USGS
science for a changing world

Prepared in cooperation with the
South Florida Water Management District

Quantification of Hydrologic Processes and Assessment of Rainfall-Runoff Models in Miami-Dade County, Florida

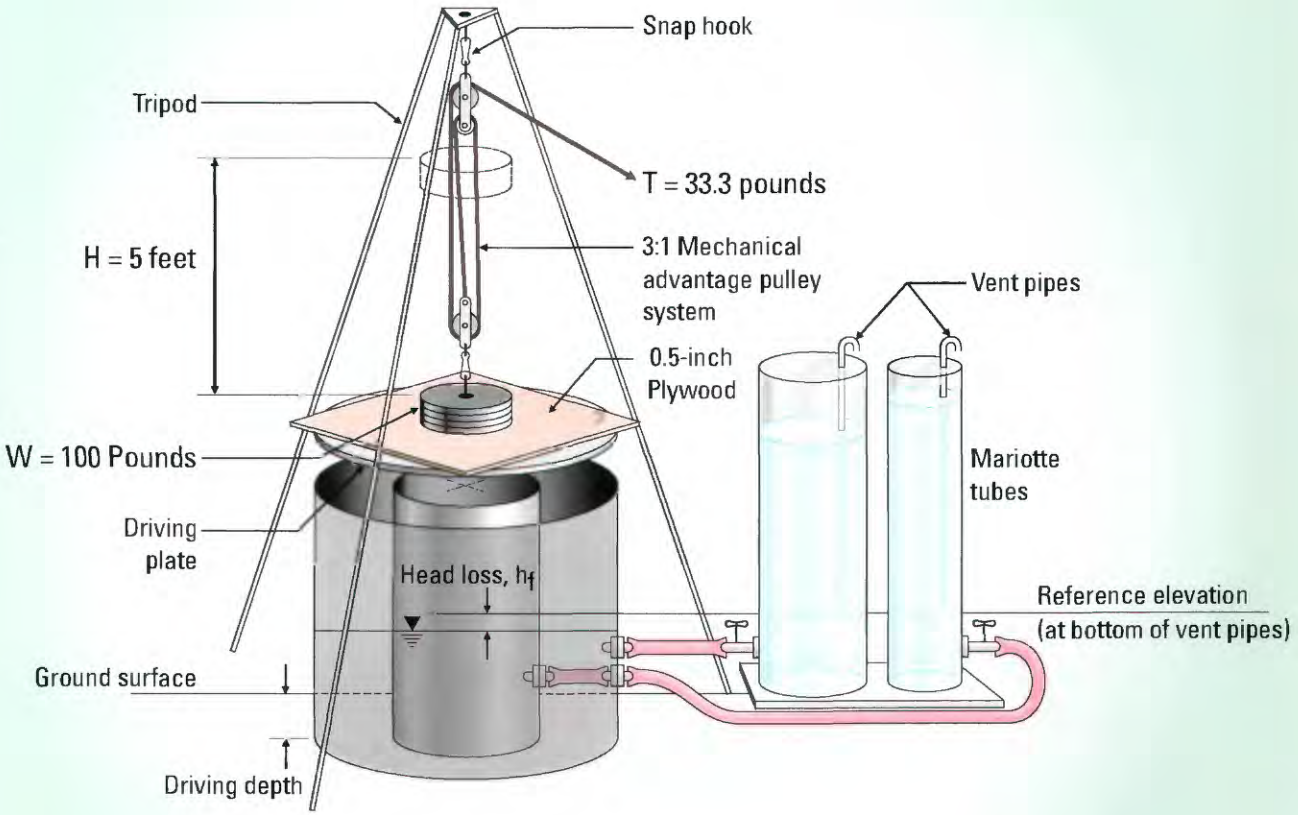

Scientific Investigations Report 2004-5191

U.S. Department of the Interior
U.S. Geological Survey

Quantification of Hydrologic Processes and Assessment of Rainfall-Runoff Models in Miami-Dade County, Florida

By David A. Chin and Raul D. Patterson

Prepared in cooperation with the
SOUTH FLORIDA WATER MANAGEMENT DISTRICT

Scientific Investigations Report 2004-5191

U.S. Department of the Interior
U.S. Geological Survey

U.S. Department of the Interior
Gale A. Norton, Secretary

U.S. Geological Survey
Charles G. Groat, Director

U.S. Geological Survey, Reston, Virginia: 2005
For sale by U.S. Geological Survey, Information Services
Box 25286, Denver Federal Center
Denver, CO 80225

For more information about the USGS and its products:
Telephone: 1-888-ASK-USGS
World Wide Web: http://www.usgs.gov/

Chin, D.A., and Patterson, R.D., 2005, Quantification of Hydrologic Processes and Assessment of Rainfall-Runoff Models in Miami-Dade County, Florida: U.S. Geological Survey Scientific Investigations Report 2004-5191, 100 p.

Contents

Figures

Tables

Conversion Factors, Acronyms, Abbreviations, and Datums

Multiply	By	To obtain
inch (in.)	25.4	millimeter
inch per hour (in/hr)	25.4	millimeter per hour
inch per day (in/d)	25.4	millimeter per day
inch per year (in/yr)	25.4	millimeter per year
foot (ft)	0.3048	meter
foot per day (ft/d)	0.3048	meter per day
square foot (ft^2)	0.09290	square meter
square foot per day (ft^2/d)	0.09290	square meter per day
cubic foot per second (ft^3/s)	0.028317	cubic meter per second
cubic foot per second per mile (ft^3/s)/mi	0.01760	cubic meter per second per kilometer
mile (mi)	1.609	kilometer
square mile (mi^2)	2.590	square kilometer
acre	4,047	square meter
pound (lb)	0.4536	kilogram
pound per square foot (lb/ft^2)	0.4882	kilogram per square meter
pound per cubic foot (lb/ft^3)	2.768×10^4	kilogram per cubic meter

Vertical coordinate information is referenced to the National Geodetic Vertical Datum of 1929 (NGVD 1929); horizontal coordinate information is referenced to the North American Datum of 1983 (NAD83)

Temperature in degrees Fahrenheit (°F) may be converted to degrees Celsius (°C) as follows:

°C = (°F - 32) / 1.8

Altitude, as used in this report, refers to distance above the vertical datum.

Acronyms

ASTM	American Society for Testing Materials
CN	Curve number
DCIA	Directly connected impervious area
DCPA	Directly connected pervious area
DERM	Department of Environmental Resources Management
GIS	Geographic Information System
MOUSE	Modeling of Urban Sewers
NDCIA	Nondirectly connected impervious area
NRCS	Natural Resource Conservation Service
PC	principal component
PVC	polyvinyl chlorinated
SFWMD	South Florida Water Management District
SFWMM	South Florida Water Management Model
SRPM	Stormwater Runoff and Pollutant Model
SWIP	Subsurface Waste Injection Program
SWMM	Surface Water Management Model
USACE	U.S. Army Corps of Engineers
USCS	Unified Soil Classification System
USDA	U.S. Department of Agriculture
USEPA	U.S. Environmental Protection Agency
USGS	U.S. Geological Survey

Abbreviation

kPa	kilopascal

Quantification of Hydrologic Processes and Assessment of Rainfall-Runoff Models in Miami-Dade County, Florida

By David A. Chin and Raul D. Patterson

Abstract

A study was conducted to identify phenomenological equations that accurately describe the hydrologic processes fundamental to modeling runoff from individual storm events in southern Florida. The ability to accurately model these processes at a variety of spatial and temporal scales is essential to the adequate design of stormwater-management infra-structure and the selection of computer codes that incorporate realistic models of hydrologic processes.

Analysis of 8 years of hourly rainfall measurements within a 100-square mile study area in Miami-Dade County indicates that rainfall amounts in individual storm events tend to be significantly correlated over distances of about 2 miles, rainfall durations tend to be significantly correlated over distances of about 4 miles, and storm events with durations of at least 24 hours have rainfall amounts significantly correlated over distances of about 4 miles. These statistics should be considered in assessing the adequacy of rain-gage densities used in regional models. A review of the temporal distribution of rainfall within individual storm events indicates that 24-hour hyetographs tend to be much more uniform than the South Florida Water Management District/U.S. National Resources Conservation Service Type III hyetograph, which has a characteristic peak in the center of the storm.

Infiltration is an important hydrologic process, and the infiltration capacities of surface soils can have a controlling influence on the amount of runoff resulting from individual storms. Double-ring infiltrometer tests were conducted at 97 sites within the 100-square mile study area, and measured infiltration capacities were related to U.S. Department of Agriculture estimated hydrologic soil group, soil texture, and land use. Relations derived in this study indicate that: (1) infiltration capacities can be reasonably estimated from either soil group or soil texture; (2) estimates of infiltration capacities are relatively insensitive to land use; and (3) the infiltration capacities reported in this study area are substantially higher than those typically associated with the native soil characteristics. The higher infiltration capacities reported in this study are attributed to the influence of soil cover and anthropogenic soil disturbances.

In applying the Horton model to the infiltration measurements, the decay factor is relatively insensitive to either the soil group or soil texture, and a typical decay factor of 0.32 minute^{-1} is associated with all soils. This indicates a rapid transition from the initial to the final infiltration capacity. Most measured infiltration capacities exceed the maximum (hourly) rainfall rate measured between 1997 and 2002, indicating that the majority of rainfall in pervious areas infiltrates and that the Hortonian model may not be adequate to explain runoff from pervious areas.

A rainfall-recharge relation of the form $y = m(x - \delta)$ is consistent with observed data where y is the change in the elevation of the water table in response to a rainfall event of depth x, δ is the threshold rainfall below which no recharge occurs, and m is the slope of the rainfall-recharge relation that can be approximated by the inverse of the specific yield of the surficial aquifer. The threshold rainfall, δ, depends on antecedent moisture conditions and varies between zero and a maximum value.

Analyses based on hourly rainfall-recharge data at five monitoring wells in the study area indicate an average specific yield of 0.23 and a threshold storm-event rainfall of 0.24 inch, whereas analyses based on 15-minute data indicated a specific yield of 0.26 and a maximum threshold rainfall of 0.37 inch. Results based on the 15-minute data are probably more accurate because rainfall extrapolation errors are not present. Analyses of daily average rainfall-recharge data indicate that the rainfall-recharge relations cannot be established using daily time increments. The rapid dissipation of recharge mounds on daily time scales causes little observable change in the daily average water table in response to daily rainfall. Upscaling of the rainfall-recharge relation for daily time scales must be based on the rainfall-recharge relation at the storm-event scale.

Analyses of evaporation from the saturated zone during extended dry periods indicates that the evaporation process

can be described by a linear model where the saturated-zone evaporation rate is equal to the ground-surface evaporation rate for a depth d_o and then decreases to zero at a depth d_{cr}. Four of the five locations investigated in this study support this model where the average value of d_o is 4.5 feet, and the average value of d_{cr} is 8.3 feet. In some cases, the evaporation rate may be independent of the depth to the water table, which occurred at the most urbanized location. Local saturated-zone evaporation rates can be estimated with a good degree of certainty from careful analysis of hourly measurements of water-table elevations.

Steady-state leakage from canals in southern Florida can be estimated from the relation presented in an earlier study, which was validated using measurements in and around the L-31N canal. Results from this study demonstrate that the relation in the earlier study is also applicable in unsteady-state cases where the time scale of fluctuations substantially exceeds 10 minutes. Analyses of data collected in the study area indicate that the estimated hydraulic diffusivity derived from tidal propagation theory combined with an effective storage coefficient of 0.007, can be used to estimate local transmissivities and then the leakage relation.

The accuracy of conventional urban runoff models was assessed by comparing field measurements of peak runoff from two urbanized catchments with the predictions of two conventional runoff models. This comparison indicated fair agreement between the measured and simulated peak runoff rates. The conventional urban runoff models used the nonlinear reservoir model to estimate surface runoff from rainfall excess, and rainfall excess was computed using the Horton model. These analyses indicate that conventional models perform adequately in estimating peak flows as a means to design drainage structures.

The formulation of several software codes, reports of previous experiences using these codes, and the consistency of these codes with the findings of this study were reviewed and the following conclusions are drawn: (1) on the urban-catchment scale, both the Surface Water Management Model (SWMM) and Modeling of Urban Sewers (MOUSE) adequately account for the key processes, and relatively accurate results can be expected; and (2) the MIKE SHE model seems to better simulate regional-scale conditions, primarily because of the integrated nature of this model; however, sufficient and accurate data are, in most cases, not available to take advantage of the distributed and integrated nature of this model.

Conclusions drawn from this study are based mostly on data collected within the 100-square mile study area, and where possible, the results have been extrapolated to the greater southern Florida area. The fundamental relations derived and validated in this study provide a sound basis for modeling event-scale rainfall-runoff processes in southern Florida, and should form the basis for selecting and developing computer codes that are useful in the development of hydrologic models at catchment, basin, and regional scales.

Introduction

The hydrology of southern Florida has been and continues to be altered by population growth and human encroachment onto the natural landscape. Urbanization causes changes in the rainfall-runoff process in various ways. As more land area becomes covered with impervious surfaces (for example, roads, buildings, and parking lots), and as natural vegetation is removed and the soil compacted, the natural infiltration capacity is lowered, causing an increased fraction of rainfall to become runoff. Increased agricultural use can also lead to increases in surface runoff (Kim and others, 2002). In southern Florida, the increased surface runoff associated with urbanization is partially accommodated by stormwater-management structures that typically are designed to remove surface runoff from rainfall events with return periods of about 5 to 10 years. The most common stormwater-management systems in southern Florida include exfiltration trenches (also known as French drains) and retention ponds that are intended to route surface runoff to ground-water recharge.

Lin and Perkins (1989) reviewed many of the conventional methods for predicting predevelopment runoff in southern Florida, and assessed the applicability of various conventional models for predicting or simulating these runoff conditions. Conventional approaches relate a runoff hydrograph to such factors as the intensity and duration of rainfall, initial abstraction, initial soil-moisture content, soil-infiltration capacity, flow length, and average slope of the land surface. The conventional computer codes used in simulating the hydrologic response of urban areas consist of node-link formulations where catchment areas are divided into subcatchments, and runoff hydrographs from these subcatchments are routed through drainage structures and conduits to yield runoff hydrographs at the catchment outlet. Inundation (flooding) occurs when surface runoff exceeds the capacity of the drainage system.

Conventional urban hydrology models do not generally simulate inundation, and site-specific models must be developed when needed. Hsu and others (2000) developed such a model, wherein a two-dimensional overland flow submodel is applied when the capacity of the drainage system is exceeded. The identification of inundation zones typically requires an accurate digital elevation model. Accurate simulation of areas of inundation can support decisions on preventing flood damages by redesigning and enlarging the capacities of storm drainage systems in inundation-prone areas. Regular flooding in urban areas normally is not life threatening but can cause a temporary inconvenience and financial burden on community residents. Such flooding is sometimes called "nuisance flooding" (Fennessey and others, 2001).

In rural areas that include agricultural fields and undeveloped land, overland flow is controlled by the topography, land cover, and soil type; and overland flow can be appropriately simulated by two-dimensional diffusive overland flow models. This is particularly true in undeveloped

areas of southern Florida that are characterized by low slopes, widespread ponding, and slow regional-flow dynamics (Lal, 1998). Kinematic-wave models are inadequate for these cases because they neglect backwater effects. Topographic depressions that hold water in the form of small lakes, wetlands, and ephemeral ponds have important hydrological functions. To account for these depressions in hydrologic models, the depressions must be characterized by their depth-storage relations; however, digital elevation models usually do not have sufficient resolution to provide these depth storage relations. Hayashi and van der Kamp (2000) demonstrated the applicability of power functions to describe the depth-volume relation in depressions. Nevertheless, more research is required to determine if these equations adequately describe conditions in southern Florida.

The canal basins of eastern Miami-Dade County were first delineated in the 1950s by the U.S. Army Corps of Engineers (USACE) in their General Design Memorandum for the Central and Southern Flood Control Project. Presented in that memorandum were the USACE analysis of the hydrology of each basin and an assessment of the flood risk from a storm of specified intensity and duration. Based on the hydrology of the basins, the USACE designed the system of canals, levees, and control structures to provide a desired level of flood protection for each basin. The canal system in southern Florida was designed to accommodate about 40 percent of the standard project flood, which is defined as the runoff resulting from a rainfall event equal to 1.25 times the 100-year 5-day storm. According to Allman and others (1979), this relation approximately corresponds to the 10-year 5-day storm within Miami-Dade County. A unit-hydrograph approach was used by the USACE to route the overland rainfall excess to the canals. Abstractions included storage in the unsaturated zone and evapotranspiration, which could probably have been neglected for individual storm events. Allman and others (1979) proposed a simple rainfall-runoff model where surface runoff occurs only when the storage is filled in the unsaturated zone.

The canal network in southern Florida acts as a strong hydraulic control, affecting surface runoff, water-table elevations, and the exchange of ground water with the canals. Positive drainage systems transport surface runoff into receiving water bodies without any detention or retention pretreatment; in southern Florida, a limited number of positive drainage systems provides for the discharge of surface runoff directly into the canal network. Canals in Miami-Dade County are primarily designed to provide flood protection for the corresponding basins, with secondary functions including land drainage for agricultural, urban, and residential developments as well as regulation of ground-water elevations to prevent saltwater intrusion (Cooper and Lane, 1987).

Gated spillways in the canals regulate flow by discharging excess water from the canal basins during flood conditions and maintaining minimum water levels in the canals during drought periods. In some cases, the water table may take several days to respond to lower canal stages, limiting the effectiveness of flood control (Khanal, 1982).

In western Miami-Dade County, the contribution of canals to the hydroperiod in Everglades National Park also is a concern. Damage to crops can be caused when the water table is too close to the ground elevation for an extensive period of time. For example, Wedderburn and others (1981) defined unacceptably high ground-water conditions within a particular agricultural area as the water-table elevation being less than 1.5 ft below land surface for 48 hours or more. A ground-water model is necessary to predict the lowering of the water table in the aquifer in response to a lowering of the stage in the canal.

A wide selection of numerical models has been used to simulate the rainfall-runoff process in southern Florida. The U.S. Environmental Protection Agency Surface Water Management Model (USEPA/SWMM) by Huber and Dickinson (1988) was applied by the Department of Environmental Resources Management (DERM) in Miami-Dade County where canal basins were delineated into several subbasins. The appropriate runoff formulation for all subbasins was left unresolved because most rainfall was retained within the subbasins, and direct rainfall and runoff measurements were not taken for positive drainage basins.

The South Florida Water Management Model (SFWMM) is a large-scale regional model (MacVicar and others, 1984; South Florida Water Management District, 1997) where rainfall-runoff relations are approximated for large spatial domains (2- × 2-mi cells) with time steps of 1 day. This model uses a two-dimensional diffusion flow model to simulate overland flow (Fennema and others, 1994; Lal, 1998). The ground-water component of this model is two dimensional and can neither simulate cones of depression around well fields nor flow in the unsaturated zone. Yan and Smith (1994) proposed combining the SFWMM with MODFLOW to produce an improved model, but this has yet to occur.

In an effort to model the performance of the canal system in response to rainfall in southern Miami-Dade County, Swain and others (1996) developed the MODBRANCH package that combines the BRANCH network dynamic flow program to simulate the canal system with the MODFLOW program to simulate the ground-water system. In many applications of this model, a fraction of the rainfall is allocated to ground-water recharge, and the rest is allocated to evapotranspiration. The MODBRANCH model was not designed to account for runoff processes directly. Other models have been developed primarily for stormwater runoff applications in southern Florida, such as the South Florida Water Management District Stormwater Runoff and Pollutant Model developed by Xue (1996). Such models have been used primarily to assess the environmental impact of urban development. Although numerous hydrologic models have been applied in southern Florida, validated rainfall-runoff relations in Miami-Dade County do not exist (Savabi and others, 2001).

The interaction of surface water and ground water is an important component in the hydrology of southern Florida and generally must be accounted for in any large-scale model that attempts to calculate runoff from rainfall (Yan and Smith,

1994). The use of integrated ground- and surface-water models (also called conjunctive models) is highly desirable because inconsistent results are likely to be generated when two separate models are used to simulate the highly interactive hydrologic systems.

Low topographic gradients, high interconnectivity between ground water and surface water, a network of canals that penetrate the water table, and numerous flow-regulation structures along the canals exist in southern Florida. To construct the models needed for flood-control operations, efficient and accurate algorithms are needed to represent the subprocesses in the rainfall-runoff relation. The results of this study, conducted by the U.S. Geological Survey (USGS) in cooperation with the South Florida Water Management District (SFWMD), provide an essential basis for constructing models that can accurately analyze large-scale stormwater-management practices in southern Florida.

Purpose and Scope

The purpose of this report is to delineate the predominant hydrologic processes that affect the representation of rainfall-runoff in numerical models of the urban areas in Miami-Dade County, southeastern Florida. This report describes the experimental protocol used to collect and analyze hydrologic data in Miami-Dade County and documents conclusions drawn from these data with respect to temporal and spatial characteristics of rainfall in southern Florida; the relation between infiltration characteristics, soil hydrologic group, and soil texture; the relation between rainfall and direct (ground-water) recharge; the relation between direct evaporation from the water table and depth of the water table below land surface; estimation of canal leakage; and estimation of surface runoff. Equations that describe hydrologic processes identified in this study are contrasted with the process models that are built into various computer codes, including MIKE SHE, Surface Water Management Model (SWMM), Modeling of Urban Sewers (MOUSE), MODBRANCH, and MODNET. Previous research on rainfall characteristics, infiltration, direct recharge, canal leakage, and overland flow processes at the storm-event scale are discussed in detail in the appendix.

Acknowledgments

This report embodies the contributions of many individuals. Eric Swain (USGS) was involved in many discussions related to this project and provided much valued advice. Marc Stewart (USGS) performed much of the field work by installing rain gages, adjusting water-level recorders, downloading data from recorders, installing flow-measurement hardware into culverts and channels, performing field calibrations, and securing data from a variety of agencies. Michael Zygnerski (USGS) performed many of the double-ring exfiltration tests, analyzed the majority of data collected in those tests, and made several other contributions to this study. Jeff Rogers (formerly of the USGS) performed the model runs for SWMM and MOUSE, Hong Xu extracted the rainfall-recharge relations from historical measurements as well as the water-table decline rates, and Richard Rojas further refined the historical rainfall-recharge measurements and derived the rainfall-recharge relations from data collected during this study. The authors of this report would also like to acknowledge the contributions, advice, and support of Elizabeth Debiak and Barbara Howie (USGS), Jayantha Obeysekera (SFWMD), and Reza Savabi (U.S. Department of Agriculture).

Description of Study Area

The study area encompasses about 100 mi^2 in Miami-Dade County, southeastern Florida (fig. 1). The hydrologic features include the C-102, C-103, C-103N, Military, North, and Florida City Canals in and around Homestead. The physiographic features present in the study area include parts of the Everglades, Atlantic Coastal Ridge, and coastal marshes and mangrove swamps (fig. 2). The Atlantic Coastal Ridge is 2 to 10 mi wide and has ground elevations ranging from 8 ft to as much as 20 ft above NGVD 1929 in some parts of Miami-Dade County (Lietz, 1999). The Everglades and coastal marshes and mangrove swamps have ground elevations that are lower than the Atlantic Coastal Ridge.

Land use is quite variable in the study area, with agriculture being the most predominant type. Highly urbanized areas (commercial, industrial, and residential) are located in the central part of the study area (fig. 3). Agriculture is diverse (row crops, fruit tree groves, and plant nurseries) and commonly located on soils suitable for the specific purpose. For example, most field nurseries are located on marl soil, because this type of soil facilitates the harvest of palms or large trees and shrubs; and container nurseries are located on rock land, because plants require land that is level, compacted, and well drained. A third type of nursery utilizes greenhouses for producing bedding plants or tropical foliage, such as orchids and bromeliads.

Meteorologic Characteristics

Climate in Miami-Dade County is marine subtropical characterized by long, warm, rainy summers and mild, dry winters. Meteorological data, summarized in table 1, indicate the range of conditions present in the study area. These data include the average monthly temperature, average monthly total rainfall, and average maximum evapotranspiration rate for a representative calendar year. The mean annual temperature is 75.6 °F, the average annual total rainfall is about 57.5 in., and the maximum average evapotranspiration rate is 0.17 in/d.

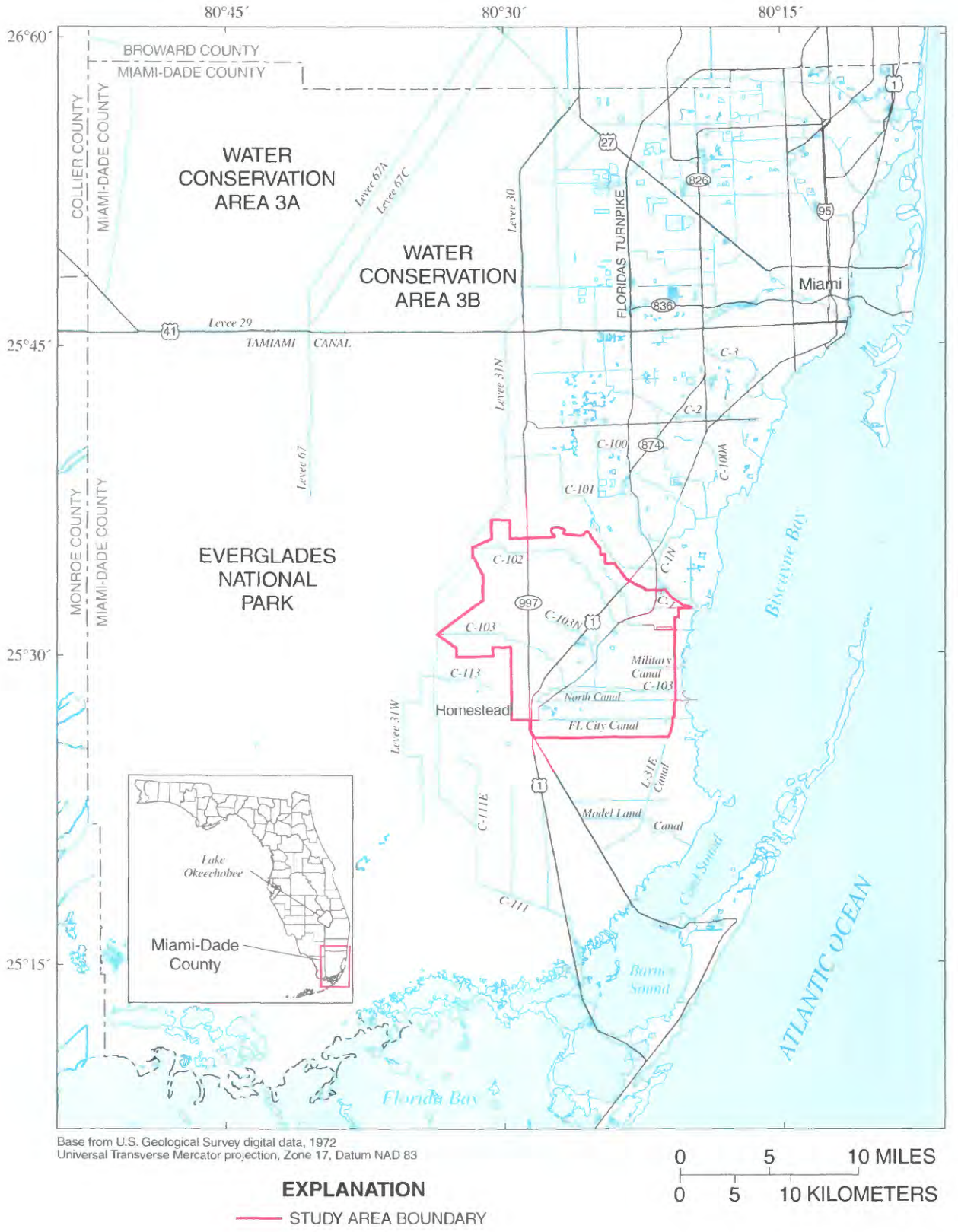

Figure 1. Location of study area in Miami-Dade County, Florida.

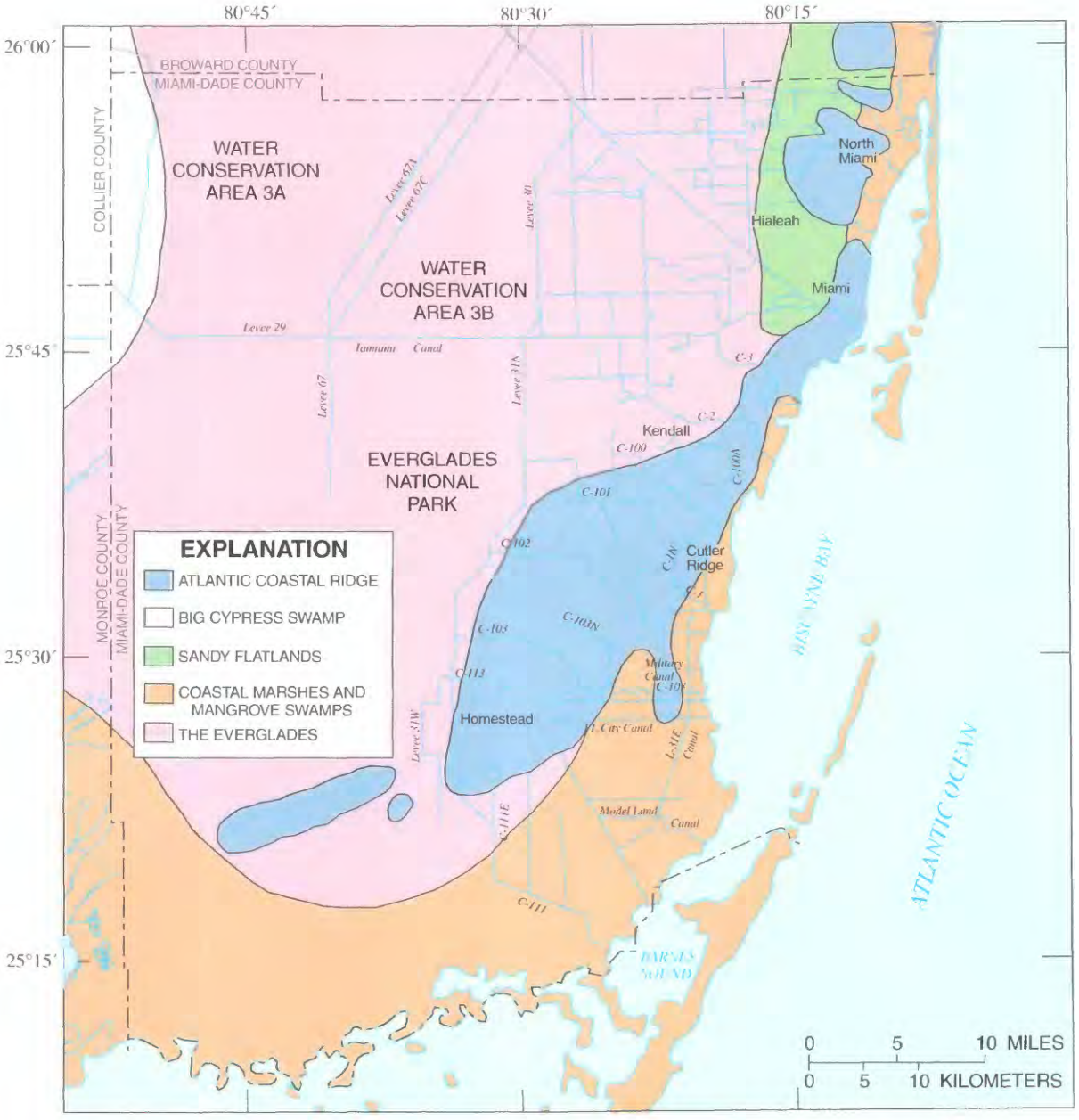

Figure 2. Physiographic features of Miami-Dade County prior to development (from Lietz, 1999).

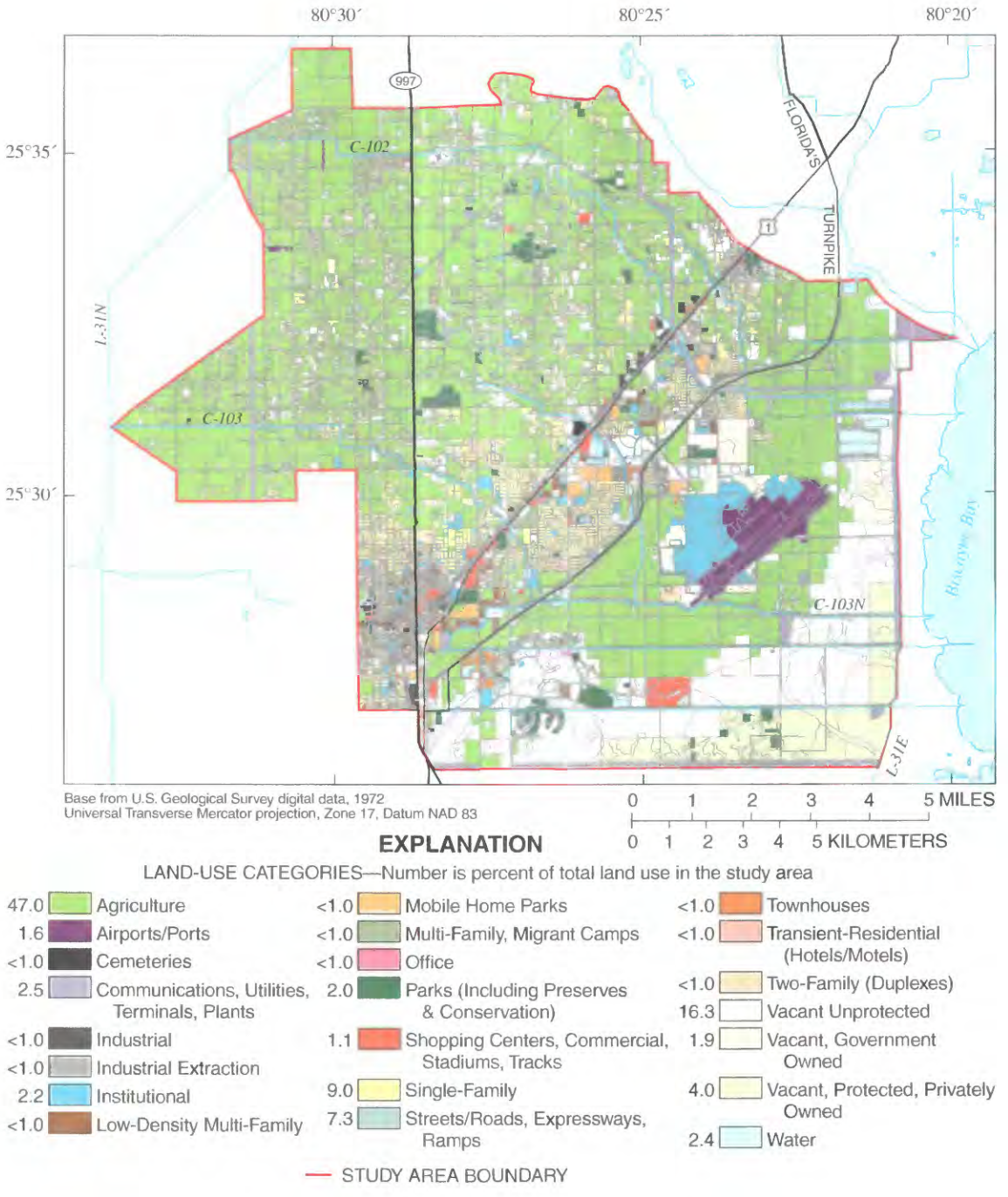

Figure 3. Distribution of land use in the study area. Detailed 1998 land-use classification provided by the Miami-Dade Department of Building, Planning, and Zoning. The < symbol is less than the value.

Table 1. Meteorologic characteristics in Miami-Dade County

[Data provided by the Natural Resources Conservation Service, 1996]

Month	Average temperature (degrees Fahrenheit)	Average rainfall (inches)	Maximum evapotranspiration (inches per day)
January	67.1	2.1	0.12
February	67.8	2.0	.12
March	71.7	1.9	.16
April	75.3	3.1	.19
May	78.5	6.5	.20
June	81.0	9.1	.19
July	82.4	6.0	.21
August	82.8	7.0	.21
September	81.8	8.1	.19
October	77.9	7.1	.18
November	72.8	2.7	.14
December	68.5	1.9	.11

Temperatures in Miami-Dade County are moderated by the Atlantic Ocean and Gulf of Mexico, but the moderating effects quickly diminish inland. Subfreezing temperatures occur about every 2 years, with moderate to severe damage to agricultural commodities.

Rainfall in southern Miami-Dade County averaged 62 in/yr between 1940 and 1992 and ranged from a minimum of 37 in. in 1971 to a maximum of 94 in. in 1947. (Merritt, 1996; Lietz, 1999). The combination of seasonally low rainfall between November and April and the porous nature of rock soils in the growing area necessitates the use of irrigation during these months. Rainfall between June and September generally is associated with localized thunderstorms and tropical cyclones, whereas rainfall during other times of the year typically is the result of frontal systems having a larger spatial scale. Peninsular Florida is affected on the average by one named storm each year and by a hurricane every 2 to 3 years, with most of the storms (79 percent) occurring in August through October (Neumann and others, 1993). The majority of annual rainfall (75-80 percent) occurs between May and October, with June and September producing the highest monthly rainfall and December producing the lowest monthly rainfall. In 1999, Miami-Dade County received 24-hour, 48-hour, and 72-hour maximum rainfall amounts that would occur once in 100 years (Abtew and Huebner, 2000).

The mean annual relative humidity is 62 percent, and evapotranspiration typically is 70 to 90 percent of total annual rainfall (Duever and others, 1994). Direct measurements of evapotranspiration rates in the Everglades and other parts of southern Florida indicate that rates between 48 and 51 in/yr (84-89 percent of mean annual rainfall) are typical in areas where the water table is relatively high (Langevin, 2001).

Table 2. Description of hydrologic soil groups in Miami-Dade County

[From Soil Conservation Service (1986) and Natural Resources Conservation Service (1996)]

Group	Description
A	Soils having a high infiltration rate (low runoff potential) when thoroughly wet. These consist mainly of deep, well-drained to excessively drained sands or gravelly sands. These soils have a high rate of water transmission
B	Soils having a moderate infiltration rate when thoroughly wet. These consist chiefly of moderately deep or deep, moderately well-drained or well-drained soils that have moderately fine texture to moderately coarse texture. These soils have a moderate rate of water transmission
C	Soils having a slow infiltration rate when thoroughly wet. These consist chiefly of soils having a layer that impedes the downward movement of water or soils of moderately fine texture or fine texture. These soils have a slow rate of water transmission
D	Soils having a very slow infiltration rate (high runoff potential) when thoroughly wet. These consist chiefly of clays that have high shrink-swell potential, soils that have a permanent high water table, soils that have a claypan or clay layer at or near the surface, and soils that are shallow over nearly impervious material. These soils have a very slow rate of water transmission

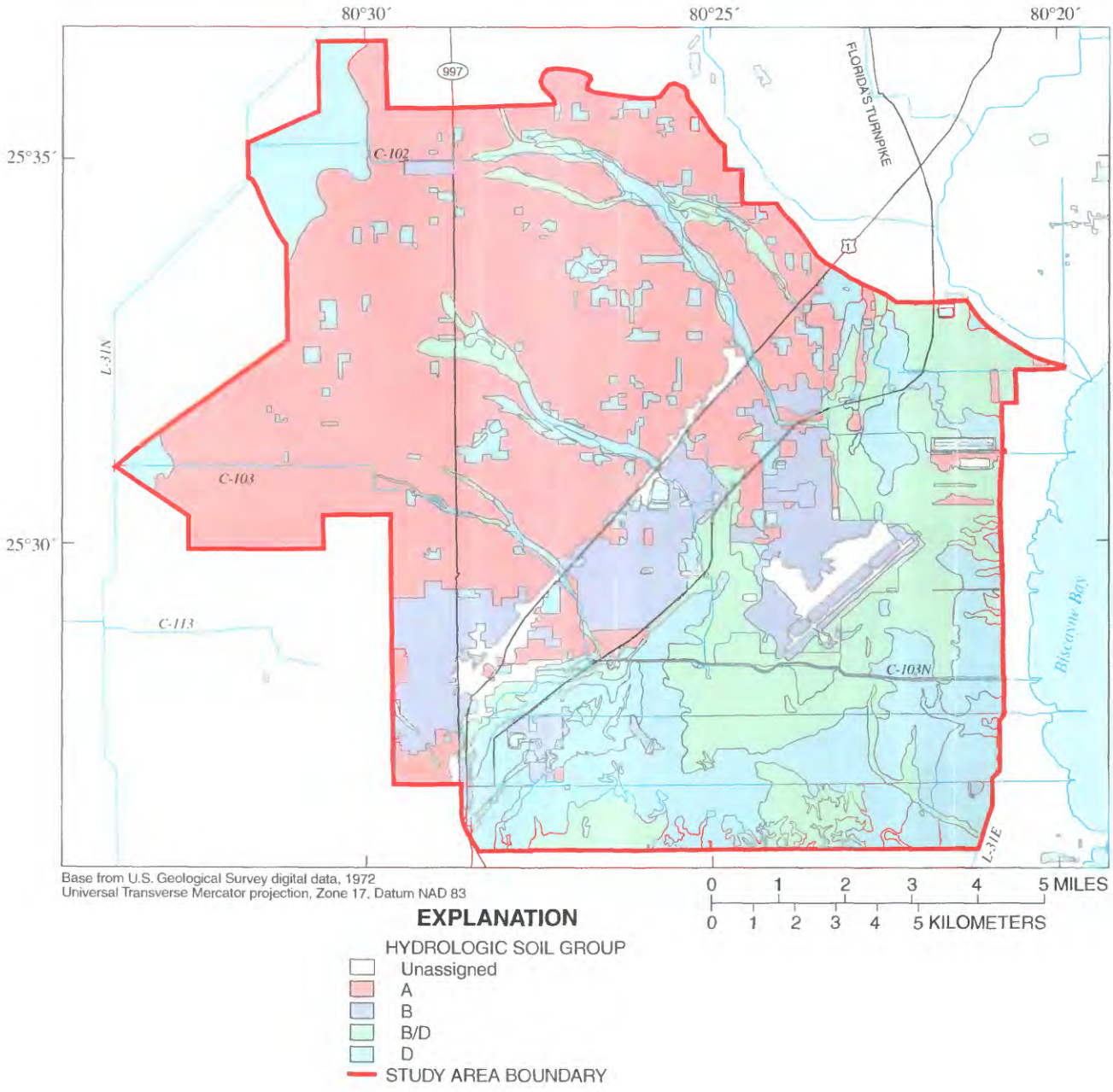

Figure 4. Generalized soil classification in the study area. Description of hydrologic soil groups (Natural Resources Conservation Service, 1996) is presented in table 2. If a soil is assigned to two hydrologic groups, the first letter is for drained areas and the second is for undrained areas.

Merritt (1996) developed a model to study the water budget in southern Miami-Dade County, and estimated that mean annual evapotranspiration was about 91 and 98 percent of annual rainfall between 1968-82 and 1983-89, respectively.

Soil and Water Features

The sedimentary material underlying Miami-Dade County consists of a thin layer of soil overlying porous limestone. Topsoils are weathered geologic materials arranged in more or less well developed layers. Various soils within the study area can have very different characteristics (depth, texture, bulk density, mineral composition, and chemical properties) that can affect the movement of water through the soil. Soils are classified by the U.S. Department of Agriculture (USDA) into different soil groups; the four hydrologic soil groups A, B, C, and D (Natural Resources Conservation Service, 1996) are described in table 2 and shown in figure 4. Soils classified as B/D are in group B under drained conditions and group D under undrained conditions.

Table 3. Soil and water features in the study area

[From Natural Resources Conservation Service (1996). Description of hydrologic soil groups is given in table 2. If a soil is assigned to two hydrologic groups, the first letter is for drained areas and the second is for undrained areas; --, no data; >, greater than the value]

Soil subclass	Percent of total land area	Hydrologic soil group	Permeability (inches per hour)	Water capacity	Depth (inches)
Krome very gravelly loam	43.0	A	0.6-2.0	0.08-0.12	
Biscayne marl, drained	14.2	B/D	.6-6.0	.15-.20	
Perrine marl, drained	12.1	D	.2-2.0	.15-.20	0-10
			.6-6.0	.20-.45	10-26
Udorthents, limestone substratum–Urban land complex	8.3	--	--	--	
Chekika very gravelly loam	3.6	D	.6-2.0	.08-.12	
Biscayne gravelly marl, drained	3.2	B/D	.6-6.0	.10-.20	
Urban land	2.5	--	--	--	
Pennsuco marl, drained	2.3	D	.2-2.0	.15-.20	0-8
			.6-6.0	.20-.45	8-44
Cardsound–Rock outcrop complex	2.1	D	.2-0.6	.18-.23	
Pennsuco marl	1.7	D	.2-2.0	.15-.20	0-4
			.6-6.0	.20-.45	4-46
Opalocka–Rock outcrop complex	1.4	D	>20	.02-.45	
Lauderhill muck, depressional	1.0	B/D	6.0-20	.30-.50	
Biscayne marl	.8	B/D	.6-6.0	.15-.20	
Udorthents, limestone substratum, 0 to 5 percent slopes	.8	--	--	--	
Perrine marl	.7	D	.2-2.0	.15-.20	0-4
			.6-6.0	.20-.45	4-29
	.7	--	--	--	
Udorthents, marl substratum–Urban land complex	.7	--	--	--	
Udorthents–Water complex	.4	--	--	--	
Terra Ceia muck, tidal	.4	D	6.0-20	.20-.50	
Matecumbe muck	.1	D	6.0-20	.20-.24	
Pennsuco marl, tidal	0	D	.2-2.0	.15-.20	

The predominant soils within the study area are members of the Krome, Biscayne, Perrine, and Chekika Series (Natural Resources Conservation Service, 1996). Parts of the study area are covered by natural soils, but other areas have been altered by cutting and filling with various materials called "Udorthents" and areas have been made impervious by urban development known as "urban land." Within each soil series, more specific subclasses (map units) can be defined, and their distribution within the study area is shown in figure 5. A highly urbanized area is present along U.S. Highway 1, with Krome soils predominant to the west of the urbanized area and Biscayne and Perrine soils predominant to the east of U.S. Highway 1. Chekika soils are mostly in the westernmost part of the study area. Each type of soil is associated with a certain type of landscape or a segment of the landscape. The distribution of soils in the study area can be accessed from the USDA Soil Survey Geographic Database at www.ftw.nrcs.usda.gov/ssur_data.html, and is the most detailed level of soil mapping provided by the Natural Resources Conservation Service (NRCS). The percent of total land area covered by each soil subclass along with the soil hydrologic group, permeability, and water capacity of each soil subclass in the study area are given in table 3.

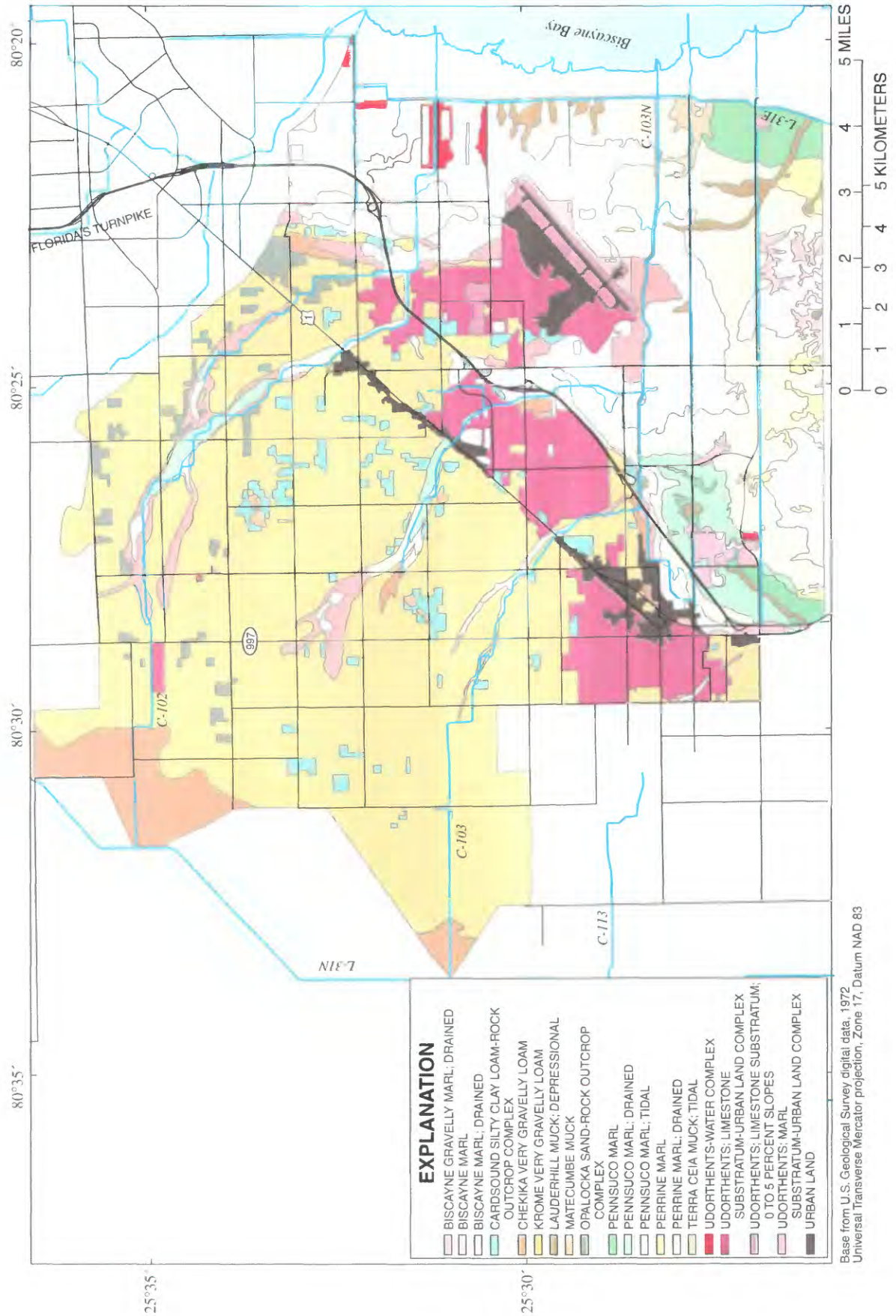

Figure 5. Distribution of soil subclasses in the study area.

Table 4. Description of soil subclasses

Subclass	Description
Krome very gravelly loam	Very shallow, nearly level, moderately well-drained soil. Typically, soil is dark brown very gravelly loam about 7 inches thick. Hard porous limestone bedrock is at a depth of about 7 inches. The water table in areas of Krome soil is within the limestone bedrock, and at a depth of 40 to 60 inches most years. Permeability is moderate (0.6 to 2 inches per hour). All areas have been rock-plowed or mechanically scarified and cultivated at some time in the past.
Biscayne marl, drained	Very shallow or shallow, nearly level, poorly drained soil. Typically, surface layer is about 5 inches of gray marl that has a texture of silt loam. The underlying layer, to a depth about 15 inches, is gray and light-gray marl that has a texture of silt loam. Hard porous limestone bedrock is at a depth of about 15 inches. The water table in the Biscayne soil remains within 10 inches of the surface for 4 to 6 months during most years, receding to as deep as 20 inches during dry periods. Permeability is moderate (0.6 to 2 inches per hour). All areas have been drained and cultivated at some time in the past.
Perrine marl, drained	Moderately deep, nearly level, poorly drained soil. Typically, surface layer is about 10 inches of grayish brown marl that has a texture of silt loam. The underlying layer, to a depth of about 26 inches, is light-brownish-gray marl that has a texture of silt loam. Soft, porous limestone bedrock is at a depth of about 26 inches. Under natural conditions, the Perrine soil has water above the surface for 1 to 3 months during most years. Generally, the water table remains within 10 inches of the surface for 2 to 4 months and is at a depth of 10 to 30 inches for most of the rest of the year. Permeability is moderately slow (0.2 to 0.6 inch per hour). All areas have been cleared, drained, and cultivated at some time in the past.
Udorthents, limestone substratum–Urban land complex	The Udorthents and urban land are either so intermixed or so small that mapping them separately is impractical. The Udorthents are found in areas of lawns, vacant lots, parks and playgrounds. The urban land consists of streets, driveways, sidewalks, parking lots, buildings and other structures in areas where the soil is covered and cannot be readily observed. Typically, the Udorthents consist of fill material that is light-gray and white extremely stony loam about 55 inches thick. The fill material is underlain by hard, porous limestone bedrock. The water table in areas of the Udorthents is within the limestone bedrock. Permeability is moderate (0.6 to 2 inches per hour) in the stony fill material
Chekika very gravelly loam	Present in the transitional areas between the Miami Ridge and the Everglades. Typically the surface layer is dark grayish brown very gravelly loam about 5 inches thick. Hard porous limestone bedrock is at a depth of about 5 inches. The water table in areas of Chekika soil is within the limestone bedrock at a depth of 12 to 36 inches in most years. Permeability is moderate (0.6 to 2 inches per hour). All areas have been rock plowed and used for vegetable crops at some time in the past

The available water capacity of a soil is equal to the difference between the water stored in the soil at the field capacity and at the wilting point. Water content for the field capacity and wilting point commonly is calculated at specified tensions of 33 and 1,500 kPa, respectively. The Soil Survey of Miami-Dade County (Natural Resources Conservation Service, 1996) lists available storage of Krome soils (typically 7 in. thick) at about 0.7 in., Biscayne Marl (typically 7 in. thick) at about 1 in., and Perrine Marl (typically 26 in. thick) at about 7 in. The five soil subclasses that compose the most total land in the study area are (table 3): Krome very gravelly loam (43.0 percent); Biscayne marl, drained (14.2 percent); Perrine marl, drained (12.1 percent); Udorthents (8.3 percent); and Chekika very gravelly loam (3.6 percent). These soils collectively cover 81.2 percent of the study area. Detailed descriptions of the five soil subclasses are given in table 4.

Soils of one series can be different in texture in the overlying layer and the underlying layer (Natural Resources Conservation Service, 1996). The physical properties of the Krome, Perrine, and Chekika series are given in table 5, and the soil-water retention curves are shown in figure 6 (Savabi and others, 2001). These retention curves are

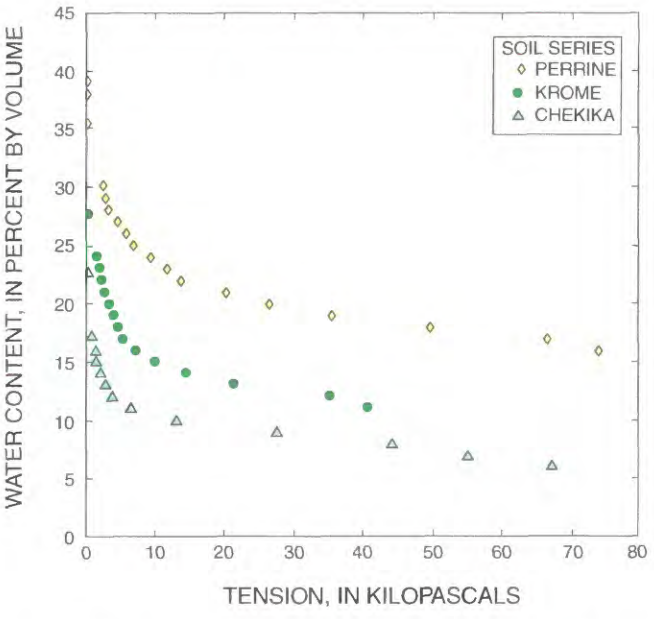

Figure 6. Soil retention curves for the Perrine, Krome, and Chekika series (from Savabi and others, 2001).

Table 5. Physical properties of Krome, Perrine, and Chekika Series in the study area

Soil series	Texture	Typical depth (inches)	Saturated hydraulic conductivity (inches per hour)	Sand (percent)	Silt (percent)	Organic matter (percent)	Rock greater than 0.08 inch or 2 millimeters (percent)
Krome	Sandy loam	8	1.0-1.1	59	31	2.1	11.4
Perrine	Silty clay loam	5	0.1-0.4	5	63	1.3	1.4
Chekika	Sandy loam	12	1.0-1.3	61	25	3.1	20.2

relatively consistent with expected curves based on the texture of the soils (Rawls and others, 1993). Nevertheless, the fact that the Krome and Chekika series are characterized by different soil retention curves, even though they both have the same soil texture, indicates that soil texture alone is not sufficient to determine the movement of water through these soils.

In soil containing a large percentage of clay (greater than 10 percent), clay mineralogy or clay type has a great effect on soil-water properties (Rawls and others, 1993). According to Savabi and others (2001), soils in the study area are mostly calcareous, and therefore, the available water is low (7-10 percent by volume). Assuming that the field capacity corresponds to a tension of 33 kPa and the wilting point corresponds to a tension of 1,500 kPa, Savabi and others (2001) determined that the field capacity of Krome soil ranges from 0.11 to 0.42, Perrine marl ranges from 0.19 to 0.51, and Chekika soil ranges from 0.08 to 0.31. Based on the typical relation between water retention properties and soil texture (Rawls and others, 1993), Krome and Chekika soils (sandy loam) should have field capacities that range from 0.13 to 0.29 with a mean of 0.21, and Perrine soils (silty clay loam) should have capacities that range from 0.30 to 0.43 with a mean of 0.37. In a calibrated hydrologic model of the study area, DERM estimated the field capacity of the soils to be 0.08 and the wilting point to be 0.03.

Although little published data exist on the measured infiltration capacities of soils in the study area, hydrologic soil group classifications indicate that Krome soil (43 percent of the study area) has a minimum infiltration capacity that exceeds 0.3 in/hr, drained Biscayne marl (about 14 percent of the study area) has a minimum infiltration capacity that ranges from 0.2 to 0.3 in/hr, and Perrine marl (12 percent of the study area) has a minimum capacity that ranges from 0 to 0.04 in/hr. These soils are expected to achieve their minimum infiltration rates within hours of continuous surface ponding; however, these rates based on these soil classifications are much less than the saturated hydraulic conductivities reported in table 5. In a calibrated hydrologic model of the study area, DERM assumed a spatially uniform Horton infiltration curve with a maximum infiltration rate of about 12 in/hr, a minimum infiltration rate of 8 in/hr, and a decay rate of 4.14 hr^{-1}. These values were allowed to vary as calibration parameters.

Soils in the study area can be classified broadly as rocky (rock land) soils in the Miami Ridge area and marl soils in the former freshwater marsh areas in the southeastern part of the study area. Rock land soils generally are well drained with a gravelly loam surface layer ranging between 3 and 9 in. thick, whereas marl soils are dense, fine-textured soils that are prone to flooding. Crops grown on rock soils where rocks are crushed into small particles require frequent irrigation. Land with marl soils must be contoured and shaped to allow appropriate drainage of excess water. Soils typically are underlain by 15 to 40 ft of porous oolitic limestone (Miami Limestone) that has a relatively low water-holding capacity and is riddled with secondary solution holes that commonly are partly to completely filled with lime mud and sand. Parker and others (1955) estimated that about 1 in. of water is retained for every 4.5 ft of rock matrix above the water table, corresponding to a specific retention of about 0.02. When the depth to the water table is greater than 5 ft, vertical flow in the unsatuarated zone generally is assumed to be predominant, and the saturated hydraulic conductivity of the unsaturated zone generally is assumed to be equal to the permeability of the most limiting horizon (Burden and Sims, 1999).

Hydrogeology and Aquifer Characteristics

The study area is underlain by a surficial aquifer system including the uppermost water-bearing unit, the Biscayne aquifer (fig. 7). The Biscayne aquifer, which is the principal source of potable water for more than 5 million people in southeastern Florida (McPherson and others, 2000), consists primarily of porous limestone that ranges in age from Pliocene to Pleistocene. The Biscayne aquifer increases in thickness from about 45 ft in the western part of the study area to about 100 ft in the eastern part (Fish and Stewart, 1991). In the study

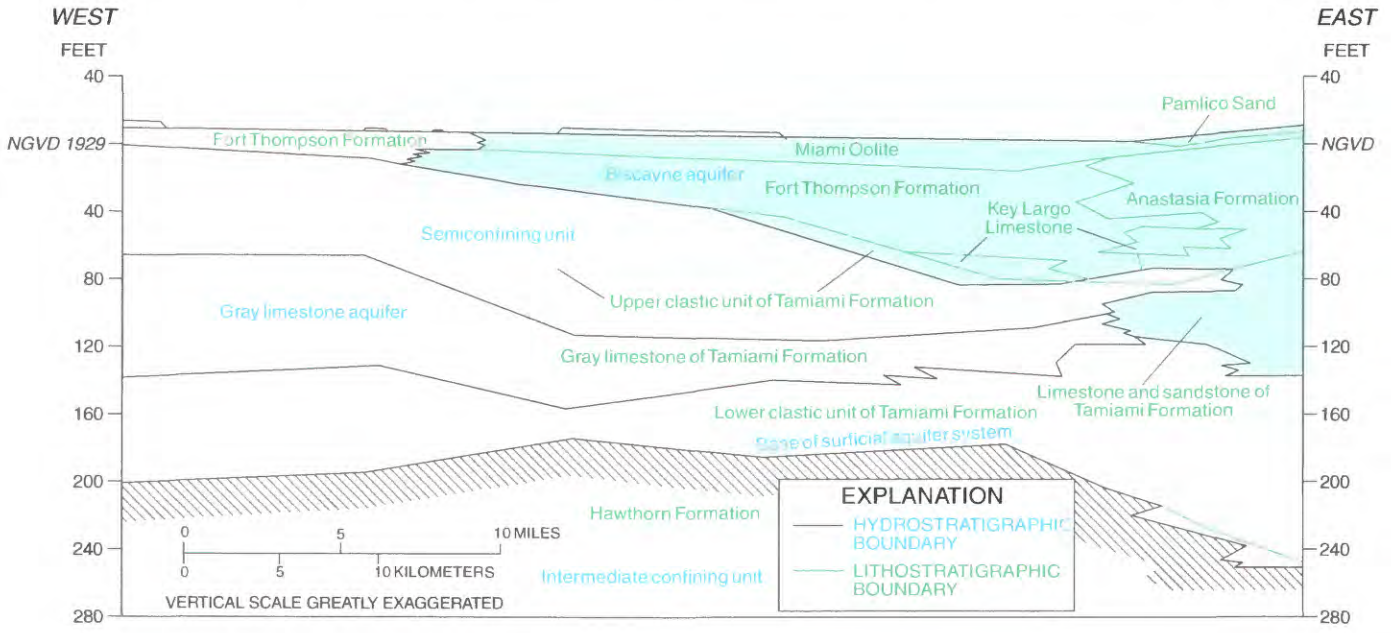

Figure 7. Generalized section showing geologic formations, aquifers, and confining units of the surficial aquifer system in central Miami-Dade County (from Fish and Stewart, 1991).

area, the Biscayne aquifer primarily comprises two limestone formations: 10 to 30 ft of the Miami Limestone underlain by 35 to 45 ft of the Fort Thompson Formation.

The water table in the study area generally is present in the Miami Limestone (marine origin), which is predominantly oolitic and contains substantial amounts of bryozoans in many parts of the area (Fish and Stewart, 1991). Shaw (1985) reported that solution channels in the Miami Limestone range in diameter from 0.4 to 1.6 in., with an average of about 0.6 in. The Fort Thompson Formation is mainly marine in origin (sandy, shelly, limestone, and largely coquina), but with some fine-grained freshwater beds (Fish and Stewart, 1991). The Miami Limestone and Fort Thompson Formation have undergone extensive secondary dissolution, making the Biscayne aquifer extremely porous and permeable. Shaw (1985) reported that solution channels in the Fort Thompson Formation range in diameter from 0.2 to 1.0 in.

In the study area, parts of the C-103 Canal basin also are underlain by the Key Largo Limestone interfingered with the Fort Thompson Formation (Shaw, 1985). The Key Largo Limestone is coralline, consisting of white to tan coral, fine-grained crystalline limestone, and generally grayish-white sandy limestone reef deposits.

Values of porosity measured in the laboratory using cores taken from the Biscayne aquifer indicate that porosity fluctuates about a mean that is independent of depth, up to at least 30 ft below land surface (fig. 8; K.J. Cunningham, U.S. Geological Survey, written commun., 2001). Typical porosity is on the order of 0.26.

Hydraulic conductivity of all geologic formations in the Biscayne aquifer typically is greater than 1,000 ft/d (Fish and Stewart, 1991), and the average hydraulic conductivity over the depth of the Biscayne aquifer is 25,000 ft/d (Genereux and Guardiario, 1998). Field experiments conducted in the upper part of the Biscayne aquifer in southwestern Miami-Dade County show that the hydraulic conductivity in the Miami Limestone and the Key Largo Limestone is substantially higher than that in the Fort Thompson Formation (Shaw, 1985; Genereux and Guardiario, 2001). Tests in the western part of the C-103 Canal basin (fig. 1) show that the Miami Limestone has a hydraulic conductivity ranging from 320 to 1,100 ft/d, with a mean of 530 ft/d, whereas the Fort Thompson Formation has a hydraulic conductivity ranging from 1 to 1,100 ft/d with a mean of 100 ft/d. Sonenshein (2001) estimated the average hydraulic conductivity to be 29,000 ft/d in the Biscayne aquifer and 470 ft/d in the Tamiami Formation (the lower boundary of the Biscayne aquifer). Fish and Stewart (1991) reported a hydraulic conductivity of less than 10 ft/d in the Tamiami Formation. Langevin (2001) estimated the average horizontal hydraulic conductivity to be 29,500 ft/d in the study area where it was used to describe the Miami Limestone, Fort Thompson Formation, and permeable zones of the Tamiami Formation. The preponderance of hydrogeologic data indicates that hydraulic conductivity is very high in the surficial aquifer system in Miami-Dade County.

Genereux and Guardiario (2001) conducted field studies using borehole flowmeters to measure the heterogeneity in the hydraulic conductivity of the Biscayne aquifer. Averaging for aquifer volumes of about 6 ft in the horizontal direction and 1 ft in the vertical direction, Genereux and Guardiario (2001) estimated a log-hydraulic conductivity variance (σ) of 2.53, a horizontal correlation length scale (λ_h) of 24 ft, and a vertical

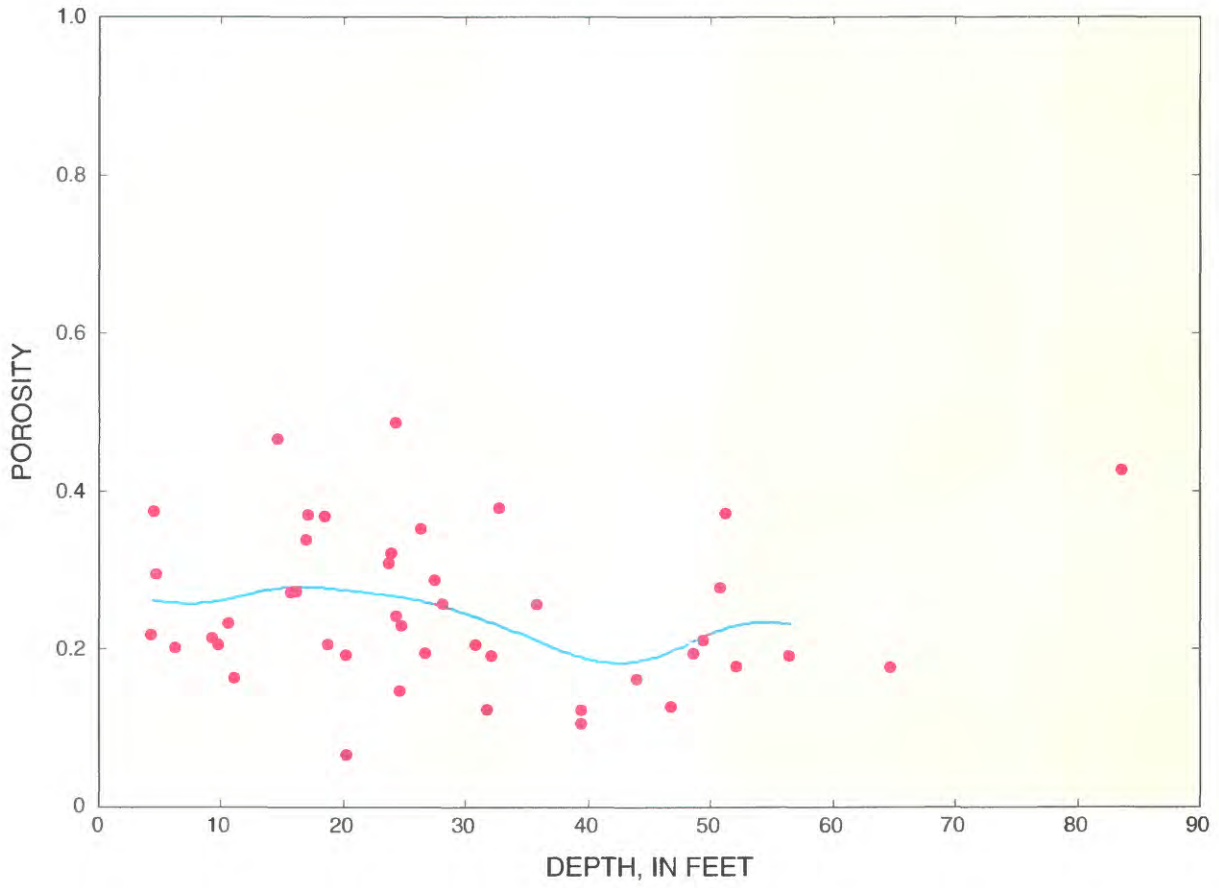

Figure 8. Measured porosity in the Miami Limestone of the Biscayne aquifer.

correlation length scale (λ_v) of 1.9 ft. Based on these data, the anisotropy ratio (λ_h/λ_v) is 12.8. The Hawthorn Formation at the base of the surficial aquifer system is at a relatively uniform elevation of 180 to 220 ft below NGVD 1929. Vertical gradients in piezometric head can be assumed to be negligible in the Biscayne aquifer (Shaw, 1985). In developing a three-dimensional model of the Biscayne aquifer, Restrepo and others (1992) assumed a specific storage of 5×10^{-6} ft^{-1}, with an anisotropy ratio of 7.

Parker and others (1955) noted that rain percolates rapidly downward to the water table, which seldom is deeper than 10 ft below land surface; high water-table conditions are at or near land surface over much of the area. Assuming that all rainfall infiltrates, and dividing rainfall amounts by corresponding water-table rises in several parts of Miami-Dade County, Parker and others (1955) concluded that 0.2 is a typical value for the specific yield of the surficial aquifer system, with several observations in the range of 0.2 ± 0.05. To determine specific yield from rainfall and water-table measurements, the area should have a high infiltration capacity, the land surface should be nearly level, and the water table should have a gentle slope and not be unduly influenced by nearby canals.

Wedderburn and others (1981) plotted the relation between daily rainfall at a station and daily change in water-table elevation at a well in Miami-Dade County, and estimated a nonlinear relation referred to as a "rating curve." For rainfall amounts less than 5 in., results indicated a specific yield substantially less than the commonly cited value of 0.2. This estimate, however, is affected by the combined effects of canal drainage, surface runoff, and aquifer response at the daily time scale. Because aquifer-response effects usually are more rapid than canal drainage effects, a shorter duration analysis is required to provide a better estimate of the rainfall-recharge relation.

Merritt (1996) estimated a specific yield of 0.2 by analyzing water-table fluctuations at a monitoring well in response to heavy rainfall. Dufresne and Davis (2001) reported that rainfall-recharge is the predominant hydrologic stress in some parts of the Biscayne aquifer, and the response of the water table to rainfall can be used as a means to calibrate ground-water models in these areas. As such, the maximum rise of the water table in response to recharge is influenced primarily by the magnitude of the recharge, specific yield, and horizontal hydraulic conductivity, with vertical hydraulic conductivity having a smaller effect in association with high

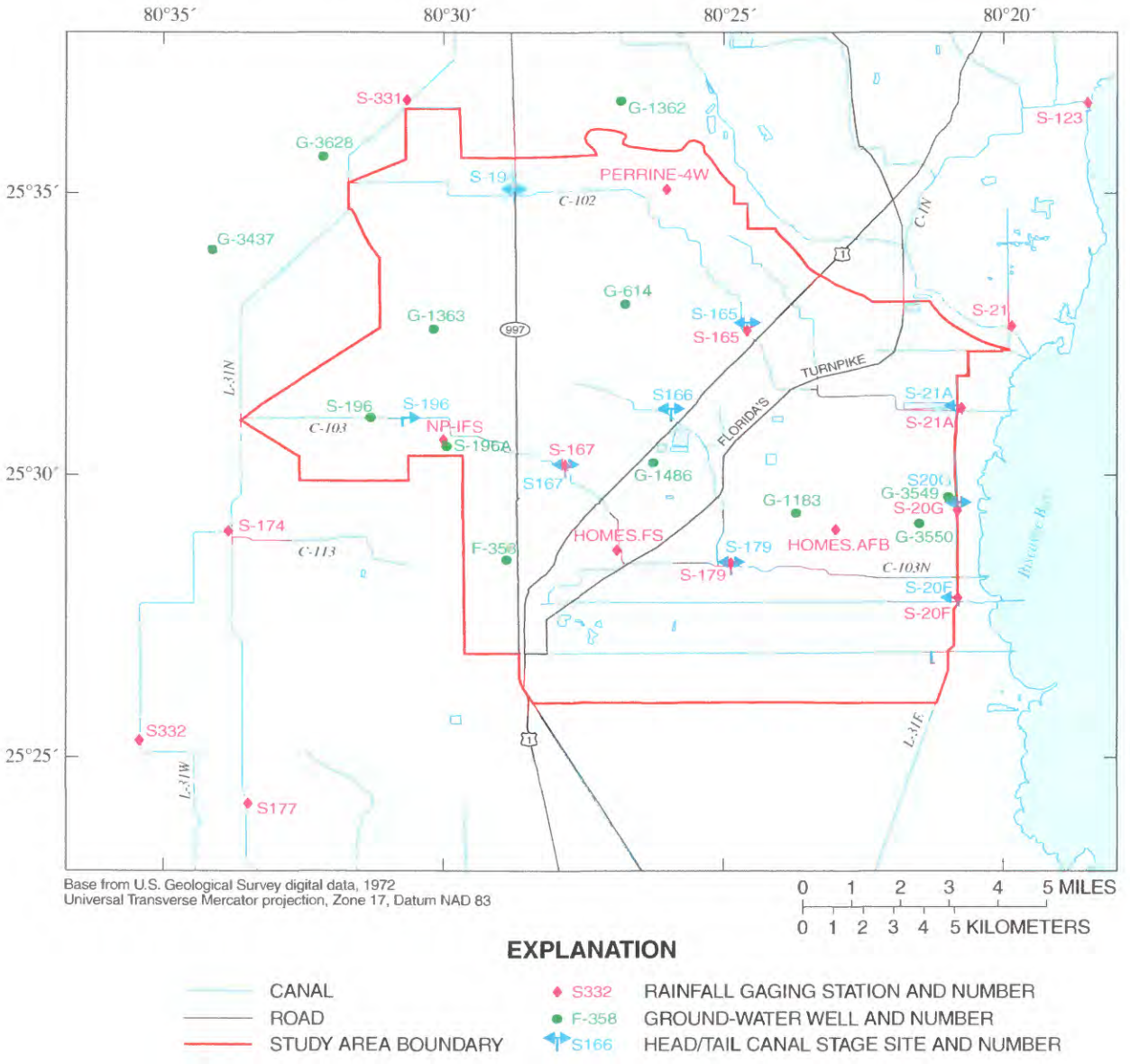

Figure 9. Location of field instrumentation sites used for the study in Miami-Dade County, Florida.

values. Dufresne and Davis (2001) noted that recession of the water table was controlled primarily by water levels in drainage canals; model calibration in the part of the Biscayne aquifer underlying northern Miami-Dade County indicated specific yields of 0.12 to 0.23.

Quantification of Hydrologic Processes

Key processes that are important in describing the hydrology of urban catchments at the storm-event scale are rainfall, infiltration, direct ground-water recharge, canal leakage, and surface runoff. Over time scales longer than those associated with storm events, evaporation from the water table also is an important process. In the subsequent sections, data collected in the study area are used to identify functional relations that accurately describe these important hydrologic processes.

Rainfall

Substantial spatial variations in rainfall are associated with thunderstorm activity in southern Florida. In general, the spatial scale of a rainfall event (storm) is proportional to the duration of the rainfall event. During the summer wet season, spatial variations in rainfall intensity tend be large, and therefore, the recorded precipitation at a measuring site could be misleading if used as an indicator of average rainfall occurring over a large area (Merritt, 1996). Most rain gages in southern

Table 6. List of rainfall stations collecting hourly data in and around the study area

[Locations shown in figure 9. Referenced to the North American Datum of 1983. All stations are South Florida Water Management District, except for PERRINE-4N, which is National Oceanic and Atmospheric Administration Station. Data from PERRINE-4W used for daily-rainfall analysis only. Abbreviation: ddmmss, degrees minutes seconds]

Station identification	Latitude (ddmmss)	Longitude (ddmmss)	Universal Transverse Mercator (UTM coordinates)	
			x (feet)	x (feet)
HOMES.AFB	25°29′01″	80°23′00″	1,843,847	9,248,006
HOMES-FS	25°28′39″	80°26′54″	1,822,419	9,245,692
NP-IFS	25°30′36″	80°30′00″	1,805,390	9,257,393
PERRINE-4W	25°35′01″	80°25′59″	1,827,294	9,284,266
S-20F	25°27′46″	80°20′51″	1,855,701	9,240,493
S-20G	25°29′21″	80°20′50″	1,855,746	9,250,081
S-21	25°32′35″	80°19′51″	1,861,053	9,269,687
S-21A	25°31′09″	80°20′46″	1,856,059	9,260,983
S-165	25°32′33″	80°24′34″	1,835,140	9,269,363
S-167	25°30′09″	80°27′48″	1,817,435	9,254,755
S-174	25°29′01″	80°33′48″	1,784,484	9,247,772
S-177	25°24′10″	80°33′30″	1,786,230	9,218,409
S-179	25°28′25″	80°24′52″	1,833,602	9,244,327
S-331	25°36′39″	80°30′35″	1,801,994	9,294,056
S-332	25°25′18″	80°35′23″	1,775,850	9,225,239

Florida report daily rainfall amounts, with hourly measurements recorded at relatively few stations.

Several recent studies have documented the effect of the spatial distribution of rainfall on runoff volume, peak flow, and time lag in the runoff hydrograph (Arnaud and others, 2002). Studies documenting the advantages of using rainfall fields as opposed to spatially averaged rainfall are relatively rare.

Rainfall Events and Hourly Rainfall

Rainfall events can be broadly defined as periods of rainfall separated by intervals of no rainfall. In applying this definition to the study area, rainfall events occur when measurable rainfall is recorded at any gaging station in the study area. In cases where rainfall is measured at 1-hour intervals, rainfall events are bounded between periods when no rainfall is recorded anywhere in the study area for at least 1 hour. This is the same definition of a storm event used by Syed and others (2003). In this study, rainfall stations collecting hourly data were located in and around the study area (fig. 9 and table 6). The collection of hourly rainfall data in southern Florida is a relatively recent practice, and before March 1997, hourly data were available only at two stations (HOMES-FS and NP-IFS). Data collected at stations listed in table 6 between March 1997 and October 2002 were used to study the spatial and temporal characteristics of rainfall events. These spatial and temporal characteristics are particularly important in assessing the density of rainfall measurements required to adequately calibrate rainfall-runoff models and the catchment scales for which spatially uniform rainfall assumptions are valid.

Using the previously stated definition of a storm event, about 3,300 storm events occurred in the immediate vicinity of the study area between March 1997 and September 2002. For each storm event, the rainfall amount at each station was calculated as the total measured rainfall at that station during the storm event, and the duration of the rainfall at each station was calculated as the time between the first and last measured rainfall within the storm event. The correlation between rainfall amounts at all individual rainfall stations in the study area for all storm events was calculated, and combining this with the known distance between stations yields the spatial correlation shown in figure 10. Assuming an exponential relation, these results can be described by the relation:

$$y = \exp(-0.07x), \qquad (1)$$

where y is the correlation coefficient (dimensionless) and x is the separation in miles. If close correlation is measured by a correlation coefficient of at least 0.9, then rainfall amounts from individual storms tend to be significantly correlated over distances of about 2 mi, as shown in figure 10. This result is particularly useful in assessing the separation in rainfall measurements required to give an accurate representation of the rainfall distribution in synoptic rainfall events.

The distribution of storm-event rainfall in the study area is presented in table 7. Although these rainfall statistics are for all storms between March 1997 and October 2002, the annual rainfall cycle in southern Florida indicates that these statistics are representative of the annual rainfall distribution. Thus, on an annual basis, about 70 percent of the rainfall events produce less than 0.25 in. of rainfall (accounting for about 13 percent of the total annual rainfall), and about 9 percent of the rainfall events produce more than 1 in. of rainfall (accounting for about 54 percent of the total annual rainfall). These statistics clearly indicate that more than half of the annual rainfall is contained in relatively few large storms.

From a water-management perspective, these data support the practice of retaining stormwater runoff from larger rainfall events to increase the availability of water during dry periods of the year. Additionally, the practice of using relatively few large rainfall events to calibrate water-management models would seem justified. Another salient feature of the rainfall statistics given in table 7 is that coastal stations S-20F, S-20G,

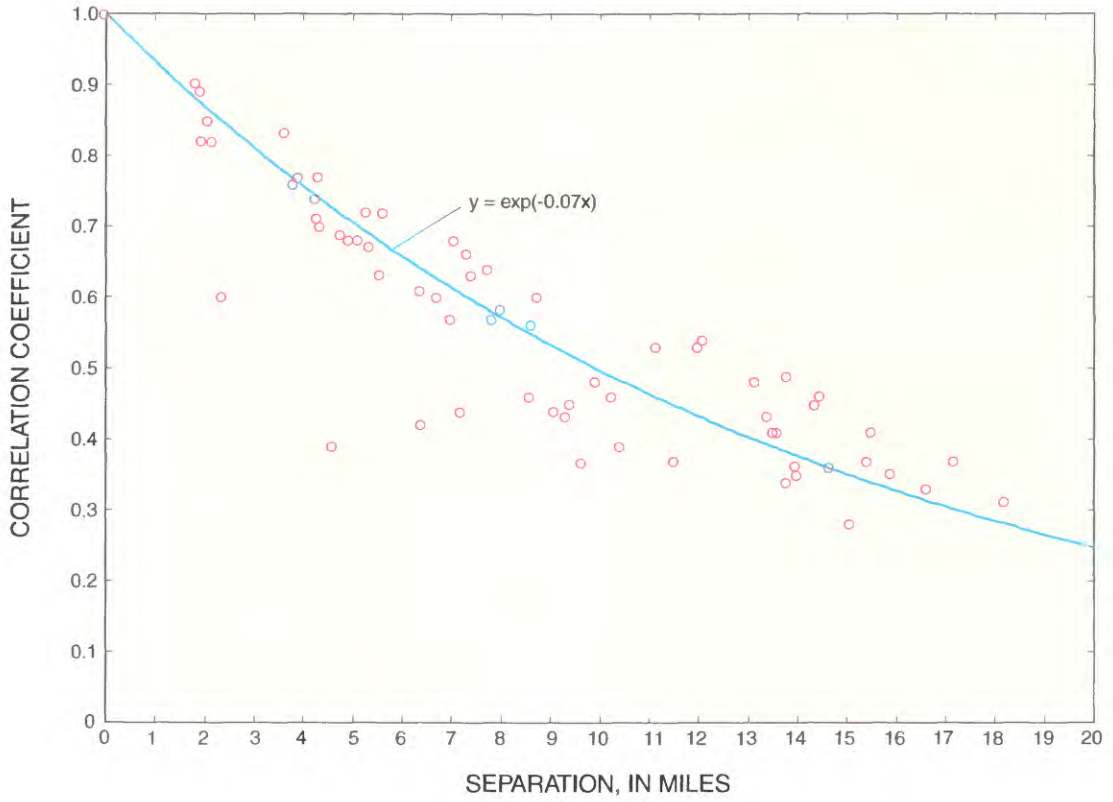

Figure 10. Spatial correlation of rainfall amount from storm events.

S-21, and S-21A tend to have a slightly higher percentage of small storms than inland stations, indicating a small heterogeneity in storm characteristics near the coastline.

Because storm events are characterized by amount and duration, spatial correlations between rainfall durations at rainfall stations in the study area also were addressed. These results, shown in figure 11, can be described by the relation:

$$y = \exp(-0.02x), \qquad (2)$$

where y is the correlation coefficient between rainfall durations, and x is the separation in miles. These results indicate that rainfall durations are correlated over longer distances than rainfall amounts. If close correlation is measured by a coefficient of at least 0.9, then rainfall durations tend to be significantly correlated over distances of about 4 mi, compared with 2 mi for significant correlation of rainfall amounts. This indicates that, within an individual storm event, more spatial uniformity exists in rainfall duration than in rainfall amount. Because storms are characterized by both amount and duration, however, these results collectively indicate that spatial uniformity in rainfall events should only be assumed for a distance of 2 mi. The results shown in figures 10 and 11 apply to all storms, and rainfall associated with longer duration storms is expected to be spatially correlated over distances that exceed 2 mi. This issue was addressed by investigating the spatial correlation of rainfall amounts for storm events with durations greater than or equal to 24 hours, and the resulting correlation function is shown in figure 12. These results can be described by the relation:

$$y = \exp(-0.025x), \qquad (3)$$

where y is the correlation between rainfall amounts, and x is the separation in miles. These results indicate that for storm events with durations of at least 24 hours, significant correlation (equal to or greater than 0.9) exists in rainfall amounts over distances of about 4 mi. Therefore, to adequately reproduce the spatial distribution of rainfall events with durations exceeding 24 hours, rainfall measurements with separations of the order of 4 mi are adequate. Furthermore, spatially homogeneous rainfall can be assumed for catchments with length scales equal to or less than 4 mi. Note that more scatter occurs in the correlation relation for storms with durations that exceed 24 hours than for all storms because substantially fewer data points occur when only 24-hour duration storms are considered.

The correlation length scales obtained here are particularly useful in determining the density of rainfall stations required to adequately represent the space/time characteristics of rainfall events in southern Florida. In a similar context, McCue and others (2002) calibrated a detailed

Table 7. Distribution of storm-event rainfall at rainfall stations in the study area from March 1997 to October 2002

Station identification	Storms less than or equal to 0.25 inch		Storms less than or equal to 1 inch	
	Number (percent)	Rainfall (percent)	Number (percent)	Rainfall (percent)
HOMES-FS	67	11	90	42
NP-IFS	69	12	90	45
S-20F	74	15	91	45
S-20G	70	16	92	50
S-21	74	15	94	51
S-21A	75	16	93	48
S-123	69	12	89	49
S-165	63	12	89	44
S-167	66	12	92	48
S-174	63	12	90	45
S-177	65	13	91	47
S-179	69	13	91	45
S-331	71	14	93	50
S-332	66	11	91	44
Average	69	13	91	46

surface-water/ground-water (conjunctive) model of central Broward County and concluded that rainfall was the largest uncertainty factor in the model calibration process. The four rainfall stations used in the 384-mi^2 area in central Broward County were insufficient for a detailed temporal and spatial resolution of the rainfall variability. McCue and others (2002) noted that single rainfall events may sometimes contribute 25 percent of the total annual runoff, so even small uncertainties in the rainfall data on such large events greatly affect the modeling results. According to McCue and others (2000), improved spatial resolution of rainfall events is needed for further development of integrated hydrologic models in southern Florida.

An important issue in hydrologic modeling concerns the appropriate hyetograph to use in describing storms. The SFWMD permit information manual cites hyetographs for both 24- and 72-hour duration storms. Between October 1994 and September 2002, 16 rainfall events with a 24-hour duration occurred, and the (cumulative) average hyetograph of these storms is compared with the SFWMD 24-hour hyetograph in figure 13. These results indicate that the observed (USGS) 24-hour hyetograph tends to be much more uniform than the SFWMD hyetograph, which has a characteristic peak in the center. To confirm the typical uniformity of the 24-hour hyetograph in the study area, cumulative observed hyetographs for both 23- and 25-hour storms (15 events each) also are shown in figure 13. These hyetographs are similar (in uniformity) to the 24-hour hyetograph, and support the assertion that a uniform hyetograph is more characteristic of 24-hour rainfall events in the study area. In making this observation, it should be noted that the SFWMD 24-hour hyetograph is entirely consistent with the Soil Conservation Service Type III hyetograph (fig. 13) that has been recommended by NRCS and is used widely in Florida.

Relative errors in rainfall measurements are assumed to decrease with increasing rainfall amounts, and for purposes of uncertainty analysis in hydrologic simulations, quantifying the uncertainties in measured rainfall is an important aspect. Most rainfall analyses in this study used hourly measurements, and for the duration of this study a large amount of synoptic hourly measurements was available at three rainfall stations spaced 300 ft apart. These stations were operated by the USGS, Everglades National Park, and the University of Florida (Institute of Food and Agricultural Sciences). Individual storms were bounded by intervals of no measured rainfall at all three stations, and the measured rainfall for each storm was determined by summing the measured rainfall amounts between the no-rainfall intervals.

The variability of measured rainfall for each storm event was assessed using the ratio of the range of rainfall measurements divided by the average rainfall measured at three closely spaced stations. The relation between the variability and the average measured rainfall for individual storm events is shown in figure 14. These results validate the intuitive assumption that uncertainty in rainfall measurements is inversely proportional to the measured rainfall amount. Data indicate that errors of 50, 25, and 10 percent should be associated with storm-event rainfall amounts of about 0.1, 0.2, and greater than 1 in., respectively (fig. 14). These differences are substantially higher that the measurement errors of the tipping-bucket rain gages used in this study and likely represent real differences in rainfall at gaging stations.

The average storm event in and around the study area can be characterized by total rainfall and duration that are spatially uniform areas in length scales on the order of 2 mi. Although rainfall amounts and durations may be spatially homogeneous over this length scale, the time sequence of rainfall may not be so uniform. To study the homogeneity of rainfall time sequences, spatial correlation of hourly rainfall was determined in the study area from March 1997 to September 2002. Results of this analysis indicate that the correlation decreases exponentially with distance, with hourly rainfall tending to have significant correlations (equal to or grater than 0.9) over distances less than 1 mi (fig. 15). Thus, rainfall measurements with separations of less than 1 mi would be required to accurately characterize the temporal and spatial details of rainfall events measured at hourly intervals in the study area. A comparison can be made with the results described earlier.

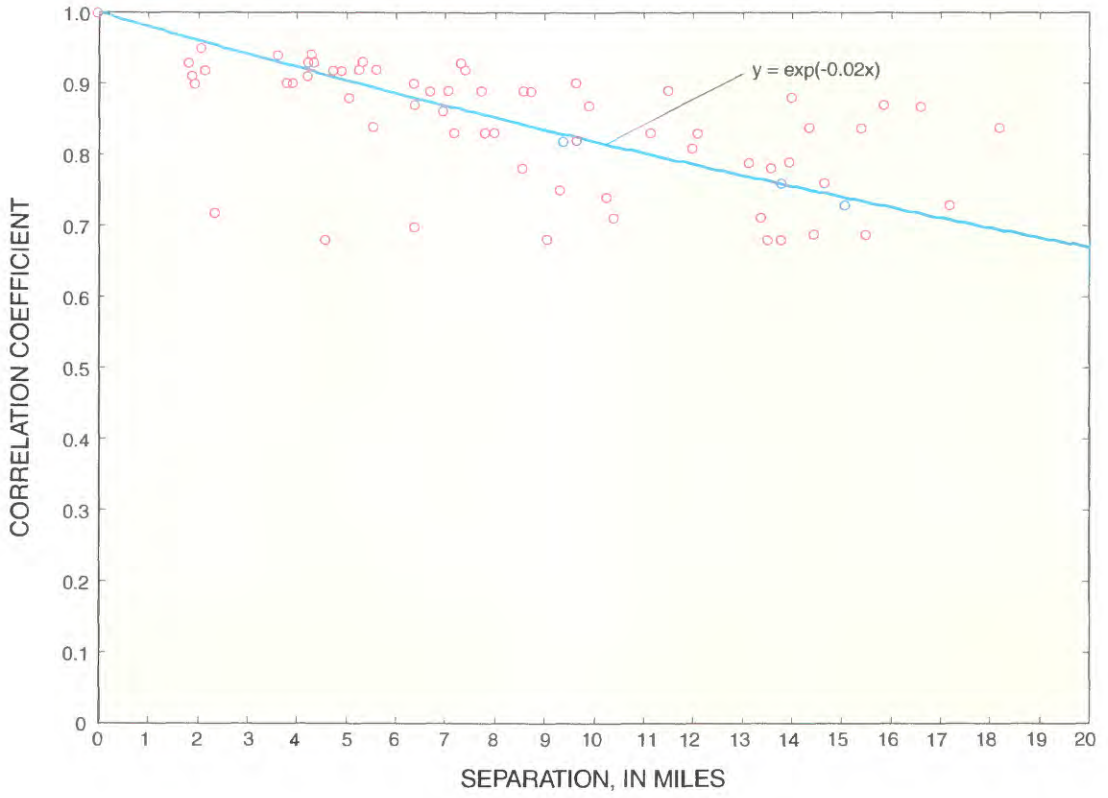

Figure 11. Spatial correlation of duration of storm events.

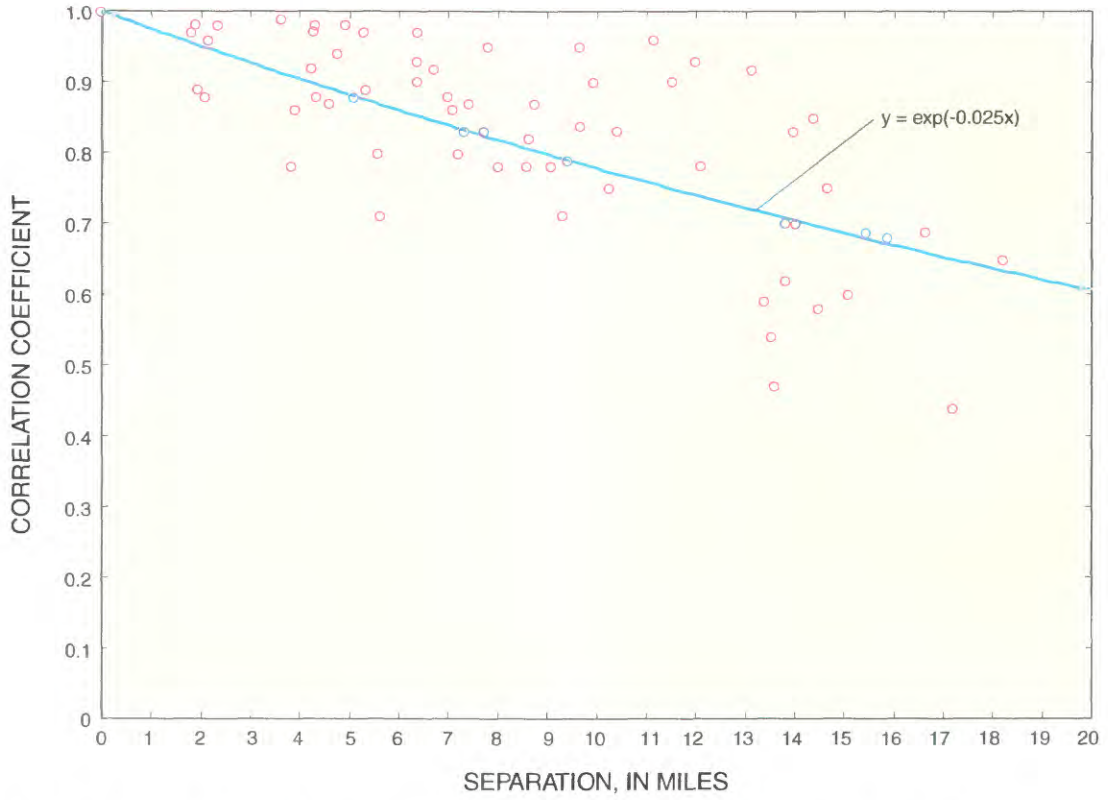

Figure 12. Spatial correlation of rainfall amount from storm events with duration of at least 24 hours.

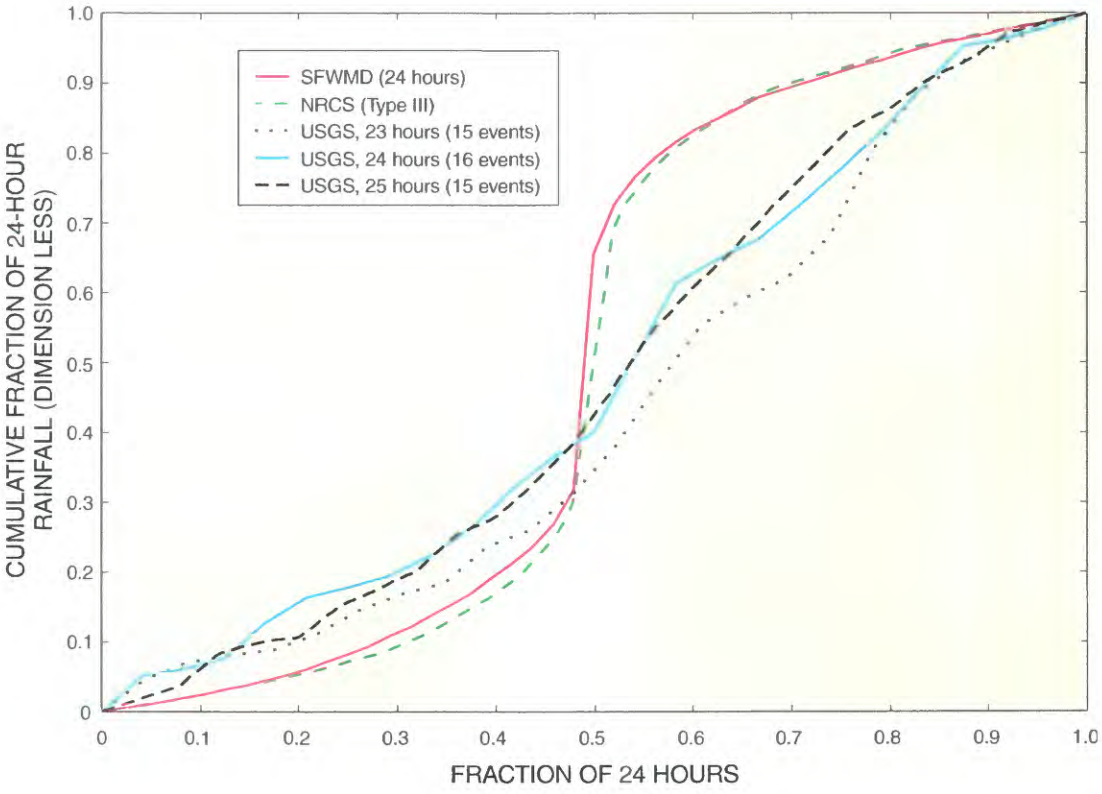

Figure 13. Cumulative fraction of rainfall with time for 24-hour storm events. SFWMD is South Florida Water Management District. NRCS is Natural Resource Conservation Service. USGS is U.S. Geological Survey.

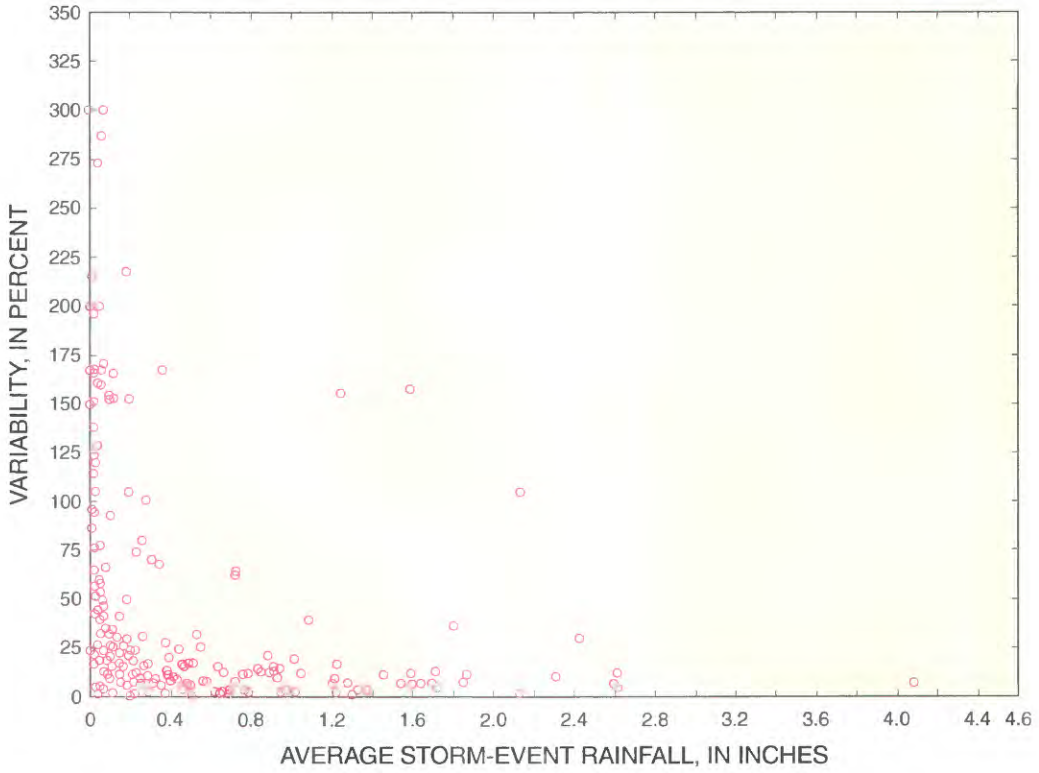

Figure 14. Relation between the variability and average measured rainfall for local storm events.

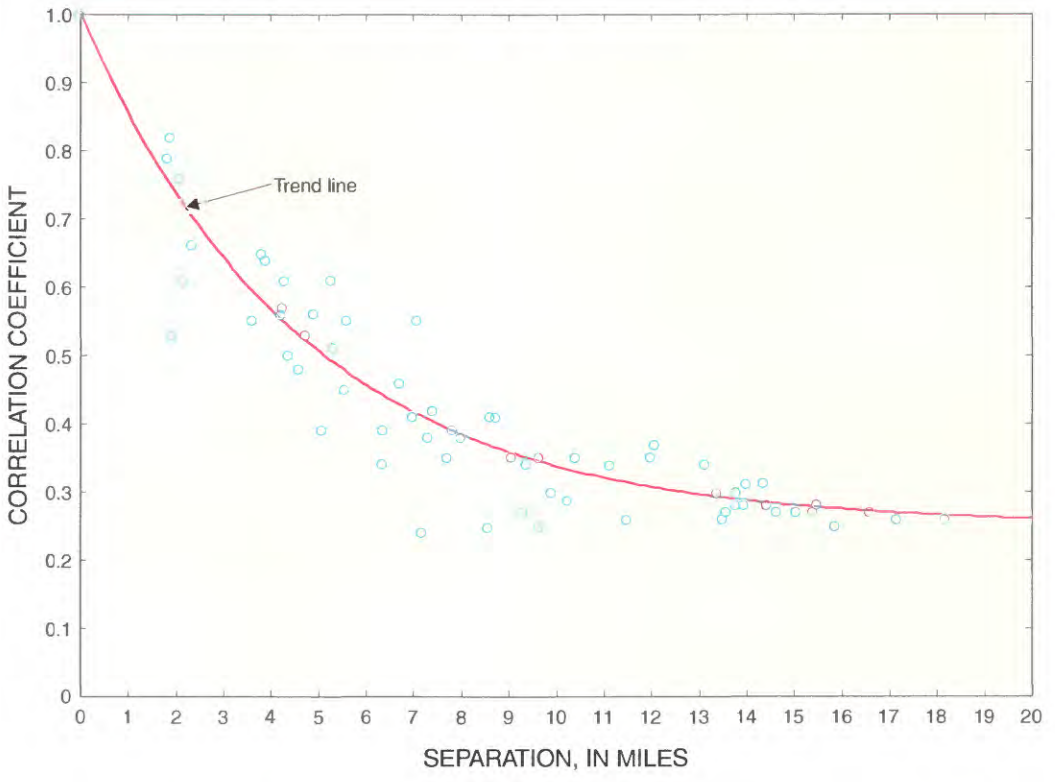

Figure 15. Spatial correlation of hourly rainfall.

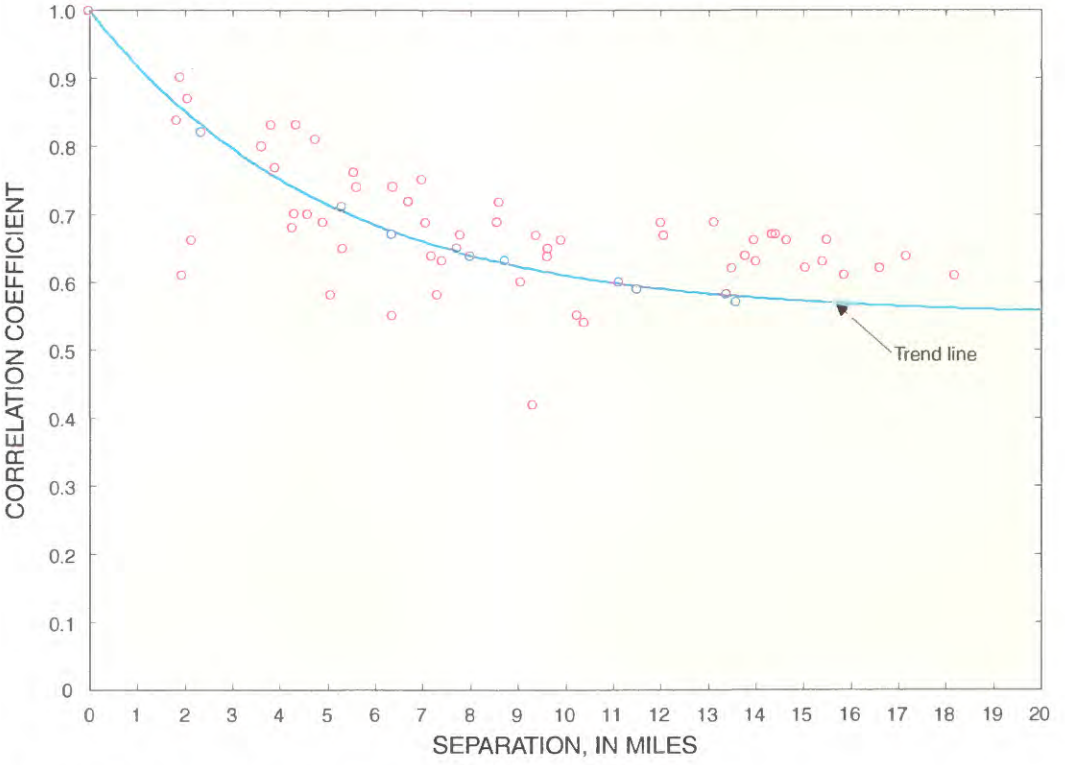

Figure 16. Spatial correlation of daily rainfall.

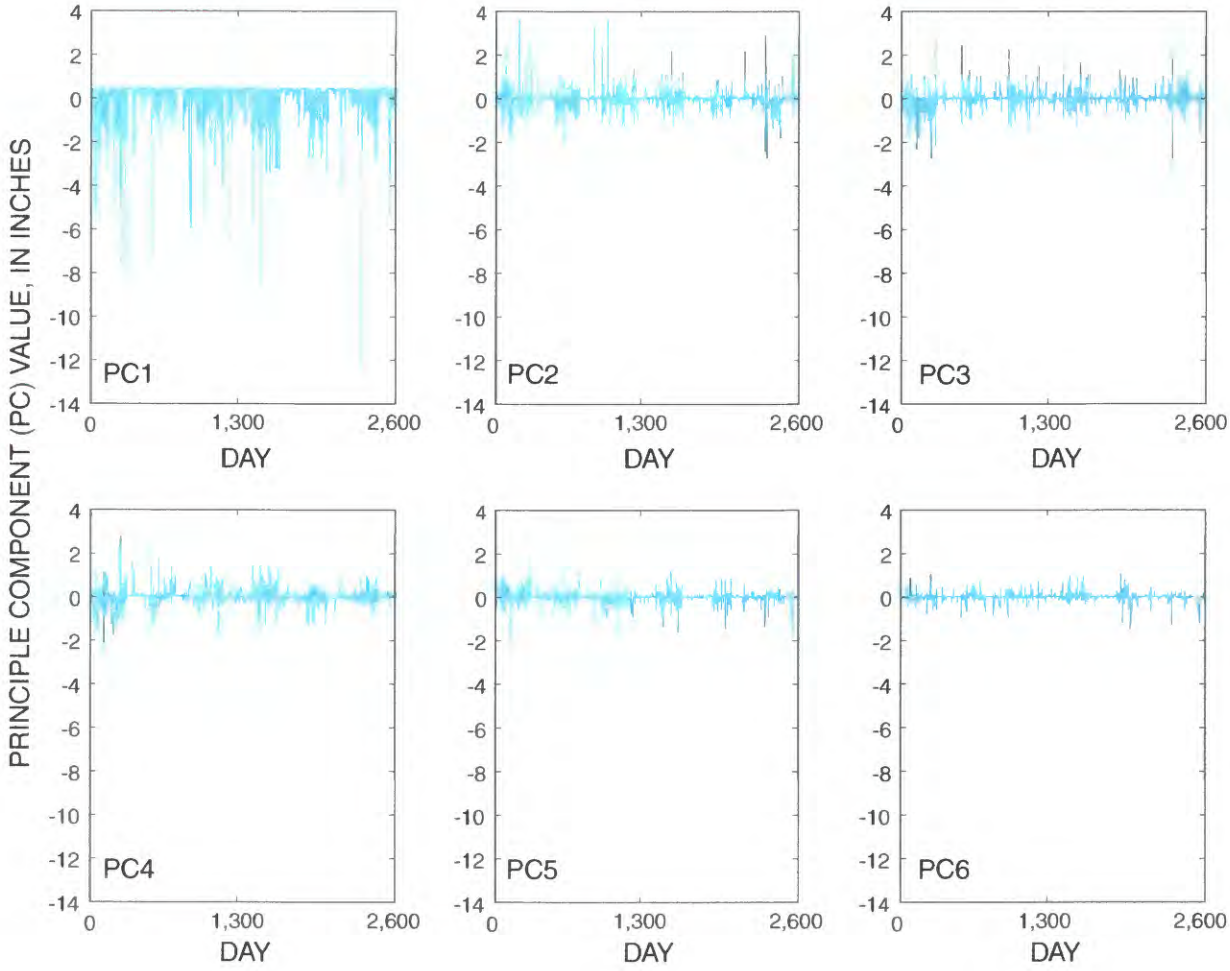

Figure 17. Principal components (PC) of daily rainfall.

Spacings of rainfall measurements of about 2 mi adequately reproduce the rainfall amounts in typical individual storms, and spacings of about 4 mi reproduce only the rainfall amounts associated with storms having durations equal to or greater than 24 hours.

Daily Rainfall

The hourly rainfall measurements analyzed in the previous section were summed to daily rainfall measurements, and the spatial correlation of the daily rainfall amounts are shown in figure 16. These data indicate that significant correlation (equal to or greater than 0.9) of daily rainfall amounts typically extend for 1 to 2 mi from a measurement location, and the spatial correlations decay more gradually than for hourly rainfall measurements. A time series of daily rainfall amounts is correlated over longer length scales than hourly rainfall; therefore, a smaller density of rainfall measurements is justified in hydrologic models with daily time steps, compared with models using hourly time steps.

The space/time characteristics of daily rainfall within the study area were investigated by analyzing daily rainfall measurements from January 1, 1990, to December 31, 2000, at stations HOMES-FS, PERRINE-4W, S-20F, S-20G, S-21A, and S-174 (fig. 9 and table 6). Applying the principal component (PC) analysis based on the covariance matrix to the synoptic daily rainfall measurements, the daily rainfall time series at each station was expressed as a linear combination of the uncorrelated PC time series shown in figure 17. The variability of the PCs shown in figure 17 clearly decrease from PC1 to PC6, and the cumulative fractions of total variance in measured rainfall explained by each of these components (communalities) are given in table 8.

These results indicate that PC1 explains more than half of the variance (59-79 percent) at each rainfall station included in

Table 8. Contribution of principal components (PCs) to rainfall measurements at selected gaging stations

Station identification	Cumulative fraction of total variance in measured rainfall					
	PC1	PC2	PC3	PC4	PC5	PC6
HOMES-FS	0.688	0.760	0.812	0.987	1.000	1.000
PERRINE-4W	.690	.781	.994	.996	1.000	1.000
S-20F	.647	.732	.746	.772	.995	1.000
S-20G	.772	.925	.926	.928	.934	1.000
S-21A	.789	.913	.916	.921	.966	1.000
S-174	.589	.669	.803	.999	1.000	1.000

the analysis. PC1 incorporates the large-scale rainfall processes in the study area, and large-scale processes account for most of the variance in the measured daily rainfall. Other PCs account for small-scale rainfall processes that primarily affect specific rainfall stations. PC2 affects coastal stations S-20G and S-21A, PC3 affects PERRINE-4W in the northern part of the study area, PC4 affects HOMES-FS in the south-central part of the study area and S-174 west of the study area, PC5 affects coastal station S-20F; and PC6 affects coastal station S-20G.

The coefficients of the PCs that express the rainfall at each station as a linear combination of PC1 and PC2 are shown in figure 18. As indicated by figure 18, the rainfall characteristics in the study area are very different in the coastal areas (S-20F, S-20G, and S-21A) compared with the inland areas (HOMES-FS, PERRINE-4W, and S-174).

Based on these results, it seems reasonable to characterize the rainfall into two modes: one for the coastal areas, and one for the inland areas. In hydrologic models that require daily rainfall time series, representative rainfall stations that are appropriate to the areas being modeled should be used.

Infiltration

A total of 97 sites was selected for infiltration measurements in the study area. Geographic Information System (GIS) maps of soil type and land-use classification were used to obtain a spatially representative number of tests in the various soils types and land uses within the study area. The double-ring infiltrometer test was used to measure the infiltration capacities at selected sites, and a hand-auger was used to collect soil samples. The support area for each infiltration measurement is the area of the inner ring in the double-ring apparatus, which has a diameter of 12 in. Horton-model infiltration parameters were estimated at each measurement location.

In analyzing the results of each infiltration test, it was recognized that infiltration characteristics can be affected by several factors, including: soil structure, condition of the soil surface, distribution of soil moisture or soil-moisture tension, chemical and physical nature of the soil, head of applied water, depth to ground water, chemical quality and turbidity of the applied water, temperature of the water and soil, percentage of entrapped air in the soil, atmospheric pressure, length of time of application of water, biological activity in the soil, and the method used to measure infiltration (Johnson, 1963). Additionally, measured infiltration rates are scale dependent, and several tests usually are necessary to arrive at a representative infiltration rate for a particular type of area. Due to the limited number (97) of infiltration tests that were conducted in this study, the number of variables that could be included were necessarily limited to those commonly assumed to have the greatest influence on the infiltration capacity of soils. In this study, the relation between USDA assigned hydrologic soil group, land use, soil texture, and infiltration capacity was investigated.

Experimental Method

All infiltration tests were conducted in accordance with the American Society for Testing Materials (ASTM) Standard Test Method for Infiltration Rate of Soils in Field Using Double-Ring Infiltrometer (American Society for Testing Materials, 1994), hereinafter referred to as the "standard method." The double-ring infiltrometer test consists of

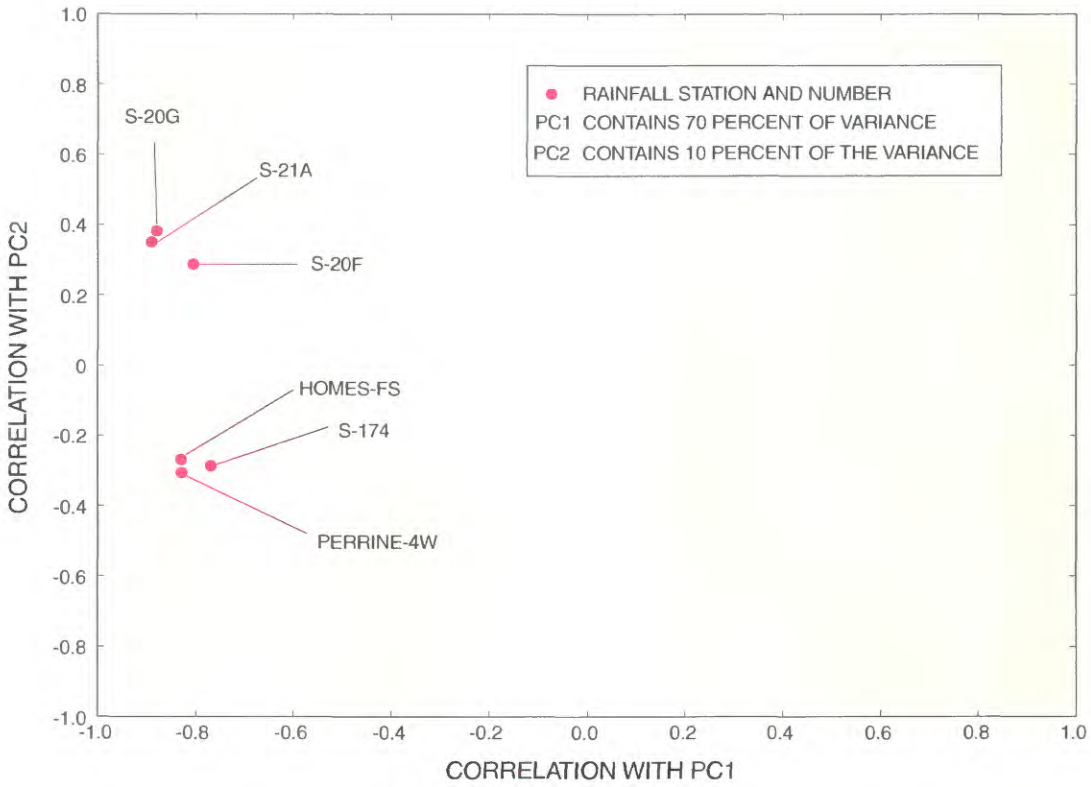

Figure 18. Principal component (PC) correlations of daily rainfall at selected gaging stations. Site locations are shown in figure 9.

driving two concentric open cylinders into the ground, partially filling the rings with water, and then maintaining the water at a constant level while the water in the rings infiltrate into the soil. The volume of water added to maintain a constant level is equal to the volume that infiltrates. The volume that infiltrates during timed intervals is converted to an incremental infiltration rate and plotted relative to elapsed time.

Operational modifications to the standard method were necessary because of the unique soil conditions in the study area. As a guide for future studies, cross references are made to the standard method in cases where the method used in this study differs from the standard method, and cross references with sections in the standard method are given within parentheses. Deviations from the standard infiltration method occur in the Apparatus (Section 6, Driving Equipment and Depth Gauge) and Procedure (Section 8, Driving Infiltration Rings, Maintaining Liquid Level, and Measurements). These changes do not add significant measurement error to the test results. The test apparatus was the same as specified in the standard method, however, neither a sledge hammer nor the jack-and-reaction method using a truck was effective in driving the rings.

The double-ring infiltrometer test begins by driving the rings into the ground at the selected test location, connecting the water supplies, and quickly filling the rings with water to the level of the bottom of the Mariotte tube vent pipes. Readings were taken immediately and every 30 seconds thereafter until the infiltration rate stabilized, and then every minute thereafter. Water levels in the inner and outer Mariotte tubes and in the inner and outer rings were recorded at the end of each time interval during the test.

Driving the Rings

The method used to drive the infiltrometer rings into the ground differed from the method recommended in the infiltration standard (American Society for Testing Materials, 1994, sections 8.3 and 8.4). The apparatus used to conduct the double-ring infiltrometer measurements is shown in figure 19. The test procedure was to first place the inner ring at a selected location under the shop-made tripod with 9-ft-long legs. The inner-ring cover plate then was centered over the inner ring, a 3/4 in. sheet of protective plywood placed on the cover plate, and the 100-lb weight, consisting of four 25-lb-weight plates, centered above the plywood.

The stationary pulley was attached to the apex of the tripod, and the moving pulley was attached to the 100-lb weight (fig. 19). A weight guide consisting of a 14-in.-diameter polyvinyl chlorinated (PVC) pipe was used to direct the falling 100-lb weight to strike the plywood and drive the rings. To place the weight guide on the plywood, the weight was lifted about 3 ft, the weight guide was encased around the

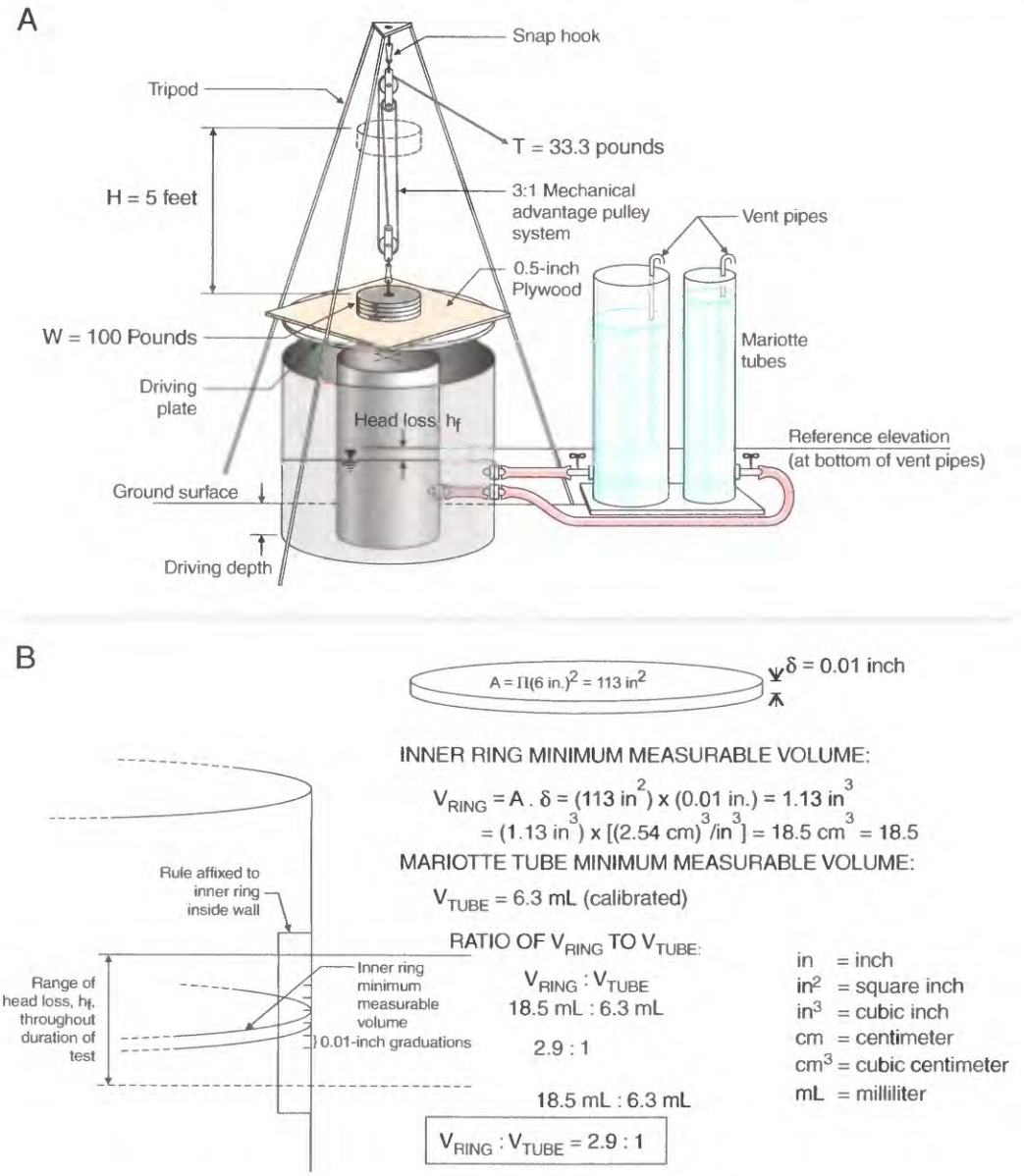

Figure 19. Infiltrometer apparatus showing (A) infiltrometer ring test setup, and (B) comparison of minimum measurable volumes of inner ring and Mariotte tube.

weight and then lifted until the bottom cleared the plywood, then slid over the plywood and centered. A small carpenter's level (about 6 in. long), with two bubble levels set perpendicular to each other, was placed on top of the driving plate to ensure a vertical and even advancement of the ring throughout the driving process.

The weight was lifted about 5 ft above the rings and dropped repeatedly, driving the ring into the ground until the desired penetration of 4 to 6 in. was achieved. The outer ring was placed concentrically around the inner ring and driven utilizing the same procedure used to drive the inner ring. In some tests, the 4- to 6-in. penetration could not be achieved for both rings, so a minimum penetration depth of 3.5 in. was used in these cases. Penetration depths and the number of strikes were recorded in field notes.

Maintaining Water Level

Mariotte tubes were used to supply water to the rings as the water infiltrated into the ground. These tubes supply water at constant head equal to the elevation of the bottom of the vent pipe as specified in the standard method. Because the Mariotte tube is sealed except for the bottom of the vent pipe, as the water is delivered to the inner and outer rings, a vacuum builds in the airspace that forms above the water surface.

The only way for air to enter is by bubbling from the bottom of the vent tube. This happens only when the level in the ring drops below the level of the bottom of the vent tube. Under these conditions, water is dispersed from the Mariotte tubes at a rate to maintain a water level in the ring equal to the level of the bottom of the vent tube.

Because the rate of infiltration can exceed the rate at which water is delivered by the Mariotte tube, the stage in the inner ring fluctuates slightly throughout the test. These fluctuations must be quantified because they are large relative to the amount of water that infiltrates for a measurement interval, thus affecting the mass balance from which infiltration rates are calculated. This is especially a problem at the beginning of the experiment when the highest infiltration rates occur and the level of water in the rings drops considerably below the reference elevation.

Because of the high infiltration rates common in the study area and as described by the Horton model, the initial infiltration rate (f_o) is the highest and then infiltration rates diminish until the infiltration capacity (f_c) is reached. To account for imbalances in the infiltration and water-delivery rates, more accurate recording of the inner-ring stage is required than specified by the standard infiltration method.

A finely graduated steel ruler was fixed vertically against the inner-ring wall to read the stage with an accuracy of 0.01 in. with a 3× magnifying glass. The improved accuracy in measuring the water level in the inner ring was required; in applying the mass balance at each time interval, the amount of water decreased in the inner ring is added to the amount dispensed by the Mariotte tube to compute the volume of infiltrated water. The area of the inner ring is about 12 times that of the Mariotte tube, and because the Mariotte tube graduations are about 0.04 in. (1 mm), it would be required to record inner-ring stage at 0.003 in. (1/12 mm) increments to preserve the accuracy provided by the Mariotte tube in the mass balance.

Data Collection and Processing

Data collected as part of each double-ring infiltrometer test included date, location and site conditions, weather conditions, driving depth, number of strikes to install the rings, time series of water levels in the Mariotte tubes, and time series of water levels in the inner and outer rings. A soil sample also was collected at each test site. All collected data were entered into a field notebook, except for the time series of water levels, which for the latter tests, were entered directly into a laptop computer.

Recorded site conditions included the appearance of the land surface (bare or vegetated soil), type of vegetation (if any), degree of soil moisture (dry, moist, or wet), and whether the area was located under a tree canopy. Recorded weather conditions were air temperature, humidity, and cloud coverage.

The driving depth (to the nearest 0.5 in.) and number of strikes required for both the inner and outer ring were recorded. Due to the extensive use of rock-plowing, trenching, and scraping throughout the study area, which creates rock fragments in the soil, the recorded number of strikes could be useful in identifying outlier tests for the given soil type/land use. This record would indicate the presence of rocks under the rings, which could affect the test results.

The Mariotte tube water levels were recorded in centimeters with one decimal place accuracy to millimeters. The ring stages were recorded to 1/8 in. accuracy for the first 49 tests, and with 0.01 in. accuracy for the inner ring for all subsequent tests (1/8 in. accuracy for the outer ring for all tests).

Selection of Test Sites

Test-site selection was guided by the following objectives: (1) to distribute the tests among the soil types and land uses in relation to their proportion of the total study area, and (2) to obtain a uniformly distributed set of tests across the study area. The locations of the infiltration test sites are shown in figure 20. Some test sites were clustered in pairs to compare small-scale variation in infiltration within a land use or soil type. Without compromising the site-selection objectives mentioned above, special focus was placed on agricultural and residential land uses. Contacting landowners or obtaining permission to conduct tests on private land was sometimes difficult, which limited the number of tests conducted on row-crop land uses. The influence of soil type and land use on measured infiltration capacity was determined by overlying soil type and land use. The relation between land use and USDA assigned hydrologic soil groups in the study area is presented in table 9.

Table 9. Relation between land use and hydrologic soil group

[All values are in acres. Description of hydrologic soil groups is presented in table 2. If a soil is assigned to two hydrologic groups, the first letter is for drained areas and the second is for undrained conditions]

Land use	Total area (acres)	Hydrologic soil group				No group assigned
		A	B	D	B/D	
Densely developed	6,544	1,178	3,272	559	559	976
Sparsely developed	12,064	5,535	1,714	3,193	1,362	260
Undeveloped	1,002	244	0	491	265	2
Agriculture (row/field crops)	14,105	7,165	16	2,721	4,194	9
Agriculture (groves)	9,178	8,133	4	881	160	0
Agriculture (nurseries)	7,698	3,850	11	1,483	2,354	0

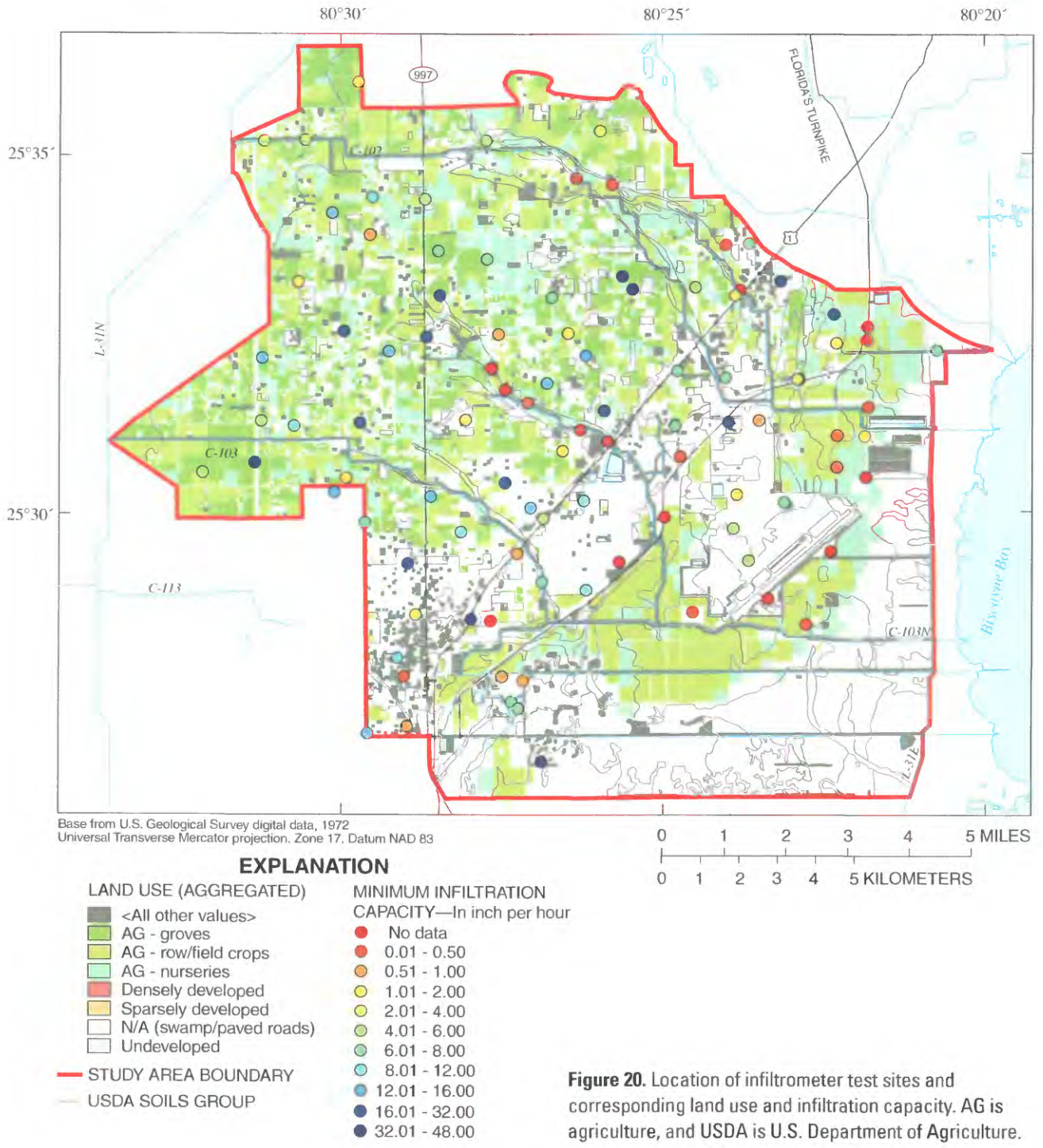

Figure 20. Location of infiltrometer test sites and corresponding land use and infiltration capacity. AG is agriculture, and USDA is U.S. Department of Agriculture.

The hydrologic soil group represents the potential for runoff due to soil texture and structure. The soils are classified as (Soil Conservation Service, 1986):

- Group A—sand, loamy sand, and sandy loam with bare-soil infiltration rates exceeding 0.3 in/hr;
- Group B—silt loam and loam with infiltration rates between 0.15 and 0.30 in/hr;
- Group C—silt and sandy clay loam soils with infiltration rates ranging from 0.05 to 0.15 in/hr; and
- Group D—clay loam, silty clay loam, sandy clay, silty clay, and clay with infiltration rates less than 0.05 in/hr.

Land use was classified as densely developed, sparsely developed, undeveloped, and agriculture. Densely developed

land includes single-family, multifamily, commercial, and industrial properties. Sparsely developed land (urban) includes low-density residential, estate-home residential, green areas in Florida Department of Transportation rights-of-way, and canal rights-of-way. Undeveloped land is unused and unoccupied. Agricultural land includes three categories: row/field crops, groves, and nurseries. The row/field crops are commonly tilled, whereas the fruit groves are not commonly tilled, but initially subject to cross trenching. There are three types of plant nurseries specializing in: mature or young landscaping trees, container-grown plants, or greenhouse seedling plants.

Data indicate that the densely developed land mainly contains group B soils, sparsely developed land mainly contains group A soils, undeveloped land mainly contains group D soils, and agriculture mainly contains group A soils, primarily because of rapid drainage (table 9). Very little development occurs in the southern and eastern extremes of the study area (fig. 3), primarily because this area is flooded for extended periods of time during the year. As a result, no infiltrometer tests were conducted in these areas.

Analysis of Infiltrometer Data

Fitting the Horton infiltration model to each individual test consisted of computing infiltration rates at each time interval, identifying and removing outliers, and regressing the data to the Horton model to obtain the parameters f_o, f_c, and k, which are defined by the Horton model for ponded infiltration capacity, f_p, given by $f_p = f_c + (f_o - f_c)e^{-kt}$, where f_o is the initial infiltration capacity, f_c is the asymptotic (minimum) infiltration capacity, and k is the decay factor. Infiltration rates were computed using the standard ASTM method, with the added refinement of including the inner-ring stage fluctuations in the water mass-balance computations. Outlying data values include: (1) those immediately following refills of the Mariotte tubes (stoppage of the water supply is a temporary transient stress on the system); and (2) the first few data points for some of the faster infiltrating soils at the beginning of the test when conditions were changing too quickly to be recorded accurately. All outliers were removed if not part of a trend. Some tests results could not be fitted to the Horton model. In cases where the transient Horton model did not fit the measured data and where the last few data points fluctuated regularly about a horizontal line, the average value was taken and reported as f_c.

Estimation of Infiltration Capacity from Hydrologic Soil Groups

According to the USDA, about 20 distinct soil types are present in the study area. The Miami-Dade Department of Planning and Zoning (2002) produced a 1998 land-use map identifying 93 separate land-use classifications, which generally adhere to the Florida Land Use and Cover Classification System, with modifications for specialized local land uses. The number of combined soil type/land-use categories (a potential of 1,860) and the number of infiltration tests (only 97) made it impossible to analyze each combination individually.

To facilitate meaningful analysis, land use and soil types were aggregated into groups based on semiquantitative criteria (in the case of soils), field observations, and interviews with local land managers (in the case of land use). For example, high-density single-family residential, multifamily residential, commercial, and light-industrial areas all had similar types of landscaping; namely, sod underlain with a thin layer of dark, highly organic soils. These land uses also had similar land-management practices prior to development— the land was cleared and the organic top soil was removed from building-pad or paved-surface areas and relocated offsite or used to create landscaping mounds. As such, these were categorized as "densely developed." Large single-family homes on 1-acre lots, estate homes on 5 acres or more, and canal and powerline easements were classified as "sparsely developed," regardless of the underlying natural soil.

Because of the flat topography, the four basic types of original land covers (pine rockland on the coastal ridge, freshwater marshes, slow moving streams or sloughs, and tidal wetlands east of the ridge) are expected to be relatively homogeneous and separated by relatively sharp boundaries. The soil map used in this study (fig. 4) is the digital version of the Miami-Dade County soil survey, which was published in 1980 and converted recently to a GIS layer in the USDA Soil Survey Geographic standard format by the SFWMD. The assumption of homogeneity within soil types allows for the discrete separation of tests into groups corresponding to the major soil types, which were aggregated by their hydrologic group. The USDA soil survey for Miami-Dade County (Natural Resources Conservation Service, 1996) classifies the 20 soil types in the study area into four hydrologic groups: A, B, B/D, and D (fig. 4). Classification of these soil groups is based on laboratory measurements of permeability (performed by the USDA) on the major soil groups in the study area.

An important consideration is that the assignment of soils to hydrologic soil groups based on texture is appropriate for uncompacted disturbed soils. A detailed description of each hydrologic soil group is presented in table 2.

Hydrologic soil groups reflect infiltration characteristics under bare-soil conditions, and the influence of ground cover is an added effect. In addition to groups A, B, C, and D, three dual classes also are used: A/D, B/D, and C/D. These dual groups are assigned for certain wet soils that can be adequately drained. The first letter applies to the drained condition, the second to the undrained. Only soils that are rated D in their natural condition are assigned to dual classes. Soils may be assigned to dual groups if drainage is feasible and practical. Beyond the hydrologic group of a soil, treatment and cover type are factors that affect the infiltration characteristics. Treatment refers to both mechanical practices (such as

contouring and terracing) and management practices (such as crop rotations and reduced or no tillage).

The hydrologic soil group at each infiltrometer test site (fig. 20) was obtained from the USDA soil map (fig. 4), and the distribution of hydrologic soil groups at the sites where usable infiltration data were collected are given in table 10. These data indicate that most of the sites (43 sites) contained soil group A, with soil groups B, B/D, and D distributed relatively evenly at the remaining sites.

The infiltration capacity at each site was taken as the Horton asymptotic (minimum) infiltration capacity (f_c), and the mean and standard deviation of f_c for each soil group are given in table 10. These results indicate significantly higher infiltration capacities than are usually associated with hydrologic soil groups. For example, as previously indicated, group B soils are typically associated with infiltration capacities ranging between 0.15 and 0.3 in/hr, whereas measurements in this study indicate infiltration capacities of 8.2 ±7.0 in/hr for group B soils. The reason for this discrepancy is probably because infiltration capacities typically associated with soil groups are for bare soil (without vegetation) and infiltration capacities used to assign hydrologic groups are derived from

Table 10. Distribution of hydrologic soil groups in the study area

[Description of hydrologic soil groups is presented in table 2. If a soil is assigned to two hydrologic groups, the first letter is for drained areas and the second is for undrained areas]

Hydrologic soil group	Number of samples	f_c, Infiltration capacity (inches per hour)	
		Mean	Standard deviation
A	43	14.8	10.5
B	19	8.2	7.0
B/D	19	6.4	11.0
D	16	4.4	6.3

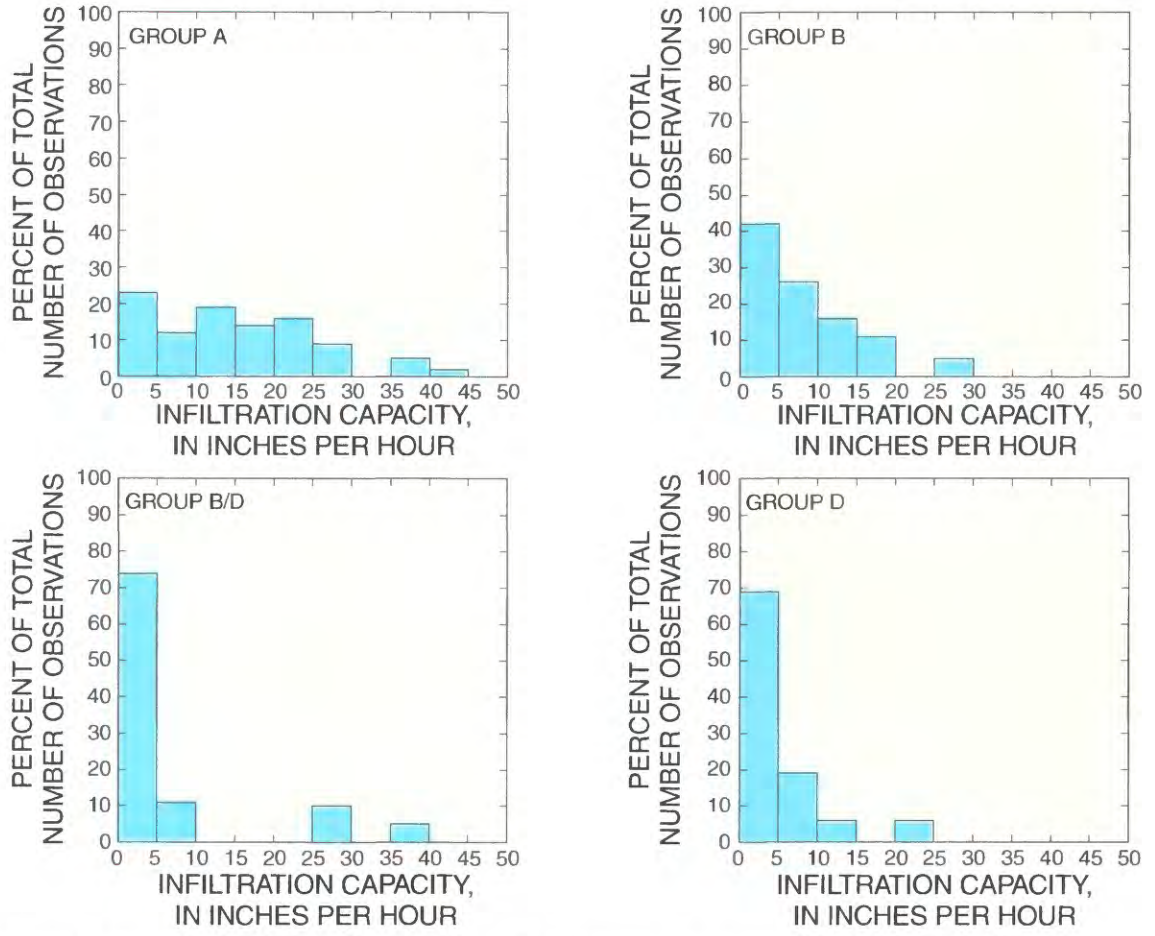

Figure 21. Distribution of infiltration capacities within hydrologic soil groups. Description of hydrologic soil groups (Natural Resources Conservation Service, 1996) is presented in table 2. If a soil is assigned to two hydrologic groups, the first letter is for drained areas and the second is for undrained areas.

laboratory permeability measurements. With the exception of agricultural areas, infiltration measurements in this study were conducted at sites where there was ground cover. The results suggest that ground cover causes the infiltration capacity normally associated with the soil to be significantly higher. The distribution of measured infiltration capacities within soil groups is shown in figure 21.

These distributions indicate that soil group A soils has a relatively uniform likelihood of infiltration capacities of 0 to 25 in/hr, with declining likelihood of infiltration capacities greater than 25 in/hr. In contrast, soil groups B, B/D, and D tend to have a substantially greater likelihood that the associated infiltration capacities will range from 0 to 5 in/hr. In practical terms, the precision of infiltration-capacity estimates based on soil groups is least for soil group A and greatest for soil groups B and D.

Because of the varying number of infiltrometer measurements between soil groups, the standard error of the mean infiltration capacity varies between soil groups. The standard error , $s_{\bar{x}}$, of each estimated mean, $\bar{x}$, was calculated using the relation:

$$s_{\bar{x}} = \left(\frac{s^2}{N}\right)^{1/2}, \qquad (4)$$

where s^2 is sample variance given by:

$$s^2 = \frac{1}{N-1}\sum_{1}^{N}(x_i - \bar{x})^2 , \qquad (5)$$

where N is the number of samples, x_i is an individual sample value, and $\bar{x}$ is the average of the sample values.

Results illustrating the mean, standard error of the mean, and standard deviation of the infiltration capacity for all hydrologic soil groups in the study area are shown in figure 22. As depicted, the standard error of the mean typically is 3 to 5 in/hr. The results also support the relative infiltration capacities expected for hydrologic soil groups because the mean infiltration capacity decreases with groups A, B, B/D, and D, as expected. Actual infiltration capacities, however, substantially exceed those suggested by the USDA for soils in the study area.

In addition to the hydrologic soil group, land use generally is assumed to further influence the infiltration capacity of soils. To investigate the influence of land use, the infiltration capacity as a function of land use within each hydrologic soil group was identified. The results indicate that the infiltration capacities associated with various land uses within any soil group are typically within one standard

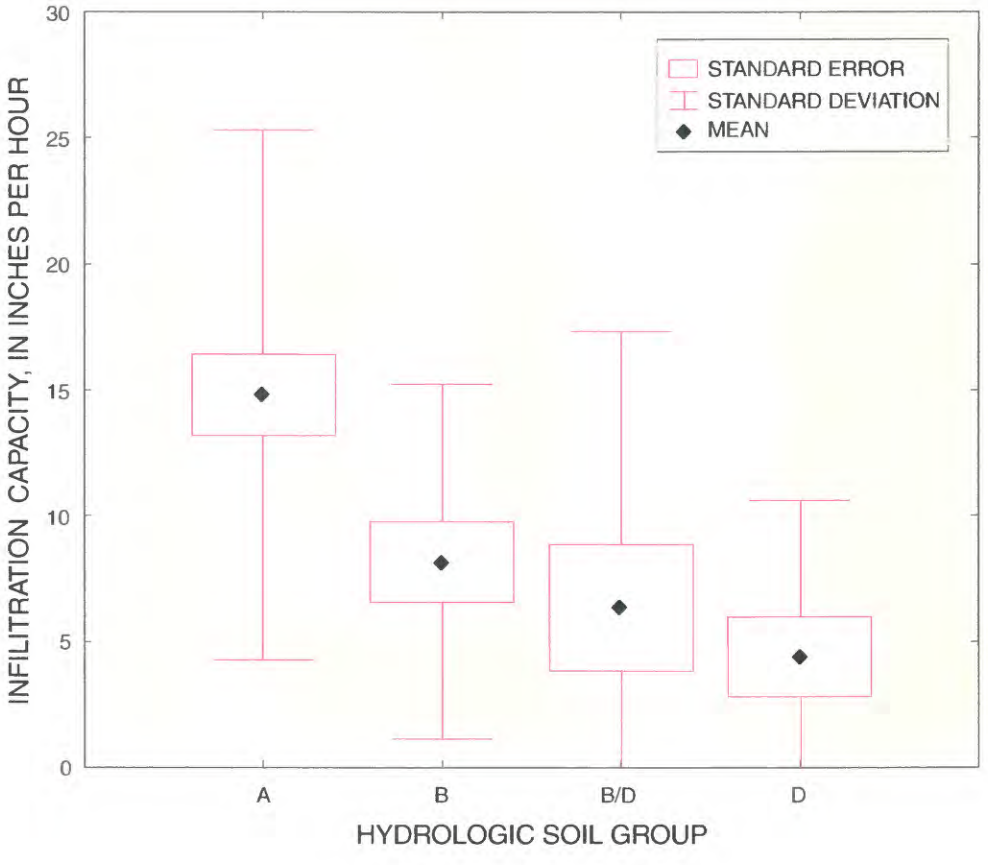

Figure 22. Infiltration capacity relative to hydrologic soil group. Description of hydrologic soil groups (Natural Resources Conservation Service, 1996) is presented in table 2. If a soil is assigned to two hydrologic groups, the first letter is for drained areas and the second is for undrained areas.

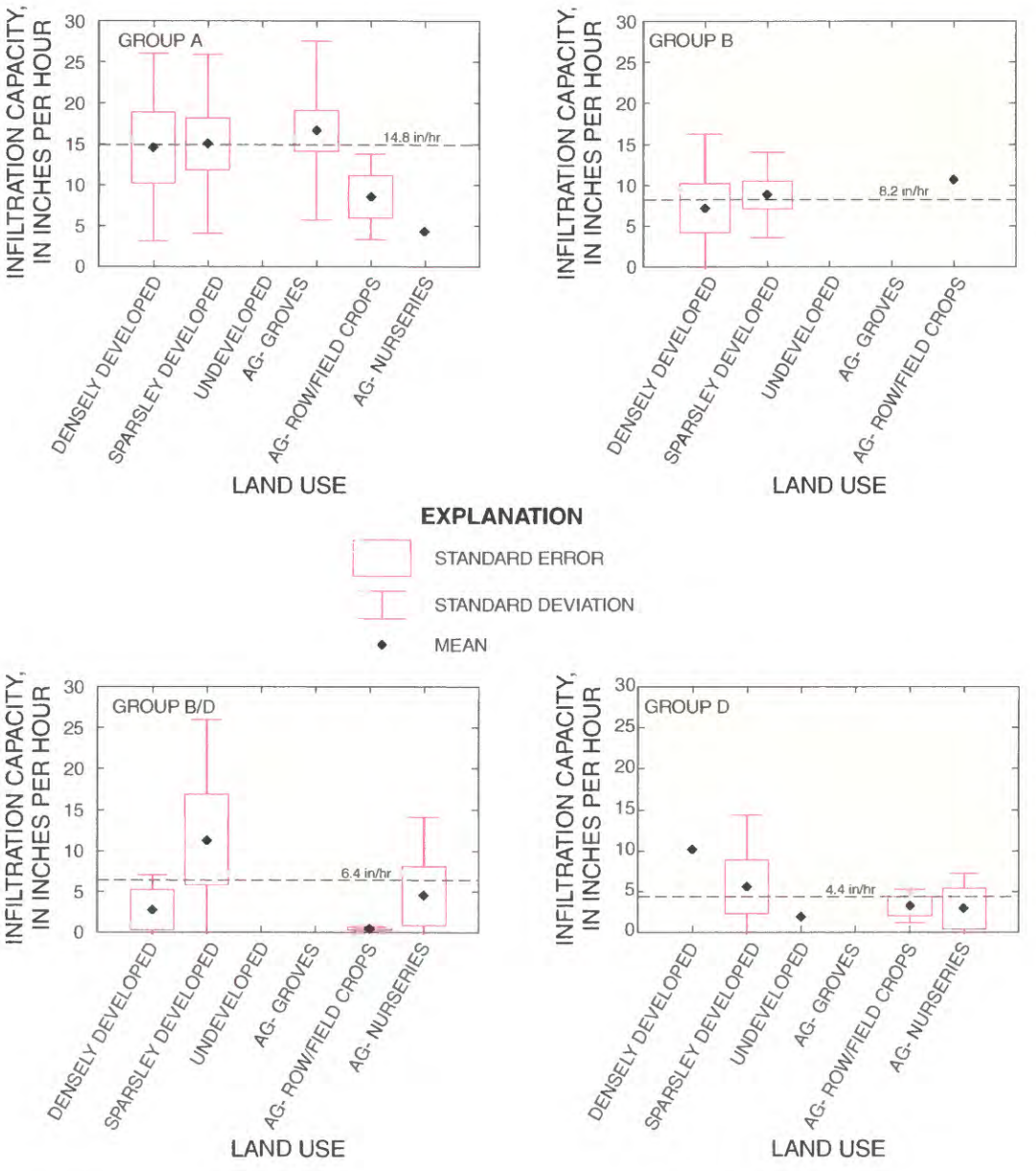

Figure 23. Infiltration capacity relative to land use. Description of hydrologic soil groups (Natural Resources Conservation Service, 1996) is presented in table 2. If a soil is assigned to two hydrologic groups, the first letter is for drained areas and the second is for undrained areas. AG is agriculture, and in/hr is inches per hour.

deviation of the mean infiltration capacity for the soil group (fig. 23). The infiltration capacity assigned to each soil group is relatively independent of land uses identified in this study, and the infiltration capacity is related primarily to the USDA assigned hydrologic soil group. Furthermore, multiple land use is associated with individual soil groups within the study area.

A histogram showing the relation between land use and hydrologic soil group (fig. 24) illustrates that no clear association exists between land use and hydrologic soil group, with multiple soil groups having a large presence within individual land uses. These data indicate that land use is not a reliable basis for estimating infiltration capacities that are primarily related to the hydrologic soil group.

Estimation of Infiltration Capacity from Soil Texture

Two soil-classification systems are used in the United States: (1) the USDA system, primarily used by soil scien-

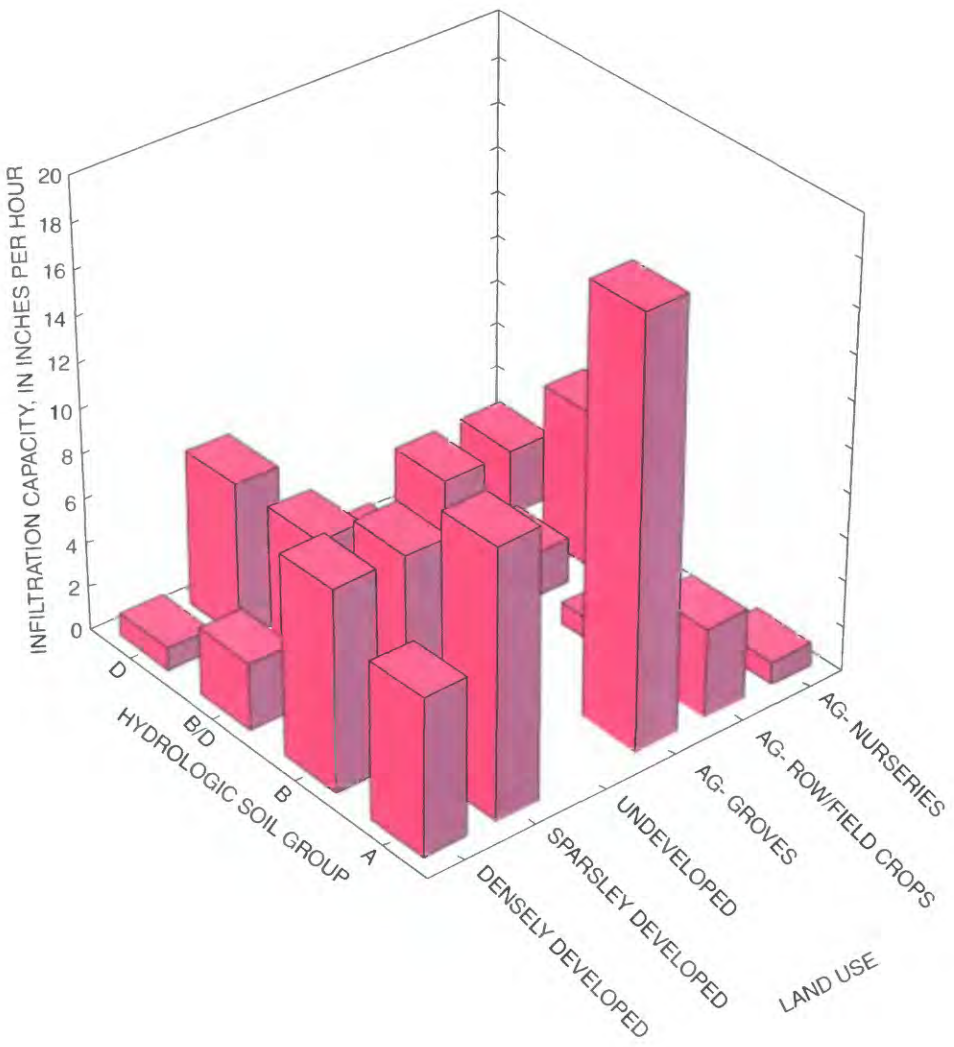

Figure 24. Land use relative to hydrologic soil group. Description of hydrologic soil groups (Natural Resources Conservation Service, 1996) is presented in table 2. If a soil is assigned to two hydrologic groups, the first letter is for drained areas and the second is for undrained areas. AG is agriculture.

tists, whereby soil is classified by the amount of sand-, silt-, or clay-sized particles (Soil Conservation Service, 1982); and (2) the Unified Soil Classification System (USCS), primarily used by engineers to describe the engineering properties of soils, whereby soil is characterized based on amounts of certain sizes of soil particles as well as the response of the soil to physical manipulation at varying water contents (American Society for Testing Materials, 1993). This report uses the USDA system.

In the USDA soil classification system, soil particles smaller than about 0.08 in. (2 mm) are divided into three soil texture groups: sand, silt, and clay; the percentage of each is used to define the textural class (Soil Conservation Service, 1982). In the USDA system, soil infiltration capacity is primarily determined by soil texture, with coarser materials commonly having higher conductivities (Burden and Sims, 1999). Other factors that influence infiltration capacities are soil structure, presence of macropores, condition of the soil surface, and the type of vegetation on the soil surface. Infiltration capacities are increased by lower bulk densities and higher porosities or by an increase in the number of macropores connecting to the soil surface.

Based on the USDA soil-texture classification, Meyer and others (1997) developed generic probability distributions for unsaturated and saturated-soil hydraulic parameters. These distributions are particularly useful for modeling the uncertainty in soil hydraulic properties when information about the soils at a site is limited to the soil texture.

In this study, soil samples were collected at most of the sites where double-ring infiltrometer tests were conducted, and these samples were sent to a commercial laboratory for USDA textural analyses. Using the results of these analyses (table 11), the relation between soil texture and the Horton asymptotic infiltration capacity (f_c) was developed (table 12).

Table 11. Analysis of double-ring infiltrometer tests and soil and land-use characteristics

[Description of hydrologic soil groups is given in table 2. If a soil is assigned to two hydrologic groups, the first letter is for drained areas and the second is for undrained areas. Land use: 1, densely developed; 2, sparsely developed; 4, undeveloped; 5 agriculture-groves; 6, agriculture-row/field crops; 7, agriculture-nurseries; --, no data available; ?, unknown]

Test No.	f_0, Initial infiltration rate (inches per hour)	f_c, Asymptotic infiltration rate (inches per hour)	k, Decay coefficient (minute^{-1})	Hydrologic soil group	Soil texture	Land use
1	19.0	5.9	0.30	A	Sandy loam	5
2	21.0	15.5	.13	A	Loamy sand	2
3	9.7	.3	.51	B/D	Loam	2
4	18.8	3.0	.19	D	Sandy loam	2
5	12.6	.7	.04	B/D	Silt loam	6
6	--	33.9	--	?	Sandy loam	2
7	11.0	.1	.30	D	Loam	5
8	7.2	1.9	.14	D	Loam	4
9	12.6	.8	.39	D	Silt loam	7
10	30.5	20.8	.08	A	Sandy loam	5
11	27.8	3.3	.77	D	Silty clay loam	6
12	--	24.7	--	D	Loamy sand	2
13	--	16.0	--	A	Sandy clay loam	6
14	6.7	.5	.25	A	Loam	2
15	13.6	7.5	.04	A	Sandy loam	5
16	--	36.1	--	A	Sandy loam	2
17	--	2.0	--	B	Loam	2
18	--	7.9	--	D	Sand	7
19	14.4	4.3	.56	A	Sandy loam	5
20	--	6.3	--	D	Sandy loam	2
21	20.0	5.3	.42	D	Loam	6
22	--	24.9	--	A	Loamy sand	2
23	4.4	.4	.18	D	Loam	2
24	21.1	8.7	.03	B	Sandy loam	2
25	93.4	4.1	.34	A	--	2
26	--	7.8	--	B/D	Loamy sand	1
27	--	28.7	--	A	--	2
28	--	13.1	--	A	--	2
29	13.3	4.9	.10	D	Loam	2
30	27.6	.1	.29	D	Loam	2
31	11.1	3.0	.31	B/D	Loam	2
32	--	9.6	--	B	--	2
33	11.1	1.3	.11	B/D	--	2
34	6.0	1.2	.13	B/D	Loam	2
35	93.2	10.7	1.31	A	--	2
36	--	16.4	--	B	--	2
37	--	10.7	--	B	--	6
38	30.3	3.5	.26	B	Loamy sand	2
39	12.8	1.7	.74	A	Clay loam	5

Table 11. Analysis of double-ring infiltrometer tests and soil and land-use characteristics--Continued

[Description of hydrologic soil groups is given in table 2. If a soil is assigned to two hydrologic groups, the first letter is for drained areas and the second is for undrained areas. Land use: 1, densely developed; 2, sparsely developed; 4, undeveloped; 5 agriculture-groves; 6. agriculture-row/field crops; 7. agriculture-nurseries; --, no data available; ?, unknown]

Test No.	f_o, Initial infiltration rate (inches per hour)	f_c, Asymptotic infiltration rate (inches per hour)	k, Decay coefficient (minute^{-1})	Hydrologic soil group	Soil texture	Land use
40	57.4	28.3	.06	B/D	Sandy loam	2
41	--	3.7	--	A	Sandy loam	6
42	22.3	12.8	.26	A	Loamy sand	2
43	--	.5	--	B/D	Clay	7
44	10.8	.3	.25	D	Sandy loam	2
45	8.3	.3	.28	B/D	Silty clay loam	6
46	40.3	9.8	.10	B/D	Sandy loam	2
47	--	21.2	--	A	Sandy loam	5
48	35.1	26.2	.05	A	Sandy loam	5
49	--	24.4	--	A	Sandy loam	5
50	4.7	.6	.31	B	Sandy loam	1
51	22.7	10.3	.19	A	Sandy loam	2
52	10.3	2.1	.62	A	Sandy loam	2
53	20.4	3.6	.57	B	Sandy loam	2
54	--	21.4	--	A	Sandy loam	2
55	--	16.3	--	B	Loamy sand	2
56	--	27.9	--	B	Sandy loam	1
57	24.1	9.6	.20	B	Sandy loam	2
58	96.4	35.7	1.12	B/D	Sandy loam/sandy-clay loam	2
59	--	1.1	--	B	Silty clay loam	1
60	24.3	1.5	.59	A	Silty clay loam	1
61	40.3	29.0	.16	A	--	1
62	16.9	10.3	.09	D	Sandy loam	1
63	30.3	14.0	.37	B	Sandy loam	1
64	22.1	10.0	.26	A	Loamy sand	1
65	--	.7	--	A	Sandy loam	1
66	31.4	10.1	.25	B	Sandy loam	2
67	8.2	23.2	.55	A	Sandy loam	1
68	12.3	1.9	.16	B	Sandy loam	1
69	62.1	12.4	2.48	A	Loamy sand	1
70	13.4	2.2	.29	B	Sandy loam	1
71	18.1	.3	.46	B/D	Sandy loam	1
72	18.9	9.4	.23	?	Loamy sand	1
73	37.8	26.2	0.09	B/D	Silty clay loam	7
74	14.7	.3	.48	B/D	Clay loam	7
75	--	.9	--	B/D	Silty clay loam	7
76	4.2	1.2	.43	D	Silty clay loam	6
77	--	1.0	--	B/D	Silty clay loam	7
78	--	2.8	--	B/D	Silty clay loam	7
79	49.3	25.3	.22	A	Sandy loam/sandy-clay loam	1
80	16.9	.0	.42	B/D	Silty clay loam	7

Table 11. Analysis of double-ring infiltrometer tests and soil and land-use characteristics--Continued

[Description of hydrologic soil groups is given in table 2. If a soil is assigned to two hydrologic groups, the first letter is for drained areas and the second is for undrained areas. Land use: 1, densely developed; 2, sparsely developed; 4, undeveloped; 5 agriculture-groves; 6, agriculture-row/field crops; 7, agriculture-nurseries; --, no data available; ?, unknown]

Test No.	f_o, Initial infiltration rate (inches per hour)	f_c, Asymptotic infiltration rate (inches per hour)	k, Decay coefficient (minute^{-1})	Hydrologic soil group	Soil texture	Land use
81	10.0	.4	.32	B/D	Loam	1
82	26.7	.5	.53	B	Sandy loam	1
83	1.3	7.4	.28	A	Sandy clay loam	6
84	85.4	41.6	.40	A	Sandy loam (sandy clay loam)	5
85	17.3	8.6	.03	B	Sandy loam	1
86	70.4	8.4	.72	B	Loamy sand	1
87	12.9	7.4	.06	A	Sandyloam	6
88	35.5	19.2	.03	A	Sandy loam	5
89	28.2	3.1	.02	A	Sandy loam	5
90	19.6	11.4	.15	A	Sandy loam	5
91	20.7	10.7	.03	A	Sandy loam	5
92	10.2	5.8	.21	A	Loamy sand	5
93	72.0	35.3	.21	A	Sandy loam	5
94	36.1	19.3	.02	A	Sandy loam	5
95	25.6	18.4	.06	A	Sandy loam	5

Sandy loam was by far the most frequently sampled soil texture, with loamy sand, loam, and silty clay loam having substantially less representation, but having at least 10 measurements in each textural class (table 12). There were relatively few samples of clay loam, silt loam, sandy clay loam, sand, and clay. The mean and standard deviations of the infiltration capacities within each textural class also were determined at the test sites (table 12). Few measurements were taken in several textural classes, and the data for these classes should be considered statistically unreliable. The distribution of infiltration capacities by soil texture for cases having at least 10 measurements is shown in figure 25. These results indicate that loam and silty clay loam have the greatest likelihood that the infiltration capacity ranges from 1 to 5 in/hr, with higher infiltration capacities more likely for sandy loam and loamy sand. In the cases of loam and silty clay loam, the expected infiltration capacity can be stated with much more certainty.

To account for the relatively few number of samples in several textural classes, the standard error of the mean infiltration capacity was calculated for each soil texture. The results along with the standard deviation of the infiltration-capacity measurements for all soil textures in the study area are shown in figure 26. The standard error and standard deviation are not shown in cases having only one data point. A clear relation

Table 12. Distribution of soil texture and infiltration capacities at test sites in the study area

[-- Standard deviation not calculated due to insufficient data]

Soil texture	Number of measurements	f_c, Infiltration capacity (inches per hour)	
		Mean	Standard deviation
Sandy loam	42	12.2	10.1
Loamy sand	13	13.4	6.9
Loam	12	1.7	1.8
Silty clay loam	10	3.8	7.9
Clay loam	3	.7	.9
Silt loam	2	.7	.1
Sandy clay loam	2	11.7	6.1
Sand	1	7.9	--
Clay	1	.5	--

is evident between soil texture and infiltration capacity, with coarse-textured soils (those with a significant sand fraction) having greater infiltration capacities than fine-textured soils (those with a significant silt/clay component). These results indicate that coarse-textured soils in the study area have infiltration capacities of about 13 in/hr, with much smaller infiltration capacities associated with the fine-textured soils.

Land use is frequently cited as an independent parameter for estimating the infiltration capacity of soils. The distribution of infiltration capacity for each land use within four textural classes is shown in figure 27. These classes had at least 10 field measurements of infiltration capacity; the mean, standard error of the mean, and standard deviation of the infiltration capacity are illustrated for each land use. Given the relatively few number of measurements, it is difficult to make any firm conclusions as to the role of land use in determining infiltration capacity. Overall, the results indicate that infiltration capacity within a textural class is not greatly influenced by land use.

Particular weight in this analysis should be given to the case of sandy loam, where there were 42 measurements of infiltration capacity. To interpret these data, it can reasonably be asserted that if the mean infiltration capacity for all sandy loam soils (12.2 in/hr) is within one standard deviation of the mean infiltration capacity for any given land use within that textural class, then land use is not a significant variable in determining the infiltration capacity. Based on this criterion, the mean infiltration capacity is not demonstrably influenced by land use, with the single exception of agricultural use for row/field crops. Results of this analysis indicate that the land-use classes are not significant parameters in determining the infiltration capacity of soils in the study area.

To further investigate the role of land use in infiltration capacity, the relation between land use and soil texture is shown in figure 28. These results give a clear indication that densely developed land tends to have soils with much coarser texture than agricultural land used for nurseries. Agricultural lands containing row and field crops have soils with inter-

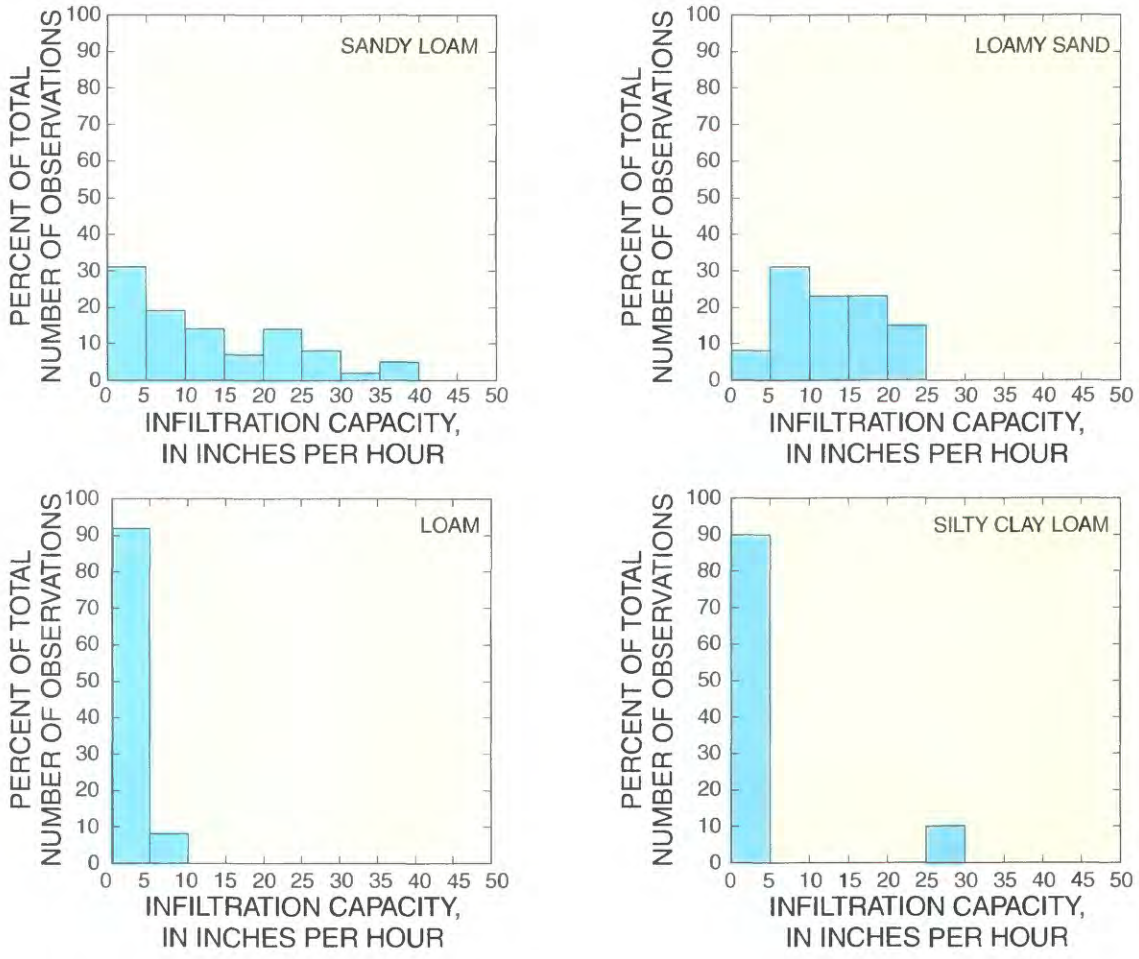

Figure 25. Distribution of infiltration capacities within textural classes.

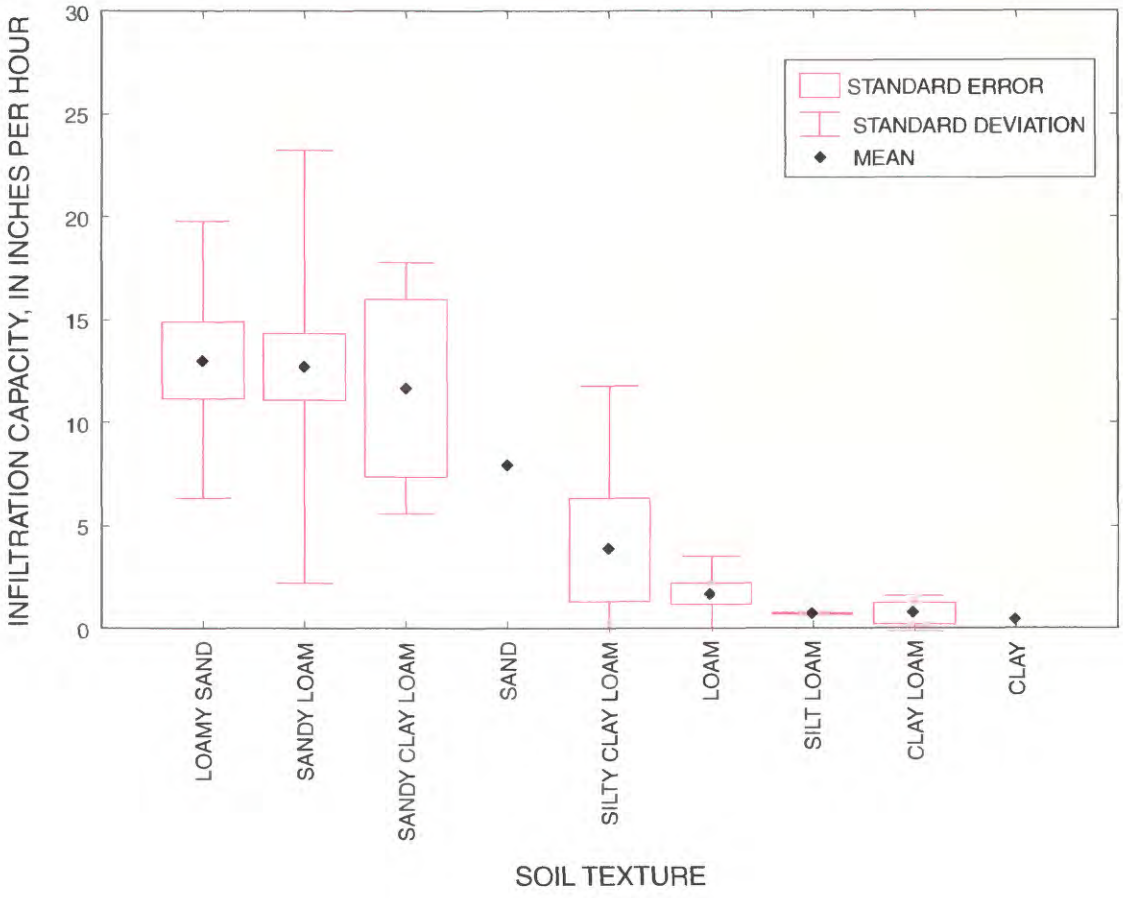

Figure 26. Infiltration capacity relative to soil texture.

mediate soil textures. Clearly, sandy loam is the predominant soil type in densely developed areas, with silty clay loam the predominant soil texture in agricultural areas.

Based on the data in figure 28, it is reasonable to expect lower runoff rates in pervious areas of densely developed land than in land used for nursery operations because higher infiltration capacities are associated with densely developed land compared with land used for nursery operations. Furthermore, the apparent relation between land use and soil texture indicates that using soil texture as a sole basis for estimating infiltration capacity may be justified because the soil texture also accounts for the associated land use. If soil texture is used as a basis for estimating the infiltration capacity of an area, then figure 27 indicates the validity of using this relation.

Probability distributions and parameter values of saturated hydraulic conductivity (equal to the infiltration capacity) that are commonly recommended for soils with various USDA textures are given in table 13 (Meyer and others, 1997). When these data are compared to the data in table 12 and figure 26, infiltration capacities measured during this study appear to be substantially higher than expected based on the results reported in table 13. The reason for this discrepancy might be that the infiltration capacities reported in table 13

Table 13. Saturated hydraulic conductivities of various soils

[Values are in inches per hour; --, no data]

Soil texture	Meyer and others (1997)			Carsel and Parrish (1988)	Rawls and Brakensiek (1983)
	Distribution	Mean	Standard deviation	Typical value	
Sand	Beta	11.6	6.2	1.2	9.3
Loamy sand	Beta	5.7	4.5	.59	2.3
Sandy loam	Lognormal	1.7	1.9	.17	.86
Sandy clay loam	Lognormal	.46	.85	.51	.11
Loam	Lognormal	.41	.70	.39	.51
Silt loam	Lognormal	.13	.32	.18	.27
Silt	Lognormal	.07	.04	.10	--
Clay loam	Lognormal	.14	.36	.10	.08
Silty clay loam	Lognormal	.02	.05	.03	.08
Sandy clay	Lognormal	.05	.21	.05	.05
Silty clay	Lognormal	<.01	<.01	.02	.04
Clay	Lognormal	.05	.15	.16	.02

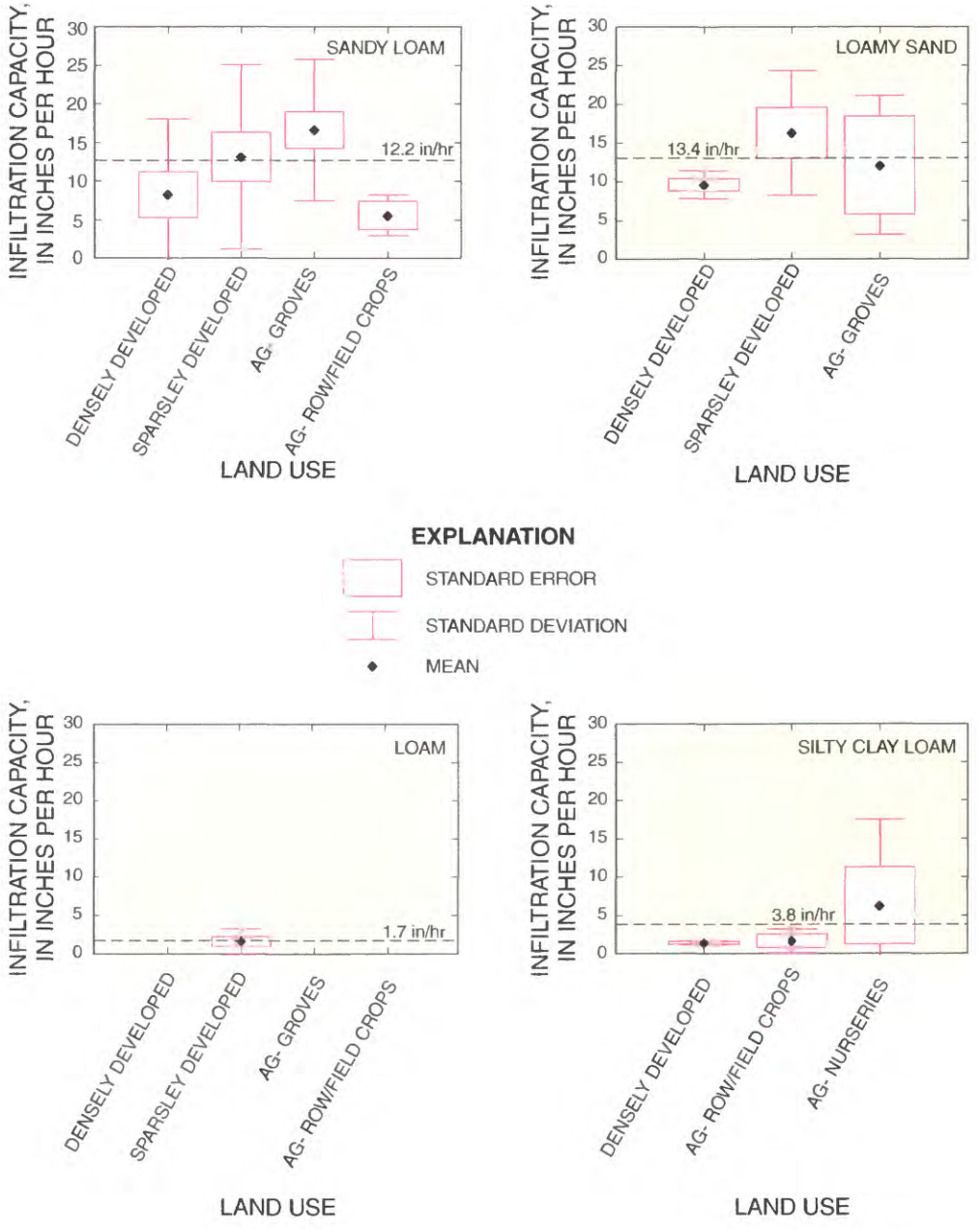

Figure 27. Distribution of infiltration capacity for land use within selected textural classes. AG is agriculture, and in/hr is inches per hour.

were derived mostly from laboratory measurements rather than field measurements that were used in this study. Furthermore, conventional relations between soil texture and infiltration capacity typically assume bare-soil conditions, and the presence of surface vegetation (such as grass) typically tends to increase the infiltration capacity for a given soil texture.

Infiltration capacities found in this study are consistent with those reported by Pitt and others (1999), who found mean infiltration capacities of 15 in/hr for uncompacted sandy soils in urban areas of Birmingham and Mobile, Alabama. Pitt and others (1999) also noted that measured infiltration capacities were higher for individual soil textures than expected from

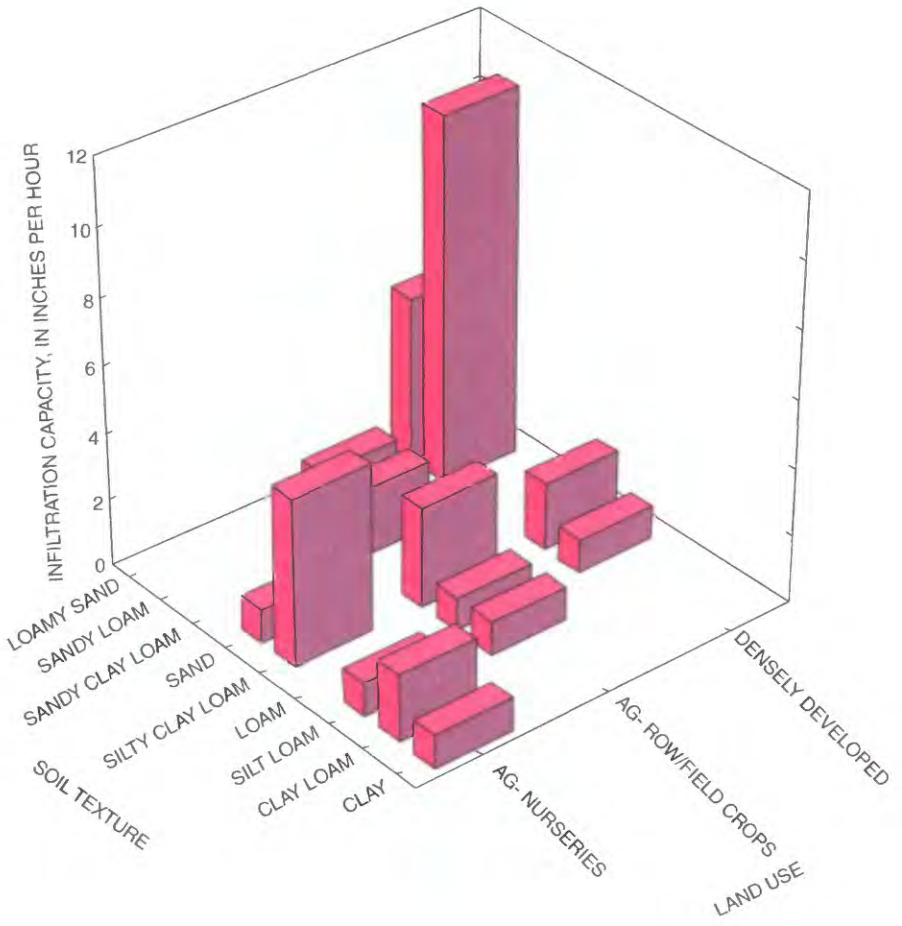

Figure 28. Relation between soil texture, land use, and infiltration capacity.

published literature, and compaction was a major factor affecting the infiltration capacity of some urban soils. An important fact is that textural measures in this study do not account for the amount of organic matter; Rawls (1983) reported that increasing the organic matter of the soil lowers the bulk density, increases porosity, and hence increases infiltration. Additionally, one-dimensional (vertical) flow is not entirely simulated by double-ring infiltrometers; there is always some lateral spreading, and as time proceeds, deviations from one-dimensional flow are to be expected (Smettem and Smith, 2002). Deviations from one-dimensional flow will cause overestimates of the infiltration capacity.

Infiltration capacities measured in this study are consistent with the typical values of the Horton parameters for bare agricultural land where f_c = 0.24 to 8.7 in/hr, and typical values of the Horton parameters for turfed agricultural land where f_c = 0.79 to 11 in/hr. Although too few measures are available in this study for a comprehensive analysis of the probability distribution of infiltration capacities within individual textural classes, sample measurements of soil-saturated hydraulic conductivities within textural classes consistently have been found to be significantly variable, and the lognormal distribution is commonly a good description of the data from such sampling (Nielsen and others, 1973; Viera and others, 1981).

The importance of soil infiltration in the rainfall-runoff process can be inferred from the distribution of infiltration capacities measured in the study area (fig. 29). These results demonstrate that the most frequently measured infiltration capacities ranged from 0 to1 in/hr (19 percent). About 40 percent of the measured infiltration capacities were less than 4 in/hr. Additionally, all of the rainfall intensities during the 7-year period of record (1995-2002) that were analyzed for this study ranged from 0 to 4 in/hr. Because the infiltration capacity test sites were relatively uniformly distributed throughout the study area, and 40 percent were less than 4 in/hr, one can conclude that most of the area has a sufficiently high infiltration capacity to absorb all measured incident rainfall during the 7-year period, the amount of runoff is limited, and most rainfall is either contributing to groundwater recharge, or producing runoff by a saturation-excess

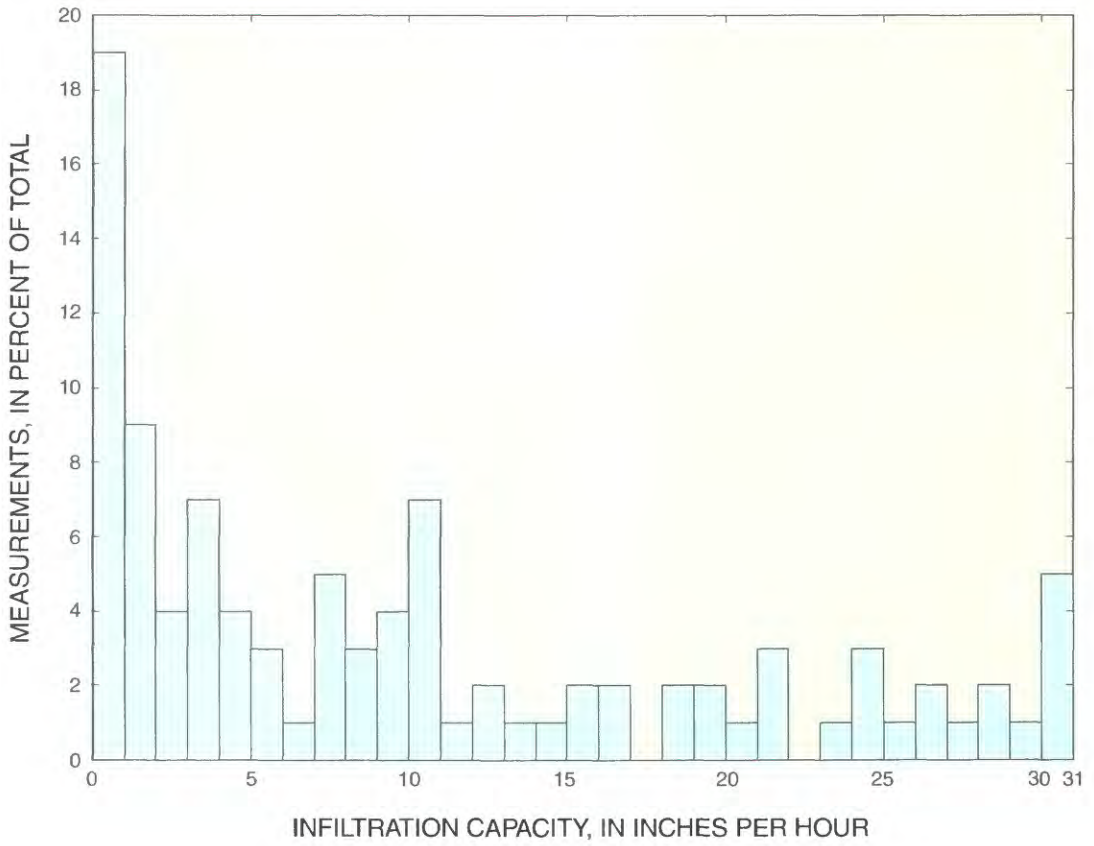

Figure 29. Distribution of infiltration capacity in the study area.

(no Hortonian) mechanism. An average intensity of 4 in/hr during a 1-hour interval has a return period of about 25 years, also giving further indication that surface runoff from most of the pervious area by a Hortonian mechanism may be a relatively rare occurrence. The results of this infiltration study can be contrasted to the relation between surface runoff, land slope, and infiltration capacity proposed by the U.S. Department of Agriculture (2001). These results indicate that for land slopes of less than 1 percent (typical of southern Florida), infiltration capacities of less than 0.2 in/hr are required to generate a substantial amount of runoff from a catchment area.

Other Infiltration Characteristics

Previous sections of this report address the estimation of the infiltration capacity of soils in the study area, with the objective of developing generalized estimation approaches that can be applied in other areas of southern Florida. A functional relation can be extracted between the hydrologic soil group and infiltration capacity, as well as soil texture and infiltration capacity. Both relations lead to infiltration-capacity estimates with about the same degree of precision, and in cases where USDA soils maps do not assign a hydrologic soil group, then estimation of infiltration capacity from a soil textural analysis may be the next best alternative. The relation between the hydrologic soil group and soil texture is shown in figure 30. No clear relation is evident between the soil texture and hydrologic soil group, with sandy loam being the predominant texture in soil groups A and B, silty clay loam being the predominant texture in soil group B/D, and loam being the predominant texture in soil group D. This ambiguity with respect to soil groups A and B having the same predominant texture indicates that relating the infiltration capacity to texture may be preferable. More data are needed to draw firm conclusions.

In accordance with the Horton model, the infiltration capacity, f_c, is the (asymptotic) minimum infiltration rate, which commonly is considered equal to the saturated hydraulic conductivity of the soil. Other parameters of the Horton model are the initial infiltration rate, f_o, and the decay rate, k. As previously described, curves were fitted to the double-ring infiltrometer data to estimate both f_o and k. The statistics of the estimated values of f_o by hydrologic soil group and soil texture

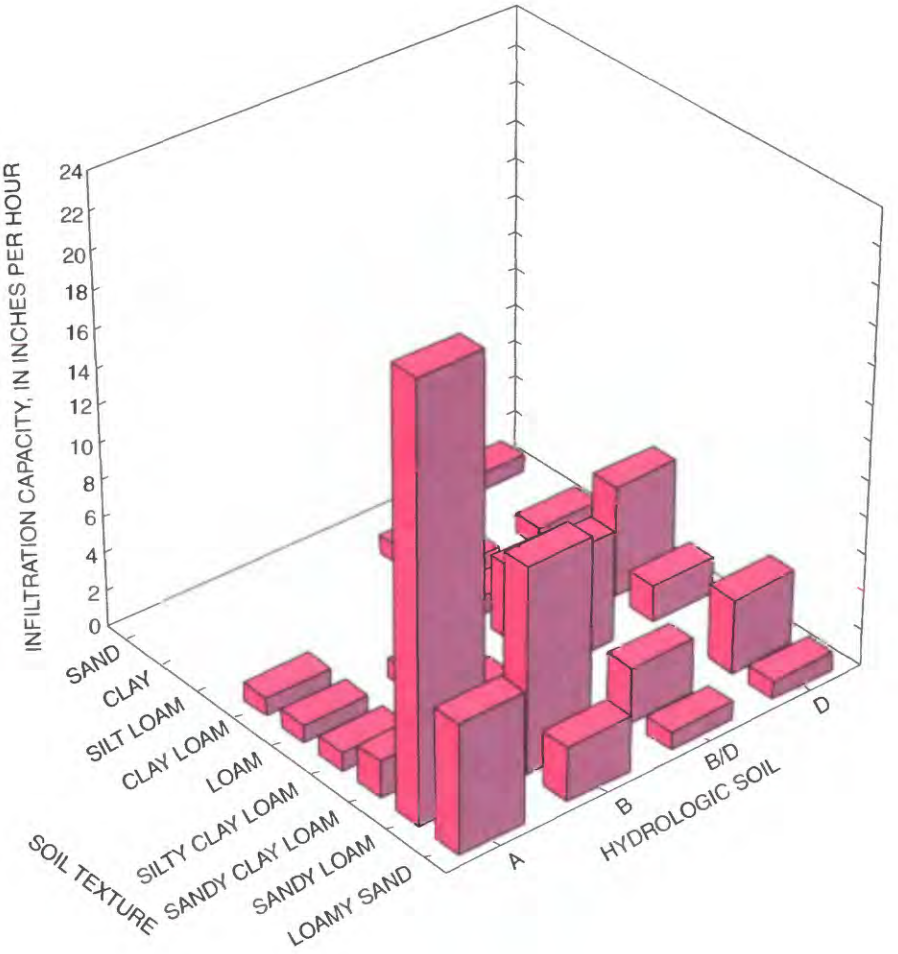

Figure 30. Relation between soil texture, hydrologic soil group, and infiltration capacity. Description of hydrologic soil groups (Natural Resources Conservation Service, 1996) is presented in table 2. If a soil is assigned to two hydrologic groups, the first letter is for drained areas and the second is for undrained areas.

are presented in table 14. The mean initial infiltration rate was highest for soil group A, and decreased with soil groups B, B/D, and D. Soil groups A and D had a mean initial infiltration rate of 31.1 and 13.7 in/hr, respectively, which can be attributed directly to the increased drainage capacity of soil group A relative to soil group D. Similar results also are evident in the relation between initial infiltration capacity and soil texture. The mean initial infiltration capacity was highest for loamy sand, and decreased with sandy loam, silty clay loam, and loam. Loamy sand soils had a mean initial infiltration capacity of 32.3 in/hr, whereas loam soils had a mean initial infiltration capacity of 11.6 in/hr. This trend is the same as that which exists for the asymptotic infiltration capacity relative to soil textures.

Values of the decay factor in the Horton model, k, were estimated for the double-ring infiltrometer measurements by hydrologic soil group and soil texture (table 15). Considering the relation between the soil hydrologic group and the mean decay factor, it is apparent that the decay factor is insensitive to the soil group, with mean decay factors contained in the relatively narrow range of 0.31 to 0.34 minute^{-1}. This result is supported by the literature on k values discussed earlier. The data obtained in this study indicate a decay time scale ($1/k$)

Table 14. Initial infiltration capacity in the Horton model by hydrologic soil group and soil texture

[Description of hydrologic soil groups (Natural Resources Conservation Service, 1996) is presented in table 2. If soil is assigned to two hydrologic soil groups, the first letter is for drained areas and the second is for undrained areas]

Soil group/texture	Number of measurements	f_0, Infiltration capacity (inches per hour)			
		Mean	Minimum	Maximum	Standard deviation
Soil Group					
A	33	31.1	1.3	93.4	24.5
B	12	25.2	4.7	70.4	16.4
B/D	14	25.0	6.0	96.4	25.4
D	13	13.7	2.8	27.8	8.3
Soil Texture					
Loamy sand	9	32.3	10.2	70.4	20.4
Sandy loam	33	24.4	4.7	71.9	13.9
Silty clay loam	6	19.9	4.2	37.8	12.6
Loam	11	11.6	4.4	27.6	6.8
All other soils	72	25.8	1.3	96.4	22.0

Table 15. Decay factor in the Horton model by hydrologic soil group and soil texture

[Description of hydrologic soil groups (Natural Resources Conservation Service, 1996) is presented in table 2. If soil is assigned to two hydrologic groups, the first letter is for drained areas and the second is for undrained areas]

Hydrologic soil group and soil texture	Number of measurements	k, Decay factor (per minute)			
		Mean	Minimum	Maximum	Standard deviation
Hydrologic Soil Group					
A	33	0.34	0.02	2.48	0.47
B	12	.31	.03	.72	.21
B/D	14	.32	.04	1.12	.29
D	13	.31	.08	.77	.19
Soil Texture					
Loamy sand	9	.52	.13	2.48	.75
Sandy loam	33	.21	.02	.62	.19
Silty clay loam	6	.43	.09	.77	.23
Loam	11	.27	.10	.51	.13
All other soils	72	.32	.02	2.48	.36

of 3 minutes, which typically indicates a very rapid decrease of infiltration capacity from an initial value to the asymptotic infiltration capacity. The range of decay rates is wider when soil textures are considered, ranging between 0.21 minute^{-1} for sandy loam and 0.52 minute^{-1} for loamy sand. This range represents decay time scales of between 2 and 5 minutes, which still represents a relatively rapid decrease from the initial infiltration capacity. All of these results collectively indicate that the decay rate does not vary much between individual soil groups and textures, thus using an average decay rate, k, of 0.32 minute^{-1} in the Horton infiltration model is reasonable. This rate of decay is sufficiently rapid in that an alternative model, which assumes that the infiltration capacity remains constant and independent of time, may be a valid approximation for many storm events of longer duration.

Direct Ground-Water Recharge

Direct ground-water recharge is defined as rainwater that percolates through the unsaturated zone and enters the saturated zone. In contrast to direct recharge, indirect recharge includes water that enters the saturated zone by other means, such as canal leakage. In this report, direct recharge is referred to simply as recharge, and canal leakage is treated as a separate process. Well-hydrograph analysis relates changes in water-table elevation to changes in the amount of water stored in the aquifer (Rasmussen and Andreason, 1959). Recharge, $R(t_j)$, can be expressed as:

$$R(t_j) = S_y \times \Delta H(t_j), \qquad (6)$$

where t_j is the j^{th} time step, $R(t_j)$ is the recharge occurring between times t_{j-1} and t_j, S_y is the specific yield of the surficial aquifer, and $\Delta H(t_j)$ is the water-table rise attributed to the recharge.

Delin and others (2000) suggested that $\Delta H(t_j)$ be estimated by visually extrapolating the hydrograph recession preceding the water-level rise to the time when the water-level peak occurs. Therefore, $\Delta H(t_j)$ equals the difference between the projected water-level decline and the peak of the hydrograph at the time of the peak water-level rise. The specific yield, S_y, is the difference between the field capacity (or specific retention) and the porosity.

The method of well hydrograph analysis is simple to apply, but is limited by its inability to detect slow or constant recharge that occurs in the absence of relatively rapid changes in the water table, and by the following assumptions (Delin and others, 2000): (1) recharge is the only process causing the water table to rise; (2) recharge is represented in the measured water-level rises; and (3) the specific yield is constant. There is usually a minimum precipitation event below which no recharge occurs or none can be detected. In the study reported by Delin and others (2000), no recharge was detected for precipitation events smaller than 0.6 in.

Bierkens and others (2001) developed and applied a time-series model relating water-table depth to rainfall excess. This model was applied successfully in an area in the Netherlands where the water table was 3 to 6 ft below land surface. The form of the model is given by:

$$H_t - c = a\{H_{t-1} - c\} + bP_t + \varepsilon_t, \qquad (7)$$

where H_t is the water-table depth; P_t is the effective precipitation between $t-1$ and t; a, b, and c are constants; and ε_t is a discrete white noise process. Daily time steps were used, and the effective rainfall was defined as the daily rainfall minus evapotranspiration.

In this study, the rainfall-recharge relation was investigated using water-table elevation measurements at wells G-614, G-1183, G-1363, G-1486, and S-196A (fig. 9). The latitude and longitude, depths, and land-surface elevations at these wells are given in table 16. Because of the shallow water table and porous soils in the study area, a close relation exists between rainfall and water-table elevations in the study area. Typical relations between measured rainfall and water-table elevations at selected sites in the study area are shown in figure 31.

Rainfall-Recharge Analysis Based on Existing Hourly Data

Five monitoring wells were equipped with recorders that measured the water-table elevations at hourly intervals, and synoptic hourly rainfall measurements were available at several gaging stations in the study area. In choosing the nearest gaging station to a well for synoptic rainfall-recharge analysis,

rainfall data from station S-167 was chosen for wells G-1486, S-196A, and G-1363; station S-165 was chosen for well G-614; and station HOMES-FS was chosen for well G-1183 (fig. 9). Hourly water-table fluctuations recorded at the five wells were combined with hourly rainfall measurements at the nearest gaging stations to develop the rainfall-recharge relation.

A typical relation between rainfall and change in water-table elevation for a single storm at well G-1486 is shown in figure 32. Prior to most storms, there is a steady decline in the water table that usually is associated with canal drainage and evaporation. This decline in the water table during the initial part of the storm must be added to the increase in the water table to estimate the recharge resulting from the rainfall event.

Table 16. Water-table elevation measurements and other characteristics for selected wells in the study area

[Well locations are shown in figure 9. Acronym or abbreviation: NGVD 1929, National Geodetic Vertical Datum of 1929; DWT, Annual average depth to water table; ddmmss, degrees, minutes, seconds]

Well number	Latitude (ddmmss)	Longitude (ddmmss)	Depth (feet)	Diameter (inches)	Land-surface elevation (feet, NGVD 1929)	DWT (feet)
G-614	25°32′58″	80°26′43″	20	6	11.10	6.75
G-1183	25°29′18″	80°23′42″	47	9	6.17	4.25
G-1363	25°32′33″	80°30′10″	33	6	9.78	5.75
G-1486	25°30′12″	80°26′14″	32	6	10.39	7.75
S-196A	25°30′29″	80°29′56″	20	8	10.33	7.75

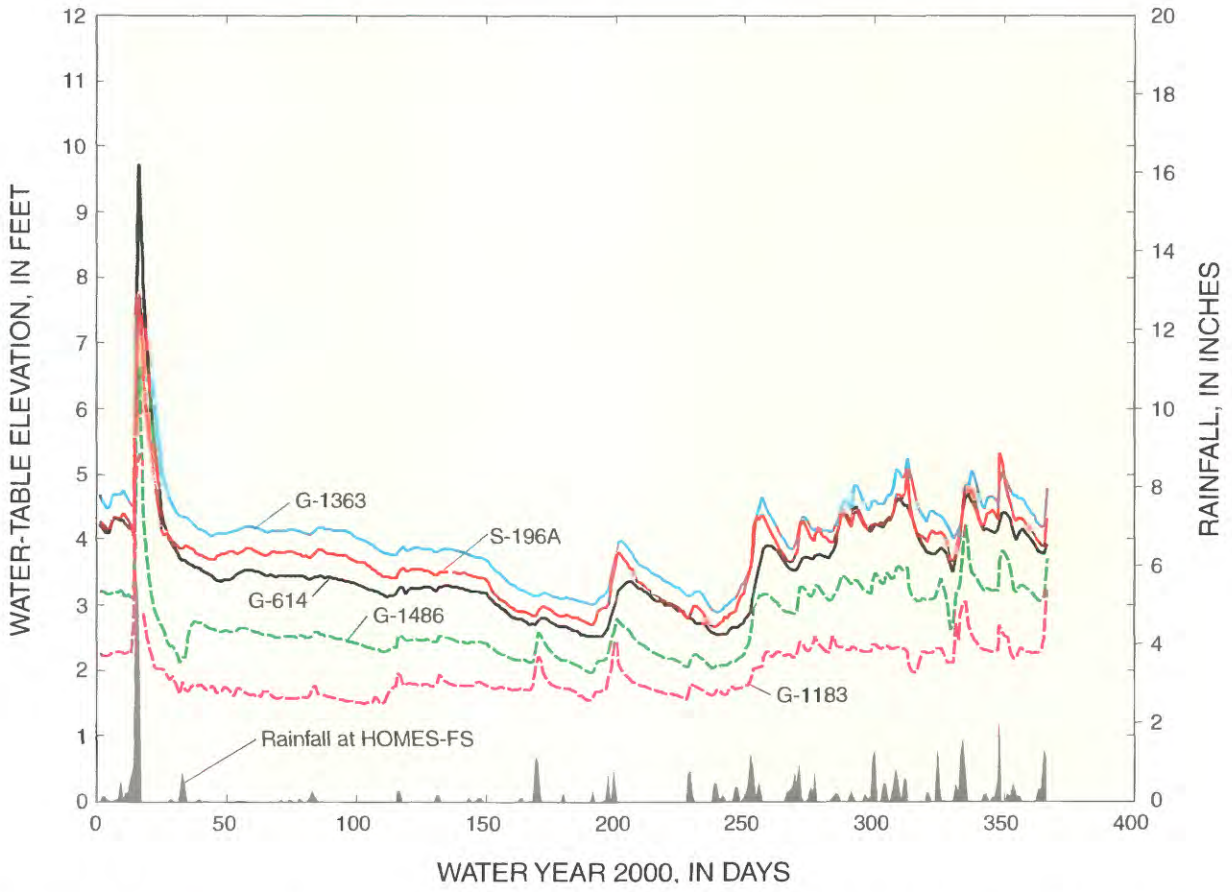

Figure 31. Relation between water-table elevations and rainfall at selected sites in the study area. Site locations are shown in figure 9. Water year 2000 begins October 1, 1999, and ends September 30, 2000.

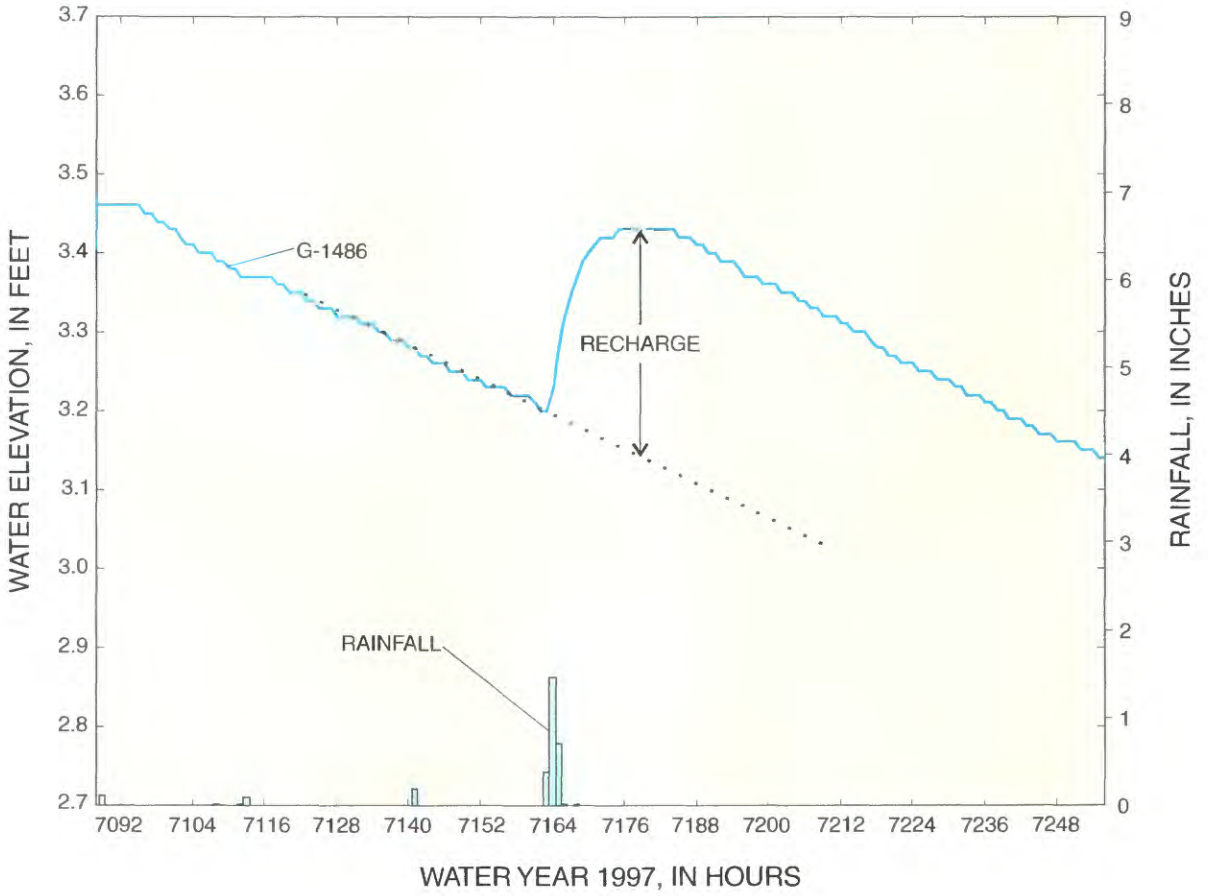

Figure 32. Relation between rainfall and recharge at well G-1486. Water year 1997 begins October 1, 1996, and ends September 30, 1997.

Direct ground-water recharge for an area can be expected to vary in space, and because of the high soil infiltration capacity and aquifer hydraulic conductivity, the recharge measured at any individual site may be related to the average rainfall and average recharge for an extended area. In all analyses that utilize point measurements of rainfall, the areal-averaged rainfall for individual storm events generally is less than the rainfall measured at single locations—a factor that must be considered in estimating the average rainfall-recharge relation over large areas. An areal reduction factor commonly cited in textbooks was developed by the National Weather Service (1958) based on major storms recorded at points in seven dense networks in the United States mainly east of the Mississippi River, with records ranging from 7 to 15 years. Storm durations ranged from 30 minutes to 24 hours, and the plots showed that the areal reduction factors for areas from 100 to 400 mi^2. The study area covers about 106.4 mi^2, and an areal reduction factor of about 75 percent is expected for 1-hour storms, with a reduction factor of about 95 percent expected for 24-hour storms. Significant deviations from the empirical rainfall reduction factor relation can be expected depending on local geographic and climate conditions (De Michele and others, 2001).

The relation between rainfall and direct recharge of an aquifer is greatly influenced by the amount of storage available both above and below ground. In pervious areas, above-ground storage consists primarily of the interception capacity of vegetation, and below-ground storage is associated with the moisture-holding capacity of the soil, which generally is limited by the field capacity. In cases where antecedent rainfall events have filled all available storage, subsequent rainfall events in pervious areas will contribute the entire rainfall to ground-water recharge. On the other hand, if antecedent conditions consist of an extended dry period, the initial rainfall will be used to fill the above- and below-ground storage capacity, and once filled, excess rainfall will contribute to direct recharge of the ground water. In the intermediate case where available storage is partially filled by antecedent rainfall, the initial rainfall in a storm event is used to fill the available capacity, and excess rainfall contributes to recharge. This rainfall-recharge model is illustrated in figure 33. For saturated initial conditions, all rainfall contributes to recharge and the relation between the rise in water table, y, and the rainfall amount, x, is given by:

$$y = \frac{x}{S_y} , \qquad (8)$$

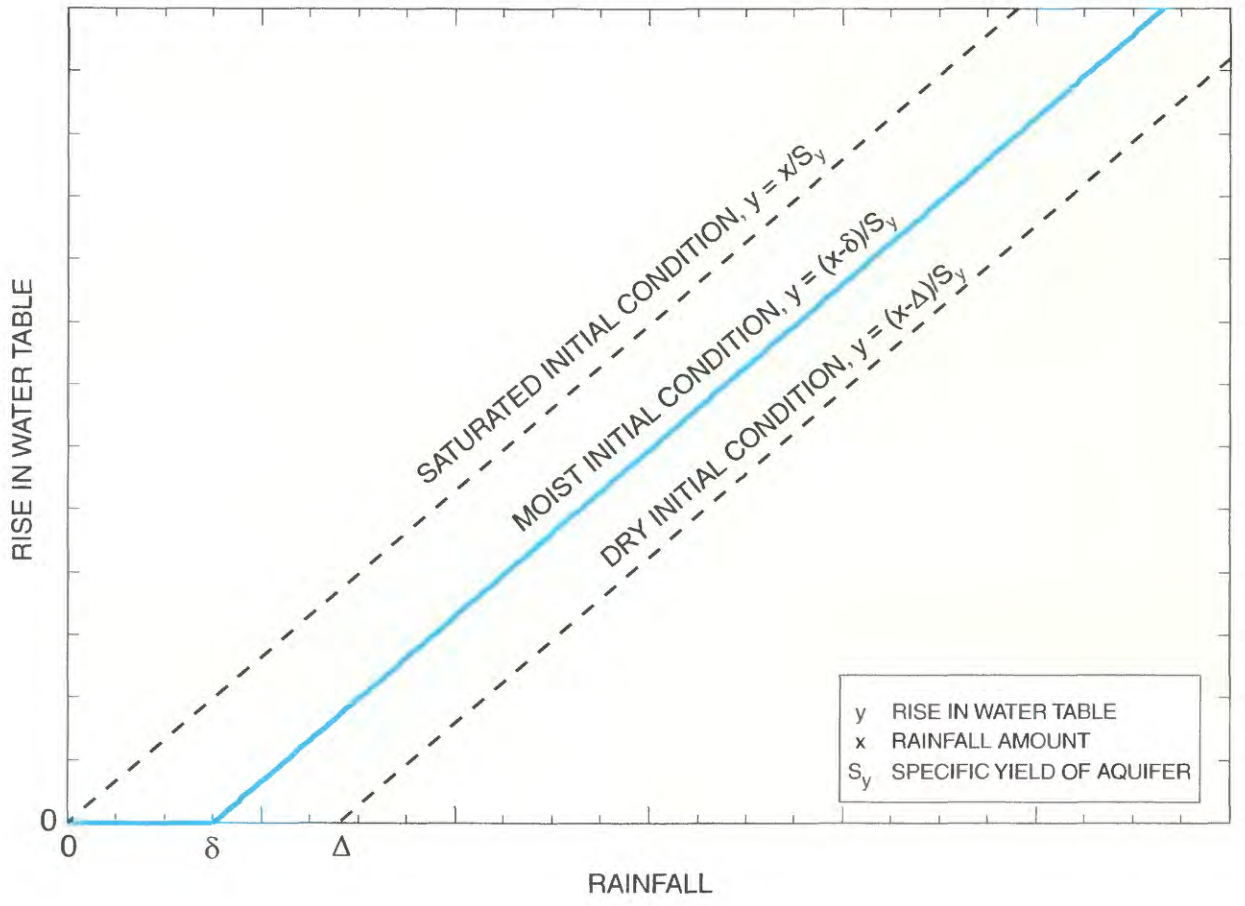

Figure 33. Rainfall-recharge model.

where S_y is the specific yield of the aquifer. In the case of dry initial conditions, the rainfall must exceed the storage capacity, Δ, for any recharge to occur. For rainfall amounts greater than Δ, the relation between water-table rise, y, and rainfall, x, is given by:

$$y = \frac{(x - \Delta)}{S_y} \quad . \tag{9}$$

For intermediate conditions where a storage, δ (which is less than Δ), is available, the rainfall-recharge relation is given by:

$$y = \frac{(x - \delta)}{S_y} \quad . \tag{10}$$

The relations between the changes in water-table elevations at wells G-614, G-1183, G-1363, G-1486, and S-196A, and the storm-event rainfall measured at the closest gaging stations are shown in figure 34. Although the rainfall data have been extrapolated to the well locations (more than 2 mi in some instances), the measured rainfall-recharge relations (fig. 34) tend to support the hypothesis that the relation between rainfall and change in the water table can be approximated by a threshold rainfall and a linear equation in the form $y = m(x - \Delta)$, where y is the change in water table occurring in response to a storm with rainfall depth x.

At wells G-614, G-1183, G-1363, G-1486, and S-196A, the threshold rainfall, Δ, was estimated by identifying all storm events where no measured change in the water-table elevation occurred, and then taking the average no-recharge rainfall as the threshold Δ. Using this threshold value, the slope of the rainfall-recharge relation that minimized the least-square error was found and taken as the parameter m in the rainfall-recharge relation. Applying this methodology to the data at the five wells resulted in the best-fit equations shown in figure 34.

The rainfall-recharge relation is expected to be influenced by the antecedent moisture conditions, with more recharge expected when the ground is wet compared to when the ground is dry. In an attempt to extract the importance of this effect, the rainfall-recharge relation was estimated using only rainfall events with intervals of at least 7 days between prior rainfall events, and these results are shown as solid points in figure 34. As evidenced, the rainfall-recharge relation for storms that are at least 7 days apart have less scatter, but the mean rainfall-recharge relation is about the same as when all storms are considered.

A significant source of uncertainty in the recharge relations (fig. 34) is the assumption that the rainfall in the vicinity

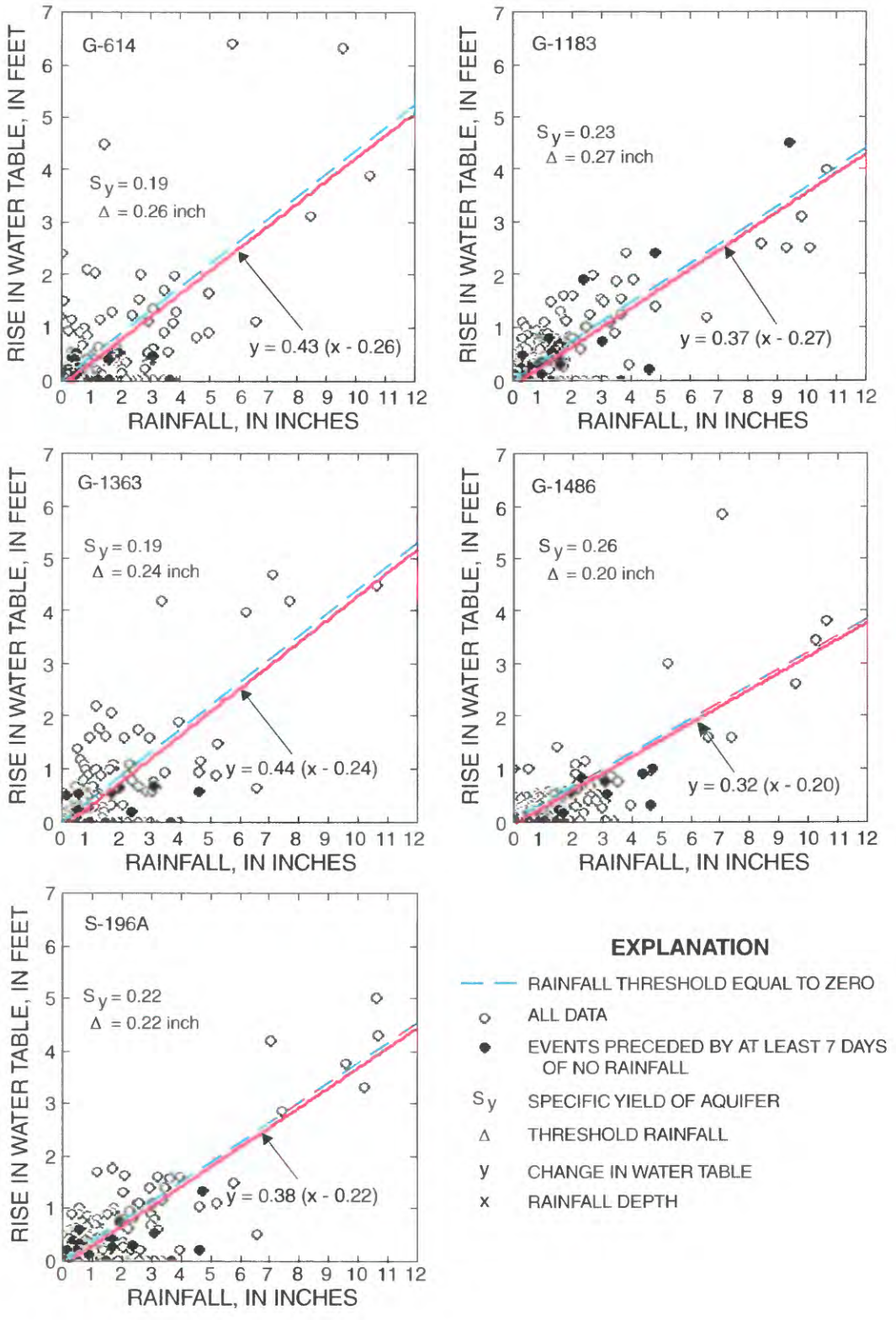

Figure 34. Change in water-table elevation relative to storm-event rainfall at selected wells. Well locations are shown in figure 9.

of all well locations is equal to the measured rainfall at the nearest gaging station. The uncertainty in this assumption was manifested in the result that some large storms apparently yielded negligible recharge. Another source of uncertainty is the difficulty in determining the rainfall-recharge relation when several storms occur within a relatively short period of time. In these cases, the storms are spaced sufficiently close together that it is difficult to separate the storms into individual storms with each having specific recharge amounts. In most cases, it was most convenient to consider several closely spaced storms as a single storm, with the recharge occurring over the collective duration of these storms.

Assuming that incremental rainfall amounts are translated directly to water-table rise, especially for large rainfall events, the specific yield of the aquifer can be estimated from the slope, m, of the rainfall-recharge relation using the equation:

$$S_y = \frac{1}{12m} \quad , \qquad (11)$$

where the factor 12 converts the slope, m, from feet per inches to a dimensionless quantity.

Applying this relation to the linear equations (fig. 34) leads to the specific yields given in table 17. These results indicate that the specific yield of the Biscayne aquifer in the study area ranges from 0.19 to 0.26, and can be reasonably estimated as 0.23. The transient drainage of soils in response to recharge events is widely recognized to result in reduced values of the specific yield. An analytical expression to quantify this effect on selected Florida soils was suggested by Nachabe (2002), who also noted that if the time step used in numerical ground-water models is larger than the time for the soil to drain, then it is justified for these models to use a constant value of the specific yield. In cases where regional ground-water models cover distinct landscapes (for example, wetlands and uplands), capturing the variation in specific yield between landscapes may be important. In applying the specific yield estimates derived from the present study, it should be noted that air entrapment during recharge and rise in the water table commonly is assumed to result in specific yield values that are less than those observed during periods when the water table is falling. The extent and validity of this assertion, however, has not been investigated for water-table fluctuations within the Miami Limestone.

Table 17. Estimated specific yields based on 1-hour data at selected wells

Well number	S_y, Effective specific yield	Δ, Threshold rainfall (inches)
G-1486	0.26	0.20
G-1183	.23	.27
G-1363	.19	.24
G-614	.19	.26
S-196A	.22	.22
Average	.23	.24

In addition to yielding estimates of the specific yield, the rainfall-recharge data (fig. 34) also yielded estimates of the threshold rainfall, Δ, below which no measurable recharge is produced. The threshold rainfall amounts at the wells range from 0.20 to 0.27 in., with an average of 0.24 in. (table 17). Consequently, storms with rainfall amounts less than about 0.24 in. are not expected to produce measurable recharge. This is less than the value of 0.6 in. reported by Delin and others (2000), and this difference may be attributed to differences in the composition of the unsaturated zone and relatively shallower depth to the water table.

The relation between rainfall and water-table rise measured at well G-1486 (fig. 34) is particularly relevant to this study because this well is located in the most urbanized part of the study area (fig. 9). The rainfall-recharge relation at well G-1486 indicates that generally there is no observable recharge to the ground water with less than 0.26 in. of rainfall. Data collected between 1995 and 2002 indicate an average depth to the water table of 7.68 ft, and therefore, a specific retention of 0.26/12(7.68) = 0.003 is obtained. Although this value is substantially smaller than the estimate of 0.02 suggested by Parker and others (1955), the difference can be partly explained by well G-1486 being in a highly urbanized area with extensive impervious land coverage. Consequently, the effective threshold rainfall in the pervious areas is greater than 0.26 in., producing a higher specific retention.

In regional models that use daily time steps, the question arises as to what part of the rainfall should be allocated to recharge. To address this question, daily rainfall relative to daily change in the water table was calculated at wells G-614, G-1183, G-1363, G-1486, and S-196A from 1996 to 2002 (fig. 35). In each case, the rainfall was the daily rainfall at the nearest gaging station, and the change in water table was the change in the average water-table elevation between the day of the rainfall and the following day. The nearest rainfall gaging stations are S-167 for wells G-1363, G-1486, and S-196A; S-165 for well G-614; and HOMES-FS for well G-1183. The daily rainfall-recharge relations (fig. 35) indicate that changes in water-table elevations over daily time scales are relatively insensitive to the daily rainfall, any model that allocates a set fraction of daily rainfall to recharge would not be valid, and it is clear that recharge must be based on storm-event rainfall rather than daily rainfall. The rapid dissipation of water-table mounds associated with canal drainage and the

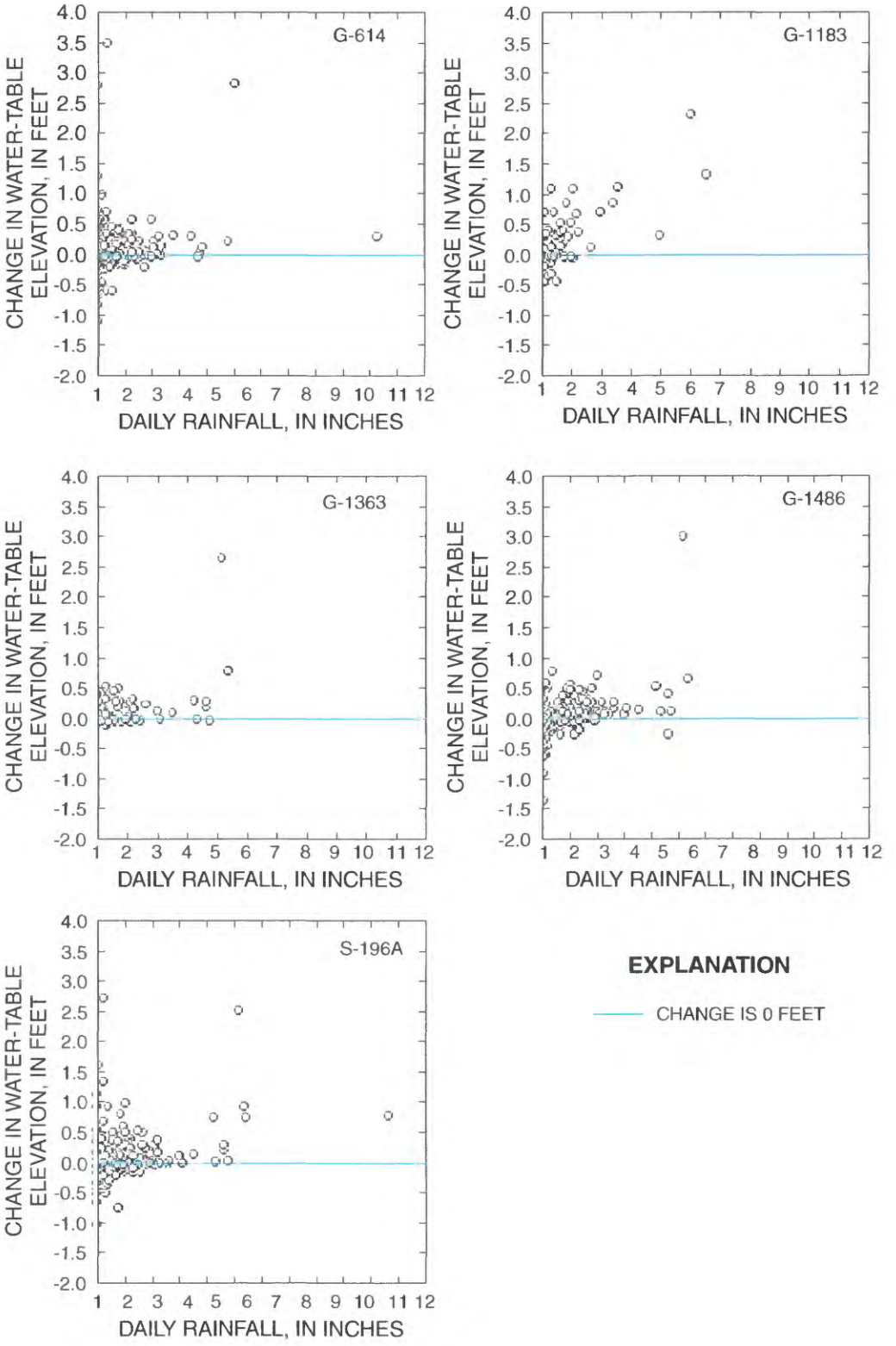

Figure 35. Daily change in water-table elevation relative to daily rainfall at selected wells. Well locations are shown in figure 9.

high transmissivity of the aquifer are certainly factors that contribute to this result. Based on these data, any rainfall-recharge relation should be applied at the scale of individual storms, and this relation should be the basis for upscaling the rainfall-recharge relation for longer time scales.

Many integrated surface-water/ground-water models express the recharge volume as a percentage of the rainfall volume for a defined time interval. Results of the annual rainfall, recharge, and ratio of recharge to rainfall for each well used in the study area from 1996 to 2001 is presented in table 18. Annual rainfall for each year was assumed to be the sum of the hourly rainfall amounts recorded at station HOMES-FS, and annual recharge was calculated by summing all rainfall-induced changes in the water table multiplied by the specific yield of 0.23. The annual recharge at wells G-614, G-1183, G-1363, and S-196A was calculated to be 41, 43, 43, and 46 percent of the annual rainfall, respectively (table 18). This percentage is substantially less at well G-1486 where the recharge is only 30 percent of the rainfall. A plausible explanation is that the area surrounding well G-1486 is more urbanized and includes positive drainage systems where some rainfall drains directly into adjacent canals instead of recharging the ground water.

Recharge rates of 10 to 40 percent of rainfall have been reported in humid to semi-arid regions around the world (Delin and others, 2000); however, the shallow water tables in the present study area may account for the higher recharge rates compared with those reported in previous studies. From 1996 to 2001, average recharge at the five wells ranged from 19 to 29 in. In contrast to these results, Langevin (2001) used an annual net recharge of 15 in. to model seawater intrusion in the study area; however, this value was recognized to be a rough estimate, and a sensitivity analysis indicated that the model results were not very sensitive to recharge.

Results of the present study showed no clear relation between the average depth to the water table and the average annual recharge. Measurements indicated that well G-1363 had an average depth to water of 5.75 ft and an average recharge of 27.1 in., whereas well S-196A had an average depth to water of 6.75 ft and an average recharge of 28.8 in. Further investigation may be warranted. The influence of surface topography on recharge was previously documented by Delin and others (2000), who studied the local recharge at upland and lowland sites located 256 ft apart. The average depths to the water table at the upland and lowland sites were 14 and 9 ft, respectively, and the amount of recharge at the lowland site exceeded that at the upland site for almost every rainfall event. Average annual recharge at the lowland site exceeded recharge at the upland site by about 30 percent.

Water-table fluctuations in the study area are greatly influenced by both direct recharge and leakage into and out of canals. The relation between water-table fluctuations at wells in the study area was investigated by using PC analysis. Using the hourly data from 1995 to 2002, these analyses indicated that the water-table fluctuations at each well location can be expressed as a linear combination of five PCs, and the variance explained by each of these PCs (communalities) is given in table 19. These results indicate that the first principal component (PC1) explains more than 95 percent of the variance at wells G-1363, S-196A, and G-614; 89 percent of the variance at well G-1486; and only 51 percent of the variance at G-1183. Considering only the first two PCs explains at least 94.5 percent of the variance at all well locations; therefore, water-table fluctuations can be explained almost entirely by two PCs.

The correlations between the water-table fluctuations and the first two PCs are shown in figure 36. The fluctuations at wells G-614, G-1363, and S-196A can be explained almost entirely by PC1, and those at wells G-1486 and G-1183 are mostly or greatly influenced by PC1 and PC2, respectively.

Table 18. Annual rainfall, recharge, and recharge/rainfall ratio for selected wells in the study area

[Well locations shown in figure 9; --, no data available]

Year	Rainfall (inches)	G-614		G-1183		G-1363		G-1486		S-196A	
		Recharge (inches)	Recharge/ rainfall ratio (percent)	Recharge (inches)	Recharge/ rainfall ratio (percent)	Recharge (inches)	Recharge/ rainfall ratio (percent)	Recharge (inches)	Recharge/ rainfall ratio (percent)	Recharge (inches)	Recharge /rainfall ratio (percent)
1996	61.0	37.5	61	16.3	27	36.9	60	22.7	37	31.8	52
1997	74.3	7.9	11	32.8	44	--	--	10.4	14	26.3	35
1998	59.2	37.2	63	37.2	63	23.0	39	18.3	31	30.9	52
1999	43.7	5.8	13	4.6	11	20.2	46	7.0	16	18.6	43
2000	59.1	27.7	47	25.0	42	26.2	44	25.6	43	25.6	43
2001	76.3	37.2	49	43.9	58	29.0	38	29.7	39	39.8	52
Average	62.3	25.6	41	26.6	43	27.1	43	19.0	30	28.8	46

Fluctuations at well G-1486 are explained mostly by PC1, and G-1183 is influenced significantly by PC2. The coefficients (eigenvectors) of the PCs are given in table 20, and these coefficients give a relative measure of the water-table fluctuations at each well location. Comparing the coefficients of PC1 for wells G-614, G-1363, and S-196A with the coefficient for well G-1486 indicates that the water-table fluctuations at the three wells tend to be about 40 percent greater than the fluctuation at well G-1486. Possible contributing factors are the higher permeability of materials in the unsaturated zone and the rural locations of wells G-614, G-1363, and S-196A, permitting more land-surface exposure to the atmosphere.

Table 19. Cumulative contribution of principal components to water-table fluctuations for selected wells

Well number	Principal component (PC) variance				
	PC1	PC2	PC3	PC4	PC5
G-614	0.958	0.963	0.998	1.000	1.000
G-1183	.508	.968	.971	.999	1.000
G-1363	.963	.982	.985	.996	1.000
G-1486	.886	.945	.954	.994	1.000
S-196A	.971	.974	.991	.991	1.000

Table 20. Coefficients (eigenvectors) of principal components for selected wells

Well number	Principal component (PC) coefficient				
	PC1	PC2	PC3	PC4	PC5
G-614	-0.545	-0.165	0.787	0.199	0.127
G-1183	-.215	.847	.126	-.456	.112
G-1363	-.542	-.319	-.224	-.527	-.526
G-1486	-.355	.377	-.270	.685	-.435
S-196A	-.486	-.109	-.492	.065	.711

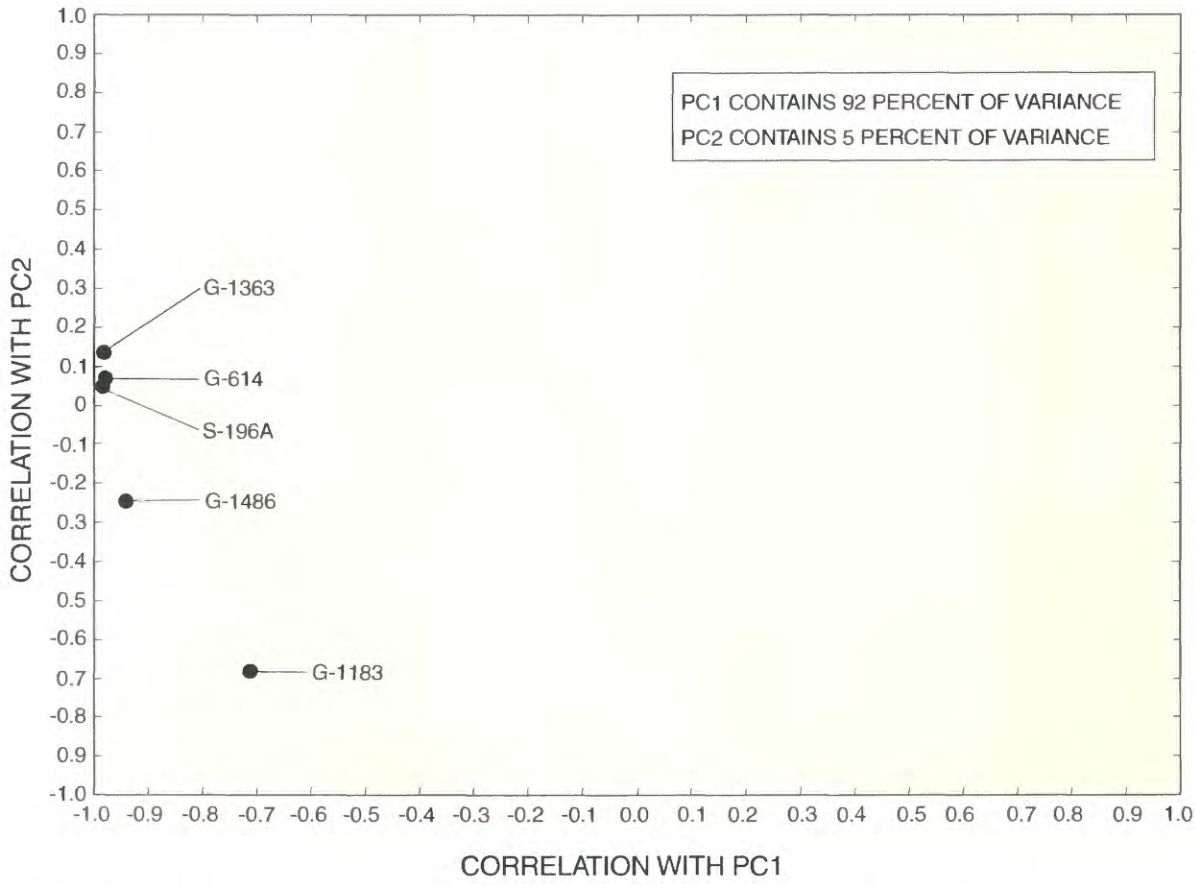

Figure 36. Principal component (PC) correlations of hourly water-table fluctuations at selected wells. Well locations are shown in figure 9.

Results of the PC analyses collectively indicate that (hourly) ground-water recharge is correlated over relatively large spatial scales. Additionally, two fundamental modes of fluctuation can occur—one related to local water-management practices and the other to topology of drainage canals.

Rainfall-Recharge Analysis Based on 15-Minute Data with Local Rainfall Measurements

As part of this study, rain gages were installed at wells G-614, G-1183, G-1363, and S-196A, and water-table elevations and incremental rainfall amounts were measured at 15-minute intervals. The wells and rain gages used in this study are shown in figure 37. The rain enters through an 8.2-in.-diameter orifice on top of the Sutron Model 5600-0420 rain gage, and is funneled into one of two tipping buckets inside the gage. After the rainfall measurement is taken, the water exits through drain tubes with screen-covered holes in the base of the rain gage. The rain gage has a 0.01-in. resolution with an accuracy of ±0.5 percent at 0.5 in/hr, and an accuracy of ±2 percent at 2 in/hr. At wells G-614, G-1183, G-1363, and S-196A, a rain gage was mounted directly above the monitoring well. At well G-1486, an existing Sutron Model 5600-0420 rain gage (HOMES-FS) located about 2 mi from the monitoring well was used to estimate the rainfall at 15-minute intervals at the well location. The time series of water-table/rainfall measurements at 15-minute intervals covered various periods between April 2001 and December 2002 as given below:

Well	Period of Record	Missing data (percent)
G-614	10/19/01-11/30/02	9.5
G-1183	04/28/01-12/31/02	10.3
G-1386	04/26/01-09/22/02	11.1
G-1486	06/01/01-10/15/02	37.0
S-196A	07/24/01-11/30/02	6.7

A cursory review of water-table fluctuations recorded at 15-minute intervals indicated features that were not observed in hourly data. For example, short-term water-table fluctuations with time scales less than 1 hour with no measured rainfall indicated indirect recharge events not associated with rainfall. In some instances, the cause of the short-term water-table fluctuations could be traced to gate operations and associated water-level changes in nearby canals. It was particularly instructive to note the time lag between the start of rainfall events and the start of recharge events. A typical lag between the beginning of a rainfall event and observation of a measurable change in water table ranged between 15 minutes and 1 hour.

The relations between single-event rainfall and the corresponding water-table rise at wells G-614, G-1183, G-1363, G-1486, and S-196A are shown in figure 38. As was the case for hourly rainfall-recharge data, the 15-minute measurements indicate that the relation between rainfall and change in water table can be approximated by a threshold rainfall and a linear equation in the form $y = m(x - \Delta)$, where y is the change in water table occurring in response to a storm with rainfall depth x. At each well, the threshold rainfall, Δ, was estimated by identifying all storm events where no measured change in the water-table elevation occurred, and then the maximum no-recharge rainfall was used as the threshold Δ. Using this threshold value, the slope of the rainfall-recharge relation that minimized the least-square error was reported and used as the parameter, m, in the rainfall-recharge relation. Applying this methodology to the data at the five wells resulted in the best-fit equations shown in figure 38.

The methodology used to determine the threshold rainfall, Δ, from the 15-minute rainfall data differed from the approach used previously for the historical hourly data. In the case of the 15-minute data, where rainfall and water-table measurements are at the same location, Δ is the maximum no-recharge rainfall, which is consistent with the physical meaning of Δ as the maximum rainfall storage available at the location of the measurements. In the case of historical hourly data, rainfall and water-table measurements were not at the same location, and extrapolation of rainfall measurements to the water-table measurement location yielded errors in the local rainfall-recharge relation, and Δ was taken as the mean rainfall occurring when there was no observable change in the water table. The data shown in figure 38 indicate values of threshold rainfall, Δ, ranging from 0.22 to 0.48 in., with a mean value of 0.37 in. The distribution of threshold rainfall amounts at the five wells used in this study are given in table 21. A fair degree of uniformity exists in the threshold rainfall amounts, and the mean threshold rainfall of 0.37 in. can be compared with the estimated threshold rainfall of 0.24 in. derived from the historical hourly data. Because the hourly data involved many more assumptions, added weight should be given to the threshold rainfall derived from the 15-minute data. A reasonable estimate can be made that a maximum of 0.37 in. of rainfall

Well number	S_y, Effective specific yield	Δ, Threshold rainfall (inches)
G-614	0.30	0.41
G-1183	.16	.37
G-1363	.26	.39
G-1486	.30	.22
S-196A	.26	.48
Mean	.26	.37

Table 21. Estimated specific yield and threshold rainfall based on 15-minute data at selected wells in the study area

[Well locations are shown in figure 9]

G-1363

G-614

G-1183

S-196A

G-1486/HOMES-FS (Rain)

G-1486 (Water Table)

Figure 37. Rainfall/water-table measurement stations used at selected wells during the study. Well locations are shown in figure 9.

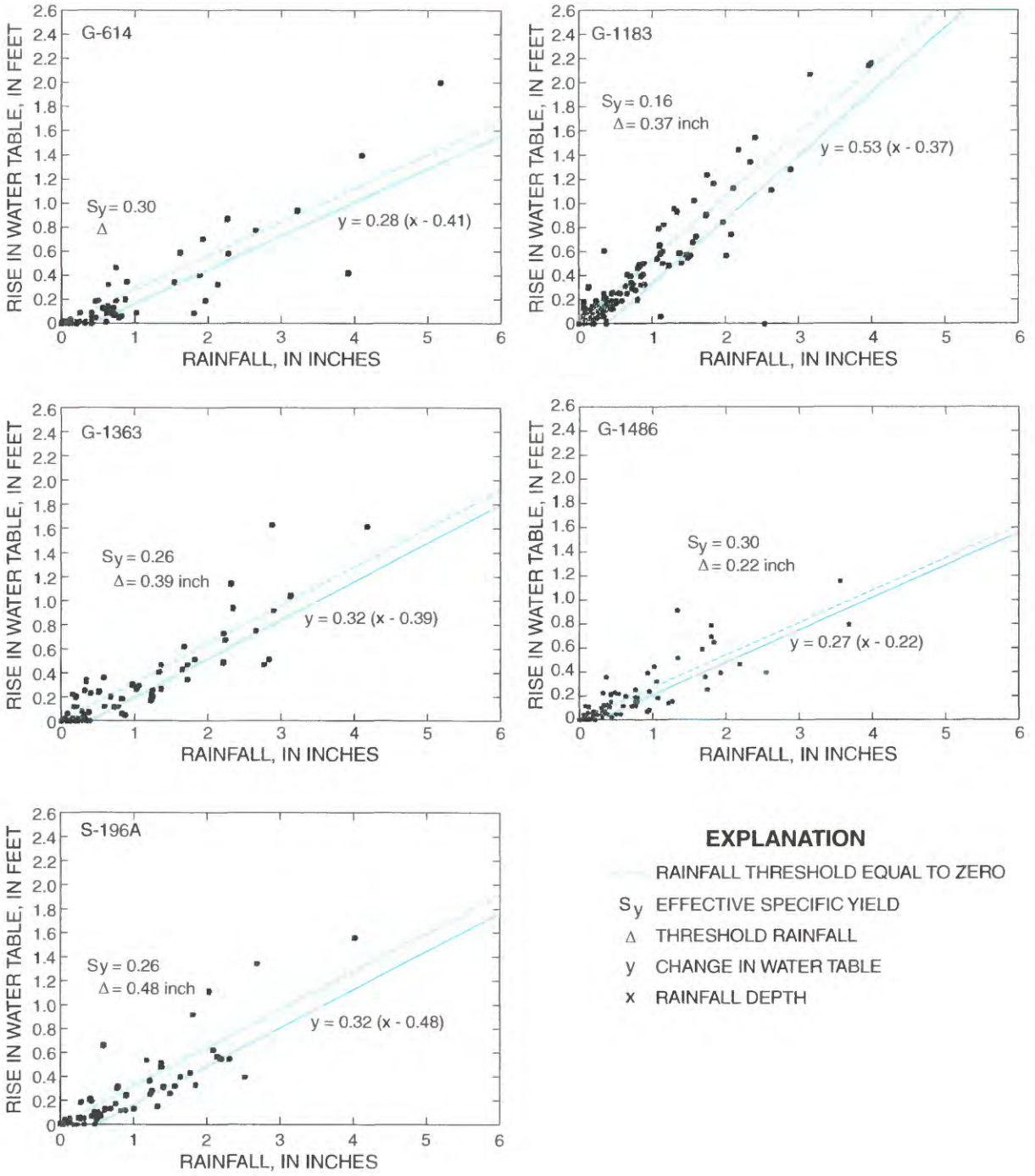

Figure 38. Water-table elevation relative to storm-event rainfall based on 15-minute data. Well locations are shown in figure 9.

typically will be required prior to any measured recharge, with a lower threshold when antecedent conditions are moist.

The specific yield of the aquifer was estimated from the slope, m, of the rainfall-recharge relation using equation 11. Applying this relation to the linear relations (fig. 38) produces the specific yields given in table 21. These results indicate that the specific yield of the Biscayne aquifer in the study area ranges from 0.16 to 0.30, with a mean value of 0.26. These results can be contrasted with those based on historical hourly data, where the aquifer specific yield was estimated to have a mean value of 0.23. The fact that rainfall and water-table changes were measured at the same location in this (15-minute data) study gives added weight to the 0.26 estimate of specific yield because errors associated with spatial extrapolation of rainfall measurements were not present. Furthermore, this estimate of specific yield is consistent with porosity measurements shown in figure 8. The estimated value of the specific yield derived from the rainfall-recharge relation is very close to the value of 0.25 based on data reported by Merritt (1996) in the vicinity of well S-196A.

Evaporation from Water Table

Evaporation from the water table, which is negative recharge, is an important process during extended periods of no rainfall. Although this investigation is concerned primarily with storm-event scale processes, a study of water-table behavior during rainfall events was easily extended to cover periods of no rainfall.

In southern Florida, the water table typically is observed to decline steadily between rainfall events. During this investigation, these declines were observed and considered to be caused primarily by canal drainage and/or direct evaporation from the saturated zone. Before canal construction, Parker and others (1955) and later Merritt (1996) reported that evaporation from the water table contributes substantially to water-table declines when canal influences are negligible. In the study area, transpiration can be eliminated as a major contributor to water-table declines, because in most of the study area, less than 1 ft of soil overlies hard limerock (the Miami Limestone), which is not penetrated by plant roots. Consequently, evaporation and canal drainage must be considered as likely causes of water-table declines between rainfall events.

A variety of formulae have been proposed to estimate evaporation from the saturated zone, and several of these formulae are discussed by Zammouri (2001). Most models that simulate evaporation rate, E, from the saturated zone can be put in the form:

$$E = E_o\left(1 - \frac{d}{d_{cr}}\right)^m, \qquad d < d_{cr}\ , \qquad (12)$$

where E_o is the potential evaporation rate at the land surface, d is the depth of the water table below the land surface, d_{cr} is the critical water-table depth below which evaporation ceases, and m is a coefficient typically equal to 1 or 2. The groundwater model MODFLOW (McDonald and Harbaugh, 1988) uses $m = 1$, and $m = 2$ is assumed in the Averianov formula (Schoeller, 1961). The critical depth, d_{cr}, at any location typically is assumed to be a constant and dependent on the local climate.

In an attempt to relate d_{cr} to climatic conditions, Zammouri (2001) suggested the following relation:

$$d_{cr} = 170 + 8T\ , \qquad (13)$$

where d_{cr} is in centimeters, and T is the annual-average air temperature in degrees Celsius. In southern Florida, the average-annual air temperature is about 25 °C, which yields d_{cr} = 370 cm = 12.1 ft. Because the depth to the water table in the study area ranges between 4 and 9 ft, observable evaporation from the water table is to be expected.

Some models assume that evapotranspiration occurs at a maximum rate above the bottom of the shallow root zone and decreases linearly from the bottom of the shallow root zone to the bottom of the deep root zone (INTERA Environmental Consultants, Inc., 1976). The absence of root penetration into the limestone formation in southern Florida does not support the application of such models. Despite this physical inconsistency, such models have been applied in the study area. For example, Merritt (1996) used such a model with an extinction depth of 20 ft in southern Miami-Dade County. The formulation was justified by Merritt (1996) based on the lack of apparent correlation between rate of recession and depth below land surface, which could indicate a large extinction depth.

In the study area, evaporation from the saturated zone should be readily observable during prolonged dry periods when drainage structures are closed and there is negligible difference between canal stages and elevations of the surrounding water table. To quantify evaporation rates from the saturated zone, hourly records of water-table elevations at wells G-614, G-1183, G-1363, G-1486, and S-196A were analyzed from 1995 to 2002. For each month, a single interval of at least 7 days (168 hours) without rainfall was identified for further study. Recognizing that aquifer drainage during dry periods is a transient phenomenon, in those cases where the rate of water-table decline during a 7-day minimum interval remained relatively steady, the decline was attributed to evaporation, and the rate of water-table decline for the selected interval was calculated using a least-squares fit to the water-table elevations during the prolonged dry period.

The hypothesis that these dry-period water-table declines are caused primarily by evaporation, and not aquifer drainage, is further supported by the frequent observation that the steady rate of water-table decline persists for almost the entire duration of the dry interval. Conditions when water-table elevations remained constant during prolonged dry periods were not found.

Water-table decline rates during 1995 to 2002 were calculated for all months when at least 7 days of no rainfall occurred. During the wet-season months of June through September, few dry intervals lasting 7 days occurred, so no conclusions could be drawn about evaporation-induced water-

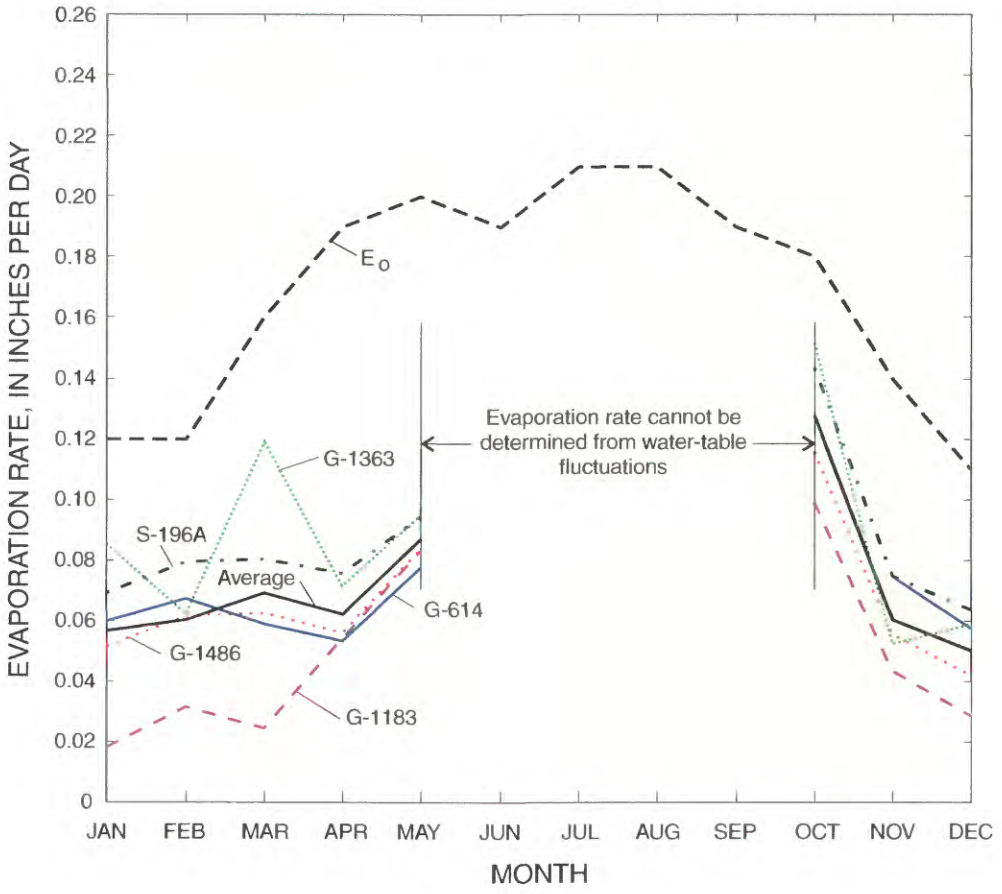

Figure 39. Monthly saturated-zone evaporation rates for selected wells and the potential evaporation rate (E_o) at the ground surface, 1995-2002.

table declines during these months. For the other 8 months, the average monthly water-table decline rates were determined, and these rates were multiplied by the estimated specific yield of 0.26 to obtain the average evaporation rates.

The monthly saturated-zone evaporation rates were determined for wells G-614, G-1183, G-1363, G-1486, and S-196A from 1995 to 2002 (fig. 39). These data along with the corresponding land-surface potential evaporation rates (maximum evapotranspiration in table 1) follow the same trend, supporting the hypothesis that water-table declines during dry periods are associated with the evaporation process. The lowest evaporation rates are at well G-1183, the highest rates are at well G-1363, and evaporation rates at the other wells are in the intermediate range. As indicated by figure 39, the saturated-zone evaporation rates are seasonal and related to land-surface potential evaporation rates.

Another important variable influencing the relation between the land-surface and saturated-zone evaporation rates is the depth of the water table below land surface. The average depth to the water table for each month from 1995 to 2002 is shown in figure 40. These data indicate that well G-1183 has the shallowest depth to the water table (4.0-4.5 ft), and wells G-614 and G-1486 have the greatest depth to the water table (7-8.5 ft).

To fully understand the relation between evaporation from the water table (E), land-surface potential evaporation rate (E_o), and depth to the water table (d), the normalized saturated-zone evaporation rate (E/E_o) is plotted relative to the depth to the water table (fig. 41). These relations can be expressed in the form:

$$\frac{E}{E_o} = \alpha - \beta d, \qquad (14)$$

where α and β are constants. At wells G-614, G-1183, G-1486, and S-196A, the data fit well with the linear model, whereas a fair degree of scatter appears at well G-1363. Data indicate that normalized evaporation rates decrease with depth, as expected, except at G-1486 where the rate appears to be independent of the depth to the water table.

At wells G-614, G-1183, G-1363, and S-196A, the data support the saturated-zone evaporation model shown in figure 42, where the evaporation rate is equal to the surface evaporation rate for a depth, d_o, below the land surface, and the

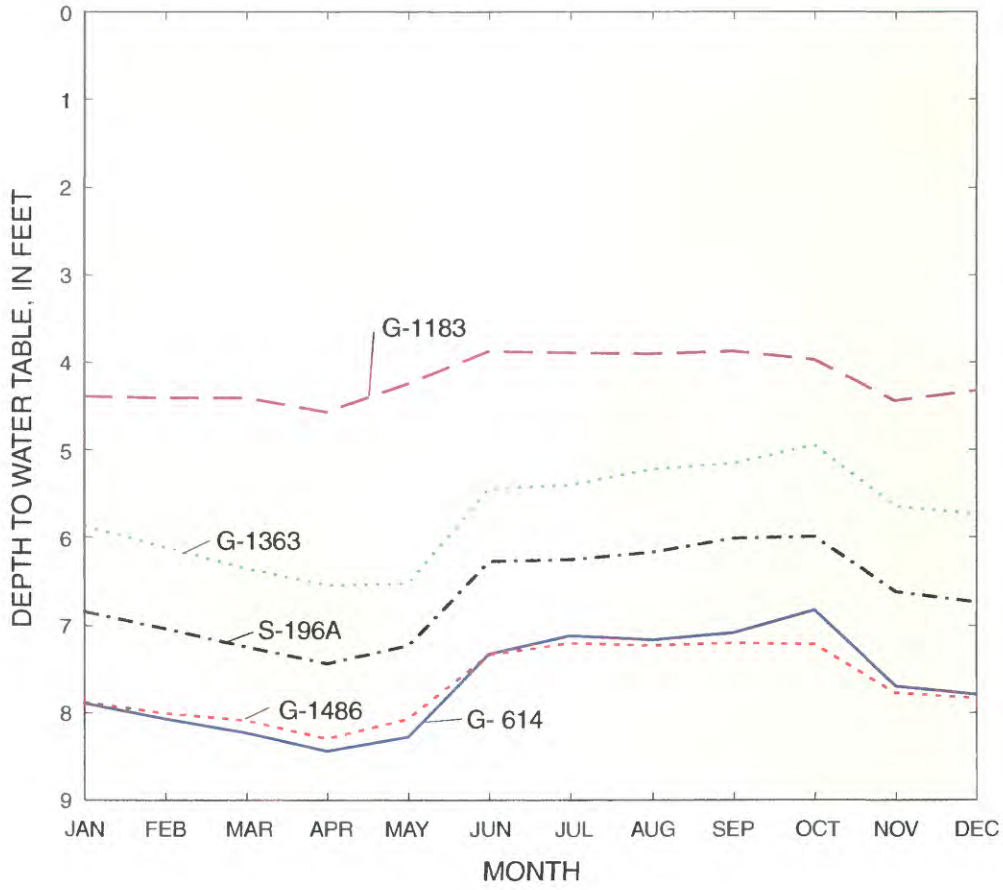

Figure 40. Average monthly water-table elevations for selected wells, 1995-2002.

saturated-zone evaporation rate decreases linearly to zero at a depth, d_{cr}, below the land surface. In accordance with this model, the saturated-zone evaporation rate can be described analytically by the relation:

$$\frac{E}{E_o} = \begin{cases} 1 & d \le d_o \\ 1 - \dfrac{d - d_o}{d_{cr}} & d \ge d_o \end{cases} . \qquad (15)$$

The d_o and d_{cr} model parameters can be estimated from the best-fit linear equation (eq. 14) by:

$$d_o = \frac{\alpha - 1}{\beta} \quad \text{and} \quad d_{cr} = \frac{\alpha}{\beta} . \qquad (16)$$

Using the relations given in equation 16, the values of d_o and d_{cr} were calculated from the linear equations shown in figure 41. These results, tabulated in figure 42, indicate that d_o ranges from 3.1 to 6.5 ft, and d_{cr} ranges from 4.9 to 9.6 ft. Values of d_o and d_{cr} could not be estimated for well G-1486, where E/E_o remains nearly constant, within the range of water-table fluctuations experienced during this study. Interestingly, well G-1486 is located in the most urbanized part of the study area, where impervious surfaces may have a moderating influence on evaporation from the saturated zone.

Results of the saturated-zone evaporation study collectively indicate that evaporation from the saturation zone can, in many cases, be described by a linear model where the saturated-zone evaporation rate is equal to the land-surface evaporation rate for a depth, d_o, and then decreases to zero at a depth, d_{cr}. Four of the five wells (mentioned above) support this model, where the average value of d_o is 4.5 ft, and the average value of d_{cr} is 8.3 ft. In some cases, the evaporation rate may be independent of the depth to the water table, which occurred at one location that also happened to be the most urbanized. This study has shown that local saturated-zone evaporation rates can be estimated with a relative degree of certainty from a careful analysis of hourly measurements of water-table elevations.

Canal Leakage

Under steady-state and small-drawdown conditions, detailed field work at the L-31N canal and Snapper Creek Extension Canal (fig. 1, C-2 Canal) has verified that the

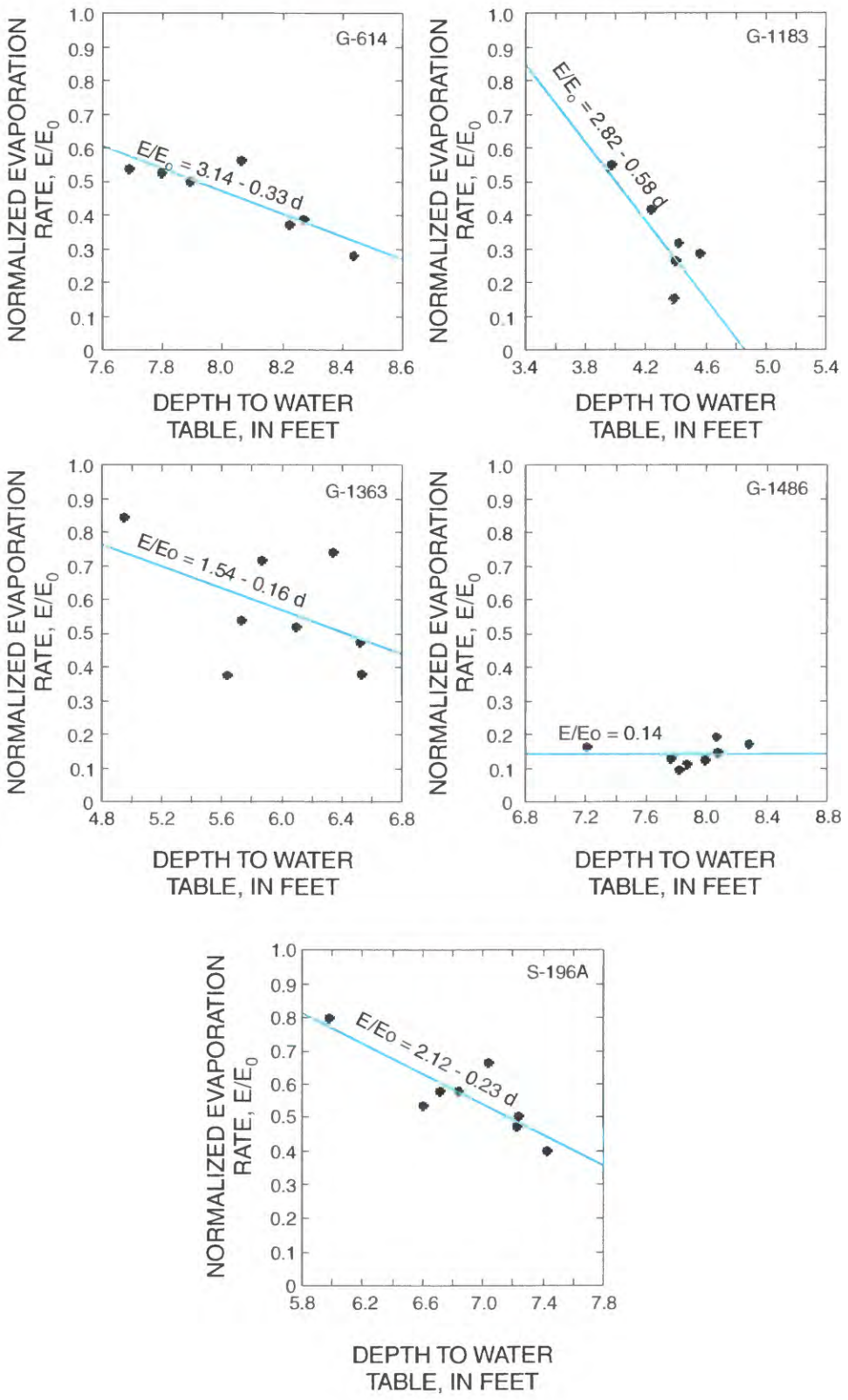

Figure 41. Relation between normalized saturated-zone evaporation rate and depth to the water table for selected wells, 1995-2002.

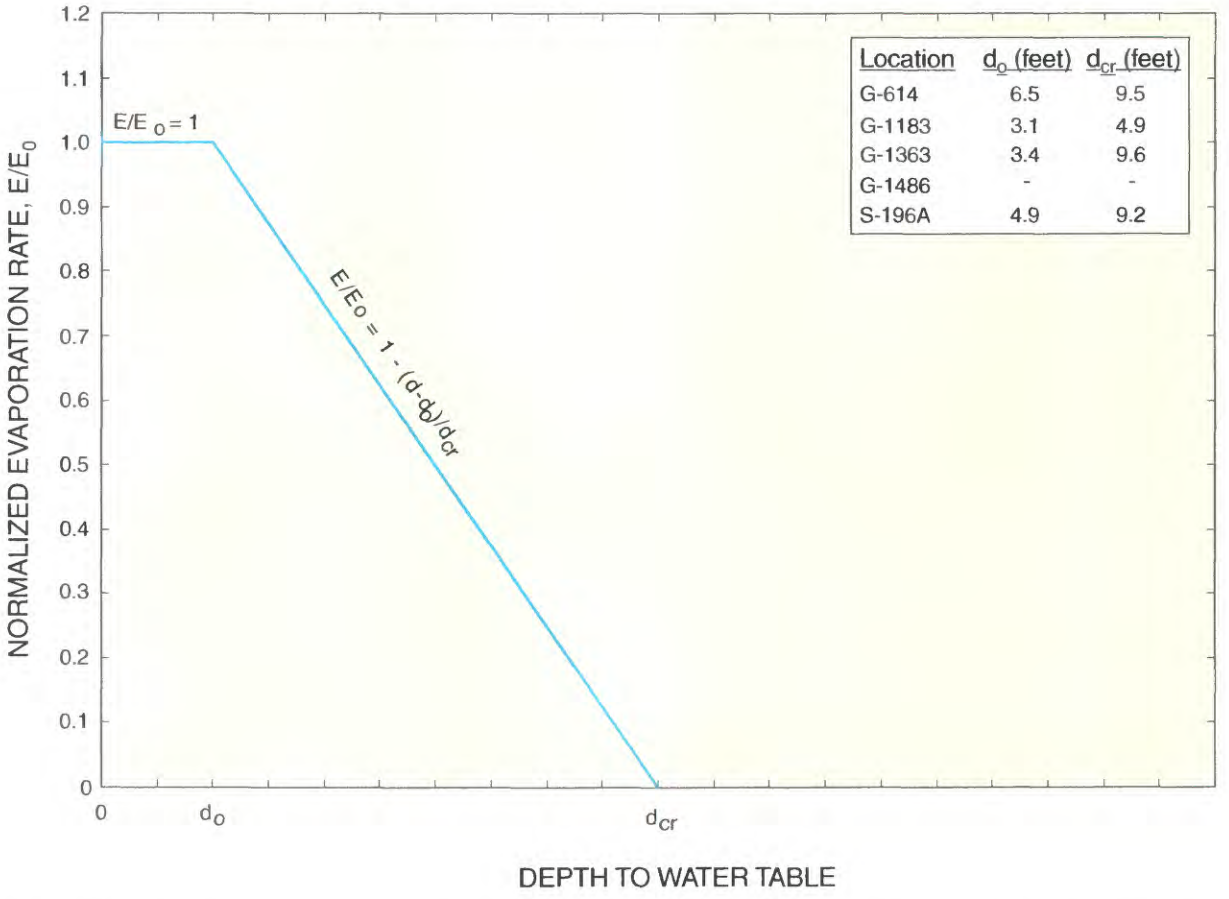

Figure 42. Saturated-zone evaporation model. The parameter d_o is the land-surface evaporation rate for a depth, and d_{cr} is where the saturated-zone evaporation rate decreases linearly to zero at a depth below land surface.

leakage, ΔQ, out of a canal per unit length of canal can be estimated using the relation (Chin, 1990):

$$\Delta Q = T\left(\frac{s_R}{x_R} + \frac{s_L}{x_L}\right), \qquad (17)$$

where s_R is the head difference between the canal and the aquifer at a distance, x_R, from the right-hand side of the canal; and s_L is the head difference at a distance, x_L, from the left-hand side of the canal.

Results of a field investigation (Chin, 1990) indicate that equation 17 is relatively accurate as long as x_R and x_L exceed 10 aquifer depths and the drawdowns are small relative to the thickness of the saturated zone. The validated leakage relation given by equation 17 requires that the transmissivity of the aquifer directly adjacent to the canal be known. The importance of accurately accounting for canal leakage has been demonstrated in model results by McCue and others (2002), who showed that canal leakage can constitute a large part of total recharge in southern Florida, and can be considerably higher than rainfall recharge during dry periods.

Accurate determination of the local transmissivity of the aquifer adjacent to a canal is difficult in many cases because of the expense of conducting aquifer tests and the high pumping rates required to cause measurable drawdowns in the highly transmissive parts of the aquifer. An alternative to using aquifer tests to determine the hydraulic properties of the aquifer near canals is to track the propagation of tidal fluctuations from the canals to nearby wells and estimate the local aquifer properties from the wave-attenuation characteristics in the aquifer. Tidal waves in canals are potentially useful for this analysis because most major coastal canals experience tidal oscillations when gates connecting them to the ocean are opened.

Tidal fluctuations in canals occur when the gates of coastal structures are opened to provide drainage during current or imminent major storm events. The close connection of the canal and aquifer and the high transmissivity of the aquifer are shown in figure 43. The synoptic tidal fluctuations at structure S-166 in the C-103N Canal and structure S-167 in the C-103 Canal propagate to well G-1486, which is located about midway between C-103 and C-103N and about 1 mi from each canal (fig. 9). For each peak or trough in the canal tidal wave, a corresponding peak or trough can be identified at the well, and the measured delay time, t_d, can be related to the

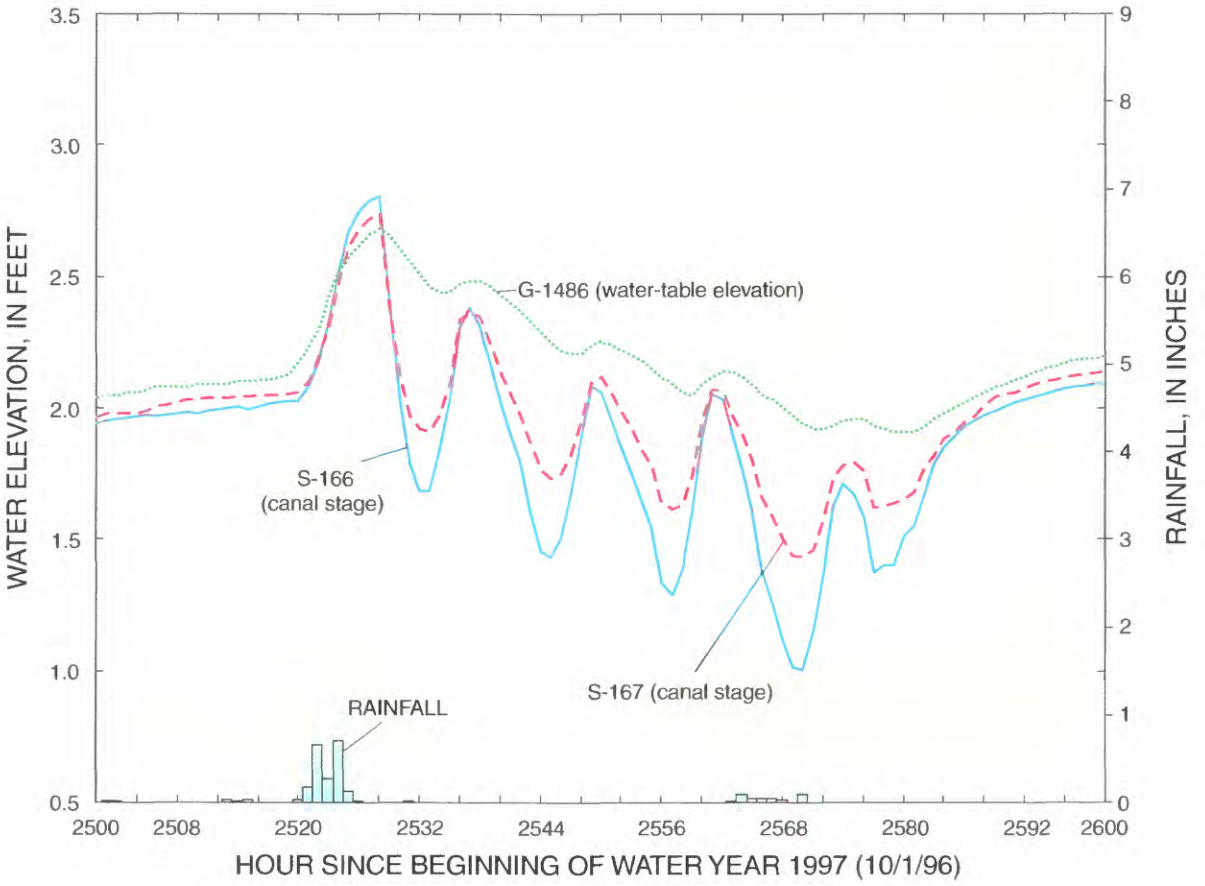

Figure 43. Propagation of tidal effects into the aquifer. Water year 1997 begins October 1, 1996, and ends September 30, 1997.

hydraulic properties of the aquifer between the canal and the well using the relation (Hermance, 1999):

$$t_d = x\sqrt{\frac{S_t}{4\pi f T}}\ , \qquad (18)$$

where x is the distance from the tidal source (canal) to the monitoring well in the aquifer, S_t is the storage coefficient of the aquifer for tidal propagations at frequency, f, in cycles per unit time, and T is the transmissivity of the aquifer between the canal and the monitoring well. The variable combination, T/S_t, is commonly referred to as the hydraulic diffusivity.

The relation given by equation 18 is based on the assumption that the canal is fully penetrating and local resistance on the perimeter of the canal is negligible. Singh and others (2002) studied the effects of partial penetration and stream resistance, which tend to increase the time lag over that estimated by equation 18. In other words, using equation 18 can potentially underestimate the hydraulic diffusivity under these conditions.

The relation between the delay time, t_d, and corresponding peak/trough sequence for the C-103 and C-103N Canals and well G-1486 for several tidal events during 1996-2002 is shown in figure 44. As indicated by the graph, the time lag varies substantially for a small number of wave/trough sequences, but seems to be more consistent as the number of wave/trough sequences increases. It is interesting to note that for a long sequence of tidal waves, the time lag approaches zero, which is the steady-state condition for a well located between two canals with coherent tidal fluctuations. A distance-weighted least-squares fit to the time lag compared to the wave sequence indicates that the time lag for wave propagation into the aquifer from the C-103 and C-103N Canals to well G-1486 is about 3 hours for the semidiurnal (period = 12 hours) tidal fluctuations in the canals. Well G-1486 is about 5,370 ft from C-103 and 5,060 ft from C-103N (fig. 9), with an average distance from the canals of 5,200 ft. If $t_d = 3$ hours, $x = 5{,}200$ ft, and $f = 1/12$ hour^{-1}, then equation 18 yields:

$$\frac{T}{S_t} = \frac{1}{4\pi f}\left(\frac{x}{t_d}\right)^2 = \frac{1}{4\pi\left(\frac{1}{12}\right)}\left(\frac{5{,}200}{3}\right)^2$$

$$= 2.87 \times 10^6 \text{ ft}^2/\text{hr} = 6.89 \times 10^7 \text{ ft}^2/\text{d}$$

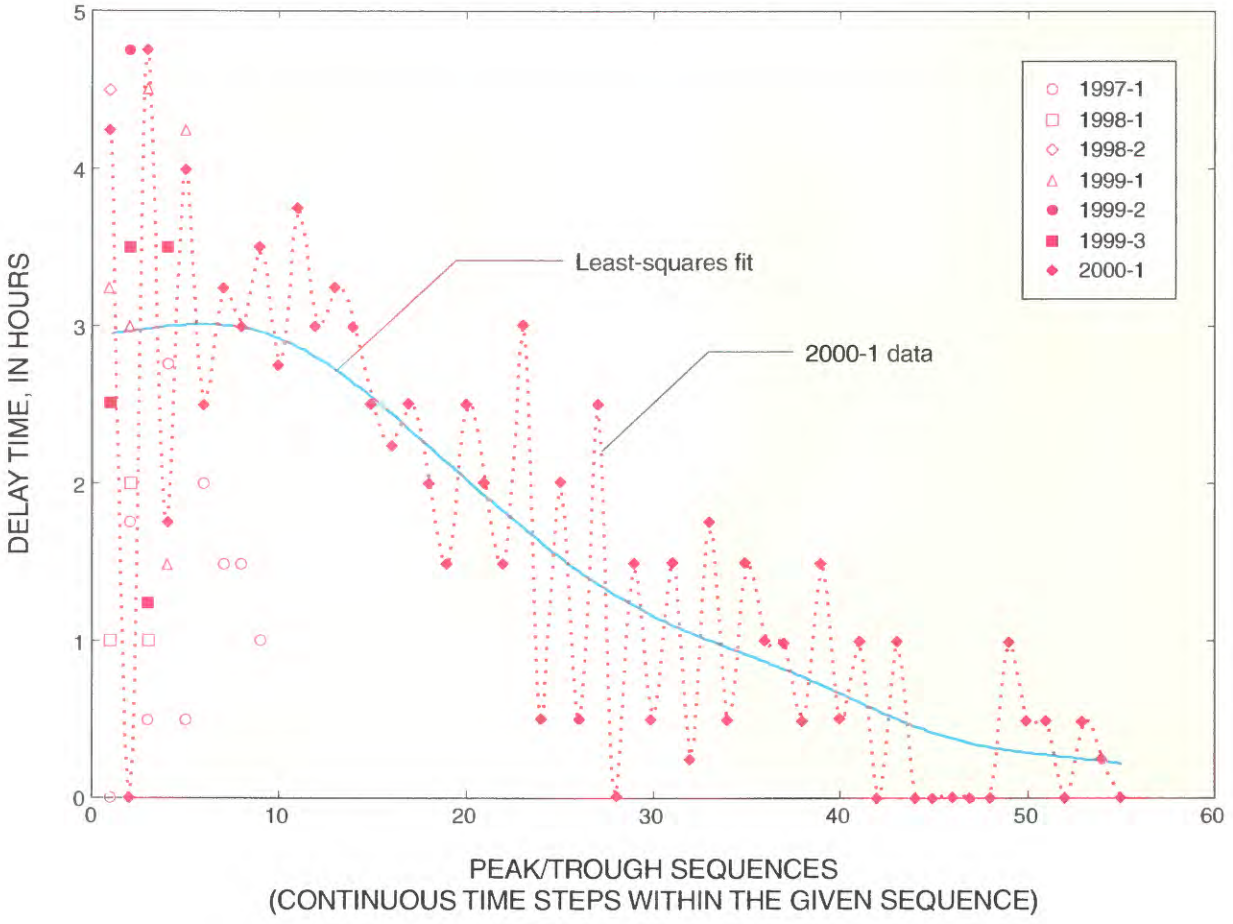

Figure 44. Delay time relative to the peak/trough sequence for the C-103 and C-103N Canals and well G-1486. The numbers (following the year in the explanation) represent sequences within the year.

Assuming that $S_t = S_y = 0.26$ is typical of the study area, and combining this result with the above estimate of the aquifer diffusivity yields:

$$T = (0.26)(6.89 \times 10^7) = 18 \times 10^6 \text{ ft}^2/\text{d} .$$

This estimate of the aquifer transmissivity between the C-103 and C-103N Canals is about an order of magnitude higher than reported by Fish and Stewart (1991), who estimated the transmissivity in this location to range from 0.3 to 1×10^6 ft^2/d. This order of magnitude discrepancy is consistent with previous studies that showed the hydraulic diffusivity estimated from equation 18 is more consistent with using an intermediate value of S_t between the specific yield, S_y, and the storage coefficient, S. This is conceptually equivalent to saying that the wave passes across a depth of the aquifer with an effective storage of S_y at the free surface and a value of S_t lower down in the aquifer. Based on the transmissivity measurements reported by Fish and Stewart (1991), the transmissivity in the aquifer between C-103 and C-103N can be estimated as 0.7×10^6 ft^2/d. The appropriate storage value, S_t, to be used in estimating the transmissivity from the hydraulic diffusivity is given by:

$$S_t = \frac{0.7 \times 10^6}{6.89 \times 10^7} = 0.010 .$$

This estimate of the tidal propagation storage coefficient, S_t, is between the estimated specific yield of 0.26 and the aquifer storage coefficient, which has been previously estimated as 0.0002 (Swain and Wexler, 1996). To validate this estimate of S_t, the tidal propagation analysis was repeated for tidal fluctuations originating in the C-103 Canal downstream of structure S-179 and monitored at well G-1183 about 5,270 ft away from C-103 at the nearest point (fig. 9). Synoptic tidal fluctuations measured in the C-103 Canal and well G-1183 are shown in figure 45, and the measured time lags relative to the peak/trough sequences are shown in figure 46. The results in figure 46 indicate that a significant and (sometimes) consistent time lag exists between the tidal fluctuations in C-103 and the water-table fluctuations measured at well G-1183. The results further indicate that a time lag of 2.5 hours is characteristic of initial tidal propagations to be

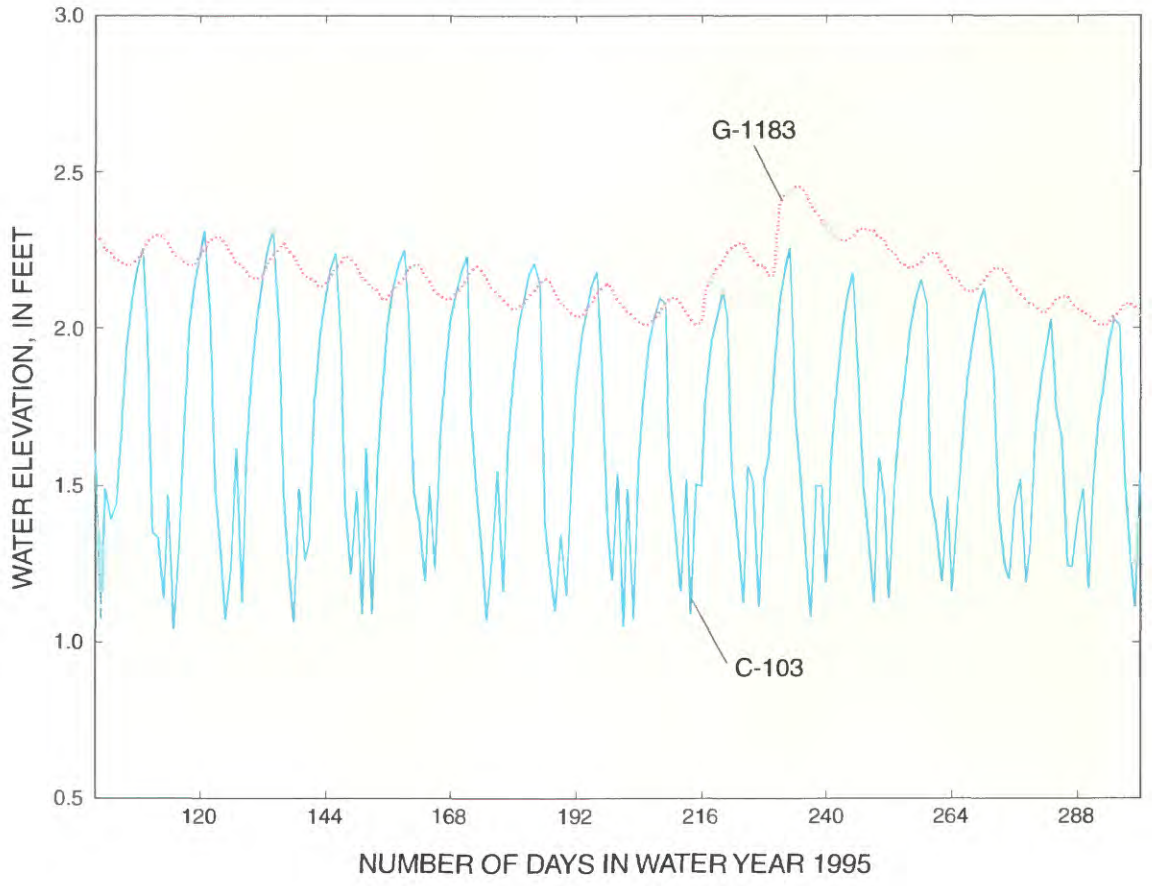

Figure 45. Propagation of tidal fluctuations from the C-103 Canal to well G-1183.

used in estimating the aquifer hydraulic diffusivity. If $t_d = 2.5$ hours, $x = 5{,}270$ ft, and $f = 1/12$ hour^{-1}, then equation 18 yields the following estimate of the hydraulic diffusivity:

$$\frac{T}{S_t} = \frac{1}{4\pi f}\left(\frac{x}{t_d}\right)^2 = \frac{1}{4\pi\left(\frac{1}{12}\right)}\left(\frac{5,270}{2.5}\right)^2$$

$$= 4.24 \times 10^6 \text{ ft}^2/\text{hr} = 10.2 \times 10^7 \text{ ft}^2/\text{d}$$

According to Fish and Stewart (1991), the transmissivity of the aquifer in the vicinity of the C-103 Canal (downstream of structure S-179) can be estimated as 0.3×10^6 ft^2/d. Therefore, the appropriate storage coefficient, S_t, to be used in estimating the transmissivity from the hydraulic diffusivity is given by:

$$S_t = \frac{0.3 \times 10^6}{10.2 \times 10^7} = 0.003$$

Comparing this result (0.003) with that derived from the previous tidal analysis for well G-1486 (0.010) shows an order of magnitude agreement in the estimate of the appropriate storage coefficient to be used in estimating the transmissivity from measurements of tidal fluctuations. The discrepancy between the appropriate storage coefficients can partially be explained by a greater casing depth in well G-1183 (47 ft) than in well G-1486 (32 ft), which is consistent (based on previous results) with a smaller tidal storage coefficient, assuming that geologic conditions are relatively homogeneous. In assessing the moderate discrepancy in tidal storage coefficients, the transmissivity estimates given by Fish and Stewart (1991) were based largely on localized measurements from specific-capacity tests. Therefore, it is reasonable to expect that the transmissivity estimated from tidal propagation analysis, which is for a much larger length scale, could differ substantially from localized transmissivity measurements.

Results presented here indicate that tidal propagation analysis in the surficial aquifer can yield fair estimates of the aquifer transmissivity, which can then be used to estimate the canal-aquifer leakage relations by using equation 17. Results from this study indicate that tidal storage coefficients range from 0.003 to 0.010, with an average value of about 0.007.

In the study area, actual measurements of transmissivity derived from aquifer tests should be used to provide the best estimate of the canal leakage relations. Based on equation 17, which was previously validated in the L-31N canal (Chin,

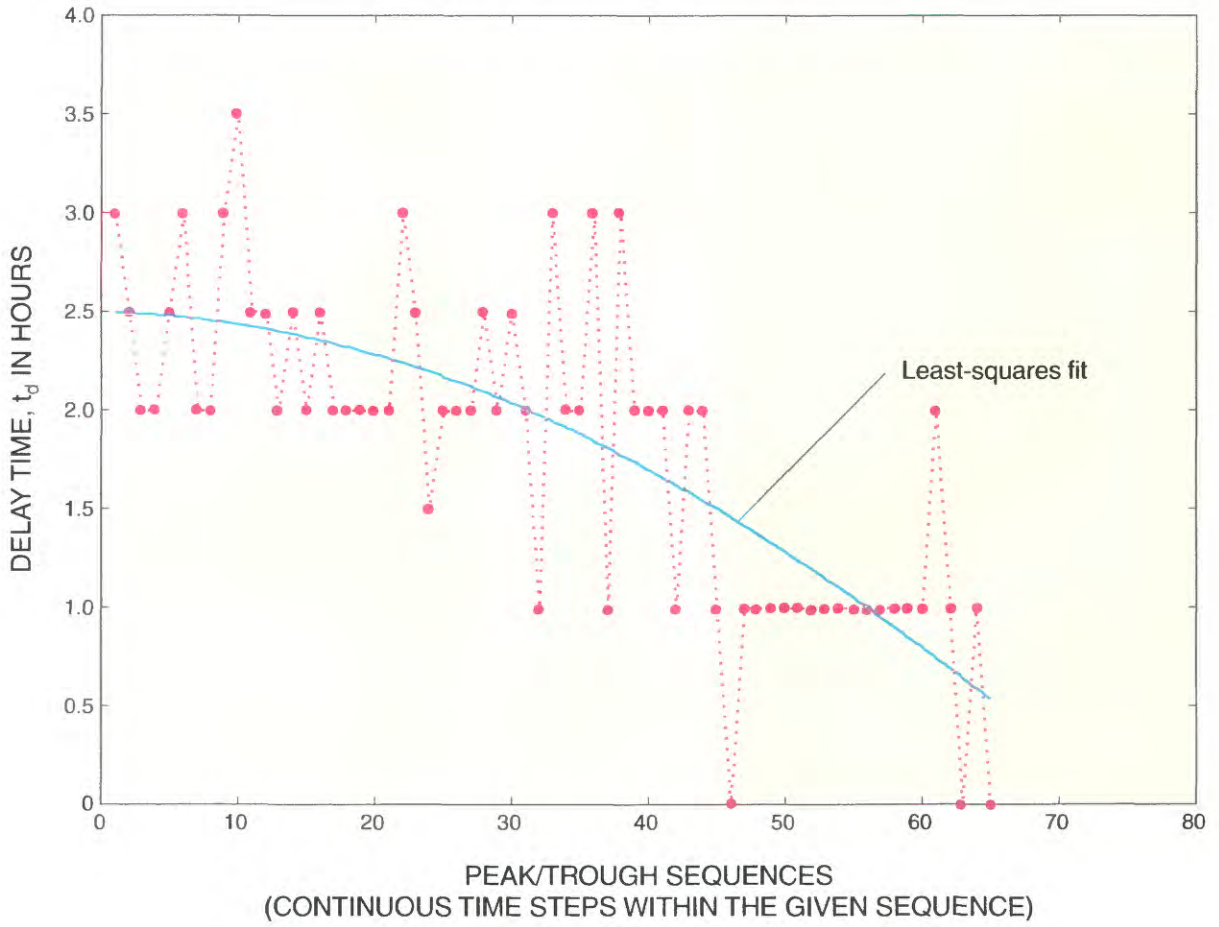

Figure 46. Phase lags in tidal fluctuations between the C-103 Canal and well G-1183.

1991), the leakage relation for the C-103 and C-103-N Canals near structures S-167 and S-166, respectively, is given by:

$$\Delta Q = 0.7 \times 10^6 \left(\frac{s_R}{x_R} + \frac{s_L}{x_L} \right) \text{ ft}^2/\text{d} , \qquad (19)$$

and the leakage relation for the C-103 Canal downstream of structure S-179 can be estimated by:

$$\Delta Q = 0.3 \times 10^6 \left(\frac{s_R}{x_R} + \frac{s_L}{x_L} \right) \text{ ft}^2/\text{d} . \qquad (20)$$

Equations 19 and 20 are appropriate for estimating canal leakage under steady-state conditions (Chin, 1991). To assess the validity of these relations under transient conditions, it is necessary to assess the time scale, t^*, for propagation of a canal disturbance to a distance, x, into the aquifer. This time scale is given by:

$$t^* = \frac{x^2 S_t}{4T} , \qquad (21)$$

where x is the distance from the canal, in feet.

In the case of the C-103 and C-103N Canals near structures S-166 and S-167, equation 21 gives:

$$t^* = \frac{x^2}{4(T/S_t)} = \frac{x^2}{4(6.89 \times 10^7)} = 3.63 \times 10^{-9} x^2 \quad d = 5.22 \times 10^{-6} x^2 \text{ min} ,$$

and for the C-103 Canal downstream of structure S-179, equation 21 gives:

$$t^* = \frac{x^2}{4(T/S_t)} = \frac{x^2}{4(10.2 \times 10^7)} = 2.45 \times 10^{-9} x^2 \quad d = 3.53 \times 10^{-6} x^2 \text{ min} .$$

If head differences between the canal and the aquifer are measured 1,500 ft from the canal (10 aquifer depths), then t^* = 12 and 8 minutes, respectively, for the two cases cited above. In response to changes in canal stage, drawdowns within 10 aquifer depths of the C-103 and C-103N Canals can

Figure 47. Outfalls 1 and 2 in the C-103 Canal.

be expected to equilibrate within minutes, and the steady-state leakage relations given by equations 19 and 20 will be applicable over longer time scales (for example, hours).

Surface Runoff

The adequacy of using conventional software codes to simulate surface runoff in an urban catchment in southern Florida was investigated by measuring the incident rainfall and corresponding surface-runoff from a selected urban catchment, and comparing the measured runoff with that predicted using conventional urban rainfall-runoff codes. An area that drains directly into the C-103 Canal has been delineated by DERM, and is referred to as the C-103/C-16 basin. This basin encompasses an area of 90.7 acres in Miami-Dade County and includes 14.2 percent vacant land, 77.9 percent single-family residential use, and 7.9 percent open water. The average ground elevation is 5.4 ft, and the average water-table elevation is about 2.2 ft NGVD 1929. In modeling this area using the USEPA SWMM code, the Miami-Dade Department of Environmental Resources Management (2000) assumed that the amount of directly connected impervious area (DCIA) is 37.6 percent of the total impervious area, and the average overland slope was estimated as 0.008 percent. The catchment basin contains 64 stormwater inlets connected to nine separate outfalls that discharge into the C-103 Canal.

To measure the runoff hydrographs from this urban catchment, ultrasonic flowmeters were installed to measure flow at 5-minute intervals in two of the nine outfalls entering the C-103 Canal. The two outfalls studied are referred to in this

Table 22. Properties of the drainage systems and catchments associated with outfalls 1 and 2

[--, no data available]

Catchment No.	Structure No.	Type	Grate elevation (feet)	Inlet invert elevation (feet)	Catchment area (square feet)	Directly connected impervious areas (percent)	Length of flow (feet)	Goes to structure	Length (feet)	Diameter (inches)	Slope
					Outfall 1						
64	64	Inlet	5.16	2.38	122,892	24.7	423	66	52	21	0.000
65	65	Inlet	5.22	1.50	73,644	25.4	310	66	35	18	.017
66	66	Inlet	5.26	.90	54,028	24.5	293	67	140	30	.006
–	67	Manhole	5.80	.00	–	–	–	68	200	36	.002
68	68	Inlet	5.35	-.40	44,438	28.9	310	69	30	36	.007
69	69	Inlet	5.31	-.60	92,144	26.6	332	70	100	36	.005
70	70	Inlet	5.60	-1.12	40,825	2.2	338	98	35	36	.005
–	98	Outfall	–	-1.30	–	–	–	–	–	–	–
					Outfall 2						
54	54	Inlet	5.33	1.08	285,523	80.0	668	56	15	21	.007
55	55	Inlet	5.47	1.42	104,531	25.3	408	56	24	21	.024
56	56	Inlet	5.32	.98	18,511	32.9	203	57	45	30	.010
57	57	Inlet	5.75	.55	26,911	16.5	292	61	220	36	.004
58	58	Inlet	5.50	2.05	14,026	25.5	191	59	50	15	.004
59	59	Inlet	5.56	1.85	52,581	21.7	459	61	60	15	.035
60	60	Inlet	5.42	1.52	46,293	28.0	325	61	34	15	.045
61	61	Inlet	5.95	-.25	24,342	30.8	232	62	75	36	.006
–	62	Manhole	5.45	–	–	–	–	63	104	36	.006
63	63	Inlet	6.00	-1.04	20,786	2.3	212	97	45	36	.007
–	97	Outfall	–	-1.85	–	–	–	–	–	–	–

report as outfall 1 and outfall 2, and the catchment areas and inlets associated with these outfalls are shown in figure 47.

The catchment areas corresponding to each of the inlets were delineated using digital orthophotos of the C-103/C-16 basin, topographical data for the roadways and stormwater infrastructure, and physical features (such as streets and houses) that would restrict the flow. Section maps of the study area were available in AutoCAD format, developed by DERM in association with Florida Power and Light. These section maps identified edge and centerline of roads, canal rights-of-way, lakes, buildings, subdivisions, and parcel lines. The detailed properties of the drainage systems and catchments associated with outfalls 1 and 2 are given in table 22. These properties were used in the SWMM and Modeling of Urban Sewers (MOUSE) codes to estimate the surface runoff utilizing the nonlinear-reservoir (kinematic-wave) model, and the computed catchment runoff was compared with the measured runoff to assess the adequacy of the model formulations. More detailed discussions of the SWMM and MOUSE codes are given later in this report. Outfall 1 has a total contributing area of 10.8 acres, a DCIA of 28.6 percent, and an estimated time of concentration of 8 minutes. Outfall 2 has a total contributing area of 9.8 acres, a DCIA of 23.5 percent, and an estimated time of concentration of 6 minutes.

Approach

The primary objective of the surface-runoff study was to assess the accuracy of using a conventional modeling approach to estimate surface runoff from an urban catchment in southern Florida. In the conventional approach, urban catchments are discretized into subcatchments, and runoff hydrographs from each of the subcatchments are routed through the drainage network to a catchment outlet. Simulated subcatchment areas consist of directly connected impervious area (DCIA), directly connected pervious area (DCPA), and nondirectly connected

impervious area (NDCIA). The runoff from each subcatchment is assumed to be equal to the sum of the runoff from the DCIA and DCPA. Runoff from pervious areas are assumed to occur only when the rainfall rate exceeds the infiltration capacity of the pervious area and the cumulative rainfall excess is greater than the depression storage. Runoff hydrographs from impervious and pervious areas commonly are derived from the rainfall and depression storage excess, using the nonlinear reservoir method.

The most frequently used code to develop conventional rainfall-runoff models in the United States is the SWMM code, and a comparable emerging code is the MOUSE code. Details on how these codes are structured are given later. Although these codes are very similar in terms of the basic hydrologic processes incorporated within them, the SWMM and MOUSE codes combine the hydrologic processes in different ways, the codes do not have exactly the same input parameters, and the codes do not yield exactly the same output for equivalent input. This study investigates the accuracy of the SWMM and MOUSE models in simulating the rainfall-runoff relation in positive drainage catchments in the study area and the difference in surface runoff produced by these codes.

Surface Water Management Model (SWMM)

The latest available version of the SWMM code (version 4.31) was used in this study. The RUNOFF module was used to calculate infiltration, depression storage, and surface runoff hydrographs of flow entering the inlets, and the EXTRAN module was used to route the surface runoff through the drainage network. The RUNOFF module generates overland flow from impervious areas with and without depression storage and from pervious areas with depression storage. In all cases, overland flow is generated by approximating the subcatchments as nonlinear reservoirs. The option exists to account for infiltration by using either the Horton or Green-Ampt model; the more conventional Horton model was used in this study. The parameters used in the SWMM code to simulate runoff from the C-103/C-16 basin are given in table 23. The infiltration capacity of the pervious area was assumed to follow the Horton model, with an initial infiltration capacity of 5 in/hr, a final infiltration capacity of 0.4 in/hr, and a decay rate of 5.4 hours^{-1}. These parameters were confirmed during the course of this study from field measurements made in the study area using a double-ring infiltrometer. A ground slope of 0.2 percent was assumed, the average ground elevation was 5.4 ft, and the average water-table elevation was 2.2 ft.

Modeling of Urban Sewers (MOUSE) Model

In the MOUSE code, surface runoff into each inlet is equivalent to the runoff from the DCIA plus direct runoff from the pervious area. The MOUSE code does not have a provision for handling NDCIAs; thus, these areas were designated as pervious. The effect of this assumption is negligible in cases where the NDCIA is small, or the infiltration capacity of the soil is much greater than the rainfall rate. The parameters used in the MOUSE code to simulate runoff from the C-103/C-16 basin are given in table 23. In the MOUSE model, a wetting depth is abstracted from the rainfall prior to infiltration, storage, or runoff, and a wetting depth of 0.002 in. was assumed for the impervious and pervious areas of the catchment. This wetting depth is based on recommendations from the developers of the MOUSE model. After the wetting capacity has been satisfied, direct runoff occurs from the impervious area and infiltration begins on the pervious area. During periods of no rainfall, the infiltration capacity recovers exponentially with a recovery rate of 0.11 hour^{-1}, and Manning's n coefficients of 0.012 and 0.25 were assumed for the impervious and pervious areas, respectively.

In accordance with the Hortonian mechanism, runoff occurs when the rainfall rate exceeds the infiltration capacity. This accumulated runoff first fills the depression storage, then the excess rainfall contributes directly to surface runoff. In specifying best estimates of the depression storage in both the SWMM and MOUSE model, reference was made to Bower and others (1990), who reported that the depression storage for impervious drainage areas varies from 0.0 in. (on a slope of 2.5 percent) to 0.11 in. (on a slope of 1 percent), and estimates of depression storage usually are determined by runoff model calibration. Depression storage values in impervious and pervious areas in the study area were used as calibration variables

Table 23. Parameters in the Surface Water Management Model (SWMM) and the Modeling of Urban Sewers (MOUSE) model

[--, parameter not applicable]

Parameter	Impervious area	Pervious area
SWMM		
Start infiltration (inch per hour)	--	5.0
End infiltration (inch per hour)	--	.4
Exponent (hour^{-1})	--	5.4
Depression storage (inch)	0.02	.04
Manning's n	.012	.25
MOUSE		
Wetting (inch)	.002	.002
Start infiltration (inch per hour)	--	5.0
End infiltration (inch per hour)	--	.4
Exponent (hour^{-1})	--	5.4
Inverse exponent (hour^{-1})	--	.108
Depression storage (inch)	.02	.04
Manning's n	.012	.25

in a similar hydrologic model developed by the Miami-Dade Department of Environmental Resources Management (2000), where initial estimates of 0.02 and 0.2 in. were used for impervious and pervious areas, respectively. In the MOUSE model, the depression storage was 0.02 in. for impervious areas and 0.04 in. for pervious areas. These assumed values were based on the recommendations of the MOUSE developers.

Field Measurements

A field study was conducted to measure the rainfall and corresponding surface runoff from outfall 1 and outfall 2 catchments (fig. 47) in the study area. Stormwater runoff from the selected catchments was captured by the existing drainage infrastructure consisting of grate inlets, catch basins, and subsurface reinforced-concrete pipes discharging by way of outfall pipes into the C-103 Canal.

Flows from the outfall pipes were measured using individual ultrasonic Doppler flowmeters mounted in each outfall pipe. The ultrasonic Doppler flowmeter (fig. 48) consists of a combination of an ultrasonic transducer assembly that is profiled to reduce flow disturbance along with signal-processing electronics. These instruments are designed to be placed at or near the bottom of a water channel for "upward-looking" measurement. A single cable connects the instrument to a 12-volt direct-current power source. Operation of the ultrasonic Doppler flowmeter is shown in figure 49. The two transducers sample a distance from the face of the meter to about 3 ft away from the meter at a 30-degree angle. With this setup, the ultrasonic flowmeter measures the average velocity for a depth of 1.5 ft.

In this study, the instruments were placed in the bottom of 3-ft-diameter outfall pipes. If the velocity is averaged over the bottom 1.5 ft and the average velocity over the bottom 1.5 ft is equal to the average velocity over the top 1.5 ft (because the outfall pipe typically is submerged and flowing full), then the velocity measured by the ultrasonic flowmeter is assumed to be equal to the average flow velocity in the outfall pipe. Consequently, the flowrate through the outfall pipe was equal to the (average) velocity measured by the ultrasonic Doppler flowmeter multiplied by the cross-setional area of the 3-ft-diameter culvert pipe. Rainfall over the catchment areas was assumed to be equal to that collected at the HOMES-FS station about 0.6 mi from the center of the catchment areas.

Analysis of Data

The discharge from (two) outfall pipes draining two urban catchments was monitored at 5-minute intervals for the duration of this study. Because both outfall pipes were mostly submerged during this study, periods of no significant runoff were marked by apparently random fluctuations in the measured flow, and only during significant runoff events were flows well above detected background levels. Measured and simulated runoff for outfalls 1 and 2 are given in table 24.

During the course of this study, eight runoff events (table 24) occurred where the measured flows in the outfall pipes were observed to be substantially above background levels. The measured peak flows are compared to the peak flows computed with the SWMM and MOUSE models (fig. 5). Results indicate that both the SWMM and MOUSE models yield peak runoff rates that are in fair agreement with measured peak runoff rates. Simulated peak flows falling on the solid line in figure 50 indicate exact agreement with measured peak flows, and simulated flows falling between the solid and dashed lines indicate errors of less than 50 percent between the measured and simulated peak flows.

Results shown in figure 50 also indicate that simulated peak flows for outfall 2 tend to be in better agreement with measured peak flows than simulated peak flows for

Figure 48. Ultrasonic Doppler flow meter.

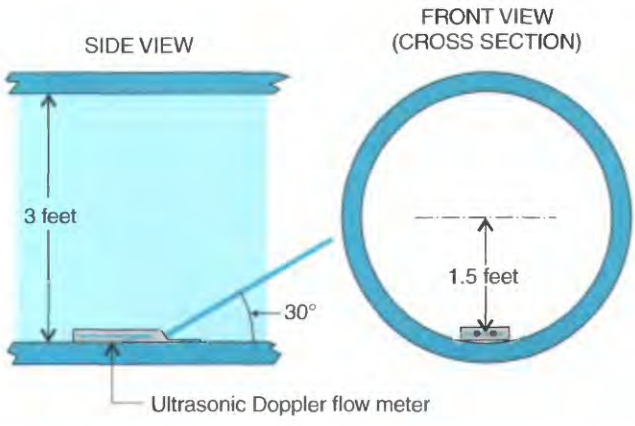

Figure 49. Installation and operation of an ultrasonic Doppler flow event.

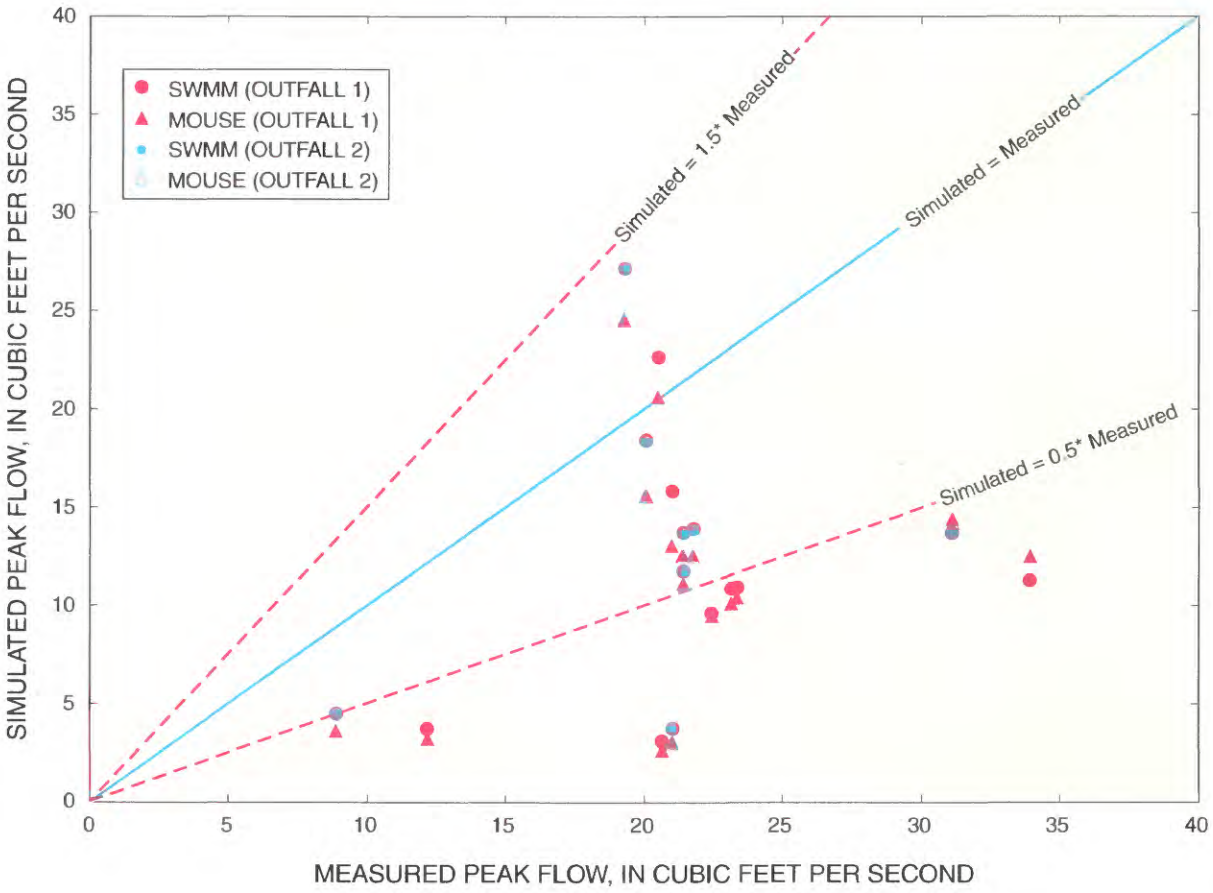

Figure 50. Relation between simulated and measured peak flows. SWMM is Surface Water Management Model, and MOUSE is Modeling of Urban Sewers model.

Table 24. Analysis of measured and simulated runoff for outfalls 1 and 2

[SWMM, Surface Water Management Model; MOUSE, Modeling of Urban Sewers; --, no data available]

Storm	Date and time		Rainfall (inches)	Outfall 1				Outfall 2			
	Start	End		Measured peak (ft^3/s)	SWMM peak (ft^3/s)	MOUSE peak (ft^3/s)	Total runoff (inches)	Measured peak (ft^3/s)	SWMM peak (ft^3/s)	MOUSE peak (ft^3/s)	Total runoff (inches)
1	09-28-01 1200	10-01-01 1200	4.87	21.0	15.9	13.0	1.47	20.1	18.3	15.6	1.68
2	07-01-02 1500	07-04-02 1200	3.75	23.2	10.8	10.2	1.01	21.4	13.7	12.6	1.25
3	07-08-02 1200	07-11-02 1200	5.00	33.9	11.3	12.5	1.43	31.1	13.7	14.3	1.65
4	08-26-01 1200	08-27-01 1200	2.85	20.5	22.7	20.6	1.33	19.3	27.1	24.5	1.41
5	09-12-01 1200	09-13-01 0300	2.54	23.3	10.9	--	.65	21.8	13.9	--	.76
6	09-28-01 1000	09-30-01 1200	4.76	22.4	9.5	--	1.23	21.4	11.7	--	1.42
7	09-01-02 1200	09-02-02 1200	.74	20.6	3.0	--	.17	21.0	3.7	--	.21
8	10-15-02 1200	10-16-02 1200	.49	12.2	3.7	--	.11	8.9	4.5	--	.13

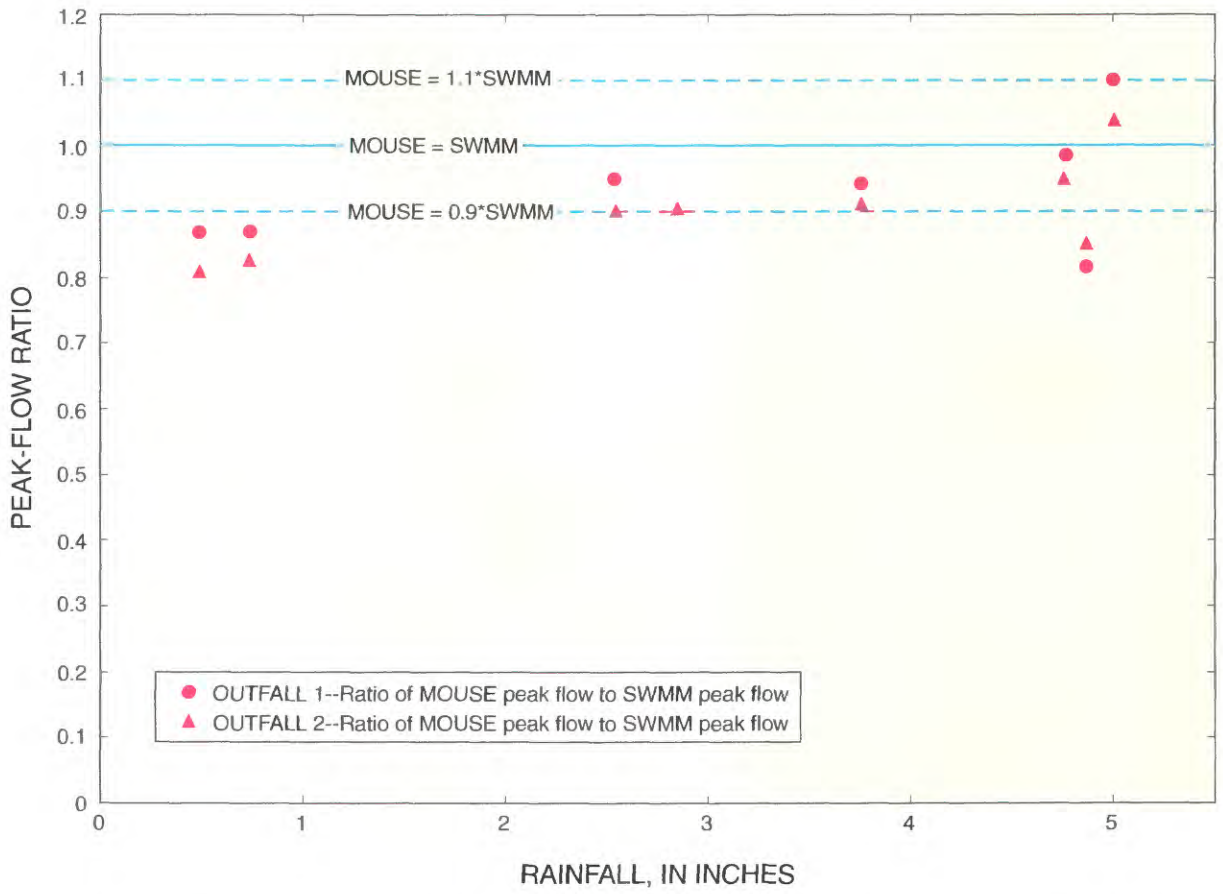

Figure 51. Peak-flow ratio as a function of rainfall for the Surface Water Management Model (SWMM) and the Modeling of Urban Sewers (MOUSE) model.

outfall 1. In assessing the level of agreement between simulated and measured peak flows, it is important to stress that the measured peak flows were not calibrated against direct flow measurements, so the accuracy of the measured peak flows cannot be certified. The measured flows could not be calibrated during the study since it was not impossible to maintain a steady controlled flow through the outfall pipes for a sufficient length of time to measure the flow by an alternative means. Overall, the results indicate that drainage structures designed on the basis of peak flows derived from conventional uncalibrated stormwater models probably have a reasonable degree of accuracy in urban areas of southern Florida.

A direct comparison of the peak runoff of the SWMM and MOUSE models (fig. 51) shows the ratio of the MOUSE peak flow to the SWMM peak flow as a function of total event rainfall for eight significant runoff events (table 24). Points on the solid line indicate exact agreement between the MOUSE and SWMM peak flows, and points falling between the solid and dashed lines indicate less than 10-percent difference between the MOUSE and SWMM peak flows. In most cases, there is less than 10-percent difference between the MOUSE and SWMM peak flows, with maximum variations not exceeding 20 percent.

Whereas both MOUSE and SWMM can provide similar results (fig. 51) for the same problem, the agreement between models is by no means exact. The apparent error, however, between measured and simulated flows (fig. 50) is much greater than that between the MOUSE and SWMM models; therefore, a preferred choice of code cannot be identified. The conclusion is that both models appear to have similar accuracies in estimating peak flows.

The SWMM and MOUSE codes yield different values of peak runoff, even though both use the Horton infiltration model, constant depression storage, the nonlinear-reservoir surface-runoff model, and effectively the same parameters to describe these processes. To provide further assurance that both models were accurately constructed, data files were sent for external review to the Danish Hydraulic Institute (the developers of MOUSE) and CDM Consulting Engineers (a company with extensive SWMM expertise), and the reviewers agreed that both models were for equivalent systems. The SWMM was found to generally predict higher infiltration amounts than MOUSE, suggesting that the discrepancy is related to the infiltration part of the codes.

Surface runoff from urban catchments typically is considered to be the sum of the runoff from the DCIA and runoff

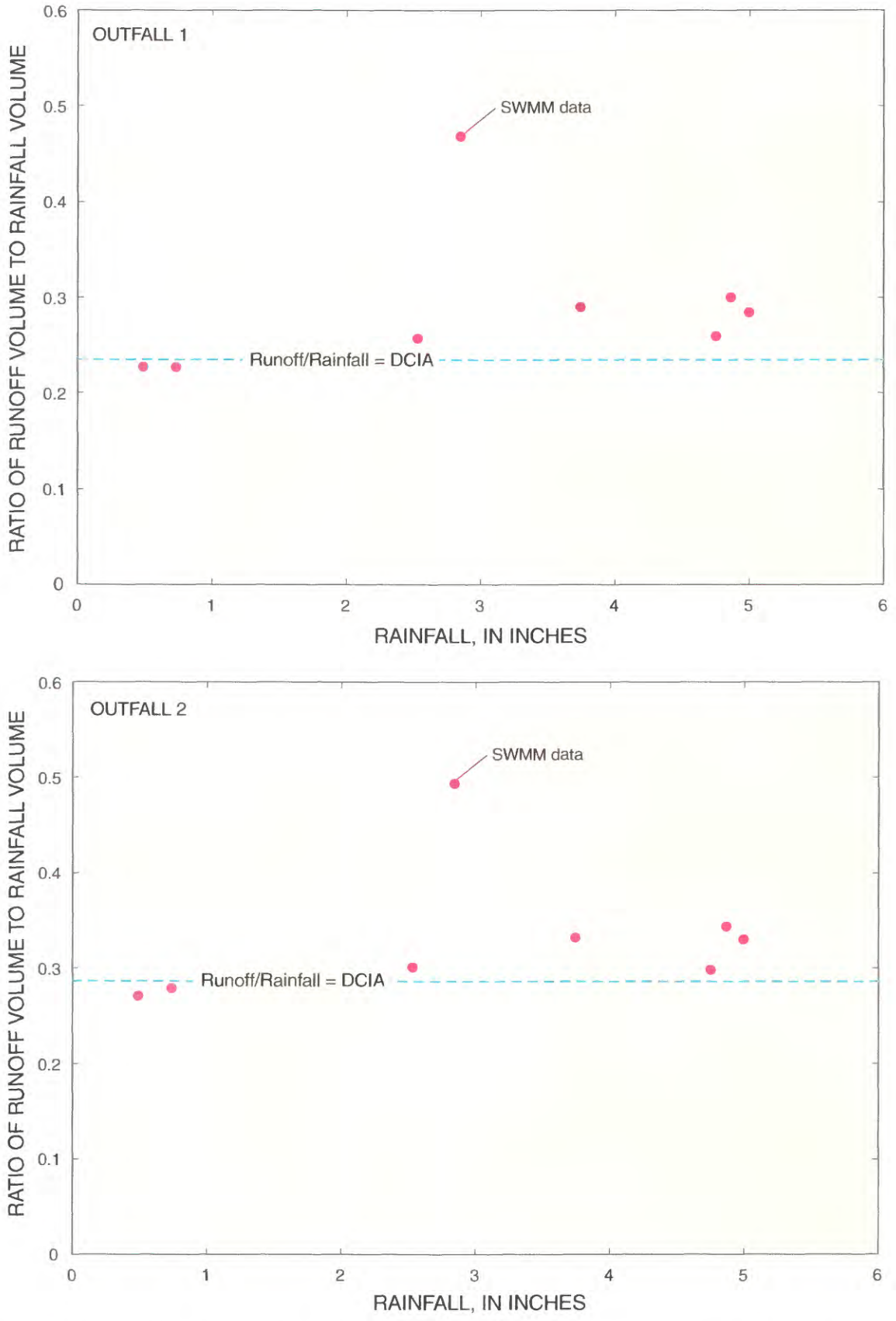

Figure 52. Ratios of the Surface Water Management Model (SWMM) runoff volume to the rainfall volume for outfalls 1 and 2. DCIA is directly connected impervious area.

from the DCPA, with runoff from the pervious area occurring only when the rainfall rate exceeds the infiltration capacity of the pervious area. Given the relatively high infiltration capacities associated with pervious areas in the study area, it is plausible to expect that the accuracy of rainfall-runoff models would be influenced by the accuracy with which DCIA is estimated.

To assess the importance of DCIA in predicting runoff, the ratios of the SWMM runoff volume to the rainfall volume for each of the significant runoff events from the outfall catchment areas were plotted (fig. 52). Points on the dashed lines indicate that the ratio of runoff to rainfall is equal to the ratio of DCIA to total catchment area, which is 23.5 and 28.6 percent for outfalls 1 and 2, respectively.

The results shown in figure 52 indicate that the rainfall-runoff ratio generally is close to the DCIA ratio, indicating that accurate estimation of DCIA is an important element in developing accurate and physically representative surface-runoff models. This assertion is tempered by the fact that estimation of DCIA in many cases can be quite speculative, particularly when the path taken by runoff from driveways and roadways cannot be guaranteed to reach stormwater inlets, such as in the residential areas of southern Florida where curbs and gutters typically do not line the roadways. This can allow DCIA runoff into the grassy areas adjacent to the roadways, thereby decreasing the effective DCIA.

The results shown in figure 52 further indicate that, although the DCIA ratio gives a good indication of the rainfall-runoff ratio, the actual rainfall-runoff ratio is, in most cases, higher than the DCIA ratio. This is most likely a result of the additional runoff from pervious areas. Based on these results, and the dominant influence of DCIA on the rainfall-runoff process in urban areas, more research on the extent of DCIA associated with individual stormwater inlets would be useful for developing more accurate surface-runoff models.

Assessment of Rainfall-Runoff Models

Urban stormwater-management systems are typically assessed using either "planning" or "design" models. Planning models are used for broad assessments of urban runoff problems, and for estimating the effectiveness and costs of abatement procedures. Data requirements are typically kept to a minimum. Conversely, design models are used for detailed simulation of individual storm events, and data requirements may be moderate to very extensive, depending on the particular model being employed (Huber and Dickinson, 1988).

The utilization of the NRCS curve number (CN) approach to calculate surface runoff from individual storm events is widely used in planning models (Bhaduri and others, 2001), and it has been estimated that 60 percent of the hydrologic studies conducted use variants of the CN method (Fennessey and others, 2001). Hydrologic soil group and soil cover are the relevant factors in determining the CN, which usually is treated as a constant even though it is actually a random variable. McCuen (2002) investigated the probability distribution of the CN in five predominantly rural watersheds and reported that the quantity 100–CN fit the gamma distribution, which can then be used to develop confidence intervals for CNs.

Integrated hydrologic models simultaneously simulate surface flow (including overland and channel flow), unsaturated-zone flow, and ground-water flow, and such models are desirable for basin-scale hydrologic models in southern Florida. Integrated models offer the greatest benefit for simulating and linking all components of the hydrologic system in a dynamic manner. Although numerous surface- and ground-water models have been developed separately and used extensively through years of research and field applications, few models have been developed with the objective of fully integrating both surface- and ground-water components of the hydrologic cycle.

A detailed review of current surface-runoff models can be found in Singh and Woolhiser (2002). Because many of these models do not account for the role of ground water on surface-water runoff, they are not applicable to basin-scale models in southern Florida.

In recent years, a few comparative studies have been made of integrated models and semi-integrated models. Kaiser-Hill Company (2001) assessed and ranked several of the most popular commercially available, integrated and semi-integrated models including: (1) MIKE SHE; (2) SWMM; (3) TOPOG-Dynamic (by CSIRO, Australia); (4) SWAT (by USDA); (5) PRMS (by USGS); (6) HSPF (by USEPA); (7) SWRRB (by USDA); (8) DHSVM (by the U.S. Department of Energy); and (9) MODBRANCH (by USGS). A study by Camp, Dresser, & McKee (2001) yielded the following overall ranking of integrated and semi-integrated hydrologic models: (1) MIKE SHE; (2) MODFLOW; (3) HSPF; (4) SWMM; and (5) MODBRANCH. Only in the case of MIKE SHE was the linkage of ground- and surface-water components created as part of a unified model development process, and this model was not at the top of the list in both comparative studies.

MODBRANCH was created by linking previously developed surface- and ground-water models, the MODFLOW ground-water code was enhanced with the addition of interactive surface-water packages, and the SWMM and HSPF catchment-scale surface-water codes were enhanced with ground-water representational capabilities. In the Tampa Bay area of west-central Florida, HSPF and MODFLOW were joined together into a single program called the ISGW model that simulates the interaction of surface water and ground water. Both MODFLOW and SWMM are used widely and have a high degree of regulatory acceptance.

Discharge through water-control structures in canals typically is calculated as a function of headwater elevation, tailwater elevation, and gate opening. The discharge equations for southern Florida structures are coded into the FLOW computer program for automatic computation. In southern Florida,

the most commonly used structures are gated spillways, gated culverts, and weirs. Details of the appropriate equations for calculating flows through control structures in southern Florida can be found in Otero (1995).

The importance of an integrated model to simulate canal flows with hydraulic structures was highlighted by Allman and others (1979), who noted that low head differentials develop across canal structures where the aquifer transmissivity is high. Accounting for this phenomenon is important because it prevents optimal canal stages from being maintained during the dry season.

The Subsurface Waste Injection Program (SWIP) code was used by Merritt (1996) to develop a comprehensive model of the surface- and ground-water system in southern Miami-Dade County, and monthly time steps were used in this model. (The SWIP code was developed by INTERCOMP Resource Development and Engineering, Inc., in 1976 under the sponsorship of the USGS.) MODFLOW was used by Restrepo and others (1992) to develop a three-dimensional model of the surficial aquifer system in Broward County. Model cells were 1,000 ft in the east-west direction and 2,000 ft in the north-south direction, and monthly time steps were used. In assessing their model, Restrepo and others (1992) noted that a fully integrated, unsaturated and saturated flow model should be developed for Broward County, with finer grid spacing and with stress periods much shorter than 1 month (ideally 5 days or less). Trimble (1986) used a node/link formulation to develop the South Florida Regional Routing Model to simulate the movement of water on monthly time scales.

The accuracy of several rainfall-runoff models was assessed by Trommer and others (1996), who measured the rainfall and corresponding runoff in 15 west-central watersheds, and then compared the peak runoff rates, runoff hydrographs, and runoff volumes with simulation results from several commonly used runoff models. The models used by Trommer and others (1996) were the: (1) rational method, (2) USGS regression equations, (3) NRCS TR-20 model (which uses the CN method), (4) USACE HEC-1 model, and (5) USEPA SWMM model. The watersheds studied by Trommer and others (1996) ranged from fully developed urban to undeveloped natural watersheds and from 90 acres to 15 mi^2 in size. Watersheds in southern Florida tend to have flatter slopes, more permeable soils, lower stream gradients, higher ground-water levels, and larger wetland areas than watersheds used in the development of many of these models (Trommer and others, 1996). The key findings from Trommer and others (1996) are as follows:

- The rational method overestimated the peak discharges for all watershed types with less error in urban than natural or mixed watersheds.
- The TR-20 CN model tended to overestimate the peak discharges and runoff volumes for storms occurring in all watershed types; errors decreased as the average CN of the watershed increases.
- In applying the SWMM model, comparisons of estimated and observed peak discharges and runoff volumes (calculated with the Green-Ampt and Horton infiltration models) report were similar; peak discharges for most storms were overestimated, and estimates of runoff volume were more accurate.

Mean estimation errors for peak discharge indicate that the Green-Ampt and Horton infiltration methods are more accurate for urban watersheds than for mixed or natural watersheds. For urban watersheds, the USGS regression equations, TR-20 model, and SWMM model using the Green-Ampt and Horton infiltration methods had standard estimation errors less than 65 percent. The rational and HEC-1 models had standard errors of 193 and 121 percent, respectively. In estimating runoff volume, the SWMM model (with the Green-Ampt and Horton infiltration methods) had standard estimation errors of 26 and 44 percent, respectively, for urban watersheds. The TR-20 and HEC-1 models had standard errors of about 60 percent, and the USGS regression equation had a standard error of about 81 percent for the urban watersheds. Comparing the model predictions based on standard errors, Trommer and others (1996) concluded that the TR-20 model was more accurate than the other models in estimating the peak discharge, and the SWMM model with the Green-Ampt infiltration was more accurate for estimating runoff volumes.

The widespread utilization of GIS is causing a fundamental shift from lumped to distributed watershed models (Ogden and others, 2001a), with the controlling factors in this shift being data availability, GIS-module development, fundamental research on the applicability of distributed hydrologic models, and regulatory acceptance of these new tools and methodologies. Rainfall-runoff relations are quite variable for small rainfall events, which can be related to the importance of initial soil moisture conditions for these events (Seibert, 2001). In these cases, continuous models may perform better than event-based models. In flood forecasting, event-response models often are sufficient, eliminating complexities of continuous moisture accounting, evaporation, and long-term dynamics.

The uncertainty in (mathematical) model output is a function of both the uncertainty in the input data (measurement errors, heterogeneity, and effective values for a grid cell) and the process description. The phenomenon that equally good model simulations might be obtained in many different ways, called "equifinality," is commonly found in hydrologic modeling (Seibert, 2001).

MIKE SHE

The MIKE SHE code is named after Michael B. Abbott (MIKE), principal author of the code, and the Systéme Hydrologique Européen, SHE (Abbott and others, 1986a; 1986b). A description of the MIKE SHE code can be found in Refsgaard and Storm (1995). The MIKE SHE code is widely used internationally, but is less well known in the United States. MIKE SHE is the standard code used for hydrologic

analysis in many European countries (Singh and Woolhiser, 2002). According to Kaiser-Hill Company (2001), MIKE SHE represents each of the three main hydrologic processes and their dynamic interaction (surface flow, unsaturated-zone flow, and ground-water flow) as well or better than all other codes reviewed. MIKE SHE is distributed in space and time; uses spatial and temporal data; and is capable of providing a variety of output types, such as time series of streamflow at different points on the drainage channel and two-dimensional maps of ground-water levels. The MIKE SHE code is limited to square grids and is capable of using digital elevation model data directly. The code uses ArcView as the basis for most of its graphical interfacing, and has several extensions written directly in ArcView for contouring and data visualization and manipulation. MIKE SHE is an externally coupled conjunctive model (Freeze, 1972; Morita and Yen, 2002), in which the surface-flow submodel and subsurface-flow submodel are solved separately in succession without iteration between the submodels.

By discretizing the catchment area into a large number of grid squares and layers, water-flow processes can be simulated, accounting for spatially variable input such as soil hydraulic properties, ground slope, and land cover. Nevertheless, previous studies have noted that the impact of grid size on simulation time is high (Xevi and others, 1997). Variability within the catchment, therefore, can be accounted for at the cost of increased calculation time, if the available measurements have the necessary detail. In a recent study that focused on the sensitivity of model output to various soil hydraulic properties, Christiaens and Feyen (2002) used grid squares of 3,281 × 3,281 ft (100 × 100 m) to model a 247.1-acre (1 km^2) catchment. The performance of the MIKE SHE code on a variety of catchments is still an active area of research (Vázquez and Feyen, 2003).

Surface Flow

Surface flow includes both overland flow and flow through canals. For overland flow, the MIKE SHE model uses the two-dimensional kinematic-wave approximation. The overland-flow equation, also called the diffusive-wave equation, is given by:

$$\frac{\partial h}{\partial t} + (8g)^{1/2}\ \frac{\partial}{\partial x}\left(\frac{S_o^{1/2} h^{3/2}}{f^{1/2}}\right) - q - r - f_i = 0\,, \qquad (22)$$

where h is the flow depth, t is time, g is the acceleration due to gravity, S_o is the slope of the ground, f is the Darcy-Weisbach friction factor, q is the lateral inflow rate, r is the rainfall rate, and f_i is the infiltration loss rate. Specific hydrologic processes, such as rill flow, are not considered in this code, but this limitation is not expected to be major at the scales normally used.

Channel and reservoir routing are simulated using the Saint-Venant equations, given by the continuity equation:

$$\frac{\partial Q}{\partial x} + \frac{\partial A}{\partial t} = 0\,, \qquad (23)$$

and the momentum equation:

$$\frac{1}{A}\frac{\partial Q}{\partial t} + \frac{1}{A}\frac{\partial}{\partial x}\left(\frac{Q^2}{A}\right) + g\frac{\partial y}{\partial x} - g(S_o - S_f) = 0\,, \qquad (24)$$

where A is the cross-sectional area of the channel, Q is the flowrate, y is the water depth, x is the distance along the channel, S_o is the channel slope, and S_f is the friction slope. Control structures, such as gates and culverts, also can be simulated. Application of the Saint-Venant equations to flow in open channels is commonly called hydraulic routing, and the small slopes (less than 0.5 percent) of canals in southern Florida typically require the use of hydraulic routing equations to describe flow in the canals.

Unsaturated Zone

The MIKE SHE code assumes that flow in the unsaturated zone is one-dimensional and vertical. Flow can be horizontal in certain locations (such as near buildings/paved areas or below trenches), causing the vertical-flow assumption to be violated. This effect is probably negligible when averaged over a grid. Unsaturated-zone processes not simulated by MIKE SHE include hysteresis and air entrapment. Vertical flow through the unsaturated zone is simulated using the following form of the one-dimensional Richard's equation:

$$C(\psi)\frac{\partial \psi}{\partial t} = \frac{\partial}{\partial z}\left[K(\psi)\frac{\partial \psi}{\partial z} + K(\psi)\right] - S\,, \qquad (25)$$

where $C(\psi)$ is the specific water capacity (also called the specific moisture capacity), ψ is the pore-water pressure, $K(\psi)$ is the unsaturated hydraulic conductivity, and S is the sink term.

Two hydraulic functions are required as input to simulate water flow in the soil profile: (1) the moisture-retention characteristic, $\theta(h)$; and (2) the hydraulic conductivity curve, $K(\theta)$. The MIKE SHE code utilizes the van Genuchten (1980) moisture-retention characteristic given by:

$$\theta(h) = \left[(\theta_s - \theta_r)\left(\frac{1}{1 + (\alpha h)^n}\right)^m\right] + \theta_r\,, \qquad (26)$$

where $\theta(h)$ is the soil-water content (dimensionless), h is the soil-water pressure head (L), θ_s is the saturated water content (dimensionless), θ_r is the residual water content (dimensionless), α is the inverse of the air entry value (L^{-1}), and n and m are shape parameters (dimensionless). The hydraulic conductivity curve used in the MIKE SHE code has the Brooks and Corey (1964) form given by:

$$K(\theta) = K_{sat}\left(\frac{\theta - \theta_r}{\theta_s - \theta_r}\right)^N\,, \qquad (27)$$

where K_{sat} is the saturated hydraulic conductivity. Correlations between the model parameters in the van Genuchten (1980) moisture characteristic and the Brooks and Corey (1964) hydraulic conductivity for several USDA soil textures were noted by Meyer and others (1997).

Saturated Zone

The MIKE SHE code assumes that the aquifer properties are uniform within a single grid cell, so effective parameters over the length scale of the grid must be used. The code uses a finite-difference formulation to solve the three-dimensional Boussinesq relation:

$$\frac{\partial}{\partial x}\left(K_{xx}\frac{\partial h}{\partial x}\right)+\frac{\partial}{\partial y}\left(K_{yy}\frac{\partial h}{\partial y}\right)+\frac{\partial}{\partial z}\left(K_{zz}\frac{\partial h}{\partial z}\right)-W=S_s\frac{\partial h}{\partial t}, \quad (28)$$

where K_{xx}, K_{yy}, and K_{zz} are the saturated hydraulic conductivities in the x-, y-, and z-coordinate directions, respectively; h is the piezometric head; W is a localized water source or sink; and S_s is the specific storage. Multiple layers can be used to apply the finite difference form of equation 28 to determine the distribution of piezometric head in the saturated zone.

Applications in Southern Florida

A few recent studies have applied the MIKE SHE code in southern Florida, including a study of water-management practices in central Broward County (McCue and others, 2002). Results of the aforementioned study were used to identify structural and operational changes needed to maintain or improve existing flood protection, increase the use of existing storage capacity within the stormwater-management system, increase well-field recharge, improve wetland sustainability, and reduce the threat of saltwater intrusion.

In this application, the MIKE SHE model used 500-ft square grid cells with five layers, including primary and secondary drainage canals, and hydraulic control structures such as gates, culverts, and pumps. Rainfall data at four gaging stations in an area encompassing 385 mi^2 were used to generate daily rainfall amounts, and the daily rainfall data were distributed spatially using Theissen polygons. Some soil parameters were adjusted during model calibration to correctly simulate ground-water dynamics and actual evapotranspiration. The moisture contents at saturation, field capacity, wilting point, and saturated hydraulic conductivity were used as calibration parameters and adjusted within the ranges that are typical of soils in the study area. A constant infiltration capacity was assumed in the model.

In applying the MIKE SHE code, McCue and others (2002) reported that the overland flow approach was by far the least time consuming to set up, when calculating direct runoff from impervious areas, because the driving force represents gravity and the primary input data represent land-surface elevation. McCue and others (2002) further noted, however, that this approach suffers a number of shortcomings when used to simulate an urban stormwater drainage system. A precise digital elevation model must be available, and a reasonably fine horizontal discretization must be applied to simulate flow paths with reasonable precision. If the stormwater drainage system does not follow the larger-scale topographic slopes of the digital elevation model, the overland flow approach does not simulate the actual drainage conditions. To alleviate this problem, each water-control district was considered an individual subbasin, and urban runoff was routed to a canal or a pond within the subbasin. The percentage of imperviousness was used as a runoff coefficient for each model cell and varied from 0 to 0.4. The urban runoff then is calculated by multiplying the rainfall by the fraction of imperviousness and the runoff is routed to a prescribed canal or pond within the subbasin. A possible improvement in the model could be accomplished by explicitly accounting for the DCIA in the computation of direct runoff that is routed to ponds and canals.

The MIKE SHE model also was applied in the development of an integrated model for the Caloosahatchee reservoir. This application was done primarily to assess the interactions between ground water and surface water (Jacobsen, 1999).

Surface Water Management Model (SWMM)

The Surface Water Management Model (SWMM) code is well documented and used widely for the simulation of urban-runoff quantity and flow routing to storm and combined sewers. This code uses a link-node formulation where links represent hydraulic elements for flow transport through the system (for example, pipes and channels), and nodes represent the junctions of hydraulic elements (links) as well as locations for input of flow into the drainage system. The SWMM code incorporates a wide variety of hydrologic process models, and for several processes, the user can choose which models to include in a simulation. This section focuses on those models that are addressed as part of the present study.

Surface Flow

The SWMM code is capable of using a variety of methods to simulate the infiltration process. These methods include the Horton, Green-Ampt, initial/continuing loss, proportional loss, and NRCS method with optional subsurface routing. In applying the Horton model, the infiltration capacity is estimated using the relation:

$$f_p = f_\infty + (f_o - f_\infty)e^{-\alpha t}, \quad (29)$$

where f_p is the infiltration (ponded) capacity of the soil, f_∞ is the ultimate infiltration rate under saturated conditions, f_o is the initial infiltration rate under dry conditions, α is the decay coefficient, and t is the time from the beginning of the storm.

The code incorporates nine different models for calculating runoff hydrographs, including nonlinear runoff routing, NRCS unit hydrographs (curvilinear or triangular), kinematic wave, Clark hydrograph, Snyder hydrograph, Nash hydrograph, Santa Barbara unit hydrograph, Laurenson's nonlinear runoff routing (RAFTS), and the rational method. In the nonlinear reservoir model, the runoff, Q, is related to the depth of water, d, over the catchment by the relation:

$$Q = \frac{1}{n}(d - d_p)^{5/3} S^{1/2} W \quad , \qquad (30)$$

where n is Manning's roughness coefficient, d_p is the depth of depression storage, S is the slope of overland flow, and W is the width of overland flow. The recovery of depression storage between storms is achieved by means of evaporation and exponential recovery of infiltration capacity. Up to 100 subcatchments can be defined. For channel flow, either the kinematic-wave equation or the Saint-Venant equations can be used to route the flow.

Subsurface Flow

Subsurface hydrology is simulated using the upper (unsaturated) zone and the lower (saturated) zone. The flow from the unsaturated zone to the saturated zone is controlled by a percolation equation, and evapotranspiration is the only loss from the unsaturated zone. Inflow to the unsaturated zone comes from infiltration computed either by the Horton or Green-Ampt equation. Once the unsaturated zone becomes saturated, infiltration losses are shut off and larger surface runoffs are possible from pervious areas. Losses and outflow from the saturated zone may be through deep percolation, saturated-zone evapotranspiration, and ground-water flow. Ground-water flow is a user-defined power function of water-table stage, and optionally, depth of water in the discharge channel.

Modeling of Urban Sewers (MOUSE)

The comprehensive surface-runoff MOUSE code simulates surface runoff, open-channel flow, pipe flow, water quality, and sediment transport in urban drainage systems. Rainfall excess is calculated assuming a Hortonian runoff mechanism. The surface-runoff module in MOUSE has the option of using three alternative methods for calculating the runoff hydrograph from the rainfall excess: time-area method, nonlinear reservoir method, and the linear-reservoir method.

The effective rainfall rate, I_e, at time, t, is defined by the relation:

$$I_e(t) = I(t) - I_E(t) - I_W(t) - I_I(t) - I_S(t), \qquad I_e \geq 0 \quad , \quad (31)$$

where $I(t)$ is the actual rainfall rate, I_E is the evaporation-loss rate, I_W is the wetting-loss rate, I_I is the infiltration-loss rate, and I_S is the surface-storage loss rate.

Evaporation losses are of less importance in single-event simulations; however, evaporation accounts for a large part of hydrologic losses on a long-term basis. If included in the computation, evaporation losses are accounted for by the following relations:

$$I_E(t) = \begin{cases} I_{PE}(t) & I(t) \geq I_{PE} \text{ or } y(t) > 0 \\ I(t) & I(t) < I_{PE} \text{ and } y(t) = 0 \end{cases} \quad , \qquad (32)$$

where $I_{PE}(t)$ is the potential evaporation at time t, and $y(t)$ is the accumulated depth at time t. When rainfall begins, part of it is used for wetting the surface, if the surface is dry initially. The MOUSE code assumes that the rainfall remaining after subtraction of the evaporation loss is used for wetting the catchment surface. When the catchment surface is wet, the wetting loss, I_W, is set to zero. The wetting process is described by the following relations:

$$I_W(t) = \begin{cases} I(t) - I_E(t) & y(t) < y_w \\ 0 & I(t) \leq I_E \text{ or } y(t) \geq y_w \end{cases} \quad , \qquad (33)$$

where y_w is the wetting depth. The infiltration-loss rate, I_I is calculated using the Horton equation, which can be put in the form:

$$I_I(t) = I_{min} + (I_{max} - I_{min}) e^{-\alpha t} \quad , \qquad (34)$$

where I_{min} is the minimum infiltration capacity, I_{max} is the maximum infiltration capacity, and α is the infiltration decay factor.

In the dry period following a rainfall event, the infiltration capacity gradually recovers to its initial value, using the following inverse form of Horton's equation:

$$I_I(t) = I_{IT} + (I_{max} - Q_{IT}) e^{-1/(\beta t)} \quad , \qquad (35)$$

where I_{IT} is the infiltration capacity between the wetting and drying periods, Q_{IT} is the infiltration capacity between the wetting and drying periods, β is the time factor for drying conditions, and t is the time since the start of the recovery process.

The surface-storage rate, I_S, is equal to the loss due to filling of depressions in the terrain. The surface-storage calculation begins after the wetting process is completed, and the surface storage is filled only if the current infiltration rate is smaller than the actual rainfall intensity reduced by evaporation. The surface-storage process is described by the following relation:

$$I_S(t) = \begin{cases} I(t) - I_E(t) - I_W(t) - I_I(t) & y(t) < y_w + y_s \\ 0 & y(t) > y_w + y_s \end{cases} \quad , \qquad (36)$$

where y_s is the surface-storage depth.

Substituting equations 32, 33, 34 or 35, and 36 into equation 31 yields the effective rainfall (or rainfall excess), I_e, over the catchment. This rainfall excess generates surface runoff when the effective rainfall is greater than zero.

The runoff hydrograph is calculated from the rainfall excess using a nonlinear reservoir model for the entire catchment. The surface runoff $Q(t)$ at time t is calculated using Manning's equation in the form:

$$Q(t) = MBI^{1/2} y_R^{5/3} \quad , \qquad (37)$$

where M is the Manning number, B is the catchment width, I is the surface slope, and y_R is the runoff depth determined from the continuity relation:

$$I_e(t)A - Q(t) = \frac{dy_R}{dt}A \ , \qquad (38)$$

where A is the catchment area.

The runoff hydrograph, $Q(t)$, from the catchment provides the input hydrograph for the pipe-network simulation. To simulate flow in the subsurface drainage pipes, the MOUSE code applies the one-dimensional conservation of mass and momentum equations, also known as the Saint Venant equations, given by:

$$\frac{\partial Q}{\partial x} + \frac{\partial A}{\partial t} = 0 \ , \qquad (39)$$

and

$$\frac{\partial Q}{\partial t} + \frac{\partial}{\partial x}\left(\alpha\frac{Q^2}{A}\right) + gA\frac{\partial y}{\partial x} + gAS_f = gAS_o \ , \qquad (40)$$

where x is the distance in the flow direction, A is the cross-sectional flow area in the pipe, y is the flow depth, α is the velocity distribution coefficient, S_f is the friction slope, and S_o is the pipe slope. Simultaneous solution of equations 39 and 40 determine the water depth and flowrate in the drainage pipes as a function of time.

In the MOUSE code, the drainage network is defined as nodes and links. Several types of nodes exist, with each type representing a different structural element in the drainage network. A list of the types of nodes in the MOUSE code is given in table 25. Links represent various types of conduits, including pipes and open channels, and are bounded on the upstream and downstream side by nodes. The types of links available in MOUSE include standard pipes, trapezoidal canals, and arbitrarily shaped links specified through tables or through the cross-section database.

Table 25. Types of nodes in the Modeling of Urban Sewers (MOUSE) code

Node type	Description
Inlet	Surface runoff from a catchment enters the drainage system at inlet nodes.
Manhole	Used to model all network nodes where the shape and volume can be sufficiently and accurately approximated by a vertical cylinder of a specified diameter.
Basin	An arbitrarily shaped structure resembling pump sumps, detention basins, or other structures with substantial volume.
Storage node	A dimensionless node used for a controlled routing (e.g. surcharged water).
Outlet	A node where the simulated system interacts with receiving waters.

MODBRANCH

The MODBRANCH code (Swain and Wexler, 1996) consists of the MODFLOW model (McDonald and Harbaugh, 1988) coupled with the BRANCH model (Schaffranek, 1987). This code simulates the interaction between streamflow and subsurface flow in areas with dynamic, hydraulically connected, ground- and surface-water systems coupled at the stream/aquifer interface. The USGS has applied MODBRANCH to areas in southern Florida involving the interaction of canals and the surficial aquifer system, as well as to river/aquifer systems in the Pacific Northwest. The MODBRANCH also is widely used by the USACE.

In using the MODBRANCH code, there are important limitations that must be considered. The BRANCH model does not handle loop channels or the wide variety of hydraulic structures found in southern Florida canals and surface-storage systems. The MODBRANCH code is limited to rectangular grids with constant width for each column and row, so the iterative linkage between ground water and surface water results in relatively long computation times.

Surface Flow

Storm runoff must be provided by an external model, and the dynamic-flow equations are used to simulate flow in the open-channel network. Streams in a network are divided into segments associated with cells of the MODFLOW grid in a manner similar to other MODFLOW packages that simulate rivers and streams.

Leakage between a stream and an aquifer is expressed as a function of streambed conductance and the difference between the stream stage and the head in the aquifer. The rate of leakage from the aquifer to the stream, Q_L, is estimated by assuming that leakage occurs across a low-permeability streambed, and that this leakage can be quantified using the approximate Darcy relation:

$$Q_L = -K'\frac{h-Z}{b'}LW \ , \qquad (41)$$

where K' is the hydraulic conductivity of the streambed; h is the head in the aquifer; Z is the elevation of the water surface in the stream; b' is the streambed thickness; L is the length of the stream segment within the finite-difference cell; and W is the stream width, which is an approximation to the wetted perimeter of the channel.

Equation 41 can be conveniently written as:

$$Q_L = C_s(h-Z) \ , \qquad (42)$$

where C_s is called the streambed conductance.

In cases where the stream penetrates several groundwater layers, total leakage is estimated as the sum of the contributions to the various layers using the following leakage relation:

$$Q_L = \sum_{k=1}^{N} [C_{sk}(Z - h_k)] \quad , \qquad (43)$$

where N is the number of aquifer layers penetrated by the stream, C_{sk} is the streambed conductance of the part of the stream in layer k, and h_k is the piezometric head in the aquifer in layer k.

In the MODBRANCH code, the BRANCH component is modified by adding the leakage term to the continuity equation. Recently, Nemeth and Solo-Gabriele (2003) and Nemeth and others (2000) improved the MODBRANCH code by incorporating the more realistic reach transmissivity model of Chin (1991). Besides providing a more realistic leakage formulation, the efficiency of the model code was improved substantially by reducing run times by about 40 percent for a wide range of problems. If the head in the aquifer is below the base of the streambed, then the water lost as leakage from the stream must pass through the unsaturated zone underlying the perched stream. In this case, the leakage relation is given by:

$$Q_L = -K' \frac{Z_B - Z}{b'} LW \quad , \qquad (44)$$

where Z_B is the elevation of the bottom of the stream. Perched streams do not exist for primary canals in southern Florida, but may exist for secondary drainage canals.

Unsaturated and Saturated Zones

Flow through the unsaturated zone is not simulated in the MODBRANCH model. Recharge to the saturated zone is entered directly by the user. Estimates of recharge generally are related to rainfall amounts; however, the code documentation does not provide guidance on how recharge should be estimated.

Evapotranspiration, pumpage, and injection of water from the saturated zone are simulated as separate processes handled by the MODFLOW modules. The Wetlands package was developed for MODFLOW by the SFWMD to simulate distributed overland flow in natural areas.

MODNET

The MODNET code (WEST Consultants, Inc., and Gartner Lee, Ltd., 1999) was created by coupling the SFWMD version of MODFLOW (McDonald and Harbaugh, 1988) with the UNET channel flow model (U.S. Army Corps of Engineers, 1996). The current version (2003) of UNET is 3.2, and the model is maintained and distributed by the USACE Hydrologic Engineering Center. The SFWMD version of MODFLOW differs from the standard version in that it contains a modified LAKE routine (Council, 1997; Nair and Wilsnack, 1998) and an added WETLAND routine (Restrepo and Montoya, 1997). In contrast to the BRANCH model, UNET includes the ability to simulate looped channels and numerous hydraulic structures, including spillways, weirs, levees, culverts, pumps, gates, and storage areas. The coupling between the MODFLOW and UNET components of the MODNET model follows an approach similar to that developed for MODBRANCH.

The MODNET documentation contains an erroneous illustration of the use of the reach transmissivity parameter. The channel conductance approach that is implicit in MODNET assumes that the channel is lined with a layer of known hydraulic conductivity and thickness, and that the leakage is linearly proportional to the difference between the stage in the canal and the head in the surrounding aquifer. In contrast, the reach transmissivity is based on the assumption that no restrictive channel lining exists (at least none on the sides of the channel), and the reach transmissivity is the proportionality factor between the leakage and the difference between the stage in the canal and the head in the aquifer at a specified distance from the canal. Based on the differences in formulation, the MODNET channel conductance cannot be derived directly from the reach transmissivity, and a different formulation is required.

Summary and Conclusions

The objectives of this study were to: (1) review previous hydrologic studies to identify phenomenological models appropriate for describing storm-event scale hydrologic processes in southern Florida, (2) collect field data to develop improved process equations, and (3) review and assess the adequacy of existing hydrologic models that currently are being used in southern Florida. These efforts led to the following findings:

- A study of the rainfall characteristics within a 100-mi^2 area in Miami-Dade County demonstrated that: (1) rainfall amounts in individual storms tend to be significantly correlated over distances of about 2 mi; (2) rainfall durations tend to be significantly correlated over distances of about 4 mi; and (3) rainfall amounts (for storm events with durations of at least 24 hours) tend to be significantly correlated over distances of about 4 mi.

- Observed 24-hour hyetographs tend to be much more uniform than the SFWMD/NRCS Type III hyetograph, which has a characteristic peak in the center of the storm.

- Based on comparison of data from rain gages at the same site, errors of 50 percent are associated with measured storm-event rainfall amounts of 0.1 in., errors of 25 percent are associated with storm-event rainfall amounts of about 0.2 in., and errors of 10 percent are associated with storm-event rainfall amounts greater than 1 in.

- Rainfall measurements would need to be collected from rain gages with spacings of less than 1 mi to accurately characterize the temporal and spatial details of hourly rainfall amounts.

- Daily rainfall amounts are correlated over longer length scales than hourly rainfall; therefore, a smaller density of rainfall measurements is justified in hydrologic models with daily time steps in lieu of hourly time steps.

- Models must account for a significant difference between rainfall characteristics in coastal areas compared to those in inland areas.

- Infiltration capacities can be estimated based on the USDA hydrologic soil groups assigned to local soils.

- Some infiltration capacities can be estimated based on soil texture. Because of the limited number of measurements, reliable estimates can only be achieved for sandy loam, loamy sand, loam, and silty clay loam.

- Infiltration capacities associated with various hydrologic soil groups and soil textures in the study area are higher than frequently reported in the literature. The reason for higher values of infiltration capacity is that literature values typically are for bare soil or derived from laboratory measurements, whereas the infiltration capacities determined in this study were obtained from field measurements and included surface cover and associated macropores.

- Infiltration capacities should not be assigned based on land use. Soil texture and land use, however, were found to have an identifiable relation, with coarse-textured soils predominant in densely developed areas. Hydrologic soil group and land use did not show a clear relation.

- Most infiltration capacities obtained in the study area during the investigation exceeded the maximum (hourly) rainfall rate measured from 1997 to 2002. This result indicates that most rainfall in pervious areas infiltrates and produces no runoff, unless the ground is saturated.

- The Horton infiltration model was matched to the infiltrometer measurements. The mean initial and final infiltration capacities can be estimated from soil hydrologic group or soil texture. The decay factor is relatively insensitive to soil group or soil texture. A typical decay factor of 0.32 minute^{-1} is associated with all soils, which indicates a generally rapid transition from the initial to the final infiltration capacity.

- A rainfall-recharge relation of the form $y = m(x - \delta)$ is consistent with observed data where y is the change in the elevation of the water table in response to a rainfall event of depth x, m is the slope of the rainfall-recharge relation that can be approximated by the inverse of the specific yield of the surficial aquifer system, and δ is the threshold rainfall below which no recharge occurs. The threshold rainfall, δ, varies between zero and a maximum value, Δ, depending on antecedent moisture conditions.

- The rainfall-recharge relations based on historical hourly data at five monitoring wells in the study area indicate an average aquifer specific yield of 0.23, and a threshold storm-event rainfall of 0.24 in. Analyses based on 15-minute data indicate a specific yield of 0.26 and a maximum threshold rainfall of 0.37 in. These results based on 15-minute data probably are more accurate than the historical results based on historical hourly data because rainfall extrapolation errors are not present in the 15-minute data.

- Rainfall-recharge relations cannot be established using daily time increments. The rapid dissipation of recharge mounds on daily time scales (primarily due to canal drainage) causes little observable change in the daily average water table in response to daily rainfall. Thus, upscaling of the rainfall-recharge relation must be based on storm-event relations.

- Annual recharge at rural locations ranged from 41 to 46 percent of annual rainfall, with recharge in the most urbanized areas being about 30 percent of annual rainfall. These results indicate that urbanization has a significant effect on the annual rainfall-recharge relation. Average annual recharge ranged from 19 to 29 in.

- Principal-component analysis of water-table fluctuations was determined to be an effective approach to identifying areas with highly correlated water-table fluctuations. In the 100-mi^2 study area, two fundamental modes of water-table fluctuations were identified.

- Roots of vegetation do not penetrate the Miami Limestone, which underlies the unsaturated zone in Miami-Dade County. Consequently, transpiration of water from the water table is considered nonexistent, and evaporation and canal-induced drainage are possible causes of water-table decline between storms.

- Evaporation from the water table can be described by a linear model where the saturated-zone evaporation rate is equal to the ground-surface evaporation rate for a depth d_o, and then decreases to zero at a depth d_{cr}. Four of the five locations in this study support this model where the average value of d_o is 4.5 ft, and the average value of d_{cr} is 8.3 feet. In some cases, the evaporation rate may be independent of the depth to the water table, which occurred at the most urbanized location.

- Steady-state leakage from canals in southern Florida can be estimated from a relation that was validated using measurements in and around the L-31N canal. This leakage relation also is applicable in unsteady-state cases where the time scale of fluctuations greatly exceeds 10 minutes.

- A study of the efficacy of using the lag time of tidal propagations in the aquifer to estimate local transmissivity for input into the canal leakage model has demonstrated that this is a promising area of further research. Indications from the study area are that the estimated hydraulic diffusivity derived from tidal propagation analyses, combined with a storage coefficient of 0.007, can be used to estimate local transmissivities, which can then be used to estimate the leakage relation.

- Field measurements of peak runoff from two urbanized catchments were compared to the predictions of two conventional runoff models, and the results demonstrate a fair agreement. The conventional models used the nonlinear reservoir model to estimate surface runoff from rainfall excess, and rainfall excess was computed using the Horton model. These results indicate that the accuracy of conventional catchment-scale models in estimating peak flows that are used as a basis to design drainage structures may be adequate, but needs further improvements.

- The differences between the predicted runoff rates of the SWMM and MOUSE catchment-scale models were found to be substantially less than the differences between the simulated and measured peak runoff rates. Consequently, improvements in rainfall-runoff process formulation are needed more than improvements in code formulation.

- For the eight significant runoff events during this study, the ratio of runoff to rainfall was relatively close to the percentage of DCIA. This indicates that studies that lead to a better estimation of the DCIA associated with individual stormwater inlets may lead to improved rainfall-runoff models.

- The development of several software codes, reports on previous experiences using these codes, and the consistency of these codes with the results obtained by this study were reviewed and the following conclusions can be drawn: (1) on the urban catchment scale, both the SWMM and MOUSE codes adequately account for the key physical processes, and relatively accurate results can be expected; and (2) the MIKE SHE code appears to better simulate basin-scale and regional-scale hydrologic conditions, primarily because of its integrated nature. The main concern with the MIKE SHE model is that sufficient and accurate data generally are not available to take advantage of the distributed and integrated nature of this model. The MODBRANCH and MODNET models are of comparable utility to each other, combine excellent canal-network and groundwater models, and have proven to be useful in several cases. These models, however, are not truly integrated and do not explicitly include unsaturated-zone processes.

- The canal leakage formulations in MODBRANCH and MODNET do not account for cases where there is negligible head loss associated with a channel lining on the sides of canals. In these cases, which may be very common, a reach transmissivity approach is probably more useful.

The conclusions drawn from this study are based mostly on data collected in the study area, and where possible, the results have been extrapolated to the greater southern Florida area. To confirm these extrapolations, similar studies should be conducted in other areas of southern Florida having different surface and/or subsurface conditions, such as Broward or Palm Beach Counties. Such studies will be able to address questions related to the statistical homogeneity of rainfall events, provide added data to narrow the uncertainties in estimating infiltration capacity based on USDA estimated hydrologic soil group and/or soil texture, identify local properties affecting the rainfall-recharge relation, assess the effectiveness of using tidal propagation theory in aquifers to estimate the leakage characteristics of canals, and confirm the validity of using conventional runoff models to design drainage structures in southern Florida.

The fundamental relations derived and validated in this study provide a sound basis for modeling several hydrologic processes in southern Florida. The information should form the basis for selecting and developing computer codes that are useful in hydrologic models at catchment, basin, and regional scales.

References Cited

Abbott, M.B., Bathurst, J.C., Cunge, J.A., and others, 1986a, An introduction to the European hydrological system [Systéme Hydrologique Européen], "SHE," 1. History and philosophy of a physically-based, distributed modelling system: Journal of Hydrology, v. 87, no. 1, p. 45-59.

Abbott, M.B., Bathurst, J.C., Cunge, J.A., and others, 1986b, An introduction to the European hydrological system [Systéme Hydrologique Européen], "SHE," 2. Structure of a physically-based, distributed modelling system: Journal of Hydrology, v. 87, no. 1, p. 61-77.

Abtew, W., and Huebner, R.S., 2000, Hydrologic impact of Hurricane Irene on south Florida (October 13-17, 1999): West Palm Beach, South Florida Water Management District Technical Publication EMA 386.

Akan, A.O., 1993, Urban stormwater hydrology: Lancaster, Pennsylvania, Technomic Publishing Co.

Allman, D.W., Jakob, P.G., and McCann, T., 1979, Improvement of the canal-aquifer flow regime in the C-1N basin: West Palm Beach, South Florida Water Management District Technical Publication 79-2.

American Society for Testing Materials, 1993, Standard classification of soils for engineering purposes (Unified Soil Classification System): ASTM International Report D2487-93.

American Society for Testing Materials, 1994, Standard test method for infiltration rate of soils in field using double-ring infiltrometer: ASTM International Report D3385-94.

Anderson, M.G., and Burt, T.P., 1990, Process studies in hillslope hydrology: An overview, *in* Anderson, M.G., and Burt, T.P., eds., Process studies in hillslope hydrology: New York, John Wiley, p. 1-8.

Arnaud, P., Bouvier, C., Cisneros, L., and Dominguez, R., 2002, Influence of rainfall spatial variability on flood prediction: Journal of Hydrology, v. 260, p. 216-230.

Beck, M.B., 1991, Forecasting environmental change: Journal of Forecasting, v. 10, p. 3-19.

Beighley, R.E., and Moglen, G.E., 2002, Trend assessment in rainfall-runoff behavior in urbanizing watersheds: Journal of Hydrologic Engineering, v. 7, no. 1, p. 27-34.

Beldring, S., 2002, Multi-criteria validation of a precipitation-runoff model: Journal of Hydrology, v. 257, p. 189-211.

Berger, K.P., and Entekhabi, D., 2001, Basin hydrologic response relations to distributed physiographic descriptors and climate: Journal of Hydrology, v. 247, p. 169-182.

Betson, R.P., 1964, What is watershed runoff? Journal of Geophysical Research, v. 69, no. 8, p. 1541-1552.

Bhaduri, B., Minner, M., Tatalovich, S., and Harbor, J., 2001, Long-term hydrologic impact of urbanization: A tale of two models: Journal of Water Resources Planning and Management, v. 127, no. 1, p. 13-19.

Bierkens, M.F.P., Knotters, M., and Hoogland, T., 2001, Space-time modeling of water-table depth using a regionalized time series model and the Kalman filter: Water Resources Research, v. 37, no. 5, p. 1277-1290.

Bolster, C.H., and Saiers, J.E., 2002, Development and evaluation of a mathematical model for surface-water flow within the Shark River Slough of the Florida Everglades: Journal of Hydrology, v. 259, p. 221-235.

Bower, R.F., Adams, K.M., and Restrepo, J.I., 1990, A three-dimensional finite-difference ground water flow model of Lee County, Florida: West Palm Beach, South Florida Water Management District Technical Publication 90-01.

Brakensiek, D.L., Engelman, R.L., and Rawls, W.J., 1981, Variation within texture classes of soil water parameters: Transactions of the American Society of Agricultural Engineers, v. 24, p. 5-9.

Brakensiek, D.L., and Onstad, C.A., 1977, Parameter estimation of the Green and Ampt infiltration equation: Water Resources Research, v. 3, no. 6, p. 1009-1012.

Brooks, R.H., and Corey, A.T., 1964, Hydraulic properties of porous media: Fort Collins, Colorado State University, Hydrology Paper 3.

Burden, D.S., and Sims, J.L., 1999, Fundamentals of soil science as applicable to management of hazardous wastes: U.S. Environmental Protection Agency Ground Water Issue EPA/540/S-98/500.

Camp, Dresser, & McKee, Inc., 2001, Evaluation of integrated surface water and groundwater modeling tools: CDM technical report.

Capkun, G., Davison, A.C., and Musy, A., 2001, A robust rainfall-runoff transfer model: Water Resources Research, v. 37, no. 12, p. 3207-3216.

Carsel, R.F., and Parrish, R.S., 1988, Developing joint probability distributions of soil water retention characteristics: Water Resources Research, v. 24, no. 5, p. 755-779.

Chin, D.A., 1990, A method of estimating canal leakage to the Biscayne aquifer, Dade County, Florida: U.S. Geological Survey Water-Resources Investigations Report 90-4135, 32 p.

Chin, D.A., 1991, Leakage of clogged channels that partially penetrate surficial aquifers: Journal of Hydraulic Engineering, v. 117, no. 4, p. 467-488.

Chin, D.A., 2000, Water-resources engineering: Upper Saddle River, N.J., Prentice-Hall.

Christiaens, K., and Feyen, J., 2002, Use of sensitivity and uncertainty measures in distributed hydrological modeling with an application to the MIKE SHE model: Water Resources Research, v. 38, no. 9: p. 8-1 to 8-15.

Cook, F.J., and Rassam, D.W., 2002, An analytical model for predicting water table dynamics during drainage and evaporation: Journal of Hydrology, v. 263, p. 105-113.

Cooper, R.M., and Lane, J., 1987, An atlas of eastern Dade County surface water management basins: West Palm Beach, South Florida Water Management District, Technical memorandum.

Corradini, C., Morbidelli, R., and Melone, F., 1998, On the interaction between infiltration and Hortonian runoff: Journal of Hydrology, v. 204, p. 52-67.

Council, G.W., 1997, Simulating lake-groundwater interactions with MODFLOW: Proceedings of the 1997 Georgia Water Resources Conference, Athens, Georgia, March 20-22, 1997.

de Marsily, G., 1986, Quantitative hydrogeology, ground water hydrology for engineers: San Diego, Calif., Academic Press.

De Michele, C., Kottegoda, N.T., and Rosso, R., 2001, The derivation of areal reduction factor of storm rainfall from its scaling properties: Water Resources Research, v. 37, no. 12, p. 3247-3252.

Delin, G.N., Healy, R.W., Landon, M.K., and Bohlke, J.K., 2000, Effects of topography and soil properties on recharge at two sites in an agricultural field: Journal of the American Water Resources Association, v. 36, no. 6, p. 1401-1416.

Doyle, W.H., and Miller, J.E., 1980, Calibration of a distributed routing rainfall-runoff model at four urban sites near Miami, Florida: U.S. Geological Survey Water-Resources Investigations Report 80-1, 87 p.

Duever, M.J., Meeder, J.F., Meeder, L.C., and McCollum, J.M., 1994, The climate of south Florida and its role in shaping the Everglades ecosystem, *in* Davie, S.M., and Ogden, J.C., eds., Everglades: The ecosystem and its restoration: Delray Beach, Fla., St. Lucie Press, p. 225-248.

Dufresne, D.P., and Davis, V.C., 2001, Groundwater model construction and calibration for the prolific Biscayne aquifer—Problems and unique solutions: Florida Water Resources Journal, December, p. 29-35.

Eagleson, P., 1970, Dynamic hydrology: New York, McGraw-Hill.

Erskine, A.D., 1991, The effect of tidal fluctuation on a coastal aquifer in the UK: Ground Water, v. 29, no. 4, p. 556-562.

Esteves, M., Faucher, X., Galle, S., and Vauclin, M., 2000, Overland flow and infiltration modelling for small plots during unsteady rain: Numerical results versus observed values: Journal of Hydrology, v. 228, p. 265-282.

Fankhauser, R., 1995, Automatic determination of imperviousness in urban areas from digital orthophotos: Water Resources Research, v. 31, no. 3, p. 699-712.

Fennema, R.J., Neidrauer, C.J., Johnson, R.A., and others, 1994, A computer model to simulate natural Everglades hydrology, *in* Davie, S.M., and Ogden, J.C., eds., Everglades: The ecosystem and its restoration: Delray Beach, Fla., St. Lucie Press, p. 249-289.

Fennessey, L.A.J., Hamlett, J.M., Aron, G., and LaSota, D., 2001, Changes in runoff due to stormwater management pond regulations: Journal of Hydrologic Engineering, v. 6, no. 4, p. 317-327.

Ferris, J.G., 1951, Cyclic fluctuations of water level as a basis for determining aquifer transmissibility: International Association of Scientific Hydrology Publication 33.

Ferris, J.G., Knowles, D.B., Brown, R.H., and Stallman, R.W., 1962, Theory of aquifer tests: U.S. Geological Survey Water-Supply Paper 1536-E, 174 p.

Fiedler, F.R., Frasier, G.W., Ramirez, J.A., and Ahuja, L.R., 2002, Hydrologic response of grasslands: Effects of grazing, interactive infiltration, and scale: Journal of Hydrologic Engineering, v. 7, no. 4, p. 293-301.

Fish, J.E., and Stewart, Mark, 1991, Hydrogeology of the surficial aquifer system, Dade County, Florida: U.S. Geological Survey Water-Resources Investigations Report 90-4108, 50 p.

Forrester, F.H., 1981, 1001 questions answered about weather: New York, Dover Publications.

Fortin, J.P., Turcotte, R., Massicott, S., and others, 2001, Distributed watershed model compatible with remote sensing and GIS data: 1, Description of model: Journal of Hydrologic Engineering, v. 6, p. 91-99.

Freeze, R.A., 1972, Role of subsurface flow in generating surface runoff: 1, Base flow contribution to channel flow: Water Resources Research, v. 8, no. 3, p. 609-623.

Genereux, D.P., and Guardiario, J.D.A., Jr., 1998, A canal drawdown experiment for determination of aquifer parameters: Journal of Hydrologic Engineering, v. 3, no. 4, p. 294-302.

Genereux, D.P., and Guardiario, J.D.A., Jr., 2001, A borehole flowmeter investigation of small-scale hydraulic conductivity variation in the Biscayne aquifer, Florida: Water Resources Research, v. 37, no. 5, p. 1511-1517.

Genereux, D.P., and Slater, E., 1999, Water exchange between canals and surrounding aquifer and wetlands in the southern Everglades, USA: Journal of Hydrology, v. 219, p. 153-168.

Gómez, J.A., Nearing, M.A., Giraldez, J.V., and Alberts, E.E., 2001, Analysis of sources of variability of runoff volume in a 40 plot experiment using a numerical model: Journal of Hydrology, v. 248, p. 183-197.

Goodrich, D.C., Lane, L.J., Shillito, R.M., and others, 1997, Linearity of basin response as a function of scale in a semiarid watershed: Water Resources Research, v. 33, no. 12, p. 2951-2965.

Govindaraju, R.S., Modbidelli, R., and Corradini, C., 2001, Areal infiltration modeling over soils with spatially correlated hydraulic conductivities: Journal of Hydrologic Engineering, v. 6, no. 2, March/April, p. 150-158.

Grayson, R.B., Western, A.W., Chiew, F.H.S., and Blöschl, G., 1997, Preferred states in spatial soil moisture patterns: Local and nonlocal controls: Water Resources Research, v. 33, no. 12, p. 2897-2908.

Green, T.R., 1995, The role of moisture-dependent anisotropy and landscape topography in soilwater flow and groundwater recharge: Palto Alto, Calif., Stanford University, Ph.D. thesis.

Gregg, J.R., 1984, Evaluation of the water management system at a single family residential site: Hydrology and hydraulics of Timbercreek subdivision in Boca Raton, Florida: West Palm Beach, South Florida Water Management District Technical Publication 84-11, v. I.

Haiff, A.H., Haiff, H.M., and Rodriguez, J.S., 1992, Calculation of runoff from rainfall using "NURP" data; *in* T. Engman, ed., Irrigation and drainage: Saving a threatened resource—In search of solutions: Baltimore, Md., August 2-5, 1992, p. 487-492.

Hawkins, R.H., and Cundy, T.W., 1987, Steady-state analysis of infiltration and overland flow for spatially-varied hillslopes: Water Resources Bulletin, v. 32, no. 2, p. 251-256.

Hayashi, M., and van der Kamp, G., 2000, Simple equations to represent the volume-area-depth relations of shallow wetlands in small topographic depressions: Journal of Hydrology, v. 237, p. 74-85.

Hermance, J.F., 1999, A mathematical primer on groundwater flow: Upper Saddle River, N.J., Prentice-Hall.

Hornberger, G.M., Raffensperger, J.P., Wiberg, P.L., and Eshleman, K.N., 1998, Elements of physical hydrology: Baltimore, Md., Johns Hopkins University Press.

Horritt, M.S., and Bates, P.D., 2001, Effects of spatial resolution on a raster based model of flood flow: Journal of Hydrology, v. 253, p. 239-249.

Hsu, M.H., Chen, S.H., and Chang, T.J., 2000, Inundation simulation for urban drainage basin with storm sewer system: Journal of Hydrology, v. 234, p. 21-37.

Hsu, S.M., Ni, C.F., and Hung, Pi-Fank, 2002, Assessment of three infiltration formulas based on model fitting on Richards equation: Journal of Hydrologic Engineering, v. 7, no. 5, p. 373-379.

Huber, W.C., and Dickinson, R.E., 1988, Storm water management model, Version 4, User's manual, with addendums: Athens, Ga., U.S. Environmental Protection Agency Technical Report EPA-600/3-88/001a.

INTERA Environmental Consultants, Inc., 1976, Revision of the documentation for a model for calculating effects of liquid waste disposal in deep saline aquifers: U.S. Geological Survey Water-Resources Investigations Report 79-96.

Jacobsen, T.V., 1999, Caloosahatchee basin integrated surface water-ground water model: Danish Hydraulic Institute report.

Jocson, J.M.U., Jenson, J.W., and Contractor, D.N., 2002, Recharge and aquifer response: Northern Guam Lens aquifer, Guam, Mariana Islands: Journal of Hydrology, v. 260, p. 231-254.

Johnson, A.I., 1963, A field method for measurement of infiltration: U.S. Geological Survey Water-Supply Paper 1544-F.

Kaiser-Hill Company, 2001, Model code and scenario selection report site—Wide water balance Rocky Flats environmental technology site: Kaiser-Hill Report 01-RF-00337.

Kavvas, M.L., 1999, On the coarse-graining of hydrologic processes with increasing scales: Journal of Hydrology, v. 27, p. 191-202.

Khanal, N.N., 1975, Hydrologic aspects of on-site retention systems for urban storm runoff: West Palm Beach, South Florida Water Management District Technical publication 75-4, September 1975.

Khanal, N.N., 1982, Performance of District structures during critical storm events in west Miami, and proposed alternatives to reduce flooding (revised): West Palm Beach, South Florida Water Management District Technical Publication 82-7.

Kim, Y., Engel, B.A., Lim, K.J., and others 2002, Runoff impacts of land-use change in Indian River Lagoon Watershed: Journal of Hydrologic Engineering, v. 7, no. 3, p. 245-251.

Kokkonen, T.S., and Jakeman A.J., 2001, A comparison of metric and conceptual approaches in rainfall-runoff modeling and its implications: Water Resources Research, v. 37, no. 9, p. 2345-2352.

Lal, A.M.W., 1998, Performance comparison of overland flow algorithms: Journal of Hydraulic Engineering, v. 124, no. 4.

Lal, A.M.W., 2001, Modification of canal flow due to stream-aquifer interactions: Journal of Hydraulic Engineering, v. 127, no. 7, p. 567-576.

Langevin, C.D., 2001, Simulation of ground-water discharge to Biscayne Bay, southeastern Florida: U.S. Geological Survey Water-Resources Investigations Report 00-4251, 63 p., 3 pls., and appendixes.

Lietz, A.C., 1999, Methodology for estimating nutrient loads discharged from the east coast canals to Biscayne Bay, Miami-Dade County, Florida: U.S. Geological Survey Water-Resources Investigations Report 99-4094, 36 p.

Lin, S.S.T., and Perkins, W.A., 1989, Review of pre-development runoff analysis methods: West Palm Beach, South Florida Water Management District Report DRE 270, v. I.

Loague, IK., and Kyriakidis, P.C., 1997, Spatial and temporal variability in the R-5 infiltration data set: Déjà vu and rainfall-runoff simulations: Water Resources Research, v. 33, no. 12, p. 2883-2895.

MacVicar, T.K., Vanlent, T., and Castro, A., 1984, South Florida Water Management Model documentation report: West Palm Beach, South Florida Water Management District Technical Publication 84-3.

Maheepala, U.K., Takyi, A.K., and Perera, B.J.C., 2001, Hydrological data monitoring for urban stormwater drainage systems: Journal of Hydrology, v. 245, p. 32-47.

McCue, K.M., Sorensen, H.R., Jessen, O.Z., and Dunn, D., 2002, An integrated groundwater/surface-water model for central Broward County: Florida Water Resources Journal, October, p. 20-24.

McCuen, R.H., 2002, Approach to confidence interval estimation for curve numbers: Journal of Hydrologic Engineering, v. 7, no. 1, p. 43-48.

McCuen, R.H., Rawls, W.J., and Brakensiek, D.L., 1981, Statistical analysis of the Brooks-Corey and the Green-Ampt parameters across soil textures: Water Resources Research, v. 17, no. 4, p. 1005-1013.

McDonald, M.G., and Harbaugh, A.W., 1988, A modular three-dimensional finite-difference ground-water flow model: U.S. Geological Survey Techniques of Water-Resources Investigations Report, book 6, chap. A1.

McKillop, R., Kouwen, N., and Soulis, E.D., 1999, Modeling the rainfall-runoff response of a headwater wetland: Water Resources Research, v. 35, no. 4, p. 1165-1177.

McMaster, K.J., 2002, Effects of digital elevation model resolution on derived stream network positions: Water Resources Research, v. 38, no. 4, p. 31-1 to 31-7.

McPherson, B.F., Miller, R.L., Haag, K.H., and Bradner, A., 2000, Water quality in southern Florida, 1996-1998: U.S. Geological Survey Circular 1207, 32 p.

Merritt, M.L., 1996, Simulation of the water table altitude in the Biscayne aquifer, southern Dade County, Florida, water years 1945-89: U.S. Geological Survey Water-Supply Paper 2458, 148 p., and 9 pls.

Merz, B., and Plate, E.J., 1997, An analysis of the effects of spatial variability of soil and soil moisture on runoff: Water Resources Research, v. 33, no. 12, p. 2909-2922.

Meyer, P.D., Rockhold, M.L., and Gee, G.W., 1997, Uncertainty analyses of infiltration and subsurface flow and transport for SDMP sites: Richland, Wash., Pacific Northwest National Laboratory Technical Report NUREG/CR-6565.

Miami-Dade Department of Environmental Resources Management, 2000, Hydrologic/ hydraulic modeling of the C-103, Florida City, North, C-102, and C-1 Canals and tributary secondary canals in Miami-Dade County.

Miami-Dade Department of Planning and Zoning, 2002, Map of 1998 land use: Miami-Dade County Agriculture and Rural Area Study, November 2002.

Miller, W.L., 1978, Effects of bottom sediments on infiltration from the Miami and tributary canals to the Biscayne aquifer, Dade County, Florida: U.S. Geological Survey Water-Resources Investigations Report 78-36, 63 p.

Morita, M., and Yen, B.C., 2002, Modeling of conjunctive two-dimensional surface-three-dimensional subsurface flows: Journal of Hydraulic Engineering, v. 128, no. 2, p. 184-200.

Mualem, Y., 1976, A new model for predicting the hydraulic conductivity of unsaturated porous media: Water Resources Research, v. 12, no. 3, p. 513-522.

Nachabe, M.H., 2002, Analytical expressions for transient specific yield and shallow water table drainage: Water Resources Research, v. 38, no. 10, p. 11-1 to 11-7.

Nair, S.K., and Wilsnack, M.M., 1998, A comparison of two approaches to simulating lake-groundwater interactions with MODFLOW: West Palm Beach, South Florida Water Management District, Technical report.

Najafi, M.R., 2003, Watershed modeling of rainfall excess transformation into runoff: Journal of Hydrology, v. 270, p. 273-281.

National Weather Service, 1958, Rainfall intensity-frequency regime: Silver Springs, Md., NWS Technical Paper 29.

Natural Resources Conservation Service, 1996, Soil survey of Dade County area, Florida: Washington, D.C., U.S. Department of Agriculture, Technical report.

Nemeth, M.S., and Solo-Gabriele, H.M., 2003, Evaluation of the use of reach transmissivity to quantify exchange between ground water and surface water: Journal of Hydrology, v. 274, p. 145-159.

Nemeth, M.S., Wilcox, W.M., and Solo-Gabriele, H.M., 2000, Evaluation of the use of reach transmissivity to quantify leakage beneath Levee 31N, Miami-Dade County, Florida: U.S. Geological Survey Water-Resources Investigations Report 00-4066, 80 p.

Neumann, C.J., Jarvine, B.R., McAdie, C.J., and Elms, J.D., 1993, Tropical cyclone of the north Atlantic Ocean, 1971-1992: Asheville, N.C., National Oceanic and Atmospheric Administration Historical Climatology Series 6-2.

Nielsen, D.R., Biggar, J.W., and Erh, K.T., 1973, Spatial variability of field-measured soil-water properties: Hilgardia, v. 42, p. 215-259.

Ogden, F.L., Garbrecht, J., DeBarry, P.A., and Johnson, L.E., 2001a, GIS and distributed watershed models: pt. II, Modules, interfaces, and models: Journal of Hydrologic Engineering, v. 6, no. 6, p. 515-523.

Ogden, F.L., Senarath, S.U.S., and Downer, C.W., 2001b, Reply to comment on "On the calibration and verification of two-dimensional, distributed, Hortonian, continuous, watershed models," by Sharika U.S., and others: Water Resources Research, v. 37, no. 12, p. 3397-3400.

Otero, J.M., 1995, Computation of flow-through water control structures: West Palm Beach, South Florida Water Management District Technical Publication 95-03.

Panian, T.F., 1987, Unsaturated flow properties data catalog, v. II: Water Resource Center, Desert Research Institute, Technical Report DOE/NV10384-20, Publication no. 45061.

Parker, G.G., Ferguson, G.E., Love, S.K., and others, 1955, Water resources of southeastern Florida: U.S. Geological Survey Water-Supply Paper 1255, 965 p., and 24 pls.

Philip, J.R., 1957, The theory of infiltration: pt. 4, Sorptivity and algebraic infiltration equations: Soil Science, v. 84, p. 257-264.

Pitt, R., Lantrip, J., Harrison, R., and others, 1999, Infiltration through disturbed urban soils and compost-amended soil effects on runoff quality and quantity: Cincinnati, Ohio, National Risk Management Research Laboratory, U.S. Environmental Protection Agency Technical Report EPA/600/R-00/016.

Ponce, V.M., 1989, Engineering hydrology, principles and practices: Upper Saddle River: New Jersey, Prentice-Hall.

Rasmussen, W.C., and Andreason, G.G., 1959, Hydrologic budget of the Beaver Dam Creek basin, Maryland: U.S. Geological Survey Water-Supply Paper 1472.

Raudkivi, A.J., 1979, Hydrology: Tarrytown, N.Y., Pergamon.

Rawls, W.J., 1983, Estimating soil bulk density from particle size analysis and organic matter content: Soil Science, v. 135, no. 2, p. 123-125.

Rawls, W.J., Ahuja, L.R., Brakensiek, D.R., and Shirmohammadi, A., 1993, Infiltration and soil water movement; *in* D.R. Maidment, ed., Handbook of Hydrology: New York, McGraw-Hill, p. 5.1-5.51.

Rawls, W.J., and Brakensiek, D.L., 1982, Estimating soil water retention from soil properties: ASCE Journal of Irrigation and Drainage Engineering, v. 108, no. 2, p. 166-171.

Rawls, W.J., and Brakensiek, D.L., 1983, A procedure to predict Green Ampt infiltration parameters: American Society of Agricultural Engineers, p. 102-112.

Refsgaard, J.C., and Storm, B., 1995, MIKE SHE; *in* V.P. Singh, ed., Computer models of watershed hydrology: Highlands Ranch, Colo., Water Resources Publications, p. 809-846.

Restrepo, J.I., Bevier, C., and Butler, D., 1992, A three-dimensional finite-difference ground water flow model of the surficial aquifer system, Broward County, Florida: West Palm Beach, South Florida Water Management District Technical Publication 92-05.

Restrepo, J.I., and Montoya, A., 1997, MODFLOW wetland module: Boca Raton, Fla., Florida Atlantic University, Final report to South Florida Water Management District.

Reynolds, R.J., 1987, Diffusivity of a glacial-outwash aquifer by the flood wave-response technique: Ground Water, v. 25, no. 3, p. 290-299.

Romano, N., and Palladino, M., 2002, Prediction of soil water retention using soil physical data and terrain attributes: Journal of Hydrology, v. 265, p. 56-75.

Savabi, M.R., Shinde, D., and Bulgakov, D.A., 2001, Runoff, erosion, and soil water characteristics in the agricultural area of south Miami-Dade County, Florida: Unpublished manuscript.

Schaffranek, R.W., 1987, Flow model for open-channel reach or network: U.S. Geological Survey Professional Paper 1384.

Schoeller, H., 1961, Les eaux souterraines: Paris, France, Masson et Cie Editeurs.

Schueler, T., 1994, The importance of imperviousness: Watershed Protection Techniques, v. 1, no. 3, p. 100-111.

Seibert, J., 2001, Comment on "On the calibration and verification of two-dimensional, distributed, Hortonian, continuous, watershed models," by Sharika, U.S., and others: Water Resources Research, v. 37, no. 12, p. 3393-3395.

Serrano, S.E., and Workman, S.R., 1998, Modeling transient stream/aquifer interaction with the non-linear Boussinesq equation and its analytical solution: Journal of Hydrology, v. 206, p. 245-255.

Shaw, J.E., 1985, Preliminary evaluation of hydrologic data collected from the C-103 basin, Dade County, Florida: West Palm Beach, South Florida Water Management District Technical Memorandum DRE 207.

Shih, D.C.F., 1999, Inverse solution of hydraulic diffusivity determined by water level fluctuation: Journal of the American Water Resources Association, v. 35, no. 1, p. 37-48.

Shih, D.C.F., Lee, C.D., Chiou, K.F., and Tsai, S.M., 2000, Spectral analysis of tidal fluctuations in ground water level: Ground Water, v. 36, no. 5, p. 1087-1099.

Singh, S.K., Mishra, G.C., Swamee, P.K., and Ojha, C.P.P., 2002, Aquifer diffusivity and stream resistance from varying stream stage: Journal of Irrigation and Drainage Engineering, v. 128, no. 1, p. 57-61.

Singh, V.P., and Woolhiser, D.A., 2002, Mathematical modeling of watershed hydrology: Journal of Hydrologic Engineering, v. 7, no. 4, p. 270-292.

Sivapalan, M., 2003, Process complexity at hillslope scale, process simplicity at the watershed scale: Is there a connection? Hydrological Processes, v. 17, p. 1037-1041.

Sivapalan, M., and Wood, E.F., 1986, Spatial heterogeneity and scale in the infiltration response of catchments; *in* Gupta, V.K., Rodriguez-Iturbe, I., and Wood, E.F., eds., Scale problems in hydrology: Dordrecht, The Netherlands, Kluwer Academic p. 81-106.

Smettem K.R.J., and Smith, R.E., 2002, Field measurement of infiltration parameters, *in* Smith, R.E., Smettem, K.R.J., Broadbridge, P., and Woolhiser, eds., Infiltration theory for hydrologic applications: American Geophysical Union Water Resources Monograph 15, p. 135-157.

Smith R.E., and Hebbert, R.H.B., 1979, A Monte Carlo analysis of the hydrologic effects of spatial variability of infiltration: Water Resources Research, v. 15, p. 419-429.

Soil Conservation Service, 1982, Procedures for collecting soil samples and methods of analysis for soil survey: Soil Survey Investigations Report No. 1, Washington D.C.

Soil Conservation Service, 1986, Urban hydrology for small watersheds: Washington, D.C., U.S. Department of Agriculture, Technical Release 55.

Soil Conservation Service, 1993, SCS National Engineering Handbook, sec. 4, Hydrology: Washington, D.C., U.S. Department of Agriculture.

Sonenshein, R.S., 2001, Methods to quantify seepage beneath Levee 30, Miami-Dade County, Florida: U.S. Geological Survey Water-Resources Investigations Report 01-4074, 36 p.

South Florida Water Management District, 1994, Management and storage of surface water: West Palm Beach, Permit Information Manual, v. IV.

South Florida Water Management District,1997, Documentation for the south Florida water management model: West Palm Beach, Technical report.

Springer, E.P., and Cundy, T.W., 1987, Field-scale evaluation of infiltration parameters from soil texture for hydrologic analysis: Water Resources Research, v. 23, no. 2, p. 325-334.

Stephenson, G.A., and Freeze, R.A., 1974, Mathematical simulation of subsurface contributions to snowmelt and runoff, Reynolds Creek watershed, Idaho: Water Resources Research, v. 10, p. 284-294.

Swain, E.D., Howie, Barbara, and Dixon, Joann, 1996, Description and field analysis of a coupled ground-water/surface-water flow model (MODFLOW/BRANCH) with modifications for structures and wetlands in southern Dade County, Florida: U.S. Geological Survey Water-Resources Investigations Report 96-4118, 67 p.

Swain, E.D., and Wexler, E.J., 1996, A coupled surface-water and ground-water flow model (MODBRANCH) for simulation of stream-aquifer interaction: U.S. Geological Survey Techniques of Water-Resources Investigations, book 6, chap. A6.

Swayze, L.J., 1988, Ground-water flow beneath Levee 35A from Conservation Area 2B, Broward County, Florida: U.S. Geological Survey Water-Resources Investigations Report 87-4280.

Syed, K.H., Goodrich, D.C., Myers, D.E., and Sorooshian, S., 2003, Spatial characteristics of thunderstorm rainfall fields and their relation to runoff: Journal of Hydrology, v. 271, p. 1-21.

Telis, P.A., 2001, Estimation of infiltration rates of saturated soils at selected sites in the Caloosahatchee River Basin: U.S. Geological Survey Open-File Report 01-65, 16 p.

Trimble, P., 1986, South Florida regional routing model: West Palm Beach, South Florida Water Management District Technical Publication 86-3.

Trommer, J.T., Lopez, J.E., Hammett, K.M., and Bowman, G., 1996, Comparison of estimated and observed stormwater runoff for fifteen watersheds in west-central Florida, using five common design techniques: U.S. Geological Survey Open-File Report 96-129, 125 p.

U.S. Army Corps of Engineers, 1996, One-dimensional unsteady flow through a full network of open channels: Davis, Calif., Hydrologic Engineering Center, Technical Report No. CDP-66.

U.S. Department of Agriculture, National Resources Conservation Service, 2001, National Soil Survey Handbook, title 430-VI: Accessed at http://www.statlab.iastate.edu/soils/nssh/.

U.S. Environmental Protection Agency, 1998, Estimation of infiltration rate in the vadose zone: Compilation of simple mathematical models: Ada, Okla., National Risk Management Research Laboratory, U.S. Environmental Protection Agency Technical Report EPA/600/R-97/128a.

Vachaud, G., and Chen, T., 2002, Sensitivity of a large-scale hydrologic model to quality of input data obtained at different scales; distributed versus stochastic non-distributed modelling: Journal of Hydrology, v. 264, p. 101-112.

Valeo, C., and Monin, S.M.A., 2000, Variable source area modelling in urbanizing watersheds: Journal of Hydrology, v. 228, p. 68-81.

van Genuchten, M.T., 1980, A closed-form equation for predicting the hydraulic conductivity of unsaturated soils: Soil Science of America Journal, v. 44, p. 892-898.

Vázquez, R.F., and Feyen, J., 2003, Effect of potential evapotranspiration estimates on effective parameters and performance of the MIKE SHE-code applied to a medium-size catchment: Journal of Hydrology, v. 270, p. 309-327.

Viera, S.R., Nielsen, D.R., and Biggar, J.W., 1981, Spatial variability of field-measured infiltration rate: Soil Science Society of America Journal, v. 45, no. 6, p. 1040-1048.

Wainwright, J., and Parson, A.J., 2002. The effect of temporal variations in rainfall on scale dependency in runoff coefficients: Water Resources Research, v. 38, no. 12, p. 7-1 to 7-10.

Wallender, W.W., and Grismer, M.E., 2002, Irrigation hydrology: Crossing scales: ASCE Journal of Irrigation and Drainage Engineering, v. 128, no. 4, p. 203-211.

Warrick, A.W., and Nielsen, 1980, Spatial variability of soil physical properties in the field; *in* Hillel, D., ed., Application of soil physics: San Diego, Calif., Academic Press.

Wedderburn, L.A., Trost, S.M., and Lane, J., 1981, Management of water levels in the "Frog Pond" area, south Dade County, Florida: West Palm Beach, South Florida Water Management District Technical Publication 81-4.

WEST Consultants, Inc., and Gartner Lee, Ltd., 1999, MODNET: An integrated groundwater/open-channel flow model: Technical report prepared for the South Florida Water Management District.

Williams, A.G., Dowd, J.F., and Meyles, E.W., 2002, A new interpretation of kinematic stormflow generation: Hydrological Processes, v. 16, p. 2791-2803.

Wood, E.F., Sivapalan, M., Beven, K., and Band, L., 1988, Effects of spatial variability and scale with implications to hydrologic modelling: Journal of Hydrology, v. 102, p. 29-47.

Woolhiser, D.A., 2002, Infiltration and runoff on a hillslope, *in* Smith, R.E., Smettem, K.R.J., Broadbridge, P., and Woolhiser, D.A., eds., Infiltration theory for hydrologic applications: American Geophysical Union Water Resources Monograph 15, p. 159-183.

Woolhiser, D.A., and Goodrich, D.C., 1988, Effect of storm rainfall intensity patterns on surface runoff: Journal of Hydrology, v. 102, p. 29-47.

Workman, S.R., Serrano, S.E., and Liberty, K., 1997, Development and application of an analytical model of stream/aquifer interaction: Journal of Hydrology, v. 200, p. 149-163.

Xevi, E., Christiaens, K., Espino, A., and others, 1997, Calibration, validation and sensitivity analysis of the MIKE SHE model using neuenkirchen catchment as case study: Water Resources Management, v. 11, no. 2, p. 219-242.

Xue, R.Z., 1996, Stormwater runoff and pollutant model (SPRM) model documentation, version 1.3: West Palm Beach, South Florida Water Management District Technical Memorandum WRE 349.

Yan, J., and Smith, K.R., 1994, Simulation of integrated surface water and ground water systems—Model formulation: Water Resources Bulletin, v. 30, no. 5, p. 879-890.

Yen, B.C., 1991, Hydraulic resistance in open channels; *in* Yen, B.C., ed., Channel flow resistance: Centennial of Manning's formula: Highlands Rangh, Colo., Water Resource Publications, p. 1-135.

Zaghloul, N.A., and Al-Shurbaji, A.R.M., 1990, A storm water management model for urban areas in Kuwait: Water Resources Bulletin, v. 26, no. 4, p. 563-575.

Zammouri, M., 2001, Case study of water table evaporation at Ichkeul Marshes (Tunisia): ASCE Journal of Irrigation and Drainage Engineering, v. 127, no. 5, p. 265-271.

Zhou, Q.Y., Shimada, J., and Sato, A., 2002, Temporal variations of the three-dimensional rainfall infiltration process in heterogeneous soil: Water Resources Research, v. 38, no. 4, p. 1-1 to1-15.

APPENDIX

Review of Hydrologic Processes in Southern Florida

Rainfall-runoff relations have been a focus of hydrologic research for several decades, and an abundance of models for simulating runoff from rainfall have been proposed. These models can be classified as metric, conceptual, or physics based (Beck, 1991).

Metric models are strongly observation oriented, seeking to characterize system response by extracting information from existing data, and are empirically constructed with little or no consideration of the features and processes of the hydrologic system. Unit-hydrograph theory is the foundation of metric rainfall-runoff models.

Conceptual models describe all the component hydrologic processes perceived to be of importance as simplified conceptualizations. The Stanford Watershed Model is an example of a conceptual model. The more component processes that are included in the model, the higher the risk of over-parameterization (Kokkonen and Jakeman, 2001).

Physics-based models attempt to mimic the hydrologic behavior of a catchment by using the concepts of classical continuum mechanics. These models provide a mathematically idealized representation of the real phenomenon and usually require large amounts of data that can be difficult to obtain and have high computational demands. According to Capkun and others (2001), the physical reality underlying hydrologic systems is so complex that physics-based models are difficult to validate on the scant data usually available, which compromises their practical usefulness. Nevertheless, physics-based distributed hydrologic models generally are required when flow path and flow concentration are important—for example, when simulating erosion or contaminant transport in the context of land use (Ogden and others, 2001a).

Although physics-based models are widely recognized as the best tools presently available for complicated tasks, the reliability of these models using effective parameters at the scale of the computational elements is questionable (Beldring, 2002). Furthermore, the nonlinear nature of the hydrologic processes involved, as well as the structural heterogeneity of natural systems, make it unlikely that the equations of hydrologic theories developed at small space and time scales can be generalized to larger scales.

Many areas in southern Florida continue to undergo urban development, and urbanized watersheds are known to have nonstationary rainfall-runoff relations. The degree of this nonstationary relation varies depending on the rate of urbanization. For example, Schueler (1994) reported that an impervious area of 10 to 20 percent is sufficient to produce considerable changes in runoff from undeveloped areas, and Beighley and Moglen (2002) studied statistical methods to identify trends in rainfall-runoff behavior in urbanized watersheds.

In southern Florida, the extremely flat topography, highly permeable soils, and high water-table elevation as well as an extensive canal system cause ground-water levels to be heavily influenced by rainfall, surface-water stages, well-field withdrawals, and evapotranspiration (Yan and Smith, 1994). Aquifer recharge, especially in and around well fields, is an important part of the hydrologic regime.

In general, physiography (including geomorphology and lithology) and climate are two of the most important properties affecting the long-term hydrologic response relations in catchment areas (Berger and Entekhabi, 2001). Low topographic relief and intense or prolonged rainfall events associated with tropical storms produce recurring problems of flash floods. Typically, in areas of low topographic relief, the delineation of catchment boundaries is uncertain and dependent on the rainfall intensity. Very few areas drain directly into canals by way of surface runoff. Rainfall in pervious areas mostly infiltrates into the ground, and rainfall in impervious areas mostly runs into pervious areas and infiltrates, or is collected by exfiltration trenches and recharges the ground water. Canal stages respond rapidly to increased water-table elevations and vice versa. Spatial variations in the saturated hydraulic conductivity of the soil, surface-storage characteristics, and the depth to the water table can have a major effect on surface-runoff characteristics (Gómez and others, 2001).

Rainfall

Spatial and temporal variability of individual rainfall events can have a significant influence on generated storm runoff. The shape, timing, and peak flow of a runoff hydrograph have been shown to be greatly influenced by rainfall variability in both space and time (Singh and Woolhiser, 2002). Rainfall typically is measured with tipping-bucket rain gages, which measure rainfall in increments of 0.01 in. Light rainfall measurements range from a trace to 0.1 in/hr, moderate rainfall ranges from 0.11 to 0.30 in/hr, and heavy rainfall can be more than 0.30 in/hr (Forrester, 1981).

Rainfall in southern Florida typically originates from frontal storms during the dry season (November through April), and convectional thunderstorms during the wet season (May through October). The duration of a typical thunderstorm is 25 minutes, but can be highly variable (Forrester, 1981). The onset of thunderstorms is rapid, with the heaviest rainfall lasting 5 to 15 minutes before decreasing in rate.

The average diameter of a thunderstorm core is about 2 mi, depending on the definition of "rainfall intensity" associated with the core of a storm (Syed and others, 2003). A storm core typically is associated with that part of the storm that produces runoff (about 1 in/hr), and the areal coverage of a storm core usually is better correlated with runoff than the areal coverage of the entire storm (Syed and others, 2003).

Most rainfall-runoff models assume that rainfall is uniformly distributed over the catchment area, and only temporal variations in rainfall are taken into account. Justification for the assumption of spatial homogeneity generally requires that the catchment area be less than the area covered by the individual storm event which, in southern Florida, ranges from length scales of less than 1 mi for convection storms to several miles for frontal storms. Catchments where the spatial homogeneity assumption is or is not valid generally are called midsize catchments or large catchments, respectively (Ponce, 1989). At the other end of the spectrum, small catchments have times of concentration so sufficiently small that the rainfall intensity can be assumed constant over durations of the time of concentration. Assumptions of spatial homogeneity and constant rainfall intensity are appropriate in calculating the peak runoff from small catchments.

Infiltration

Infiltration is the major abstraction process in generating runoff from rainfall. The amount of infiltration that occurs during a storm can depend on several factors, including land use, soil type, moisture content, vegetative cover, topography, depth to water table, and rainfall intensity within the catchment area.

The capacity of the unsaturated zone to hold water against gravity is measured by the specific retention, the fraction of water that can be drained by gravity from saturated pores is the specific yield, and porosity is equal to the sum of the specific retention and the specific yield. Water is lost from the unsaturated zone between storms by evapotranspiration, thus reducing the water content below the specific retention. Therefore, if a prolonged dry period precedes a storm, the specific retention must be satisfied prior to recharge. If a wet period precedes a storm, then most of the infiltrated rainfall will become recharge.

Point-Scale Models

The classical point-scale infiltration theory is often used in physically based hydrologic models to predict rainfall excess. The U.S. Environmental Protection Agency (1998) reviewed several commonly used point-scale infiltration models and classified them as: empirical models, Green-Ampt models, and Richards equation models. These models are discussed in the subsequent sections.

Empirical Models

The most widely used empirical model to describe infiltration is the Horton model given by:

$$f_p = f_c + (f_o - f_c)e^{-kt}, \qquad \text{(A1)}$$

where f_p is the infiltration rate under ponded conditions, f_c is the asymptotic (minimum) infiltration rate ($t \to \infty$), f_o is the initial (maximum) infiltration rate, and k is the decay constant. Infiltration occurs at infiltration rate f_p when the water is ponded from the beginning of the storm (at $t = 0$).

In most cases, ponding occurs sometime after the storm begins, and the integrated form of the Horton equation is used (Chin, 2000):

$$F(t) = f_c t + \frac{f_o - f_c}{k}(1 - e^{-kt}), \qquad \text{(A2)}$$

where $F(t)$ is the cumulative infiltration. To determine the infiltration capacity, the cumulative infiltration is substituted into this equation, the corresponding time t is calculated, and this value of t then is substituted into equation A1 to determine the infiltration capacity, f_p, corresponding to the specified cumulative infiltration. The rate of decrease of infiltration capacity during a storm is assumed to be a property of the soil, with rapid decreases in infiltration rates more likely to occur in clay-rich soils than in sandy soils. According to Philip (1957), however, the Horton equation does not adequately represent the rapid decrease in the infiltration rate from very high values at small times. The major drawback of the Horton equation is that it does not consider the storage availability in the subsurface after varying amounts of infiltration have occurred, but considers only the infiltration as a function of time.

In applying the Horton equation, f_o, f_c, and k should be obtained from field measurements, but these parameters are rarely measured locally. Typical values of f_c, and k are shown in table A1 (Akan, 1993). The initial infiltration rate, f_o, is highly variable and depends on the moisture content and vegetation cover of the soil.

The NRCS curve-number (CN) model is widely used to partition the rainfall into initial abstraction, runoff, and storage components (Chin, 2000). This empirical model is given by:

$$Q = \frac{(P - 0.2S)^2}{P + 0.8S}, \qquad \text{(A3)}$$

where Q is the runoff depth, P is the rainfall depth, and S is the available storage.

The CN method for estimating direct runoff is a semi-empirical method that has been shown to match observed rainfall-runoff measurements at the catchment scale. This method fundamentally recognizes that runoff occurs when the rainfall rate exceeds the infiltration capacity of the soils (Soil Conservation Service, 1993). The initial abstraction consists mainly of interception, infiltration, and surface storage, all of which occur before runoff begins. Equation A3 is not appli-

cable for runoff amounts less than 0.5 in. (Soil Conservation Service, 1986). According to the South Florida Water Management District (1994), the storage, S, that should be used in calculating runoff from rainfall is a function of the depth of the water table below the land surface as given in table A2. This approach for estimating the storage capacity, S, differs from the usual method used in the CN model where the storage is estimated based on the infiltration capacity of the soil (classified according to hydrologic soil group) and the land use. Gregg (1984) investigated the application of the CN model at the scale of a 122-acre residential site in southern Florida, and reported that the model overestimated the runoff in most cases. Reasons cited for this discrepancy were:

- Most runoff associated with minor rainfall events and the early runoff associated with major events are from directly connected impervious areas (DCIAs). The CN model does not address the DCIA.
- The CN model was not intended to be used for short (less than 24 hours), relatively moderate rainfall events that occurred during the study.

The SFWMD-recommended procedure of relating S to the water-table depth has not been firmly established because it remains questionable as to whether this formulation is appropriate in cases where relative magnitudes of the rainfall intensity and infiltration capacity govern the runoff process (that is, the runoff mechanism is Hortonian).

Green-Ampt Model

The Green-Ampt equation is the preferred model of infiltration estimation in many physically based hydrologic models. This model assumes a piston-type water-content profile with a well-defined wetting front. In support of the application of this model, the U.S. Department of Agriculture (USDA), Agricultural Research Service has done extensive work to develop empirical relations for obtaining Green-Ampt model parameters (Brakensiek and Onstad, 1977; McCuen and others, 1981; Rawls and Brakensiek, 1982; Springer and Cundy, 1987). The primary use of the Green-Ampt model is to estimate the infiltration capacity of the soil; however, the actual water-content distribution in the soil cannot be simulated because the model formulation assumes a sharp wetting front. Application of the Green-Ampt model requires specification of the wetting front pressure, which can be derived from the moisture characteristics of the soil. Field verification of a rainfall-runoff model reported by Esteves and others (2000) indicated that the best results on infiltration were obtained using a calibrated value of wetting front pressure instead of those deduced from soil-moisture characteristics. Lin and Perkins (1989) noted that a limitation of applying the Green-Ampt model in southern Florida is that this approach does not account for the depth of the water table and its influence on the infiltration process.

Richards Model

The Richards model is widely used to describe the movement of water in the unsaturated zone, but this model is not simple for calculating infiltration rates. The Richards equation is derived from the Darcy-Buckingham law, which is the unsaturated zone analog of Darcy's law and is given by:

$$q = K(\theta)\nabla\Psi(\theta) , \qquad \text{(A4)}$$

where q is the water flux, K is the unsaturated hydraulic conductivity, θ is the volumetric water content, and Ψ is the soil-water head equal to the sum of the capillary head, h, and the elevation head, z.

In cases where the soil-water movement is vertical, equation A4 can be combined with the continuity equation to yield:

$$\frac{\partial\theta}{\partial t} = \frac{\partial}{\partial z}\left(K(\theta)\frac{\partial h}{\partial z}\right) - \frac{\partial K(\theta)}{\partial z} . \qquad \text{(A5)}$$

This formula is the one-dimensional Richards equation. The solution of the Richards equation requires the specification of soil characteristic functions, $K(\theta)$ and $h(\theta)$. Numerous sources in the soil-science literature provide estimates of the model parameters to calculate $h(\theta)$ and $K(\theta)$. The three most comprehensive sources for these model parameters are Brakensiek and others (1981), Panian (1987), and Carsel and Parrish (1988).

Comparison of Models

The Horton and the Green-Ampt models can be derived from the Richards equation under special circumstances. The Horton model can be obtained as a solution of the Richards equation by assuming that the hydraulic conductivity, $K(\theta)$, is independent of the moisture content, θ, (Eagleson, 1970; Raudkivi, 1979), and the Green-Ampt model can be obtained as an exact solution of the Richards equation when the unsaturated hydraulic conductivity is assumed to be a Dirac Delta-type function with a nonzero value only at the saturated

Table A1. Typical values of Horton parameters

[From Akan (1993). f_c, asymptotic (minimum) infiltration rate ($t\rightarrow\infty$); k, decay constant]

Soil type	f_c (inches per hour)	k (minute^{-1})
Clay loam, silty clay loams	0.0-1.3	0.069
Sandy clay loam	1.3-3.8	.069
Silt loam, loam	3.8-7.6	.069
Sand, loamy sand, sandy loams	7.6-11.4	.069

water content. If the Richards equation is assumed to be most representative of actual field conditions, then the work of Hsu and others (2002) is particularly illuminating in assessing the adequacy of the Green-Ampt and Horton models. Hsu and others (2002) compared the best-fit infiltration rate as a function of time in the Horton and Green-Ampt models with the infiltration rate as a function of time given by an exact (numerical) solution to the Richards equation under a constant rainfall intensity. The results of this study indicated that the only Horton parameter remaining relatively insensitive to the rainfall intensity and initial water content was the asymptotic infiltration rate, f_c, which tends to be larger than the saturated hydraulic conductivity of the soil. Other best-fit parameters of the Horton model, f_o and k, were sensitive to the rainfall intensity, particularly the decay coefficient, k. These results suggest that caution should be used when using the Horton model to describe infiltration, particularly in cases where the infiltration rate decays slowly. In contrast to the parameters of the Horton model, the parameters of the Green-Ampt model were relatively stable and independent of the rainfall conditions.

Soil Infiltration Characteristics

Soils are an integral part of the landscape, and an interaction between the soil and the landscape position can be expected (Merz and Plate, 1997). Estimation of reliable relations between soil hydraulic properties and landscape attributes is an active area of research (Romano and Palladino, 2002).

Telis (2001) used a double-ring infiltrometer to measure the infiltration rates of saturated soils at selected sites in the Caloosahatchee River basin in southern Florida. Based on landscape cover and associated drainage, soils at 23 sites were classified by landscape group as follows: rock (11 sites), flatwoods (7 sites), slough (4 sites), and depression (1 site). Infiltrometer data from 16 sites were fit to Horton's equation using a regression analysis to estimate the infiltration rates of saturated soils. For some sites, outliers were removed prior to regression analysis, and seven sites yielded no data that fit Horton's equation. In cases where the flatness of the plotted data indicated that saturated conditions may have been reached early in the test, the saturated-soil infiltration rate was estimated by averaging data collected after the first 20 minutes of the test. Estimated infiltration rates in saturated soils ranged as follows: flatwoods (4-45 in/hr), rock (1.3-26 in/hr), slough (1-22 in/hr), and depression (71 in/hr). The coefficient of variation of the data about the estimated saturated hydraulic conductivity at each site can be used as a measure of the spatial variability of the saturated hydraulic conductivity. At the Caloosahatchee River basin site (Telis, 2001), estimated coefficients of variation ranged as follows: rock (0.12-10.8), flatwoods (0.11-1.47), and slough (0.09-1.88). Loague and Kyriakidis (1997) reported an average coefficient of variation of 0.364 based on 247 measurements made in a small catchment in Oklahoma, and Warrick and Nielsen (1980) compiled the results of different field studies and reported coefficients of variation ranging from 0.9 to 1.9 (saturated) and 1.7 to 4.0 (unsaturated).

Pitt and others (1999) examined the effects of urbanization on soil structure and how compaction and moisture content of the soil affects the infiltration of rainwater. In this study, about 150 infiltration tests were conducted in urbanized areas of Birmingham and Mobile, Ala. In most developed areas, compact soils are expected to be dominant, with reduced infiltration capacity compared to predevelopment conditions. Pitt and others (1999) defined compact soils as having a cone penetrometer reading greater than 300 lb/ft^2 at a depth of 3 in. In sandy soils, results indicated that compaction was much more important than moisture content in determining the infiltration capacity of the soil (table A3). These results indicate: (1) the effect of compaction on the final infiltration capacity is very large, reducing the asymptotic infiltration rates between 5 and 10 times compared with the noncompacted soil; and (2) the decay rate, k, is very high relative to published values, and indicates that the infiltration capacity reaches its asymptotic value very quickly. In most of the infiltrometer experiments, infiltration rates became relatively steady after 30 to 45 minutes.

Pitt and others (1999) concluded that the Horton equation coefficients were relatively imprecise, and thus any infiltration model probably could be used as long as the uncertainty is considered in the evaluation. Additionally, when modeling runoff from urban soils, it may be best to assume relatively constant infiltration rates throughout an event, and to use Monte Carlo procedures to describe the observed random variations about the predicted mean value.

Table A2. Storage used in calculating runoff from rainfall as a function of the depth to the water table in the Natural Resources Conservation Service model

[From South Florida Water Management District, 1994]

Depth to water table (feet)	Storage capacity (inches)
1	0.60
2	2.50
3	6.60
4	10.90

Effects of Infiltration Variability

Field measurements can be used to develop equations that accurately describe infiltration at a given location; however, a high degree of spatial variability generally exists in infiltration parameters. Loague and Kyriakidis (1997) used a grid size of

2.5 acres (100 m^2) to study the effects of infiltration variability on the rainfall-runoff process in a small catchment in Oklahoma. Govindaraju and others (2001) investigated the upscaling of infiltration characteristics that account for the spatial variability of the hydraulic conductivities of soils, assuming statistical homogeneity in the upscaled area. Spatial variability in the soil saturated hydraulic conductivity is recognized to have a dominant role in the generation of Hortonian overland flow for storms of low intensity and short duration. These effects tend to weaken in heavier storms with longer duration for which the stochastic problem can be reasonably reduced to a deterministic formulation (Corradini and others, 1998; Zhou and others, 2002).

In general, caution should be exercised when using average infiltration characteristics to describe the infiltration properties of an area, especially in light of research by Smith and Hebbert (1979), Sivapalan and Wood (1986), and Woolhiser and Goodrich (1988) who observed considerable differences in the infiltration rate when average soil properties were used rather than spatially varied properties. Fiedler and others (2002) reported that small-scale dynamic interactions between overland flow and infiltration caused by spatially variable soil and ground-surface characteristics (run-on) can result in areal hydrologic response that is not described by classical point-scale infiltration theory.

In developing estimates of the effective infiltration capacity, which generally lead to estimates of surface runoff and ponding, landscape characteristics become increasingly important at larger scales because natural catchment surfaces generally are irregular. These surfaces may consist of uniform or random microrelief or a rill network into which flow is channelled when surface runoff occurs. Relatively uniform microrelief is created in agricultural areas by tillage, and random microrelief may be present in minimally eroded natural areas due to soil or vegetation distributions. In either case, surface-water flow is rarely uniform in depth, and generally is concentrated in certain areas. Thus, once rainfall ceases, the area for infiltration may be severely restricted, and the rate of loss from the surface may be substantially less than if it were assumed to cover the entire soil surface (Woolhiser, 2002). Additionally, runoff generated earlier at an upslope location can add to the rainfall influx, thereby substantially and suddenly changing the infiltration at given location. This case has been documented in the literature (for example, Corradini and others, 1998). In cases where rainfall rates substantially exceed infiltration rates, spatial variations in the soil infiltration capacity have a relatively minor effect on the overall runoff amount (Woolhiser, 2002).

Rainfall Simulator Test

Savabi and others (2001) provided raw data on rainfall-runoff characteristics of Krome, Chekika, and Perrine Marl soils present within the C-102 and C-103 basins in southern Florida. The soils were packed in boxes to the observed field bulk densities (75-87 lb/ft^3), and limestone rocks were placed beneath the soil to simulate the highly porous limestone bedrock that typically underlies the soil in the region. The soil boxes were placed under a programmable rainfall simulator and subjected to a 1-hr rainfall event with an intensity of about 5 in/hr. Three saturation water depths were used to simulate the presence of the water table, and results of these tests are given in table A4. To analyze these results, consider the relation between the rainfall and runoff given by the commonly used CN model:

$$Q = \frac{(P - 0.2S)^2}{P + 0.8S}, \qquad \text{(A6)}$$

where Q is the runoff depth, P is the rainfall depth, and S is the available storage. Rearranging equation A6 gives:

$$S = 5[2Q + P - \sqrt{Q(4Q + 5P)}]. \qquad \text{(A7)}$$

This formula can be used to calculate the available storage based on the rainfall and runoff measurements reported by Savabi and others (2001) in table A4. Applying equation A7 to the measured data in table A4 gives the storage, S, in the NRCS model. According to SFWMD guidelines, the storage S that should be used in calculating runoff from rainfall is a function of the depth of the water table below the soil surface as given in table A2. If the SFWMD guidelines were applied to the Savabi and others (2001) experiments, then the storage amounts in the SFWMD model would be used (table A4). Comparing the values of S in the NRCS and SFWMD models indicates that large discrepancies can occur for water-table depths on the order of 3 ft below land surface, which strongly suggests that if the CN model is used to calculate runoff for storms with durations of about 1 hr, then the available storage is not closely related to the depth of the water table. Thus,

Table A3. Observed infiltration of sandy soils

[From Pitt and others (1999). f_o, initial (maximum) infiltration rate; f_c, asymptotic (minimum) infiltration rate ($t \to \infty$); k, decay rate; --, no data available]

State	f_o (inches per hour)		f_c (inches per hour)		k ($minute^{-1}$)	
	Mean	Range	Mean	Range	Mean	Range
Noncompacted	39.0	4.3-146	15.0	0.4-25	9.6	1.0-33
Compacted	15.0	0.1-86	1.8	0.1-9.4	11	1.8-37
Published values	--	1.7-10	--	0.3-0.4	--	0.069[1]

[1]Range for this value not applicable.

infiltration functions, such as the Horton or Green-Ampt methods, which do not directly account for the depth to the water table, may be more appropriate in these cases. Because the depth to the water table generally is greater than 3.2 ft, the application of the CN model may substantially underestimate runoff from short-duration high-intensity storms in undeveloped areas.

Direct Ground-Water Recharge

Direct recharge of ground water results from the percolation of rainwater through the unsaturated zone. For direct ground-water recharge to occur, the rainfall depth must exceed some threshold amount to satisfy above-ground interception and the storage capacity of the unsaturated zone. Recharge events typically occur on the same time scale as rainfall events, even in cases where the unsaturated zone is very deep. For example, studies in a karst aquifer by Jocson and others (2002) have shown that during wet conditions, water levels in observation wells can rise in a matter of hours in response to heavy rainfall, despite the thickness (about 197-262 ft or 60 to 80 m) of the unsaturated zone.

In some instances, direct recharge from rainfall is combined with evapotranspiration of ground water from the saturated zone to yield a quantity commonly referred to as net recharge. Over storm-event time scales, direct evapotranspiration from the saturated zone generally is negligible. Over longer time scales, direct evapotranspiration from the water table depends on such factors as the depth to the water table, thickness of the root zone, and soil characteristics in the unsaturated zone. In many tropical areas, evaporation plays an important role in lowering the water table in finely textured soils (Cook and Rassam, 2002). In many parts of southern Florida, however, including the focus area in this study, the unsaturated zone is several feet thick and composed of a thin layer of soil overlying several feet of rock. Under these conditions, vegetation roots do not penetrate the rock formation, no direct transpiration from the saturated zone occurs, and the amount of direct evaporation from the saturated zone is substantially less than the potential evaporation.

Various methods have been used to relate rainfall to direct recharge. In a ground-water flow model developed by Langevin (2001) to simulate ground-water discharge to Biscayne Bay, recharge values for each cell and for each month were obtained by multiplying rainfall totals by runoff coefficients. The calculation of runoff coefficients was based on the assumption that runoff quantities are dependent on land use—an approach originally used by Restrepo and others (1992). Suggested runoff coefficients as a function of land use are given in table A5. Langevin (2001) assumed that the evapotranspiration rate decreases linearly with the depth of the water table beneath the land surface, with the maximum evapotranspiration rate occurring when the water table is at the land surface and decreasing to zero at the extinction depth, which was considered a function of land use (table A5).

In relating rainfall to direct recharge, available storage in the unsaturated zone is an essential property to know. In this context, the moisture-holding capacity of a soil, which is the amount of water required to bring the moisture content of a dry soil to its field capacity, is a useful measure. The moisture-holding capacity usually is stated in inches per inch. Therefore, for a soil horizon of thickness x in., a depth of rainfall equal to the moisture-holding capacity multiplied by x is required to fully saturate the dry soil. Storage capacity generally is recovered by evapotranspiration between storms. A simplified soil-moisture accounting model used by Khanal (1975) assumed that evapotranspiration takes place at a potential rate down to a depth of 6 in. and is reduced linearly down to a depth of 7 ft.

Merritt (1996) compared rainfall amounts with corresponding changes in the water-table elevation to estimate the specific yield in the Biscayne aquifer. Merritt (1996) compared daily rainfall measurements taken since 1932 at the Homestead Agricultural Experiment Station (HOMES. FS) with daily water-table elevation measurements made at well S-196A in Miami-Dade County. Only rainfall events prior to 1966 were used for the analysis because water-level fluctuations might have been strongly influenced by canals constructed since that time. During the entire period, the water table at S-196A remained below the local land-surface elevation (10.33 ft), and the highest water level was 9.58 ft. Rainfall events were selected when at least 4 in. of rainfall were concentrated in brief periods, preceded and followed by periods of little rainfall. The results derived by Merritt (1996) are shown in figure A1. These data collectively indicate a specific yield of 0.25. It is noteworthy that Merritt (1996) used storm-event rainfall derived from daily rainfall measurements to estimate the relation shown in figure A1. Because rainfall events do not occur on daily time increments, however, and because sub-stantial attenuation of ground-water mounds can occur within 1 day, an analysis based on hourly rainfall measurements may be more useful.

Canal Leakage

Possible pathways by which rainfall enters a canal are direct precipitation, overland flow, shallow subsurface stormflow, and ground-water inflow. The contribution of direct rainfall to the water budget of drainage channels usually is very low because such channels typically represent only a small percentage of the catchment area. Exceptions to this rule tend to occur at the beginning of large, intense rainstorms (Williams and others, 2002). Direct surface runoff into canals is relatively rare and primarily occurs through stormwater outfall pipes that drain roadways and adjacent subdivisions with positive drainage systems. The flow in most canals generally is influenced by ground-water inflow (canal leakage), so simula-

Table A4. Results from rainfall simulator test

[All data except storage capacities are from Savabi and others (2001). NRCS, Natural Resources Conservation Service; SFWMD, South Florida Water Management District]

Soil	Depth of soil (inches)	Depth to water table (inches)	Rainfall (inches)	Runoff (inches)	Storage capacity in NRCS model (inches)	Storage capacity in SFWMD model (inches)
Krome	8	0	5.04	4.13	0.9	0.0
		8	5.20	3.42	2.0	1.9
		39	4.57	3.22	1.4	7.7
Perrine Marl	5	0	4.76	4.02	.7	.0
		5	4.65	3.00	1.8	1.4
		39	4.76	2.66	2.5	7.7
Chekika	12	0	4.80	4.02	.7	.0
		12	4.84	2.95	2.2	2.5
		39	4.69	2.60	2.5	7.7

tion of the canal-aquifer interaction is an important component of any modeling effort to describe the hydrology of southern Florida. The complex network of canals in southern Florida extends for thousands of miles through wetlands, agricultural areas, and urban areas. Restrepo and others (1992) reported that their three-dimensional finite difference ground-water flow model of the surficial aquifer system in Broward County was most sensitive to changes in the canal-leakage parameters and hydraulic conductivity of the aquifer. Most drainage canals in southern Florida extend below the water table.

A common assumption is that sediment accumulation at the bottom of canals restricts leakage from the bottom and that most ground water enters and leaves through the canal sides (Miller, 1978; Sonenshein, 2001). The reach-transmissivity approach has been shown to provide good estimates of canal leakage under steady-state conditions (Chin, 1990; 1991). The reach-transmissivity approach is based on the Dupuit-Forcheimer assumption, and further assumes that the effects of clogging on the sides of canals are negligible and the effects of partial penetration of the canal into the aquifer are negligible whenever the reach-transmissivity equation is applied more than three aquifer depths from the canal. Nemeth and others (2000) applied the reach- transmissivity (canal-leakage) model developed by Chin (1990) to unsteady-state conditions, and produced acceptable results. Based on measurements of flow in canals, Sonenshein (2001) reported increases in discharge ranging between 9 and 30 (ft^3/s)/mi along a 2-mi reach of Levee 30 canal in Miami-Dade County, and Swayze (1988) reported an average inflow of 10 (ft^3/s)/mi into the Levee 35A canal in Broward County.

Genereux and Slater (1999) investigated the water balance over several canal reaches within Levee 31W and C-111 along the eastern boundary of Everglades National Park, and canal flow measurements were taken using acoustic velocity meters at seven different sites. Results of their study indicated that rainfall, evapotranspiration, and storage changes were minor components of the monthly water balance within these canals, with canal discharges and ground-water inflows and outflows dominating the water budget. A noteworthy discovery was the identification of a "short-circuiting" mechanism where water flows into the canal in the upstream reach and out of the canal in the downstream reach, effectively bypassing intermediate surface wetlands. The characteristic of a canal gaining flow in some parts and losing flow in other parts also was observed in the C-1N Canal (Allman and others, 1979). This close relation between canal stages and adjacent water-table elevations also was reported in the C-111 basin (Wedderburn and others, 1981; Shaw, 1985).

Several theoretical analyses of canal leakage have been published, of which some can be applied in southern Florida. When the Dupuit assumptions of small hydraulic gradients and virtually horizontal flow are valid, the linearized Boussinesq equation can be used to describe the water-table elevation in the vicinity of a canal (Workman and others, 1997). With the Boussinesq equation, the vertical coordinate is eliminated, and the free-surface boundary condition is not needed, thus yielding:

$$\frac{\partial h}{\partial t} - \frac{T}{S_y}\frac{\partial^2 h}{\partial x^2} = \frac{I}{S_y}, \qquad \text{(A8)}$$

Table A5. Runoff coefficients and extinction depths relative to land use

[From Restrepo and others, 1992]

Land use	Runoff coefficient	Extinction depth (feet)
Urban	0.5	1.0
Agriculture	.5	1.4
Rangeland	.2	2.0
Upland forests	.2	2.3
Water	.0	.6
Wetlands	.0	2.3
Barren land	.0	.5
Transportation	.5	1.0

where $h(x,t)$ is the hydraulic head, T is the aquifer transmissivity, S_y is the specific yield, I is the mean recharge to the aquifer, x is the distance from the channel, and t is time.

Workman and others (1997) provided a semi-analytical solution to equation A8 with the following boundary and initial conditions:

$$\begin{aligned} &0 \le x \le L_x, \qquad 0 < t, \\ &h(0,t) = h_1(t), \\ &h(L_x,t) = h_2, \\ &h(x,0) = h_o(x) \end{aligned} \quad , \qquad \text{(A9)}$$

where L_x is the distance to where h is unaffected by changes in canal stage, h_1 is the stage in the channel, h_2 is the hydraulic head at a distance L_x from the aquifer, and $h_o(x)$ is the initial condition. Workman and others (1997) compared a semi-analytical solution of equation A8 subject to equations A9 in an alluvial valley aquifer and reported that predictions were excellent at distances of up to about 2,297 ft (700 m) from the river. In cases where the aquifer transmissivity changes substantially with the stage and water-table elevations, the solution of the linearized equation (eq. A8) is not appropriate, and a nonlinear model, such as that proposed by Serrano and Workman (1998), should be used. Hermance (1999) considered the case where a water body (such as a canal) and adjacent aquifer are initially at elevation h_o, and the water level in the aquifer is instantaneously elevated to h_1 and allowed to drain into the water body (canal), which remains at elevation h_o. This condition is similar to what happens when rainfall rapidly recharges the ground water, and subsequently drains into a canal. Hermance (1999) showed that the elevation, $h(x,t)$, of the water table in the aquifer at a distance x from the canal at time t is given by:

$$h(x,t) = h_o + (h_1 - h_o)erf(\xi) \; , \qquad \text{(A10)}$$

where $erf(\xi)$ is the error function defined by the relation:

$$erf(\xi) = \frac{2}{\sqrt{\pi}} \int_0^{\xi} e^{-u^2} du \; , \qquad \text{(A11)}$$

and

$$\xi = \sqrt{\frac{x^2 S_y}{4tT}} \; , \qquad \text{(A12)}$$

Equation A10 indicates that the water table at any distance x from a canal declines at a rate given by:

$$\frac{dh}{dt} = -(h_1 - h_0)\frac{1}{\sqrt{\pi t}}\xi exp^{-\xi^2} \; , \qquad \text{(A13)}$$

which indicates that the rate of decline of the water table can be expressed in terms of time and distance from the canal.

Equation A10 was used by Wedderburn and others (1981) to assess the relation between the stage in C-111 and the surrounding aquifer. Base flow to a canal generally is defined as canal inflow derived from ground water. Base flow contributed to both sides of a canal per unit length of canal, Q_b, as a result of instantaneous elevation of the water-table elevation adjacent to a canal, can be estimated using the relation (Ferris and others, 1962):

$$Q_b = \frac{2(h_1 - h_0)}{\sqrt{\pi t}}\sqrt{S_y T} \, , \qquad \text{(A14)}$$

where t is the time after the instantaneous change in canal level.

Using the Boussinesq equation without recharge (eq. A8 with I =0), Lal (2001) investigated the modification of canal flow due to stream-aquifer interaction and showed that water-level disturbance characteristics in the canal are unaffected by its interaction with the aquifer for large values of the dimensionless parameters χ and P_d, where:

$$\chi = B\sqrt{\frac{f}{S_y T}} \; , \qquad \text{(A15)}$$

and

$$P_d = 0.3h_0\sqrt{\frac{2f}{q_o S_y}} \; , \qquad \text{(A16)}$$

where B is the width of the canal, f is the frequency of oscillations in the canal (in cycles per unit time), S_y is the specific yield of the aquifer, T is the transmissivity of the aquifer, h_o is the steady-state depth in the canal, and q_o is the discharge rate in the canal per unit width. Lal (2001) applied this criterion to the Levee 31N Canal and Snapper Creek Canal (fig. 1, C-2) and reported that interaction of these canals with the aquifer can be expected to affect the propagation of periodic disturbances in canals. Such disturbances consist primarily of tidal fluctuations that propagate within canals when the gates at the coastal structures are open. Major effects of stream-aquifer

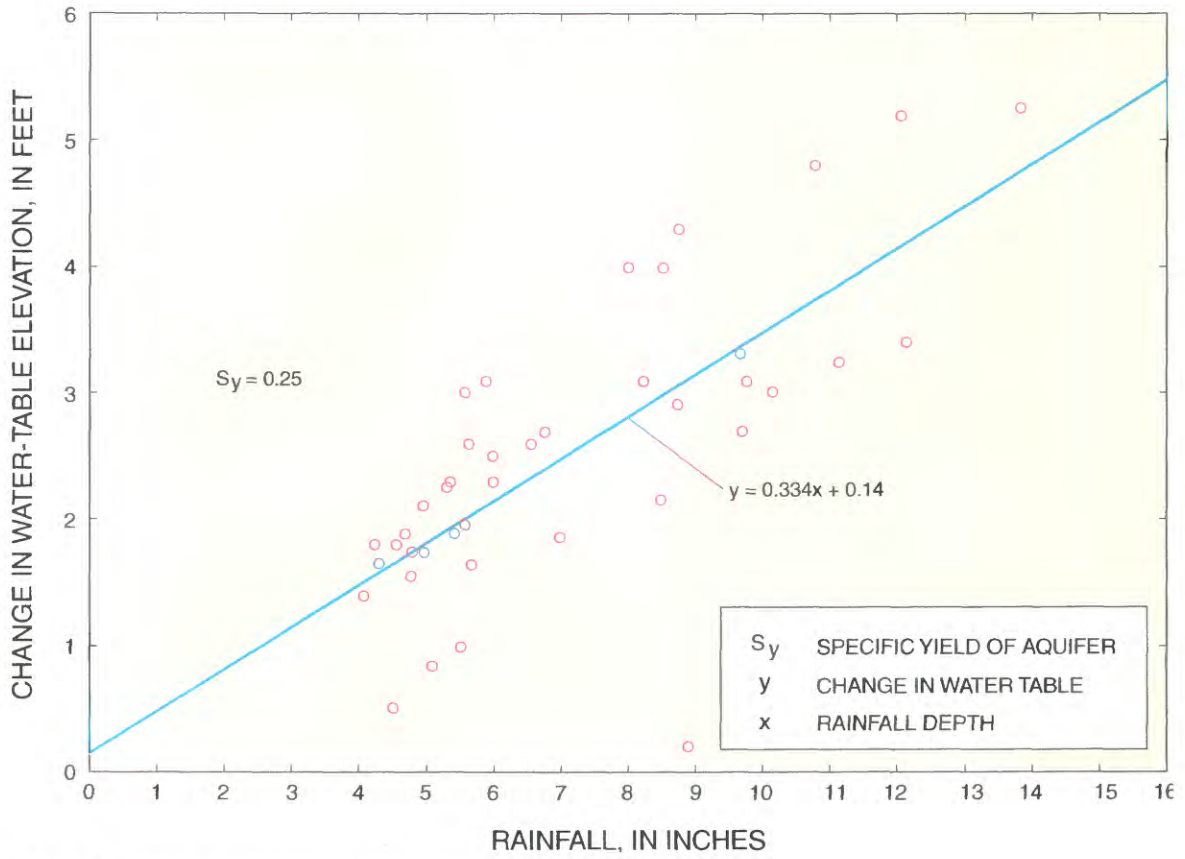

Figure A1. Change in water table relative to rainfall (from Merritt, 1996).

interaction include a reduction in amplitude and speed of tidal oscillations in the canal. Analyses of the Levee 31N canal and Snapper Creek Canal also indicated that tidal influences within these canals can be expected to propagate several miles into the aquifer. Because of the high transmissivity of the Biscayne aquifer, substantial interaction is expected to occur in major canals in southern Florida.

An ability to predict the propagation of tidal oscillations (within canals) into an aquifer can be very useful. Because the propagation of tidal fluctuations in an aquifer is influenced by the hydraulic properties of the aquifer, measurement of the tidal propagation characteristics can potentially be used to estimate the hydraulic properties of the aquifer. This is particularly useful in southern Florida where the high transmissivity of the aquifer makes measurement of the hydraulic properties difficult. The hydraulic properties that typically are of interest include transmissivity and specific yield of the aquifer. The propagation of sinusoidal oscillations from surface-water bodies into adjoining aquifers was first studied in detail by Ferris (1951) who showed that head fluctuations in a confined aquifer can be described by the relation:

$$h = h_0 \exp\left(-x\sqrt{\frac{\pi S}{t_o T}}\right) \sin\left(\frac{2\pi t}{t_o} - x\sqrt{\frac{\pi S}{t_o T}}\right), \qquad \text{(A17)}$$

where h is the ground-water head relative to the mean level, h_o is the amplitude of the tidal oscillation, x is the distance from the surface-water body where the sinusoidal fluctuations originate, S is the storage coefficient of the aquifer, t_o is the period of the sinusoidal oscillation, t is time, and T is the transmissivity of the aquifer. In addition to the confined-aquifer assumption, equation A17 assumes one-dimensional flow. According to equation A17, the time lag, t_d, and the amplitude attenuation factor, A_d, are given by the following expressions:

$$t_d = x\sqrt{\frac{t_o S}{4\pi T}}, \qquad \text{(A18)}$$

and

$$A_d = \exp\left(-x\sqrt{\frac{\pi S}{t_o T}}\right), \qquad \text{(A19)}$$

The validity of these expressions in unconfined aquifers was investigated by Erskine (1991). Results showed that the depths of piezometers used to measure the aquifer head fluctuations have an effect on the measured time lag, and nonhomogeneity and vertical flows cause deviations from ideal behavior. Measurements reported by Erskine (1991) and Shih and others (2000) in coastal unconfined aquifers clearly demonstrate that time lags in unconfined aquifers vary linearly with distance

from the shoreline, and the attenuation factor varies exponentially as expected by theory.

Erskine (1991) reported that a clear tendency exists for deeper piezometers to have smaller lags and larger attenuation factors, and this can be accounted for by the variation in effective S between the storage coefficient deep in the aquifer and the (higher) specific yield as the water table is approached. Storage coefficients typically are 1,000 to 10,000 times smaller than the corresponding specific yields (de Marsily, 1986). Using the measurements at piezometers located about 82 ft (25 m) below the water table, results reported by Erskine (1991) indicated that using values of S closer to the storage coefficient is more appropriate than to the specific yield in estimating the time lag given by equation A18. This conclusion also is supported by results reported by Reynolds (1987). Comparing equations A18 or A19 with measured data only allows the estimation of T/S, but not T and S separately. This combination of hydraulic parameters, T/S, is commonly referred to as the hydraulic diffusivity of the aquifer. Shih (1999) calculated hydraulic diffusivity in a confined aquifer using a spectral analysis of piezometric head fluctuations in a coastal aquifer and reported that the estimated hydraulic diffusivity was an order of magnitude greater than the hydraulic diffusivity estimated from aquifer tests in the area. Shih (1999) attributed this difference to aquifer tests being local measurements, whereas tidal propagation analysis measures the hydraulic diffusivity for a much larger length scale. Measured values of the amplitude attenuation factor also can be used to estimate the hydraulic properties of aquifers; however, as the attenuation factors become smaller, this approach becomes less accurate (Erskine, 1991).

Hermance (1999) analyzed the propagation of periodic (tidal) disturbances from fully penetrating canals into adjoining aquifers and defined the characteristic attenuation length scale, L, by:

$$L = \sqrt{\frac{t_o T}{\pi S_y}} \quad . \qquad \text{(A20)}$$

From an integrated-modeling viewpoint, time steps substantially less than the period of the canal disturbance should be used in the canal flow model, and a spatial resolution substantially less than the attenuation length scale in the aquifer should be used in the aquifer.

Overland Flow

Overland flow can occur from two distinct mechanisms—the Horton mechanism or the Dunne mechanism. The necessary conditions for the generation of overland flow by the Horton mechanism are: (1) a rainfall rate greater than the saturated hydraulic conductivity (equal to the infiltration capacity) of the soil; and (2) a rainfall duration longer than the required ponding time for a given initial moisture profile. Horton overland flow is generated from partial areas of a hillslope where the lowest surface hydraulic conductivities are present. Several studies have shown that Hortonian runoff is most sensitive to the spatial and temporal variability of rainfall and watershed characteristics for small excess rainfall rates (Ogden and others, 2001b).

In Dunne overland flow, the rainfall rate is less than the saturated hydraulic conductivity, and the surface soil is saturated. The surface soil may saturate from below when downward unsaturated flow is limited by restrictive subsoil or bedrock layer. The Dunne mechanism also is called saturation excess overland flow, and it is a case of subsurface soil control. This mechanism is more common to near-channel areas, and Dunne overland flow is generated from partial areas of the hillslope where the shallowest water tables are present.

Horton overland flow is considered dominant in systems where the soil profile or soil surface has been radically disturbed (for example, agricultural basins), and in urban areas where the surface is made virtually impermeable by paving and other construction. Dunne overland flow is predominant in humid regions with dense vegetation and topographic conditions that cause the water table to be located relatively close to the surface (Hornberger and others, 1998). Both Horton and Dunne mechanisms result in variable source areas that expand and contract through wet and dry periods.

The runoff/run-on phenomenon occurs whenever a more permeable soil area is located downslope from an area that generates surface runoff. A common occurrence is in urban areas where runoff from roofs, sidewalks, or streets may run onto grassed areas. In rural or natural settings, this phenomenon may occur when a soil disturbed by cultivation or compaction is upslope from pasture, hay, or a vegetated buffer zone (Woolhiser, 2002). This run-on process has important implications for ground-water recharge, and also affects the location and growth of plant species.

Peak surface runoff commonly is calculated using the rational method, which requires estimation of a runoff coefficient. This coefficient is commonly assumed to be independent of the size of the catchment area; however, a decrease in runoff coefficient with increasing size of the catchment area has been observed in many runoff studies (Wainwright and Parson, 2002). Among the factors contributing to the spatial dependence of the runoff coefficient are the spatial variation in infiltration capacity, topography, and the temporal variability of rainfall within individual storm events.

Conventional surface-runoff models are of limited use in much of southern Florida because of the relatively small land slopes. A relation between surface runoff and land slope proposed by the U.S. Department of Agriculture (2001) is given in table A6. Because land slopes in southern Florida typically are less than1 percent, average infiltration capacities of less than 0.2 in/hr would be required to generate substantial runoff from typical catchment areas.

Overland flow models describe the movement of rainfall excess and can be classified into two categories: point-scale models and catchment-scale models. Point-scale models

describe overland flow by the simultaneous solution of partial differential equations associated with laws of conservation of mass and momentum, typically solved using a finite-difference scheme. Conversely, catchment-scale models use empirical or semi-empirical equations that relate the average rainfall excess to the overland-flow hydrograph at the catchment outlet. Point-scale models typically are used to describe overland flow in rural undeveloped areas, including wetlands. Catchment-scale models are used typically in urban areas where catchment outlets connect to the drainage system. Both point-scale and catchment-scale models have been used in southern Florida.

Point-Scale Models

Point-scale models generally use the continuity and momentum equations, which are sometimes called the St. Venant equations. The two-dimensional continuity equation is given by:

$$\frac{\partial h}{\partial t} + \frac{\partial uh}{\partial x} + \frac{\partial vh}{\partial y} - i + f + ET = 0, \qquad \text{(A21)}$$

where u and v are the overland-flow velocities in the x and y directions, h is the water depth, i is the rainfall rate, f is the infiltration rate, and ET is the evapotranspiration rate.

The momentum equations applicable to overland flow in the x and y directions are given by:

$$\frac{\partial(uh)}{\partial t} + \frac{\partial(u^2h)}{\partial x} + \frac{\partial(uvh)}{\partial y} + hg\frac{\partial(h+z)}{\partial x} + ghS_{fx} = 0, \qquad \text{(A22)}$$

and

$$\frac{\partial(vh)}{\partial t} + \frac{\partial(uvh)}{\partial x} + \frac{\partial(v^2h)}{\partial y} + hg\frac{\partial(h+z)}{\partial y} + ghS_{fy} = 0, \qquad \text{(A23)}$$

where S_{fx} and S_{fy} are the friction slopes in the x and y directions. The first three terms in the momentum equations are the acceleration terms that account for inertial effects, the fourth term is the net gravitational force resulting from nonuniform flow, and the fifth term represents the shear force exerted by the land surface on the moving water. A common approach used for low-relief wetlands that facilitates solution of the governing equations is to assume that the acceleration terms of the momentum equations are negligible (McKillop and others, 1999). Under this assumption, the continuity and momentum equations can be combined to yield a single expression identical in form to the equation for heterogeneous nonlinear diffusion. Many overland flow models are based on the assumption that flow velocity can be expressed as a multiparameter power function of water depth. Traditionally, Manning's equation has been invoked to define the dependence of water velocity on friction slope. Overland flow may occur in the low range of flow Reynolds number, however, for which Manning's n is not constant, and the Darcy-Weisbach formula is preferred (Yen, 1991).

The combination of equations A21 to A23 is called the dynamic-wave model. When the velocity is expressed as a power function of the flow depth (such as in the Manning equation) and combined with equation A21, the result is called the kinematic-wave model. An overview of present-day hydrologic models indicates that the kinematic-wave theory has been widely used for simulating flow over planes where the criteria for the kinematic-wave application are satisfied. Applications of the kinematic-wave theory have been restricted mostly to urban watersheds, and to some extent, natural watersheds that have comparatively small drainage areas (Najafi, 2003). The dynamic-wave theory is considered to be the best methodology for taking into account the prevailing flow conditions over the watershed and in channels (Najafi, 2003).

The accuracy of overland flow models relies heavily on the ability to describe the topography of the land surface. Digital elevation models typically are used to describe surface topography; for accurate results, this model and the overland flow model should have resolutions greater than the average hillslope length scale (McMaster, 2002). State-of-the-art research in this area continues to explore the relations between hydrologic model accuracy, horizontal and vertical resolution thresholds of topographic data, the scale of hillslope processes, and variable landscape conditions.

Few attempts have been made to verify overland flow models with field observations. This is due primarily to the difficulty in measuring flowrates and various properties and processes that combine to influence overland flow (Bolster and Saiers, 2002).

Catchment-Scale Models

Surface runoff is typically the focus of catchment-scale urban hydrology models, with the runoff calculated by these models used to design and analyze the performance of drainage infrastructure. After reviewing several approaches to calculating surface runoff, Yan and Smith (1994) advocated using the nonlinear-reservoir model to simulate overland flow in southern Florida. Most urban hydrology codes are capable of using this model to calculate the surface runoff; however, field tests to measure the accuracy of the nonlinear-reservoir model in estimating surface runoff are limited.

Conventional urban drainage systems consist of drainage inlets connected by underground pipes leading to outfalls. The catchment area associated with each inlet is established by appropriate grading, and surface runoff entering each inlet typically consists of two components: runoff from directly connected impervious areas (DCIA) and direct runoff from pervious areas. Fully developed urban areas can be expected to have an impervious area of up to 50 percent (Khanal, 1975). In residential areas, a typical design assumption is to include all roadway pavement, connected sidewalks, and driveways as DCIA. Runoff from both DCIA and pervious areas typically

Slope (percent)	Saturated hydraulic conductivity, in inches per hour					
	>6	2–6	0.6–<2	0.2–<0.6	0.06–<0.2	<0.06
Concave	Negligible	Negligible	Negligible	Negligible	Negligible	Negligible
<1	Negligible	Negligible	Negligible	Low	Medium	High
1–5	Negligible	Very low	Low	Medium	High	Very high
5–10	Very low	Low	Medium	High	Very high	Very high
10–20	Very low	Low	Medium	high	Very high	Very high
>20	Low	Medium	High	Very high	Very high	Very high

Table A6. Index of surface runoff classes

[From U.S. Department of Agriculture (2001); >, greater than the value; <, less than the value]

are estimated using the nonlinear-reservoir method, which consists of the simultaneous solution of the continuity and Manning equations given by:

$$i_e(t)A - Q(t) = \frac{dy}{dt}A \ , \qquad \text{(A24)}$$

and

$$Q(t) = \frac{1}{n}w(y - y_d)^{5/3}S_o{}^{1/2} \ , \qquad \text{(A25)}$$

where i_e is the effective rainfall rate, equal to the actual rainfall rate minus the interception, wetting, and infiltration rates; A is the plan area of the catchment; Q is the surface runoff rate; y is the depth of water above the land surface; n is Manning's roughness coefficient; w is the width of the catchment (equal to the catchment area divided by the length of the maximum flow path); y_d is the depth of depression storage; and S_o is the slope of the ground.

In the model used by the SFWMD to calculate runoff from undeveloped land, a Manning's roughness coefficient of 0.25 and a depression storage of 2 in. was typical. In urban catchments, equations A24 and A25 are applied separately to the pervious and DCIAs contributing flow to the drainage inlet, and the resulting runoff hydrographs, $Q(t)$, are added together to give the inflow hydrograph to the inlet. To simulate flow in the underground drainage pipe connecting the inlets, urban hydrology models typically apply the one-dimensional conservation of mass and momentum equations, given by:

$$\frac{\partial Q_p}{\partial x} + \frac{\partial A_p}{\partial t} = 0 \ , \qquad \text{(A26)}$$

and

$$\frac{\partial Q_p}{\partial t} + \frac{\partial}{\partial x}\left(\alpha\frac{Q_p{}^2}{A_p}\right) + gA_p\frac{\partial y_p}{\partial x} + gA_pS_f = gA_pS_p \ , \qquad \text{(A27)}$$

where Q_p is the flow in the pipe, A_p is the cross-sectional flow area in the pipe, y_p is the flow depth in the pipe, g is the acceleration due to gravity, x is the distance in the flow direction, α is the velocity distribution coefficient, S_f is the friction slope, and S_p is the pipe slope. Simultaneous solution of equations A26 and A27 determines the water depth and flowrate in the drainage pipes as a function of time. Two popular urban hydrology codes that implement the nonlinear-reservoir method and pipeline routing to estimate discharge hydrographs from urban areas are the Surface Water Management Model (SWMM) and Modeling of Urban Sewers (MOUSE).

The linearity of the relation between peak runoff and catchment area is assumed in many standard catchment-scale hydrologic models, such as the rational method and the unit hydrograph methods, and this assumption is relatively well accepted for humid regions (Goodrich and others, 1997). Antecedent moisture conditions are not usually considered in peak runoff models, even though Haiff and others (1992) indicated that the average rainfall intensity during a storm and the cumulative rainfall over the previous 7 days are significant variables in determining the peak runoff from small basins of about 1 mi^2.

Catchment-scale models can either be distributed or lumped models. In distributed models, the catchment-scale formulation is applied to subcatchments, and the runoff from all subcatchments is combined to yield the outflow from the entire catchment. In contrast, lumped catchment-scale models describe the entire catchment with a single (lumped) catchment-scale model. Doyle and Miller (1980) applied a distributed kinematic-wave catchment-scale model to four urban sites near Miami. This distributed model was used to determine rainfall excess and route overland flow and channel flows at each site. Optimization of soil-moisture accounting and infiltration parameters was performed during the calibration phases. Results indicated that an acceptable validation of the catchment-scale model could be achieved (Doyle and Miller, 1980). In the highly porous, rapidly infiltrating soil, field data indicated that the pervious surface yields little overland runoff for most storms with rainfall less than 1 in., if there were 3 or more days prior to a storm without any appreciable rainfall. This was typical of residential and highway locations; however, in highly impervious commercial areas, most rainfall resulted in surface runoff. DCIA was a major factor in determining the runoff hydrograph, especially

for small rainfall amounts. The soils at the study sites had hydraulic conductivities ranging from about 0.6 to 1 in/hr. Field data verification (Valeo and Monin, 2000) has indicated that the urban component of a catchment dominates the low-runoff events. These results indicate that runoff from DCIA is removed by drainage systems, whereas the remaining rainfall percolates into the ground.

Zaghloul and Al-Shurbaji (1990) applied the USEPA/SWMM model at different scales to a 199-acre catchment in Kuwait. The catchment was divided into 82 subcatchments of regular shape, and the calculated runoff was compared with the runoff calculated by dividing the catchment into only four (large) subcatchments. The calculated runoff hydrographs were comparable, demonstrating that a coarser discretization was acceptable in calculating the runoff hydrograph for the entire catchment. The Horton infiltration curve was used to describe the infiltration, with a maximum infiltration of 3.1 in/hr, a minimum infiltration (equal to the saturated hydraulic conductivity) of 0.6 in/hr, and a decay factor of 0.13 minute^{-1}. In most cases, the rainfall intensities were less than the infiltration capacity of the soil and the pervious areas did not contribute to the runoff. The length of each subcatchment was equal to the distance between the drain inlet and the most remote point in the subcatchment, and the overland flow width was equal to the area of the subcatchment divided by the overland flow length. Depression storage values for pervious areas were 0.2 and 0.06 in. for impervious areas. Rainfall characteristics were mostly convectional, and substantial variations in rainfall amounts occurred for individual storms. The calculated runoff amounts were most sensitive to the depression storage and roughness coefficient for impervious areas and to the overland flow widths. In using the SWMM model to calculate the runoff entering individual storm sewers, a design runoff coefficient of 0.5 was determined as the cause in the overdesign of the sewer pipes. These results indicated that a smaller runoff coefficient should be used to account for the fact that only runoff from DCIA contributed inflow to the drainage structures.

Fankhauser (1995) developed a maximum-likelihood classification algorithm for automatic determination of imperviousness in urban areas from digital orthophotos. In sample applications on urban areas of 20 to 310 acres, the accuracy of the estimated imperviousness was within 10 percent for the entire catchment areas, with higher errors in individual subcatchments. Fortin and others (2001) described an algorithm for using a raster-type digital elevation model to delineate catchments.

Field validation of catchment-scale rainfall-runoff models is still an active area of research. Maheepala and others (2001) investigated measurement systems used to adequately monitor the performance of stormwater drainage systems. Monitoring systems included rain gages and acoustic velocity meters placed in drainage pipes to measure depth of flow and average velocity. Catchment sizes ranged from 20 to 7,400 acres, and calibration studies in a 26-in. diameter discharge pipe indicated discharge errors of less than 10 percent. For individual storm events, rain-gage measurements were considered to be representative of areas encompassing 1,000 acres. Rain gages spaced more than 1.25 mi apart produced very different hyetographs for individual storms. Ideally, rain gages should be installed at ground level to reduce wind and turbulence effects. Flowmeters can be installed in pipes just downstream of manholes (at least two pipe-diameters downstream); however, flowmeters are difficult to install in pipes with a diameter less than 15 in. Sensors should face downstream. In estimating the peak rainfall intensity, tipping bucket rain gages with resolutions of 0.02 in. perform just as adequately as those with resolutions of 0.01 in. Flowmeters with 2-minute logging intervals estimate peak runoff rates just as adequately as flowmeters with 1-minute logging intervals; however, 4-minute logging intervals introduced significant errors in the peak runoff rate and the peak time.

Scale Effects

Scale effects in hydrology arise because process relations are a function of the spatial and temporal averaging scale of the variables involved, and different processes may be dominant at different scales (Wallender and Grismer, 2002). A common practice in hydrology, however, is to use available data at scales that are not compatible with that of the application (Vachaud and Chen, 2002). Process descriptions or parameterizations that have been derived at the small spatial scales of the laboratory or experimental plot do not necessarily hold true at the much larger scales of the catchment. For example, catchment morphometry plays an important role in rainfall-runoff processes at the catchment scale, but not on local scales. Both aggregation (upscaling) and disaggregation (downscaling) are complicated by strong nonlinearities present in the hydrologic environment. Wood and others (1988) introduced the concept of a representative elementary area, which is defined as a critical area at which implicit continuum assumptions can be used without knowledge of the patterns of parameter values, although some knowledge of the underlying distributions may still be necessary. Wood and others (1988) reported that a representative elementary area of about 247 acres (1 km^2) existed for hydrologic response of an experimental watershed and was more strongly influenced by basin topography than rainfall length scales.

Numerical models have been used to study scale effects on the rainfall-runoff relation associated with the spatial variability of soil hydraulic properties; however, the effects of spatial variability are known to be event dependent. When studying a watershed, Merz and Plate (1997), reported that a small influence exists in the spatial distribution of soil hydraulic properties for both major and minor rainfall events. A large influence has been reported for medium-sized events. For events with low rainfall intensity, the impervious areas mainly contribute to surface runoff, and the effects of spatial variability are small. Increasing the rainfall intensity leads to a sensitive range with a small difference between rainfall intensity and soil conductivity. Under these conditions, runoff is very

sensitive to the spatial pattern of infiltration. A further increase of the rainfall intensity leads to an expansion of the source areas for overland flow generation and to a smaller influence of the spatial pattern of infiltration. Data from simulator plots have shown that small-scale spatial variability of saturated conductivity can cause an increase in the infiltration rate with rainfall intensity (Hawkins and Cundy, 1987).

Scale processes commonly found in hydrology are listed in table A7 (Anderson and Burt, 1990). On the local scale, runoff is influenced by properties including slope angle and upslope drainage area; however, at the hillslope scale, runoff is affected primarily by soil properties and hillslope form. At the basin or watershed scale, the runoff hydrograph is influenced by basin morphometry, which can be expressed by representative attributes for catchment height distribution (relief indices), length and form of the basin (form indices), and properties describing the drainage network. Surface and subsurface runoff to topographic lowlands can focus recharge at subregional and local scales (Green, 1995; Delin and others, 2000). The digital elevation model grid size used in hydrologic models can affect both the representation of the land surface and the results of the hydrologic simulation. Grid sizes smaller than the hillslope length scale are necessary to adequately simulate processes controlled by land form (McMaster, 2002). For event-based hydrologic modeling, the correct definition of antecedent moisture conditions is critical to accurately simulate the rainfall-runoff process (Stephenson and Freeze, 1974); however, the characterization of soil-moisture patterns and its relation to climate and catchment morphometry is still an active area of research (Grayson and others, 1997). Although much research has focused on hydrologic processes at the local, hillslope, and watershed scales, relatively little attention has been devoted to understanding the important fundamental process that ties the process models together across all scales (Sivapalan, 2003). The fact that watershed-scale surface-runoff models (for example, unit hydrographs) tend to be much simpler than hillslope-scale models is testimony for the need to identify and study the fundamental processes that link the scale models together.

Loague and Kyriakidis (1997) have noted that the "Achilles heel" of large-scale hydrologic response simulation with process-based models is characterization of small-scale variability in near-surface soil hydraulic property information at larger temporal and spatial scales. The process of run-on is an important process associated with spatial variations in infiltration capacity (Merz and Plate, 1997). Betson (1964) introduced the term "partial area concept," where the catchment discharge results mainly from infiltration excess on less permeable areas, whereas the residual areas do not contribute. Later, this concept was transferred to other runoff-generating mechanisms and named "variable contributing area," "dynamic watershed concept," or "variable source concept."

Horritt and Bates (2001) varied the resolution of a hydrologic model from about 33 to 3,281 ft (10 to 1,000 m), calibrating the model based on the location of the inundated area resulting from a specific rainfall event. The calibration was reported to be stable for resolutions less than about 328 ft (100 m), and no further improvement was found in the prediction of an inundated area for less spatial resolutions. Low-resolution predictions were subject to quantization noise, which is an error that is generated simply because the simulated boundaries of the inundated areas provide only a crude approximation to the actual boundary. Additionally, changes in scale may have a bulk effect on the flow, which is effectively independent of the quantization noise. At coarse scales, the discrepancy between model predictions and the observed boundaries of flooded areas is dominated by the quantization noise, and shortcomings in the model are obscured. Poor performance becomes evident only when models are run at a fine enough scale. Horritt and Bates (2001) proposed a two-scale modeling strategy where a low resolution model is used to predict water levels (which are less sensitive to scale). These water levels then are used to predict the inundated area using a higher resolution digital elevation model. This approach was reported to be effective in reducing the spatial resolution of the hydrologic model used to estimate the inundated area.

Scale effects generally are associated with spatial variability in catchment properties, and it is unreasonable to expect to describe hydrologic processes by models that are independent of scale. The sources of variability can be stochastic, deterministic, or both. If the mean, higher order moments, and probability density functions of the fluctuations in space/time remain constant with respect to all space/time origin locations, then the hydrologic process (or parameter) is stationary heterogeneous; otherwise, the process or parameter is nonstationary heterogeneous. Clearly, a hydrologic process (or parameter) that is nonstationary at one scale may become stationary at another scale (Kavvas, 1999).

Table A7. Scales of processes commonly found in hydrology

[From Anderson and Burt, 1990]

Scale	Dominant topographic features	Dominant hydrologic processes
1 - 10 meters	Slope angle, local parameters	Small-scale processes (such as infiltration)
10 - 1,000 meters	Hillslope form	Hillslope processes (such as overland flow)
1 - 100 kilometers	Drainage network, basin characteristics	Discharge concentration (runoff hydrograph)

125 years of science for America

1879–2004

Printed on recycled paper